Axial-Flexural Behaviour of Reinforced Concrete Masonry Columns Confined by FRP Jackets

Khalid Saqer S Alotaibi

A Thesis

In the Department

of

Building, Civil and Environmental Engineering

Presented in Partial Fulfillment of the Requirements

For the Degree of

Doctor of Philosophy (Civil Engineering) at

Concordia University

Montréal, Québec, Canada

July 2018

CONCORDIA UNIVERSITY

School of Graduate Studies

This is to certify that the thesis prepared

By:　　**Khalid Alotaibi**

Entitled:　**Axial-Flexural Behaviour of Reinforced Concrete Masonry Columns Confined by FRP Jackets**

and submitted in partial fulfillment of the requirements for the degree of

DOCTOR OF PHILOSOPHY (Civil Engineering)

complies with the regulations of the University and meets the accepted standards with respect to originality and quality.

Signed by the final examining committee:

_____ Chair
Dr. Pouya Valizadeh

_____ External Examiner
Dr. Sreekanta Das

_____ External to Program
Dr. Ion Stiharu

_____ Examiner
Dr. Ashutosh Bagchi

_____ Examiner
Dr. Lan Lin

_____ Thesis supervisor
Dr. Khaled Galal

Approved by _____

Dr. Fariborz Haghighat, Graduate Program Director

<u>August 23, 2018</u>
Date of Defence

_____
Dr. Amir Asif, Dean
Faculty of Engineering and Computer Science

Abstract

**Axial-Flexural Behaviour of Reinforced Concrete Masonry Columns
Confined by FRP Jackets**

Khalid Saqer S Alotaibi, Ph.D.
Concordia University, 2018

Confining existing concrete and masonry columns by Fibre Reinforced Polymers (FRP) is a beneficial method for enhancing the column capacity and ductility. The popularity of using FRP for strengthening and upgrading columns is mainly attributed to the high strength and lightweight characteristics of the FRP materials. Using FRP composites reduces additional dead load associated with traditional strengthening solutions and simplify the application in areas with limited access. The goal of this research is to experimentally quantify the enhancement in strength and strain capacity of Carbon FRP (CFRP) confined concrete masonry columns under concentric and eccentric loading. Research on FRP-strengthened concrete masonry columns under eccentric loads is essential to understand the effect of this retrofitting technique on the performance of columns. The experimental data was then used to propose a simplified methodology that predicts the axial force-moment interaction diagram of fully grouted reinforced concrete masonry column strengthened with FRP jackets. The methodology considers short prismatic reinforced concrete masonry columns failing in a compression controlled manner and complies with equilibrium and strain compatibility principles. To achieve the research goals, 47 scaled fully grouted concrete block masonry columns were tested under concentric, eccentric, and bending loading up to failure. Parameters investigated in this research include the thickness of CFRP jacket, corner radius of cross section and the magnitude of eccentricity. The proposed analytical methodology showed a good correlation with the experimental data. Parametric study was carried out to determine the effect of design variables on the axial-flexural interaction of fully grouted reinforced concrete masonry column strengthened by FRP jackets.

Acknowledgements

To my beloved parents; Saqer and Jawza

To my lovely wife, Jwaher Snhout Alotaibi

To my children; Alwaleed and Seba

To my brothers and sisters

Contributions of Authors and Dissemination

This thesis prepared in according to to Concordia University regulations for Manuscript-Based Thesis. This thesis presents experimental and theoretical work carried out solely by Khalid Saqer S Alotaibi. Advice and guidance were provided for the whole thesis by the academic supervisor Professor Khaled Galal. During the preparation of this thesis, some of the findings were presented and submitted in the following peer-reviewed journals:

Chapter 3

Alotaibi, K. S., and Galal, K. (2017). Axial compressive behavior of grouted concrete block masonry columns confined by CFRP jackets. Composites Part B: Engineering, 114(4), 467-479.

Chapter 4

Alotaibi, K. S., and Galal, K. (2018). Experimental study of CFRP-confined reinforced concrete masonry columns tested under concentric and eccentric loading. Composites Part B: Engineering, 155(12), 257-271.

Chapter 5

Alotaibi, K. S., and Galal, K. (2018). Axial-Flexural interaction for FRP-wrapped reinforced concrete masonry columns: design methodology and design variables, prepared for submission.

Table of Contents

VIII

X

List of Figures

XII

XIII

List of Tables

List of Equations

Notations

A_{crv}	Area under FRP confined masonry stress-strain curve
A_m	Masonry cross section area
A_s	The area of longitudinal steel reinforcement
A_{si}	Area of the ith steel reinforcement
b	Width of the cross section
c	Distance from extreme compression fibre to neutral axis
c_b	Distance from extreme compression fibre to neutral axis for balanced condition
C_c	Compression force in FRP confined masonry
d	Distance of tension reinforcement from extreme compression fibre
d_i	Distance of the ith steel reinforcement from the extreme compression fibre
e	Eccentricity
exp	Experimental value
E_f	Tensile modulus of elasticity of FRP jacket
E_s	Young's modulus of elasticity of steel reinforcement
f_l	FRP lateral confining pressure
$f_{l,eff}$	Effective confining pressure
f_{mcd}	Compressive strength of FRP-confined masonry
f_{md}	Unconfined masonry strength
f_{si}	Stress in the ith steel reinforcement
F_{si}	Force in the ith steel reinforcement
f_y	Yield strength of longitudinal steel reinforcement
g_m	Masonry mass density in kg/m^3
h	Height of the cross section
k'	Coefficient to account for the density of masonry
k_{eff}	Coefficient of efficiency for confinement
k_H	Coefficient of efficiency in the horizontal direction
k_V	Coefficient of efficiency in the vertical direction

L	Vertical height of the columns
M_{max}	Flexural capacity of FRP strengthened column
$MAPE$	Average of the absolute error
n	Total number
n_a	Environmental conversion factor
$N.A$	Neutral axis
R^2	Absolute fraction of variance
P_{max}	Axial capacity of FRP confined masonry column
r_c	Cross section corner radius
S_{crv}	First moment of area for FRP confined masonry stress-strain curve
t	Shorter dimension of the cross section
t_f	FRP jacket thickness
$theo$	Theoretical value
x	Distance of ith steel reinforcement from the neutral axis
x_{crv}	Centroid of FRP confined masonry stress-strain curve
α	Ratio of average stress in rectangular stress block to the masonry prism strength
$\alpha_1, \alpha_2, \alpha_3$	Coefficient to calibrate the model with experimental tests
β	Ratio of depth of rectangular stress block to depth to the neutral axis
γ_f	Partial factor
$\varepsilon_{fd,rid}$	The reduced value of the FRP ultimate strain
ε_{fk}	Characteristic rupture strain of FRP jacket
ε_m	Strain in masonry
ε_{mcu}	Ultimate compressive strain of confined masonry
ε_{mu}	Ultimate compressive strain of unconfined masonry
ε_y	Yield strain of longitudinal steel reinforcement
ε_{si}	strain in longitudinal steel reinforcement layer
ρ_g	Ratio of longitudinal steel area to the masonry cross section area
σ_m	Stress in masonry
δ	Absolute error percentage

Chapter 1

Introduction

1.1 General background

Masonry has been used as a structural material in construction for centuries. Many of these existing masonry constructions are in need of structural strengthening. Rehabilitation and upgrading deficient structures can be considered an economical alternative in most of the cases or the only feasible option in some.

Many concrete masonry columns cannot support additional axial loads resulting from changing the use of building or they suffer strength degradation from environmental effects or errors in their design and construction. This results in the need for developing an effective strengthening method to restore the degraded strength or to increase the bearing capacity of such existing masonry columns.

A masonry column generally consists of stone, clay brick or concrete blocks bonded with cementitious mortar. The column could be fully or partially grouted. Also, it could be reinforced with steel reinforcement bars to resist the tensile forces that arises from flexure moments acting on the column. In case of reinforced masonry columns that are part of the lateral force resisting system or designed to sway under lateral seismic load, the strengthening could improve the ductility performance to meet new seismic design requirements.

Compared to traditional methods, strengthening columns by Fibre-Reinforced Polymer (FRP) composite materials have gained popularity in recent decades due to their superior characteristics such as durability and high strength with light weight which eases the application and does not add significant dead load to the cross section.

Many researchers have established the use of FRP materials to strengthen reinforced concrete columns by confining them externally, however, there is very little research work on quantifying the effect of FRP confinement on the axial-flexural behaviour of reinforced masonry columns to satisfy the additional loading demand or improve the seismic performance by increasing the ductility.

1.2 Research significance

A large portion of the structures inventory worldwide is constructed by masonry. Unreinforced masonry buildings represent the majority of these structures. Thousands of unreinforced masonry buildings in the United States, Canada and New Zealand are structurally deficient and need retrofit (Hatzinikolas and Korany, 2005). According to Reitherman and Perry (2009), brick and hollow concrete block are the most common unreinforced masonry materials used in unreinforced masonry buildings in the United States. Considering the vulnerability of unreinforced masonry to tensile forces, the modern masonry design codes and guidelines (NZS 4230:2004, 2004; BS 5628, 2005; EN 1996-1-1, 2005; CSA S304-14, 2014; TMS 402/602-16, 2016) promote using reinforced masonry.

With more demand for strengthening reinforced and unreinforced masonry structures. The current challenge that faces structural engineers is to have a reliable estimation of the effectiveness of their strengthening system for concrete masonry columns. Quantifying the enhancement in the CFRP confined concrete masonry column performance under concentric and eccentric loading is essential for planning an effective retrofit design. This includes the increase in the confined compressive strength and ultimate strain. The latter is essential in enhancing the ductility of the strengthened structural elements, which is a highly desirable characteristic for better seismic performance.

The vast majority of the available studies that investigated the performance of FRP-confined masonry columns focused on the column's axial compression response rather than the axial-flexural interaction. This research experimentally investigates CFRP strengthened reinforced concrete blocks masonry columns that are loaded concentrically and eccentrically and develops a simplified analytical methodology to compute the axial force-moment interaction diagrams of such columns. The methodology focuses on short prismatic concrete masonry columns failing in the compression-controlled region of the axial force-moment interaction diagram.

1.3 Objectives

The objectives of this research are twofold:

- To experimentally evaluate the effect of CFRP confinement on the behaviour of reinforced concrete masonry under concentric and eccentric axial loads.
- To develop a simplified analytical methodology to compute the axial force-moment interaction diagram of prismatic fully grouted reinforced concrete masonry columns confined with FRP jacket and controlled by compression failure.

1.4 Scope of work

Predicting the behaviour of CFRP confined concrete masonry columns involves several challenges due to the nonlinear behaviour of its constituent materials (i.e. masonry blocks; mortar; grout and CFRP sheets) as well as the complex interaction between these components under axial-flexural loading. An experimental program was conducted to quantify the strength and strain capacity of CFRP confined concrete masonry columns under concentric and eccentric loading towards predicting the axial force and moment capacity of strengthened masonry columns. The tests provided necessary experimental measurements to determine the values of fundamental parameters that controls the section analysis which is essential for the theoretical prediction of axial force-moment interaction diagrams. Throughout this study, the effects of the following parameters on the axial flexural behaviour of fully grouted reinforced concrete masonry column confined with FRP jacket will be investigated;

- The thickness of CFRP jacket.
- The level of eccentricity applied on concrete masonry columns.
- The corner radius of the section.

To achieve the goals of this study, the research was divided into three phases:

Phase I focused on:

- Testing wrapped concrete block masonry prisms under concentric loading.
- The CFRP wrapping effects on the enhancement of the performance of concrete masonry columns by evaluating the complete stress-strain response.

- Investigating the effect of changing the thickness of CFRP jacket and the corner radius of cross section on the shape of stress-strain curve of masonry columns.

- Estimating the confinement pressure due to CFRP jacketing, by measuring the effective tensile strain in CFRP jackets.

- Examining analytical confinement model based on experimental results of CFRP strengthened concrete masonry columns.

- Refining the analytical confinement model based on the experimental results to give reliable correlation between experimental data and theoretical prediction.

Phase II focused on:

- Testing unwrapped reinforced concrete block masonry columns under concentric and eccentric loading to establish control data for comparison.

- Testing wrapped reinforced concrete block masonry columns under concentric and eccentric loading.

- The CFRP wrapping effects on the enhancement of the performance of eccentrically loaded concrete masonry columns.

- Investigating the effect of changing the thickness of CFRP jacket on the axial-flexural behaviour of reinforced concrete masonry columns.

- Comparison between wrapped and unwrapped masonry columns.

Phase III focused on:

- Proposing simplified analytical methodology that predicts the axial force-moment interaction diagram of short prismatic fully grouted reinforced concrete masonry column strengthened with FRP jackets.

- Determining the essential parameters to perform detailed section analysis.

- Suggesting expressions to obtain these parameters values.

- Proposing practical values for the equivalent rectangular stress block parameters.

- Comparing between experimental results and theoretical predictions obtained by proposed methodology.

- Conducting a parametric study on the effect of the design variables on the axial-flexural interaction of FRP-wrapped reinforced concrete masonry columns generated by the proposing methodology.

1.5 Organization of the Thesis

The thesis is comprised of six chapters (including this one), a list of figures, tables and equations, notations, appendix, and references. These chapters provide all the experimental and analytical details of this research project. These details were used to develop a simplified methodology to compute the axial force-moment interaction diagram for a short prismatic fully grouted FRP-wrapped reinforced concrete masonry columns falling in the compression-controlled region of the axial force-moment interaction diagram. The contents of the chapters are as follows:

- Chapter 1 consists of an introduction; general background; research significance; objectives and scope of work, and organization of the thesis.
- Chapter 2 discusses briefly relevant topics and previous research studies on confining masonry columns with Fibre Reinforced Polymers materials.
- Chapter 3 discusses the experimental compression behaviour of unreinforced half-scale concrete block masonry prisms confined with CFRP jackets.
- Chapter 4 discusses the behaviour of reinforced half scale concrete block masonry columns under concentric and eccentric loading to compare between experimental results of wrapped and unwrapped masonry columns.
- Chapter 5 proposes a simplified methodology to compute the axial force-moment interaction diagram of a short prismatic fully grouted reinforced concrete masonry column confined with FRP jacket falling in the compression-controlled region of the axial force-moment interaction diagram. Also, a parametric study was conducted to study design variables effects.
- Chapter 5 states the main conclusions of this study and the recommendations for future work.

Chapter 2
Literature Review

2.1 Introduction

This chapter covers literature related to the main research topic carried out in this thesis. Brief information about column behaviour under concentric and eccentric loads is given in first part. In the second part, traditional techniques for strengthening of masonry columns are introduced, and a brief literature review is presented. Information about FRP composite materials and their application in structural engineering is presented in the third part. The fourth part focuses on experimental works conducted on strengthening of masonry columns by FRP materials, whereas the last part reviews the models reported in the literature related to strength gain and stress-strain curve of masonry confined by FRP materials.

2.2 Column behaviour under concentric and eccentric loads

This part covers the general behaviour of masonry column under concentric and eccentric loads before applying any type of strengthening. According to Taly (2010), the column is vertical member designed to carry axial compression loads with or without flexure loads. The column could be isolated or wall column where parts of the wall acting as columns. Wall column can be called pilaster when it projects from one or two sides of the wall, as shown in Figure 2.1. If it is flushed in the wall, it can be called in-wall column. Pilasters are designed to help the walls to resistance the lateral forces. Masonry columns can be reinforced with vertical steel reinforcements to resist tensile stress and they can be without steel reinforcements to carry axial compression loads only. Masonry columns usually are constructed from concrete masonry units, clay masonry bricks, or chimney units in running bond.
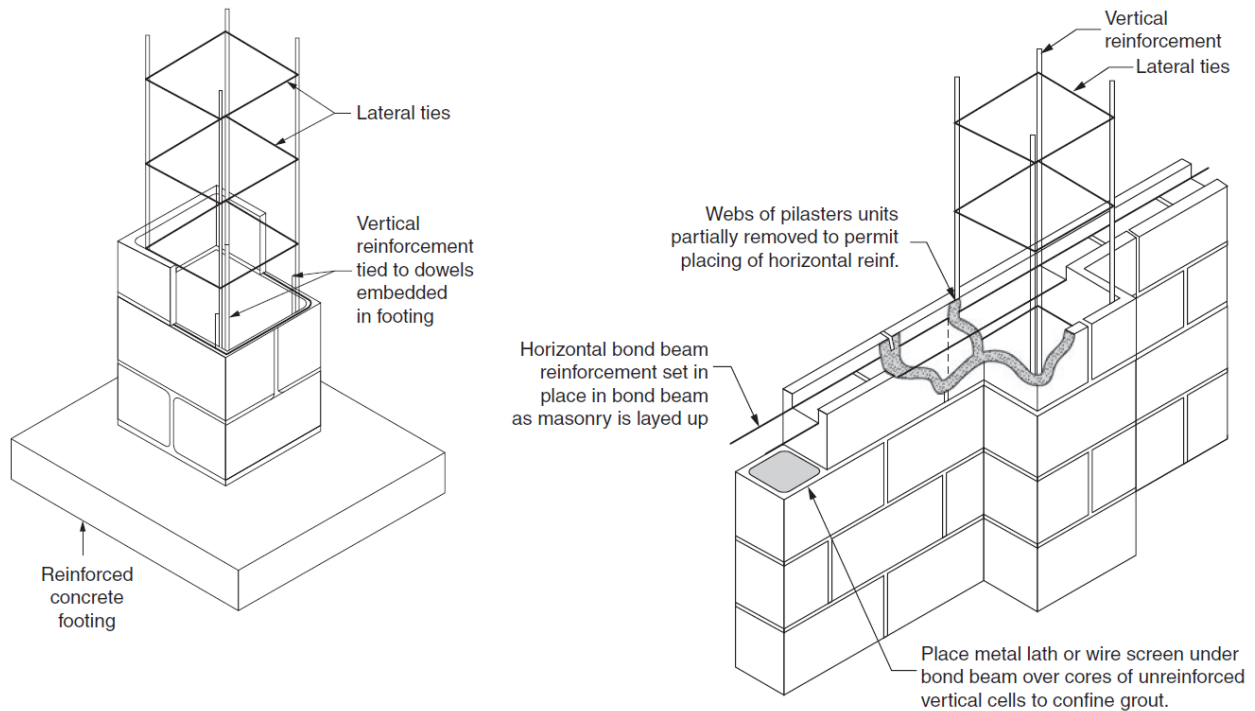
Figure 2.1 Reinforced isolated and wall columns (Taly, 2010).

Most of the columns in the site are subjected to axial compression loads and flexural bending. Where axial compression loads come from gravity loads and flexural bending is result of imperfections in the construction process, unintentional eccentricity, lateral loads transferred to the column, intentional eccentricity by beams away from the centre of column.

Interaction diagrams are helpful for designing column subjected to axial load and bending moment simultaneously. Since each point on the curve indicates the axial and flexure capacities of the column. A column can carry pure axial load without any moment applied on the column. Similarly, it can stand pure flexural load with zero axial force. Between these two cases, the column can carry combinations of axial loads and bending moments simultaneously when the magnitude of load and moment are less than the ultimate load and moment of the column. Obviously, there is ultimate number of combinations of axial load, and bending moment the column can be resisted. The interaction diagram is a plot of theses many combinations as points where each point has a unique axial load capacity on the y-axis and bending moment capacity on the x-axis, as Figure 2.2.
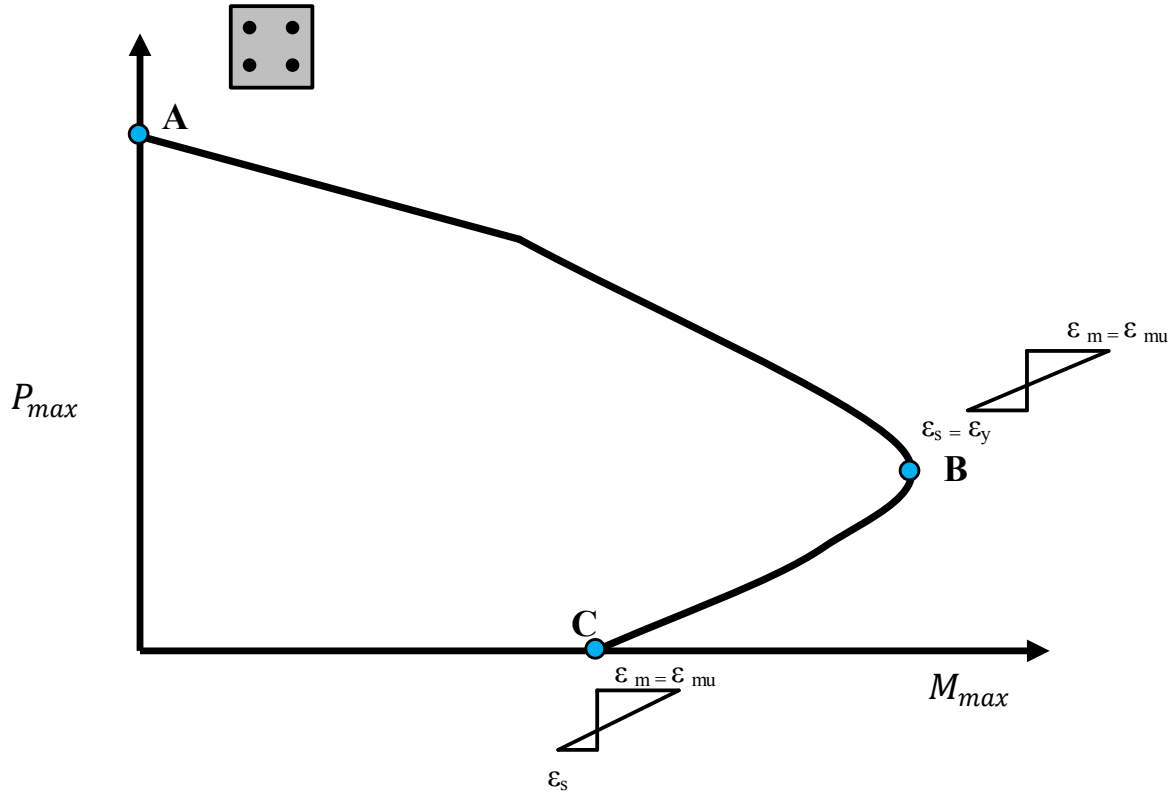
Figure 2.2 Typical interaction diagrams for masonry column.

Each column has a unique interaction diagram based on some factors that affect the axial and flexural capacities of the column. Cross section dimensions, strength of masonry and longitudinal reinforcement are the main factors affect the axial capacity of the column. Therefore, flexural capacity depends also on the same parameters beside the positions of longitudinal reinforcements in the cross section. A simplified form of the interaction diagram can be constructed from three main points, as shown in Figure 2.2: nominal axial strength (Point A), nominal moment strength (Point C) and the balanced condition (Point B). A short reinforced masonry column has nominal axial strength equals to the contribution of the axial compressive strengths of masonry and longitudinal reinforcement. The nominal moment strength of masonry column can be found by treating the column as a doubly reinforced beam and perform the well-known procedure of section analysis. The balanced condition is the load condition when masonry reaches the ultimate strain and the yield strain in tension steel simultaneously. The location of neutral axis, in this case, can be found from a linear strain distribution along the cross-section. Columns subjected to eccentric loads less than that of the balanced point will experience compression failure, whereas columns subjected to eccentric loads higher than that of the balanced point will experience tension failure.

2.3 Traditional techniques for strengthening of masonry columns

Various traditional strengthening and retrofitting techniques were reported in Witzany and Zigler (2015). The structural performance of deteriorated masonry columns can be improved by applying one of these retrofitting methods: steel plate bonding; external post tensioning; steel bracing; steel strips and cords jacketing; and inserting stirrups into bed joints. Furthermore, the masonry columns can be strengthened by casting reinforced jacketing around the columns using plaster or concrete.

The techniques mentioned above have been developed mainly to delay or prevent the failure of masonry columns under compressive loads by providing action of confinement to the cross section. The response of confined element varies depending on the retrofitting techniques utilized and the material of cross section and its shape. These effects must be considered during retrofitting design stage. Several studies have conducted to measure these effects.

Jacketing masonry columns by steel strips have proven to be viable strengthening method to increase strength and ductility of masonry columns. Ilyas et al. (2009) tested nine clay bricks columns divided into three groups. The test matrix was designed to study the amount of reinforcement and cross section aspect ratio variables. The cross section aspect ratios of 1, 2, and 3 were tested. The masonry columns were divided into unconfined, moderately reinforced and heavily reinforced columns. It is concluded from the results that confinement by steel strips enhances the strength and ultimate strain where the increase in strength is related the cross section aspect ratio.

Figure 2.3 Heavily and moderately reinforced column (Ilyas et al., 2009).

Borri et al. (2013) investigated using steel cords for strengthening solid clay bricks masonry columns. 48 masonry columns were tested under axial compression load. Octagonal, square, and rectangular cross sections were confined with different schemes of confining reinforcement. The results of experimental tests showed that masonry columns with steel cords gained a significant increase in term of strength and strain.

Figure 2.4 Hooping solid clay bricks masonry with pre-tensioned steel cords (Borri et al., 2013).

The disadvantage of using external steel strips or cords in strengthening masonry columns is the susceptibility of steel to corrosion.

Kog et al. (2001) tested brick masonry columns retrofitted by concrete jackets reinforced with longitudinal steel and stirrups. Strengthened columns exhibited a tremendous increase in axial capacity. The amount of stirrups in concrete jackets affected the bearing capacity. However, the parameters of the thickness of concrete, concrete grade, the amount of longitudinal did not affect the peak load. An analytical model and design charts for masonry columns strengthened with reinforced concrete jackets were proposed. This retrofit method has the disadvantage that the concrete jacket adds to the self-weight of the structure, which consumes portion of the increase in the compression capacity of the column. Also, the higher self-weight increases the loads transferred to the foundation system.

a	Plaster of Paris Capping
b	Masonry Core
c	Transducer Studs
d	Longitudinal Reinforcement
e	Lateral Reinforcement
f	Concrete Jacket
g	Steel Ring
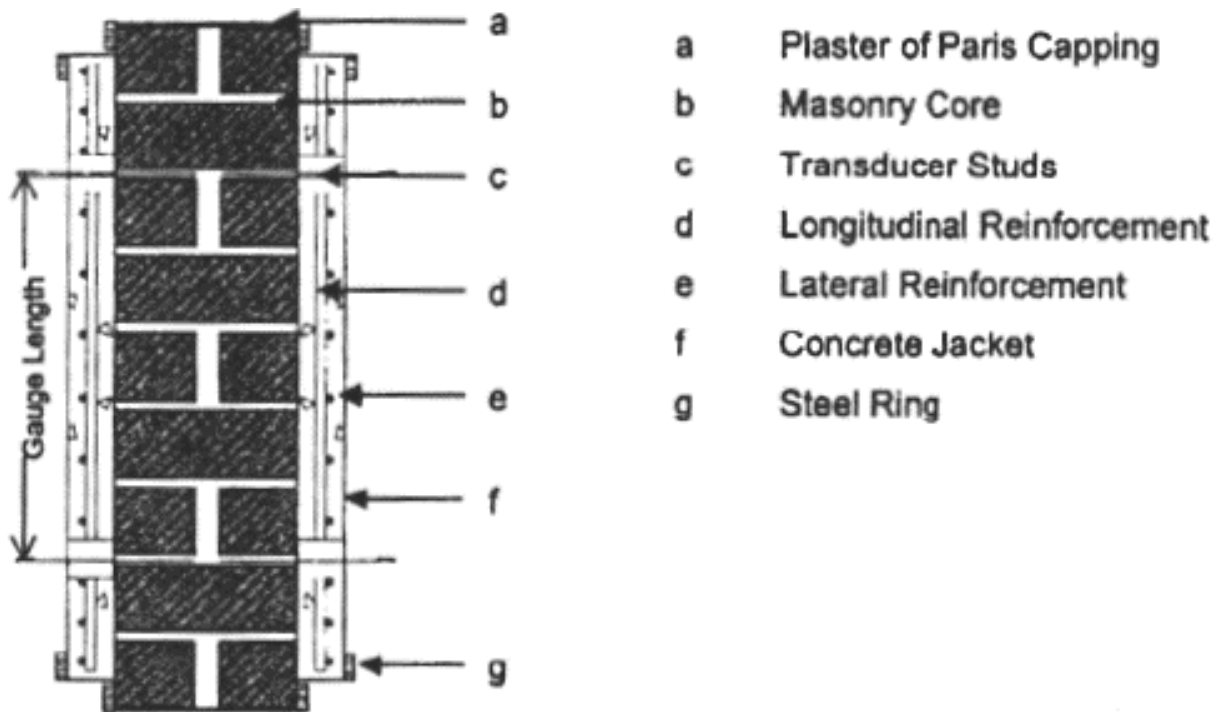
Figure 2.5 Typical concrete jacketed for brick masonry columns (Kog et al., 2001).

Priestley and Bridgeman (1974) introduced using 3.1 mm stainless steel plates in mortar beds to confine the end zone of brick masonry shear wall. These plates have been known as Priestley's plates later. In Priestley and Elder (1983), Priestley's plates were used to confine fully grouted reinforced concrete masonry prism tested under compression loads. The test results showed that Priestley's plate affected stress-strain curve of concrete masonry prisms by producing less a steeper descending curve. Also, the plates changed failure mode of masonry columns from vertical splitting at the peak load to crushing failure. Priestley and Elder (1983) proposed modified Kent-Park curve to predict stress-strain curve of unconfined and confined concrete masonry.

$1.25Kf'_c$

Kf'_c

f'_c

Confined
$\dot{\varepsilon} = 1.7\%$ /sec

Confined
$\dot{\varepsilon} = 0.00033\%$ /sec

θ_m $1.25\theta_m$

Unconfined
$\dot{\varepsilon} = 0.00033\%$ /sec

$1.25(0.2Kf'_c)$

$0.2Kf'_c$

$0.2f'_c$

COMPRESSION STRESS

0

0.002 1.25(0.002K)

0.002K

STRAIN

$$K = (1 + \rho_s \frac{f_{yh}}{f'_c})$$
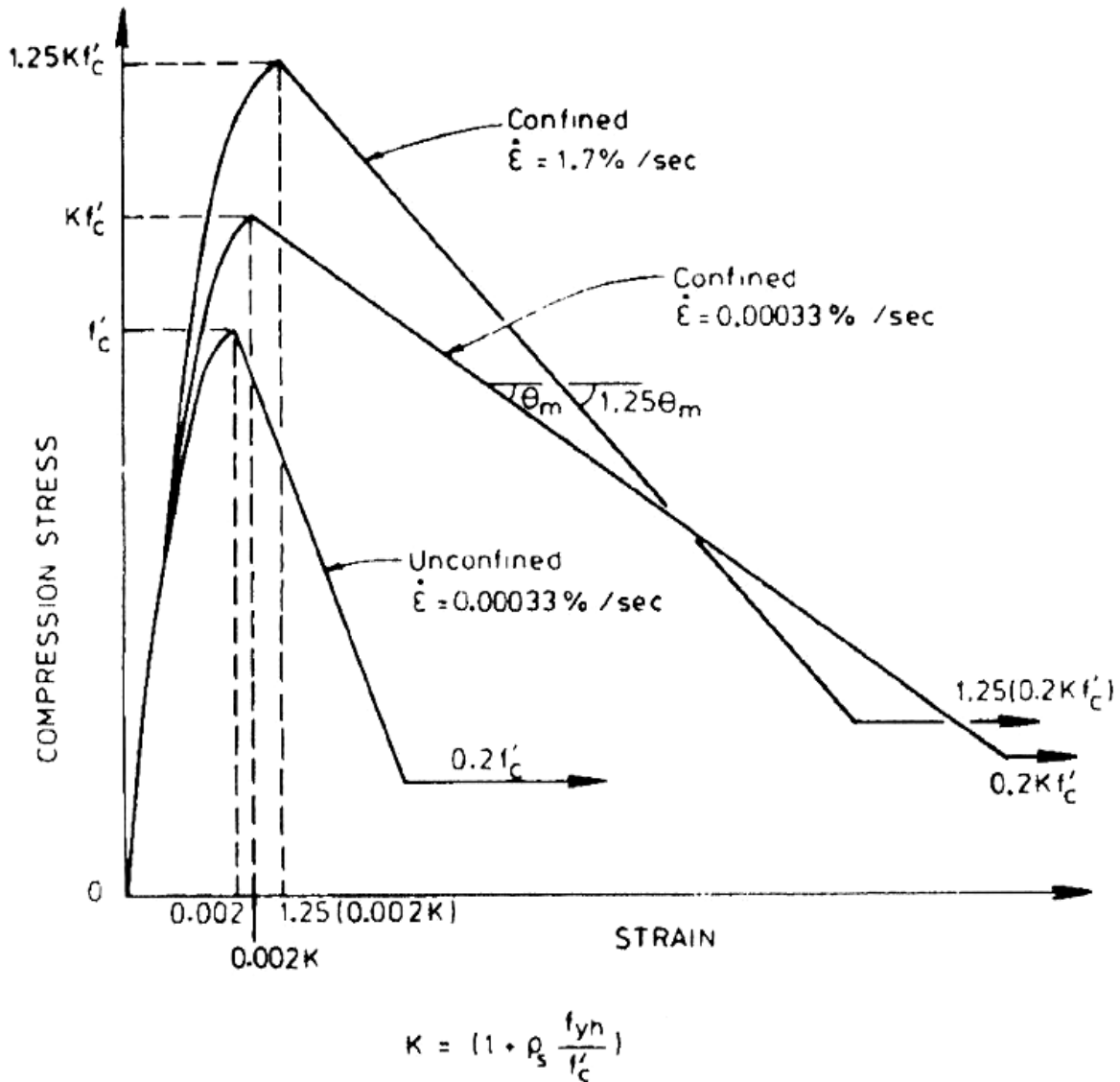
Figure 2.6 Modified Kent-Park curves for confined and unconfined concrete
(Priestley and Elder, 1983).

In the first Phase, Hart et al. (1988) studied different methods to confine fully grouted reinforced concrete masonry prims with four courses height. Seventy one prisms were confined with open or closed wire meshes, modified Priestley's plates, cages, hoops and spiral reinforcement and tested under compression. The result showed that all type of confinement has a similar ascending branch of the stress-strain curve. However, the ascending branches were controlled by confinement method. Priestley's plates gave the best behaviour in term of peak stresses, ultimate strains and the areas under the stress-strain curve. The open wire mesh was the closet to the performance of Priestley's plates.

In the second Phase Hart et al. (1989), one hundred and six concrete masonry prisms were tested including confined reinforced prisms with different methods of confinement. Two analytical models were proposed for compression stress-strain curve of concrete masonry. The first model was simple and the second model was complex and based on best fit of experimental data.

Ewing and Kowalsky (2004) tested solid and regular Priestley's plates to confine clay brick masonry. The results of fifteen prisms tested under compression showed that there was an increase in strength and ultimate strain. Also, the results of solid plates without holes in flange are close to regular Priestley's plates where the plates have holes in the flange to improve the bond to the mortar.
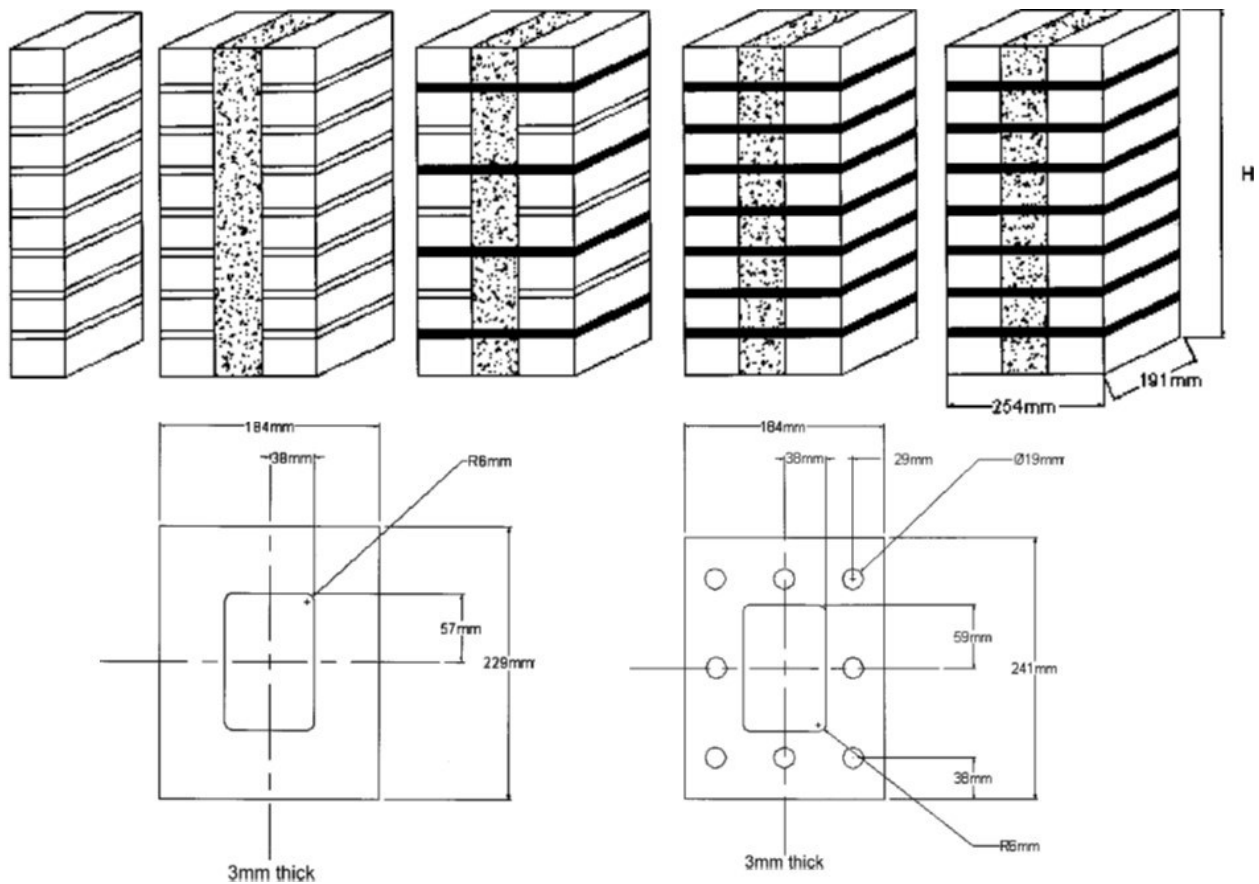
Figure 2.7 Prism configurations with solid and standard plates (Ewing and Kowalsky, 2004).

Malmquist (2004) tested forty five prisms included prims constructed with concrete blocks or clay bricks. Priestley's plates were one of the methods used to confine the prims. Test results showed that Priestley's plates increased the ultimate strain for both concrete blocks and clay bricks. Also, the confinement flattened the descending branch of the stress-strain curve.

Concrete Block Masonry - Average Stress Strain Curves
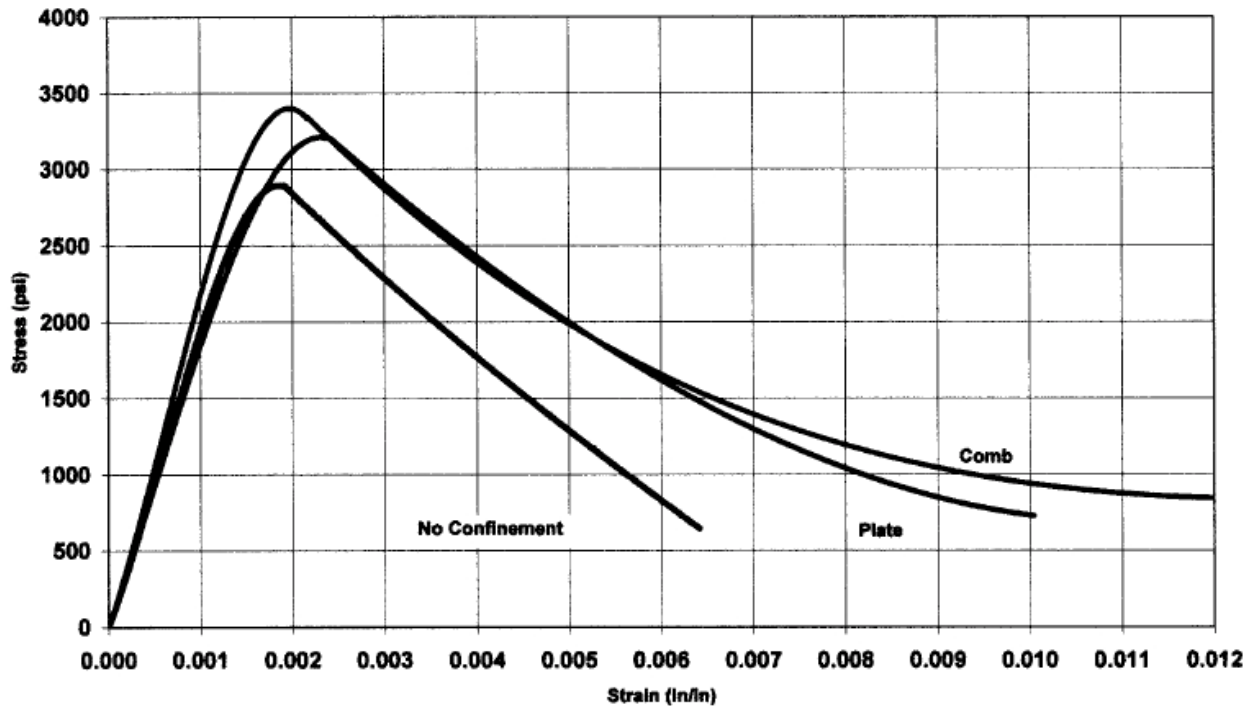
Figure 2.8 Stress-strain curves for concrete block masonry (Malmquist, 2004)
(1 MPa = 145 psi).

One of the basic approaches to improve axial carrying capacity and mainly seismic resistance of masonry is to provide sufficient transverse confinement. Confining masonry by conventional steel ties can increase the ductility of masonry beyond elastic limits without excessive strength degradation. Even though using conventional steel ties to strengthen existing masonry column is an unpractical approach, reviewing the experimental works carried out in this filed is necessary to understand the effect of confinement on the behaviour of masonry. Considering that the action of confinement produced by FRP materials is similar to steel ties confinement with some differences.

In the late seventies, Feeg et al. (1979) tested concrete masonry columns with different reinforcement detailing under compression to establish the strength behaviour. Different sizes and locations of vertical and lateral reinforcement were investigated. Sturgeon et al. (1980) proposed empirical equations to predict the capacity of concrete masonry column based on experimental tests included the variables of the amount and the grade of longitudinal reinforcement, grout strength and slump, lateral tie details, and the magnitude of eccentricity. Khalaf et al. (1993) and Singh and Cooke (1994) conducted experimental tests to study the effect of the amount of

14

longitudinal reinforcement and the lateral ties details on the compressive behaviour of concrete masonry columns.

Late studies, (Obaidat et al.; Shedid et al., 2010; Abo El Ezz et al., 2015; Obaidat et al., 2017) focused on the ductile behaviour of the confined concrete masonry under compression load to established stress-strain relationship considering different level of confinement by changing the size and the spacing of transverse tie reinforcement. It concluded that increasing the confinement improved the axial strength and the ultimate strain. Moreover, the confined concrete masonry showed a more ductile post-peak behaviour.
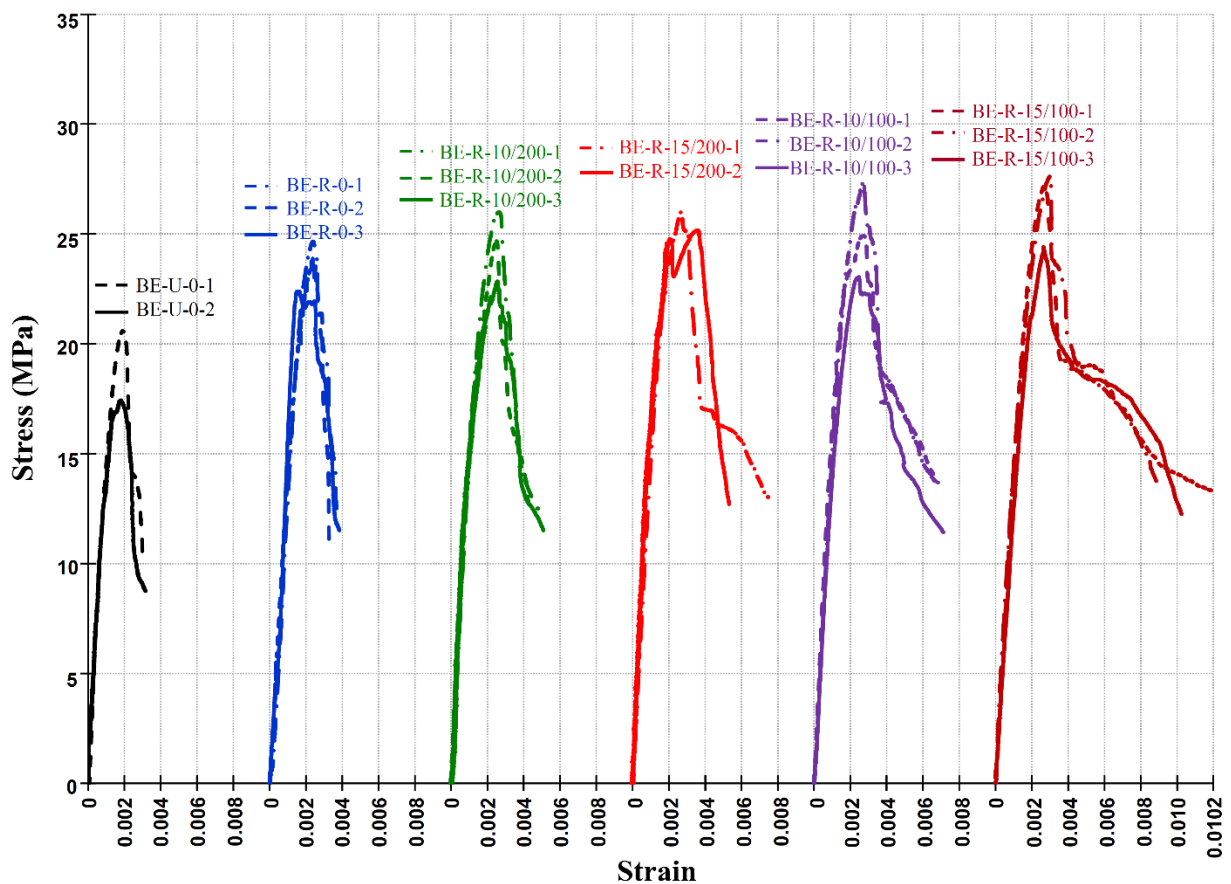
Figure 2.9 Stress-strain curves for unreinforced, reinforced concrete masonry columns (Obaidat et al., 2017).

2.4 FRP composite materials

Applications of fibre-reinforced polymer (FRP) composites in the construction industry are presented in this section. Besides using FRP composite materials as internal reinforcements, the FRP materials got considerable attention over the past two decades as externally bonded reinforcements for retrofitting and strengthening of ageing structures throughout the world. The increase of using FRP composite materials in rehabilitation could be attributed to several advantages:

- High strength and lightweight characteristics which lead to higher performance and sustainable structure with minimal resources

- Light weight which leads to reducing the additional dead load to the structure resulting from traditional retrofit technique. Also, light weight eases the handling and application in areas with limited access and increases construction speed.

- Durability in harsh and severe environments. Since, The FRP composites are resistant to corrosion, freeze-thaw cycles, and de-icing salts.

- Low thermal expansion coefficient

- High energy absorption

- Ease of fabrication where the FRP composites are typically manufactured from polymer matrix reinforced with various grades of carbon, glass, basalt, and/or aramid fibres.

- Wide selection of shapes included sheets, strips, bars, and plates.

2.5 Strengthening of masonry columns by FRP materials

Using FRP materials in strengthening masonry columns gives more advantages more than traditional strengthening methods. FRP materials are lighter and have higher strength. Considering the ease of application in limited spaces, applying FRP materials to strength existing masonry columns does not add critical dead loads to the structure.

Masonry columns are constructed with diverse materials such as clay, tuff, limestone, and concrete and can be retrofitted with different FRP techniques. Since the 2000s, few researchers conducted experimental tests to quantify the improvement in performance when applying carbon, aramid, glass and basalt FRP to confine masonry columns constructed with diverse materials.

Masia and Shrive (2003) tested damaged clay masonry columns with different masonry units and different square cross section sizes to measure the gained strength of the CFRP wrapped masonry columns. Eighteen columns were tested under axial compression. Two methods of strengthening were investigated by wrapping the clay columns with one layer of CFRP or casting a circular concrete jacket then wrapping the circular columns. Bearing capacities of clay columns treated with circular concrete jackets were significantly increased. The effect of cross section area on bearing capacity increase could not be drawn.
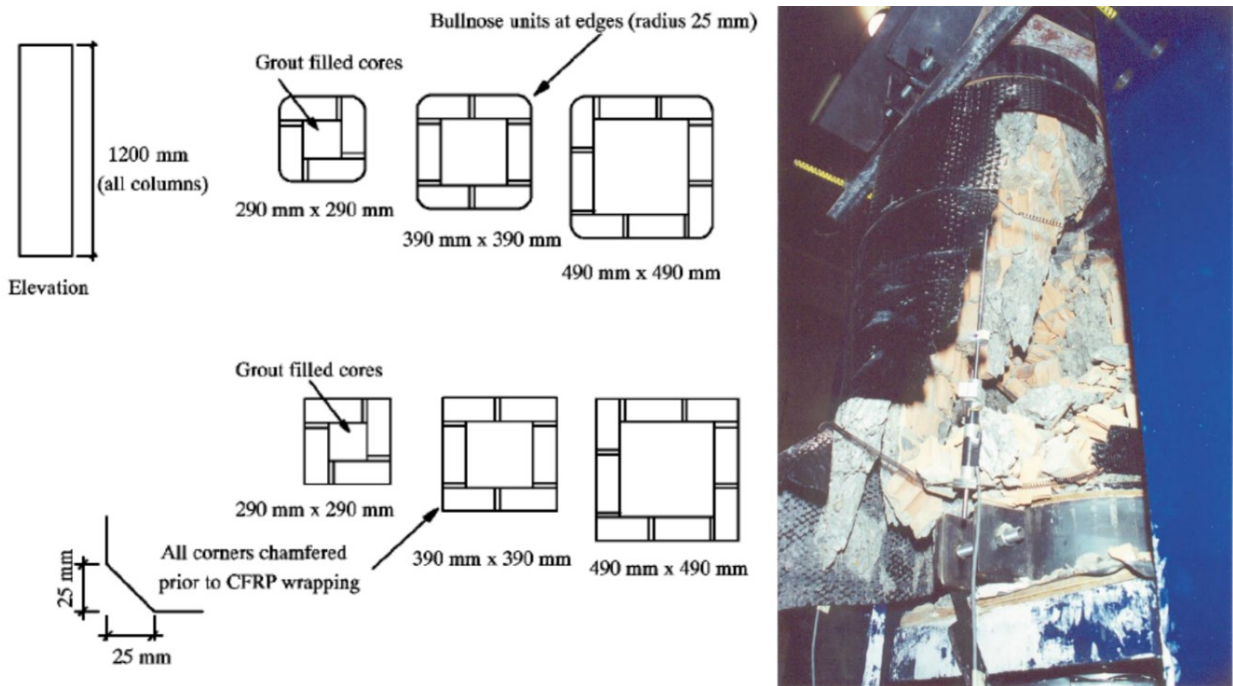
Figure 2.10 Masonry columns details and circular section column failure
(Masia and Shrive, 2003).

Krevaikas and Triantafillou (2005) proposed a confinement model for FRP wrapped clay brick columns calibrated by their experimental results of 42 specimens with different variables include number of layers, radius of the corners, cross section aspect ratio, and type of fibres. It is concluded from tests results that strengthened masonry columns with FRP behave similarly like strengthened concrete columns with FRP. The FRP confined masonry columns showed linear increases in strength and ductility with confining pressure. More details about the proposed model are given in section 2.6.1 of this chapter.
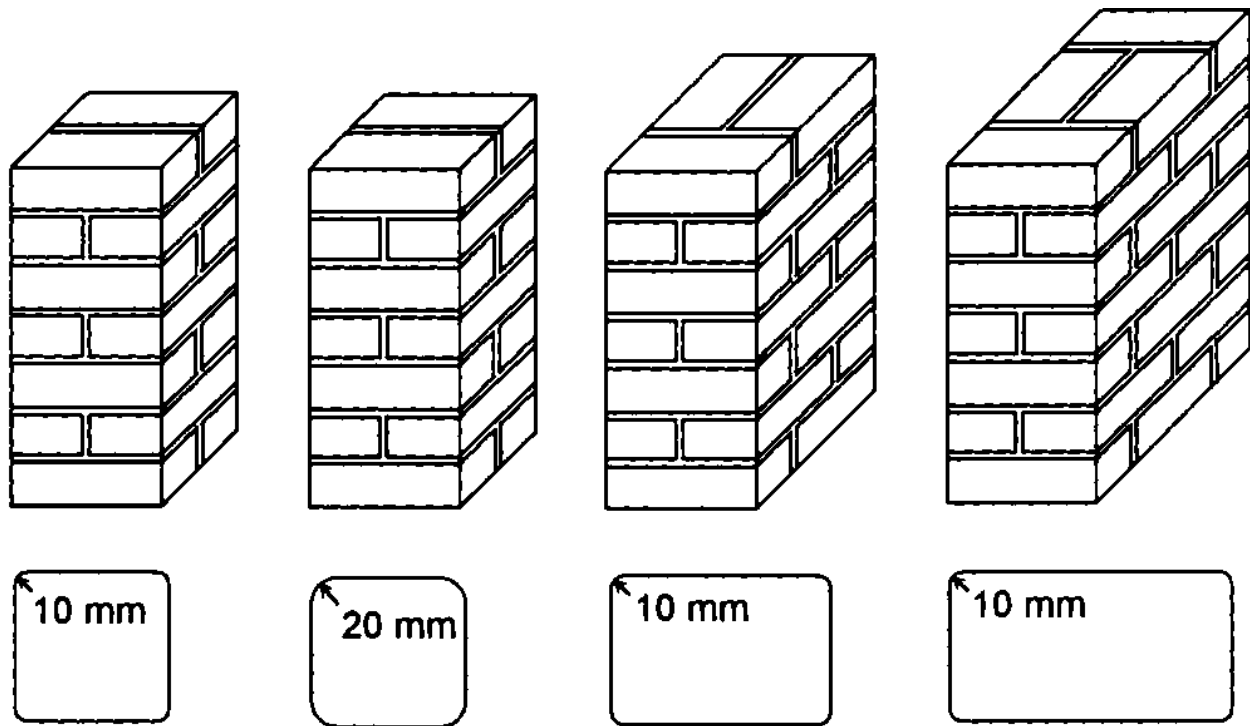
Figure 2.11 Configuration of clay brick masonry columns (Krevaikas and Triantafillou, 2005).

Corradi et al. (2007) proposed a model and tested 24 clay solid brick masonry columns with square and octagonal cross sections confined by CFRP. The results demonstrated increases in strength, ductility, and stiffness if compared to non-strengthened columns. The columns with octagonal cross sections and one or two layers of CFRP indicate very high increases in ultimate load and deformation capacity. The higher efficiency of CFRP wrap in octagonal columns is caused by the rounding the edges where that eliminates the sharp edge cutting failure. More details about the proposed model are given in section 2.6.3 of this chapter.

18

Figure 2.12 Failure of Square and octagonal cross section column (Corradi et al., 2007).

Shaheen and Shrive (2007) explored a different technique for strengthening clay masonry columns by spraying the columns with glass FRP in two thicknesses. Twenty four specimens were tested under both concentric and eccentric loading. Plain and reinforced two sizes of cross sections were tested to evaluate load and displacement increases. The result indicated that large increases in strain under concentric loading compared to small increases in strength for both plain and reinforced specimens. It is noticed the eccentric loads reduced the efficacy of strengthening method.

Figure 2.13 GFRP spray process and GFRP failure laminates (Shaheen and Shrive, 2007).

Alternate technique was investigated by some researchers, where FRP bars inserted thorough drilled holes to internally confine masonry. This can be with or without applying FRP wraps. Micelli et al. (2004) experimentally tested limestone masonry columns using injected FRP bars technique alone or in combination with FRP wraps. In all cases of confinement, a significant increase in strength capacity and ultimate displacement was noticed.

Recently, Micelli et al. (2014b) conducted the same kind of study on full-scale limestone masonry columns strengthened with similar composite systems studied in previous work. The result showed that the confinement was able to significantly increase the strength capacity and ultimate displacement in full-scale limestone masonry columns. Using FRP internal bars with FRP wraps is very effective in increasing the axial strength of masonry column. Since FRP internal bars can confine the masonry column in pre-peak phase and the confinement of FRP wraps affect more the post-peak phase. In comparison between the experimental tests on full-scale and scaled specimens, the authors concluded that the efficiency of confinement is not significantly affected by the scaling factor.
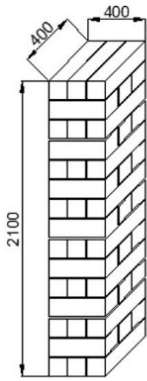
(a) S_R1 and S_R2
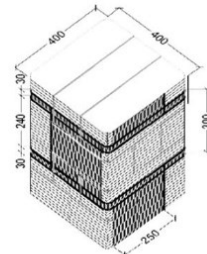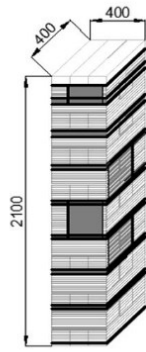
(b) S_GE_T

Horizontal overlap length = 250 mm

Vertical overlap length = 30 mm
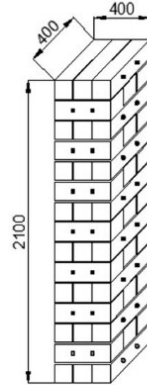
14+14 CFRP bars (Diameter 8mm)
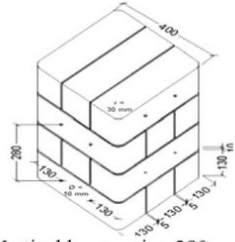
Vertical bar spacing 280mm; Horizontal bar spacing 140mm

(c) S_GRE_T
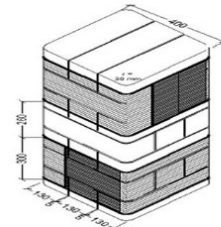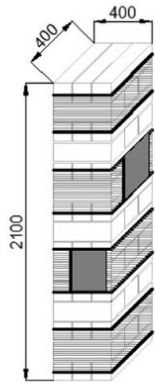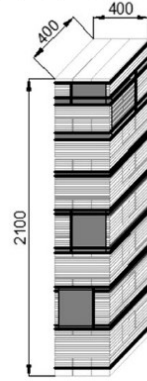
(d) S_GE_D

Horizontal overlap length = 250 mm

Strips spacing= 260 mm
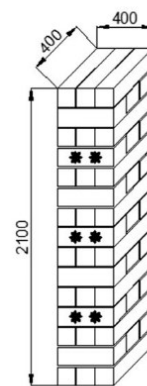
6 steel spikes
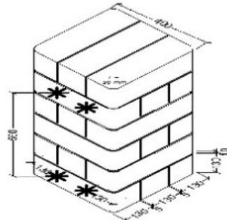
Vertical spikes spacing 560mm; Horizontal spikes spacing 140mm
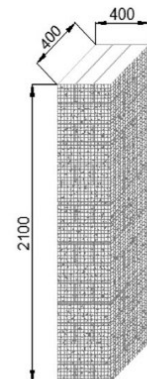
(e) S_GgridC_T

Figure 2.14 Full-scale limestone masonry columns details (Micelli et al., 2014b).

In addition, Aiello et al. (2007) studied confined circular stone columns by injected FRP bars through the columns cross section or applied carbon FRP sheets in the form of continuous jacket or discontinuous strips. Some of stone columns were loaded with 60 or 80% of the ultimate load before strengthening them. Experimental results showed that FRP strengthening was effective in increasing ultimate strength and strain in both pre-damaged and non-damaged masonry columns.
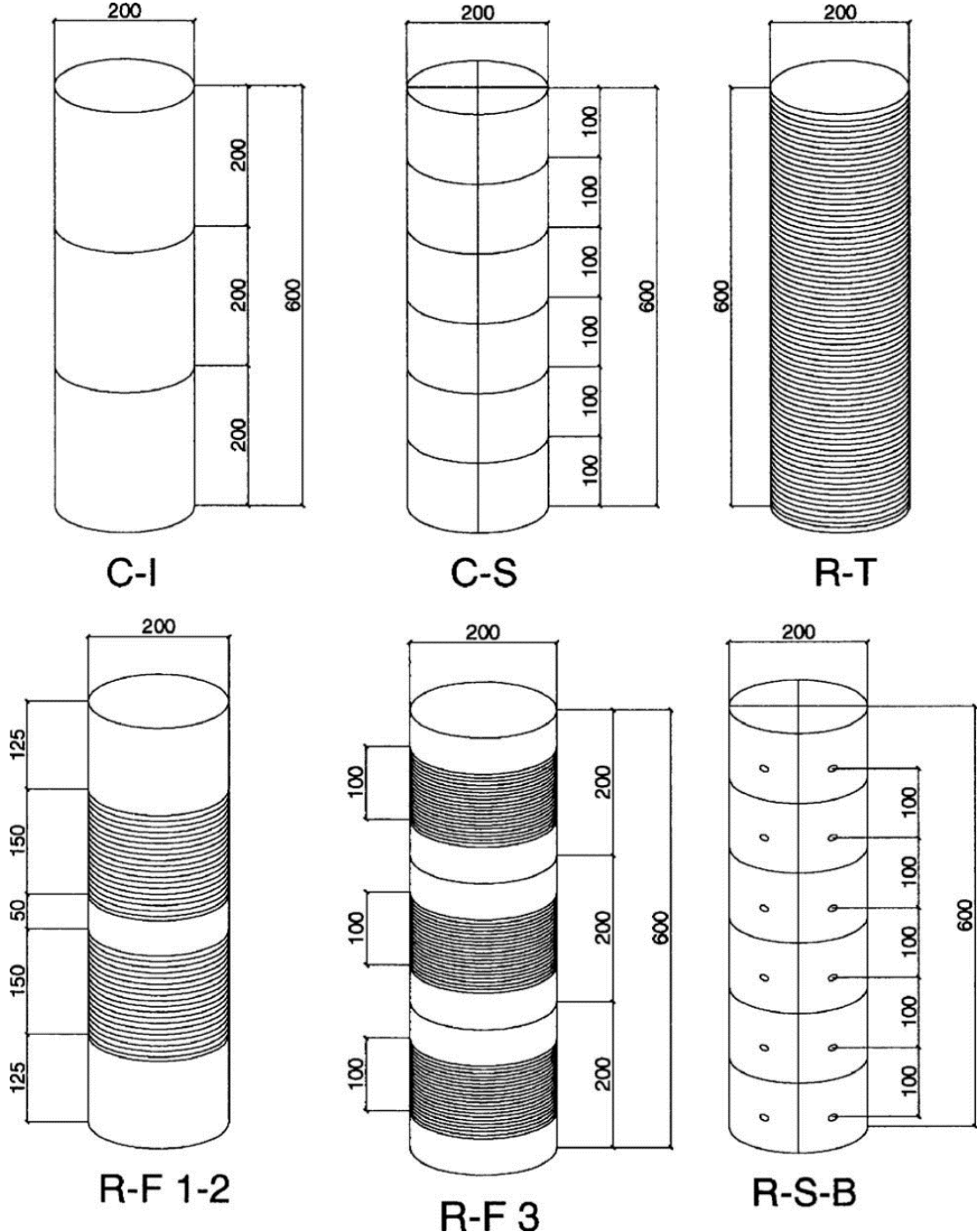
Figure 2.15 Dimensions of circular stone columns in millimetres (Aiello et al., 2007).

In another study Aiello et al. (2009) examined the injected FRP bars and glass FRP sheets strengthening techniques on limestone and clay columns. Thirty three rectangular masonry columns were tested under axial compression force. The parameters of corners radius and cross section aspect ratio were included in the experimental study. It has been concluded that all strengthening methods gave a significant increase in strength and ductility. Aiello et al. (2009) calibrated the analytical model proposed originally by Krevaikas and Triantafillou (2005) (see section 2.6.4 for more details). The calibrated model can be used to predict the capacity of limestone masonry columns with FRP wraps or injected FRP bars.
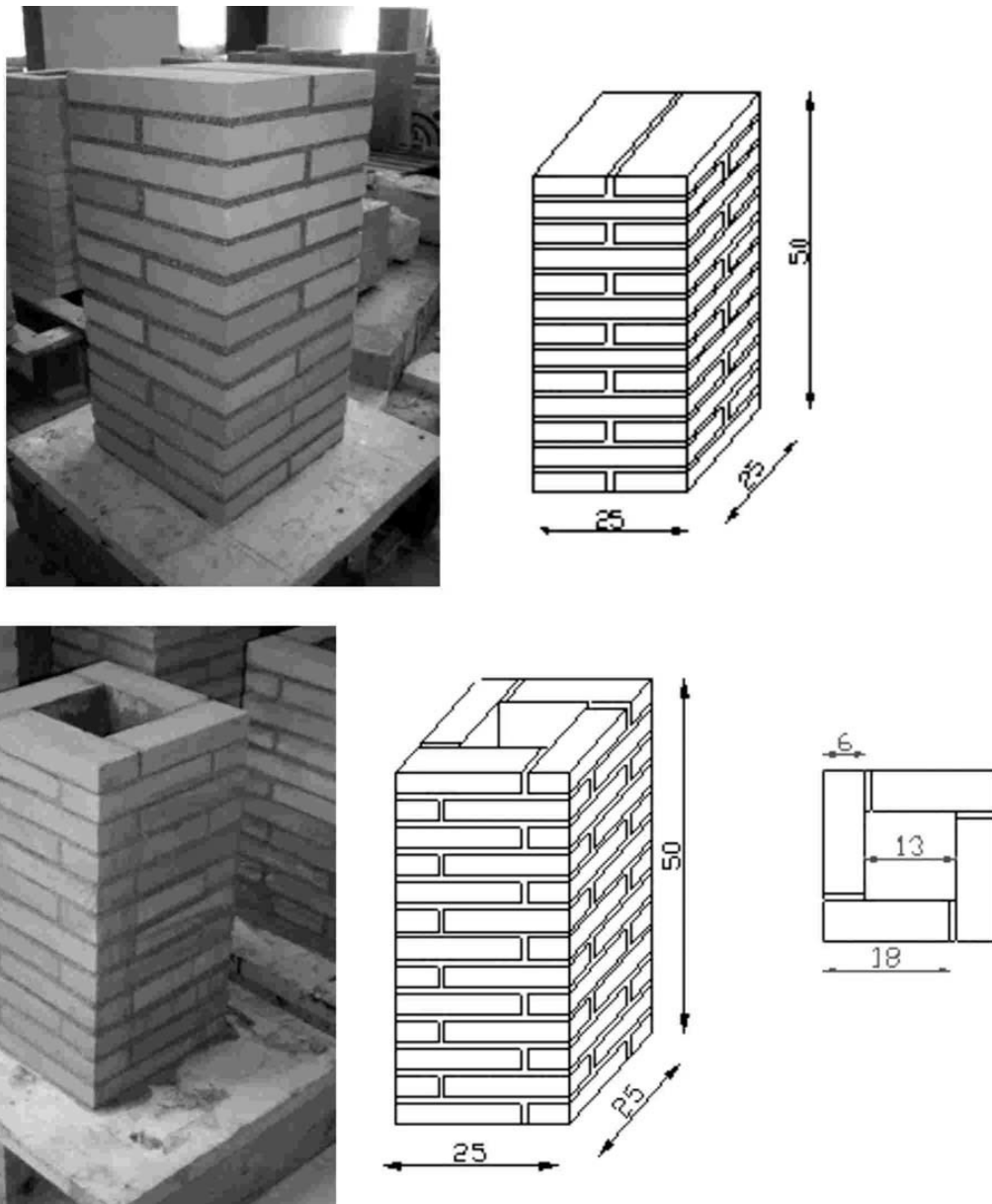
Figure 2.16 Dimensions of masonry columns in centimetres (Aiello et al., 2009).

Alecci et al. (2009) tested nineteen brick masonry specimens under uniaxial and triaxial compression. Ten of specimens were tested with a Hoek cell to produce triaxial compression. The authors compared the result with the proposed formulas from the literature and found that the results did not match.
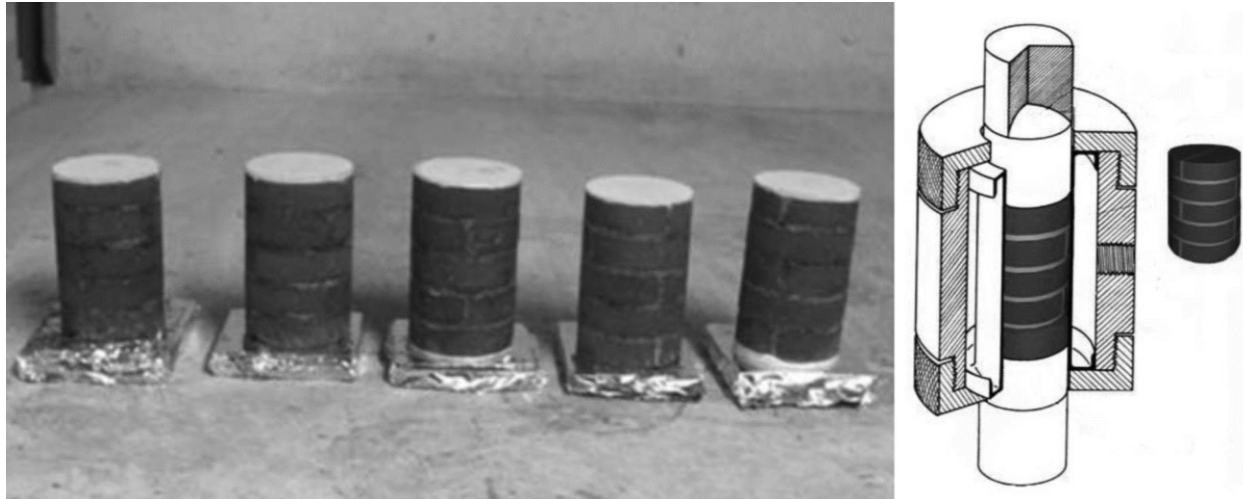
Figure 2.17 Cylindrical specimens and Hoek cell (Alecci et al., 2009).

Di Ludovico et al. (2010) tested eighteen square tuff and clay masonry columns confined with glass FRP, carbon FRP, and basalt FRP wraps under compression loads. Experimental results approved FRP wrapping effectiveness in providing significant increases in strength and ductility of masonry columns. Test results and data collected from the literature were used to evaluate the available analytical models. Refined equations were calibrated with experimental data to reduce the scattering between strength predictions and tests results (see section 2.6.5 for more details).
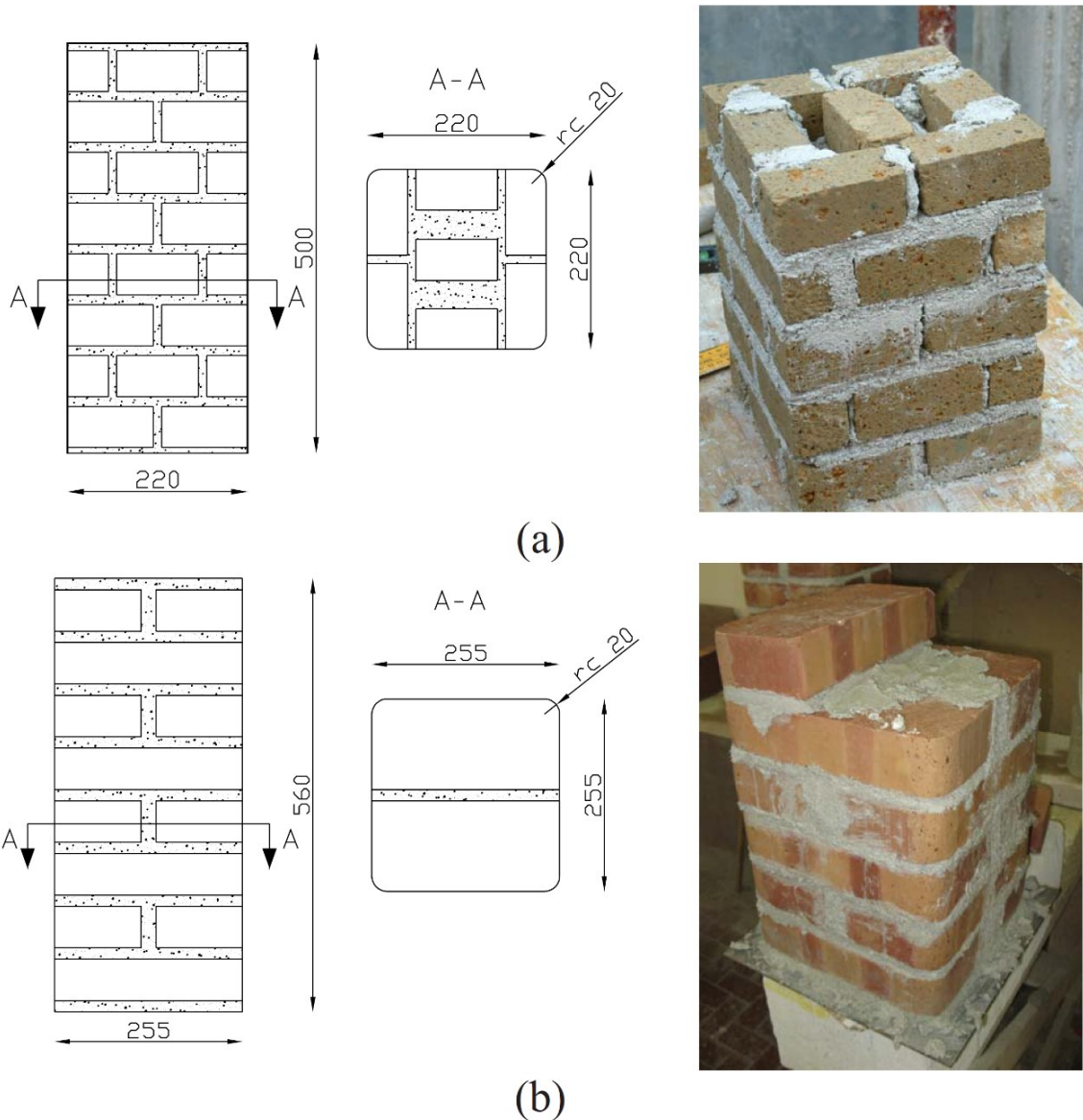
Figure 2.18 Details of tuff and clay masonry columns in millimetres (Di Ludovico et al., 2010).

Faella et al. (2011b) tested different types of masonry columns built out of natural or artificial bricks confined by carbon and glass FRP composite. Fifty-four memory column were tested under axial compression. The researchers found that the range of confined-to-unconfined strength ratio is between 1.22 and 3.94. As a general observation, the strength gain is higher when the confined material is weak, and the FRP jacket is stiffer. In a companion paper, (Faella et al., 2011a) assessed analytical formulations in the literature and calibrated a design formula for predicting the strength of FRP wrapped masonry columns using their experimental tests along with collected database from the literature.

Figure 2.19 Failure of masonry columns with FRP composite (Faella et al., 2011b).

Nanjunda Rao and Pavan (2015) investigated compression behaviour of FRP confined masonry columns constructed from burnt clay bricks. The experimental parameters included masonry bonding pattern, inclination of loading axis to the bed joint, and the type and grade of FRP. The results showed an improvement in strength, stiffness, and ductility. The FRP confinement reduced the effect of the inclination of the loading axis to the bed joint on the compressive strength and failure pattern.

<div align="center">(a)   (b)   (c)   (d)</div>
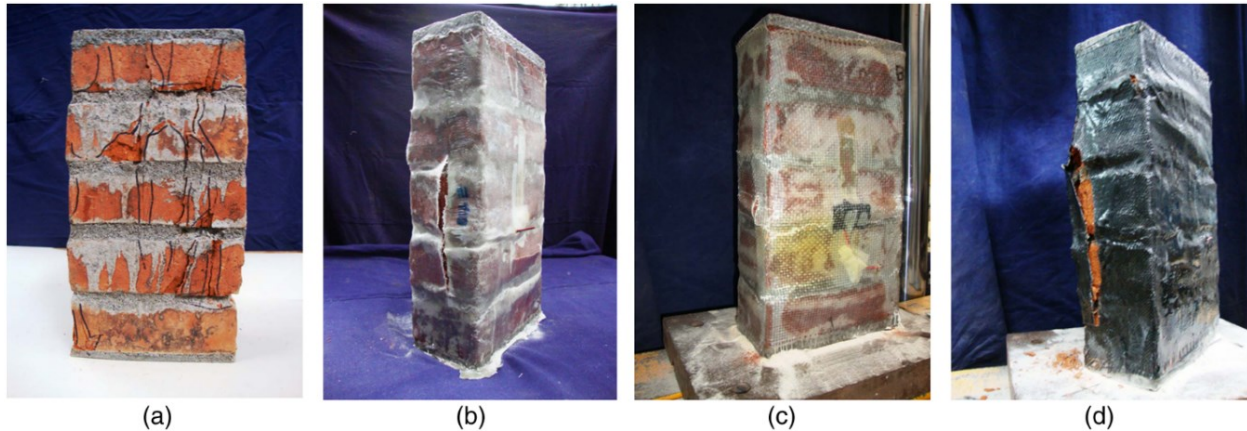
Figure 2.20 Failure pattern of 90° inclination to bed joint (Nanjunda Rao and Pavan, 2015).

Recent studies focused on discontinuous confinement by FRP strips. Witzany et al. (2014) conducted experimental research on strengthening burnt brick masonry columns by carbon and glass FRP strips. It concluded from testing thirteen columns under compression loads that the confinement with FRP strips increases the ultimate deformation and the ultimate load. They pointed out the necessity of adopting a different approach to assessing the load-bearing capacity or residual load-bearing capacity, which takes into account the different failure modes of reinforced and unreinforced brick masonry.

Non-reinforced column   CFRP reinforced column   GFRP reinforced column   GFRP reinforced column
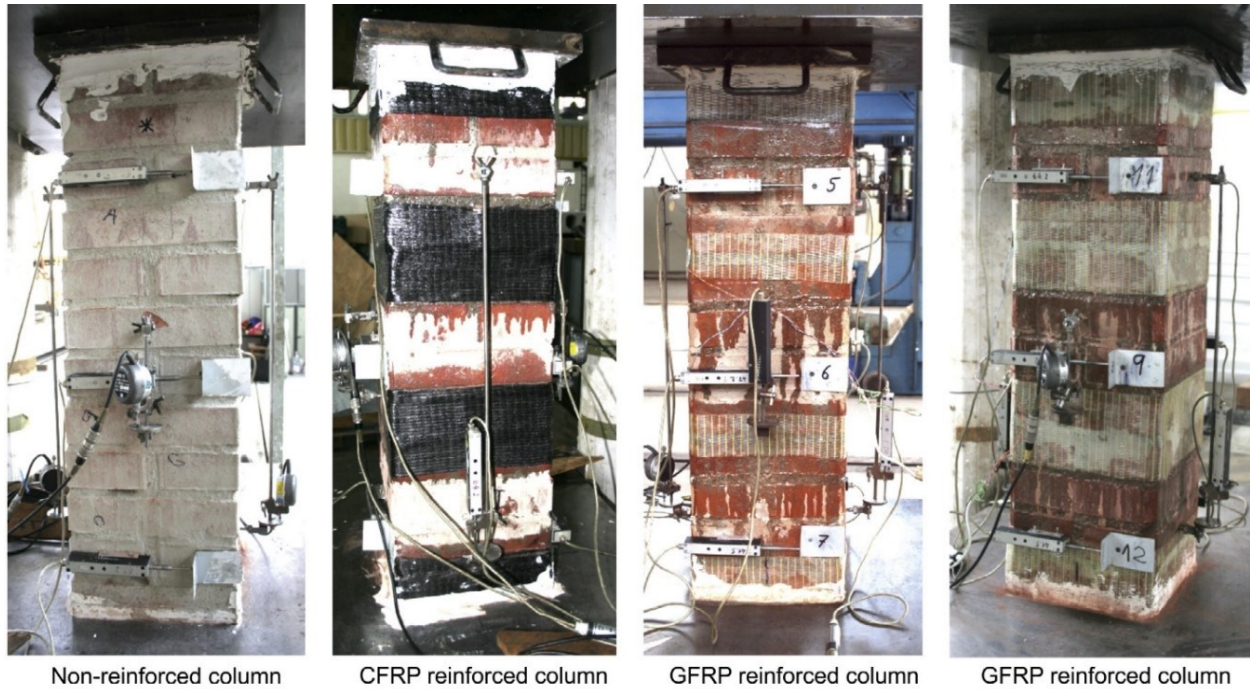
Figure 2.21 Details of brick masonry columns (Witzany et al., 2014).

Witzany and Zigler (2015) strengthened masonry columns by non-continuous wrapping of carbon FRP. The stone masonry columns constructed from regular sandstone blocks and irregular freestone blocks and tested under concentric load. Also, the researchers pointed out that the necessity of a different approach to the assessment of the load-bearing capacity, or residual load-bearing capacity of masonry composed of stone blocks.

regular sandstone   regular sandstone   irregular sandstone   irregular sandstone
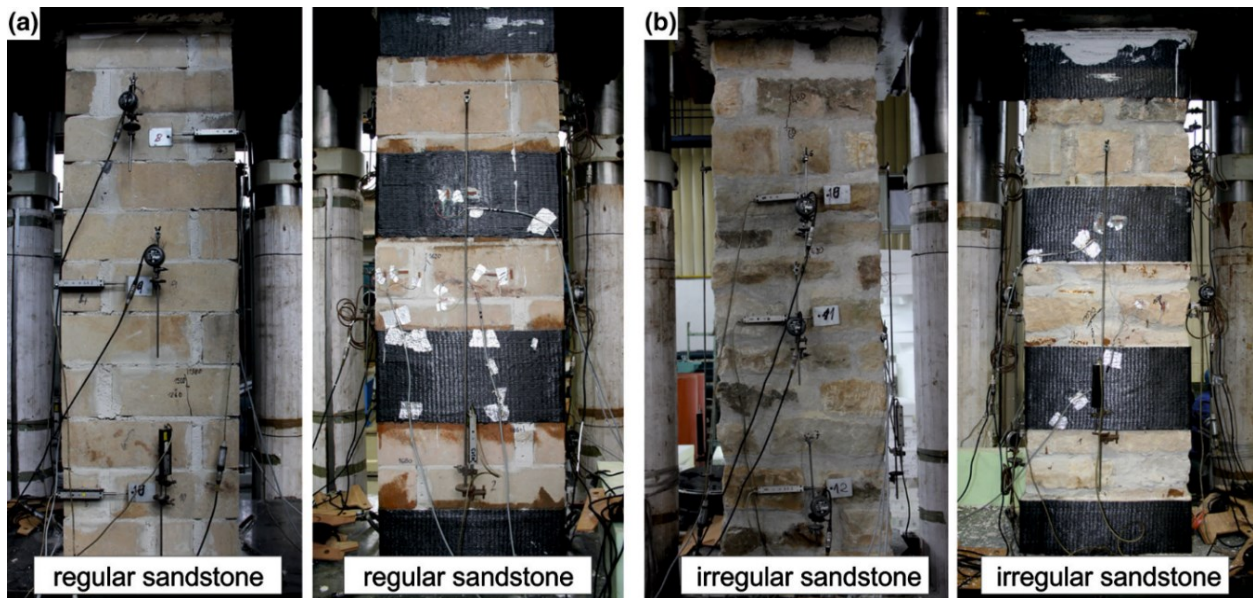
Figure 2.22 Stone masonry columns from regular or irregular sandstone blocks
(Witzany and Zigler, 2015).

Micelli et al. (2014a) studied the behaviour of circular columns constructed from natural blocks confined with glass and basalt FRP. They also studied active confinement by using a novel technique that employs Shape Memory Alloys (SMA). Twenty four masonry columns tested under axial compression loads. The results showed that FRP confinement gives significant benefit in increasing the strength and ductility of confined masonry columns. Active confinement provided by SMA wires with GFRP sheets was found to be effective in increasing the axial stiffness at early loading stages.
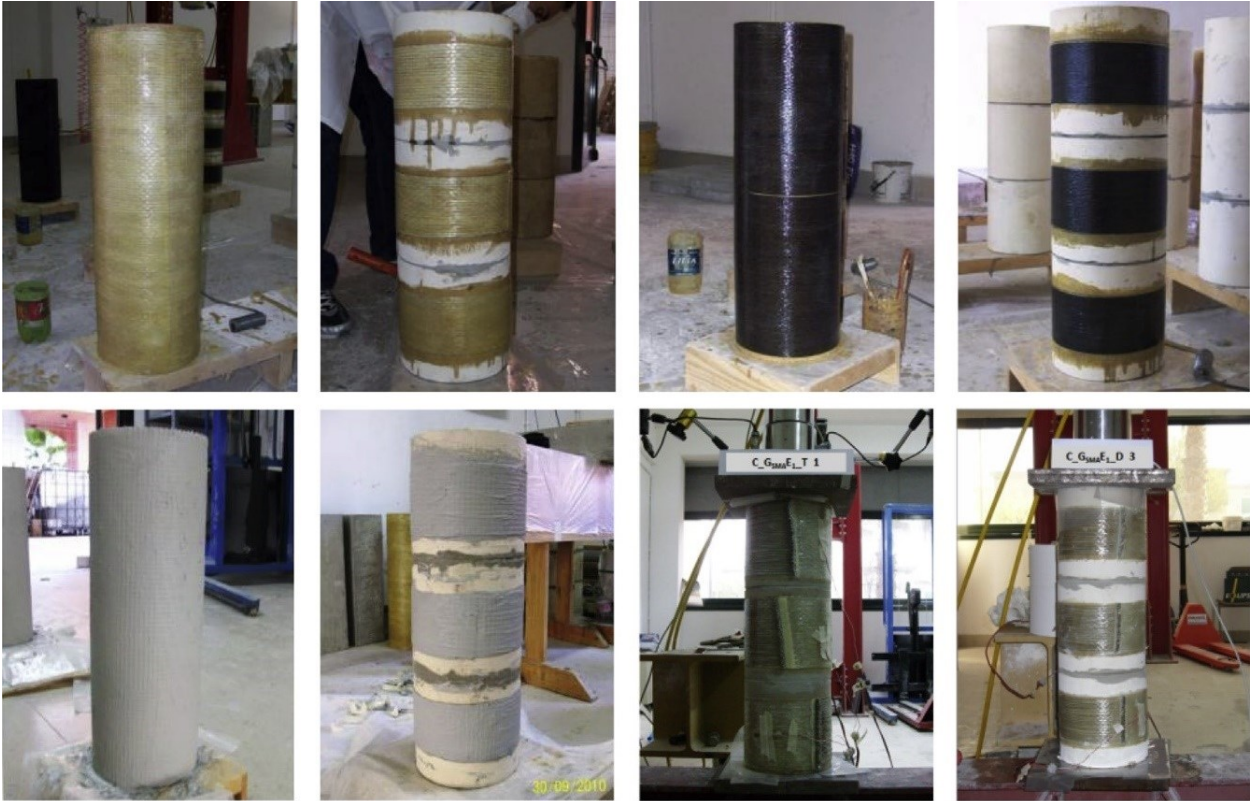
Figure 2.23 Natural blocks confined with glass and basalt FRP (Micelli et al., 2014a).

According to the authors' knowledge, there is limited research on the use of FRP composite materials in strengthening of concrete block masonry columns. Galal et al. (2012) experimentally tested reinforced concrete masonry columns strengthened with carbon FRP under combined axial load and cyclic flexure. The columns with 390 mm square cross section were constructed by bull-nosed concrete blocks. The concrete block masonry columns were wrapped with different layers of CFRP jackets with different wrapping schemes. The results proved that the seismic performance of the masonry columns was enhanced. FRP wraps increased the ductile behaviour, strength capacity, and energy dissipation.
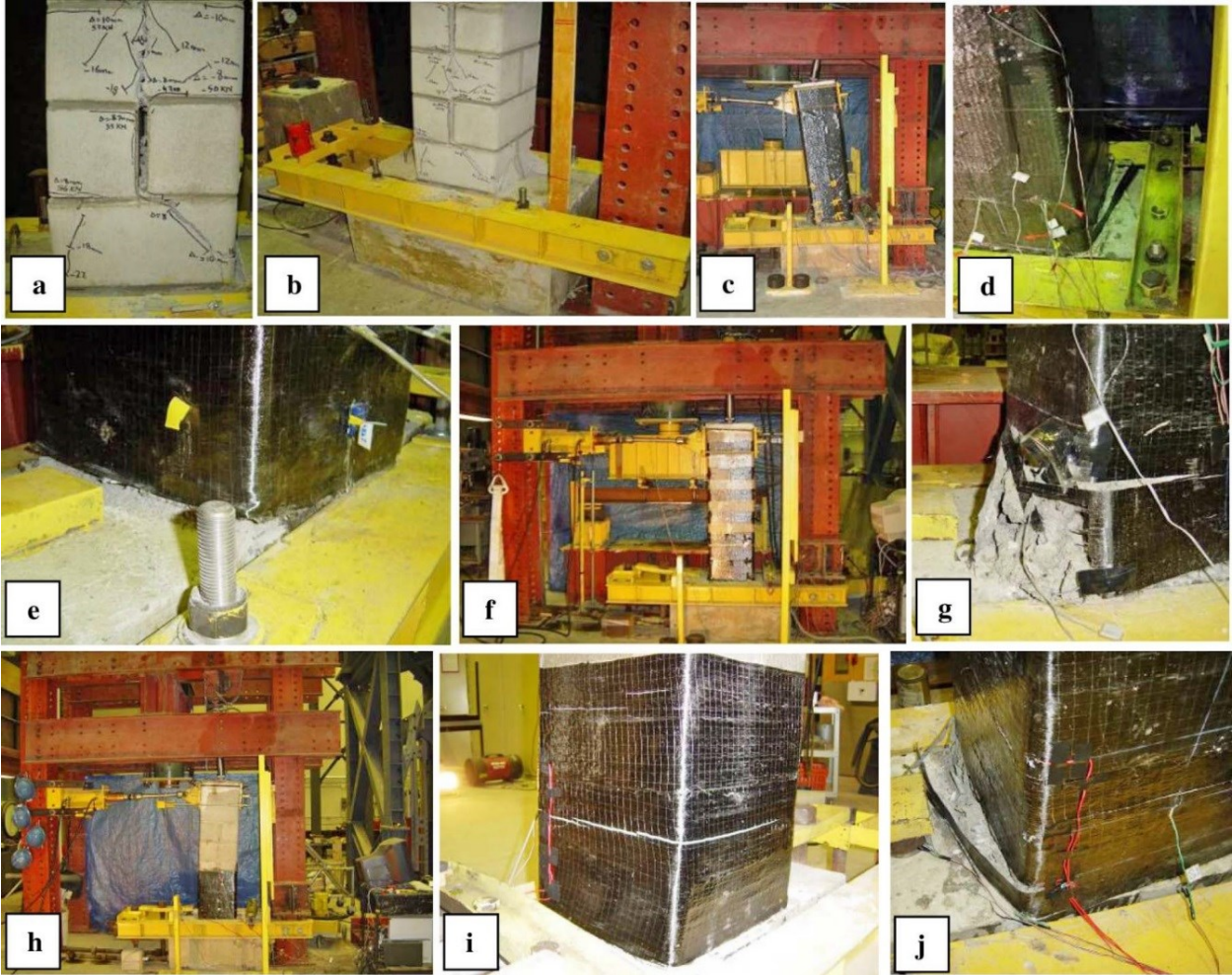
Figure 2.24 Columns' performance and failure (Galal et al., 2012).

2.6 Stress-strain behaviour of masonry confined by FRP materials

This part covers the research work found in scientific literature about the strength gain of masonry confined by FRP materials. The research work related to analytical models for FRP confinement and their assessment was briefly reviewed.

2.6.1 Krevaikas and Triantafillou (2005)

Krevaikas and Triantafillou (2005) investigated the effect of FRP confinement by conducting experimental tests, and proposed a simple confinement model for strength and ultimate strain of FRP-confined masonry.

The confinement pressure produces by FRP is not uniform at cross sections especially near the corners. The average value of confinement pressure (f_l) can be calculated as:

$$f_l = k_e \frac{b + h}{b.h} t_f E_f \varepsilon_f \qquad \text{Eq. 2-1}$$

where b and h are cross section dimensions; t_f is thickness of FRP; E_f is elastic modulus of FRP; ε_f is circumferential FRP strain; and k_e is effectiveness coefficient as Figure 2.25.

Effectiveness coefficient k_e is the ratio of the effectively confined area to the total cross section area A_m can be calculated as follows:

$$k_e = 1 - \frac{b'^2 + h'^2}{2A_m} \qquad \text{Eq. 2-2}$$
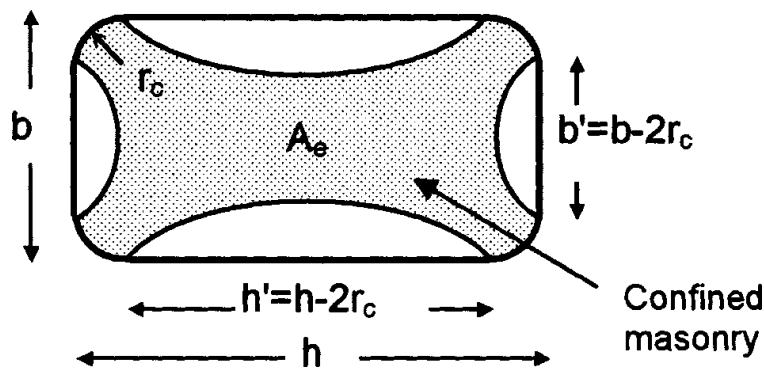
Figure 2.25 Effective confined area in rectangular columns (Krevaikas and Triantafillou, 2005).

The confinement model for strength and ultimate strain of FRP-confined masonry are based on De Lorenzis and Tepfers (2003) confinement model for confined concrete by FRP. The confinement model for masonry is determined by calibrating the empirical constants with tests results.

$$f_{mcd} = f_{md} \quad if \frac{f_l}{f_{md}} \leq 0.24 \qquad \text{Eq. 2-3}$$

$$f_{mcd} = f_{md} \left(0.60 + 1.65 \frac{f_l}{f_{md}}\right) \quad if \frac{f_l}{f_{md}} \geq 0.24 \qquad \text{Eq. 2-4}$$

where, f_{mcd} is the compressive strength of confined masonry and f_{md} is compressive strength of unconfined masonry. The confined compressive strength with low level of confinement does not exceed the unconfined value so 0.24 limit is proposed.

The expression for the ultimate axial strain of confined masonry calibrated by experimental tests in term of $\frac{f_l}{f_{md}}$ is:

$$\varepsilon_{mcu} = \varepsilon_{mu} + 0.34 \frac{f_l}{f_{md}} \qquad \text{Eq. 2-5}$$

where, ε_{mcu} is the compressive strength of confined masonry and ε_{mu} is compressive strength of unconfined masonry.

2.6.2 CNR-DT 200 R1 (2004)

Italian guideline CNR-DT 200 R1 (2004) suggested design equations for FRP-confined masonry columns. The guideline recommends the expression to find the strength of confined masonry columns as:

$$f_{mcd} = f_{md} + k'.f_{l,eff} \qquad \text{Eq. 2-6}$$

where $f_{l,eff}$ is effective lateral confining pressure; and k' is hardening factor for compressive strength.

$$k' = \left(\frac{g_m}{1000}\right) \qquad \text{Eq. 2-7}$$

g_m is the density of masonry in kg/m^3 unless a more detailed analysis is performed.

The effective confining pressure, $f_{l,eff}$, is adjusted by a horizontal and vertical coefficient of efficiency and it is expressed as

$$f_{l,eff} = k_H \cdot k_V \cdot f_l \qquad \text{Eq. 2-8}$$

where f_l is the lateral confining pressure produced by FRP jacket and can be expressed for rectangular columns as:

$$f_l = \frac{1}{2} \min\{\rho_{f,x} \cdot E_f + 2 \cdot \rho_{b,x} \cdot E_b; \rho_{f,y} \cdot E_f + 2 \cdot \rho_{b,y} \cdot E_b\} \cdot \varepsilon_{fd,rid} \qquad \text{Eq. 2-9}$$

where $\rho_{f,x}$, $\rho_{b,x}$, $\rho_{f,y}$, and $\rho_{b,y}$ are reinforcement ratios

$$\rho_{f,x} = \frac{4 \cdot t_f \cdot b_f}{d \cdot \rho_f} \; ; \; \rho_{f,y} = \frac{4 \cdot t_f \cdot b_f}{d \cdot \rho_f}; \; \rho_{b,x} = \frac{n_{b,x} \cdot A_b}{d \cdot \rho_b} \; ; \; \rho_{b,y} = \frac{n_{b,y} \cdot A_b}{d \cdot \rho_b} \qquad \text{Eq. 2-10}$$

where $n_{b,x}$ and $n_{b,y}$ are number of bars disposed in one course along the x and y directions.

In the case of continuous wrapping by FRP jacket, ρ_f can be calculated as:

$$\rho_f = \frac{4 \cdot t_f}{\max\{b,h\}} \qquad \text{Eq. 2-11}$$

the horizontal coefficient k_H is calculated from the relationship between the confined area and the total area:

$$k_H = 1 - \frac{b'^2 + d'^2}{3A_m} \qquad \text{Eq. 2-12}$$

The values of k_H is equal to 1 for continuous jacketing, while in the case of FRP strips it is given by

$$k_v = \left(1 - \frac{\rho'_f}{2 \cdot \min\{b,h\}}\right)^2 \qquad \text{Eq. 2-13}$$

where ρ_f is vertical spacing between the FRP strips. See the Figure 2.26 for more explanation. Like discontinuous wrapping, the confinement by internal FRP bars is reduced by the coefficient of efficiency k_{eff}, which can be assumed as follows

$$k_{eff} = k_H \cdot k_V =$$
$$\left[1 - \frac{1}{6}\left(2 \cdot \frac{n_{b,x} - 1}{n_{b,x}^2} \cdot \frac{d}{b} + 2 \cdot \frac{n_{b,y} - 1}{n_{b,y}^2} \cdot \frac{d}{b} + \frac{3}{n_{b,x} \cdot n_{b,y}}\right)\right]\left(1 - \frac{\rho_f}{2 \cdot \min\{b,h\}}\right)^2 \qquad \text{Eq. 2-14}$$

The value of $\varepsilon_{fd,rid}$ which is the ultimate design strain for FRP can be computed by the following equation:

$$\varepsilon_{fd,rid} = \min \left\{ \frac{n_a \cdot \varepsilon_{fk}^{(r)}}{\gamma_f^{(r)}} ; \frac{n_a \cdot \varepsilon_{fk}^{(b)}}{\gamma_f^{(b)}} \right\} \qquad \text{Eq. 2-15}$$

where n_a is environmental safety factor; $\varepsilon_{fk}^{(r)}$ and $\varepsilon_{fk}^{(b)}$ are FRP ultimate strain for wraps and bars, respectively; while $\gamma_f^{(r)}$ and $\gamma_f^{(b)}$ are material factors for FRP wraps and bars, respectively,.
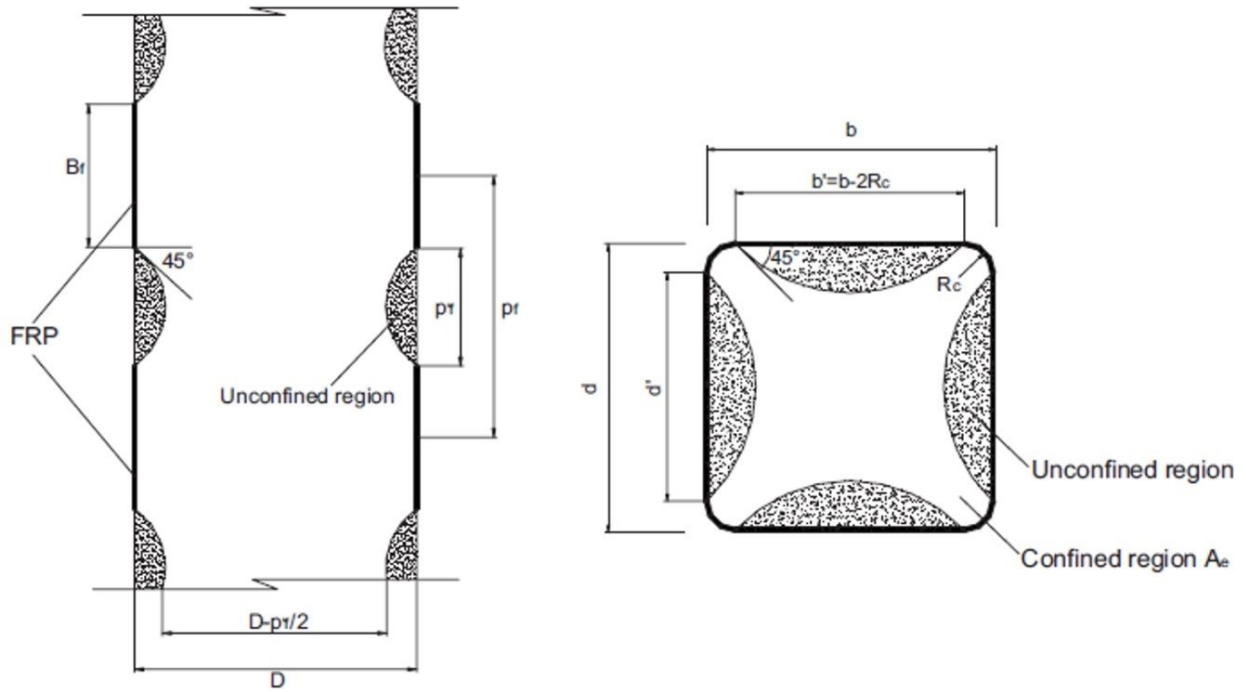
Figure 2.26 Geometry of FRP-confined masonry column (CNR-DT 200 R1, 2004).

2.6.3 Corradi et al. (2007)

Corradi et al. (2007) calibrated a simple confinement model for FRP-confined masonry. Experimental results on clay brick columns conducted by Krevaikas and Triantafillou (2005) and Corradi et al. (2007) were used to calibrate the numerical expression.

$$f_{mcd} = f_{md} + \left(1 + k' \cdot \frac{f_{l,eff}}{f_{md}} \right) \qquad \text{Eq. 2-16}$$

$$\text{where } k' = 2.4 \cdot \left(\frac{f_{l,eff}}{f_{md}} \right)^{-0.17} \qquad \text{Eq. 2-17}$$

The study presented more discussion and expressions to obtain the effective confinement pressure in square and octagonal cross-sections.

2.6.4 Aiello et al. (2009)

Aiello et al. (2009) conducted experimental tests on limestone and clay masonry columns to perform a comparison between experimental results and equations proposed in CNR-DT 200 R1 (2004). They concluded that CNR-DT 200 R1 (2004) equations could be considered reliable in describing the behaviour of FRP-confined masonry. Aiello et al. (2009) also calibrated confinement model proposed by Krevaikas and Triantafillou (2005) which originally calibrated on clay masonry columns. Aiello et al. (2009) suggested this expression with the coefficients found from their tests for limestone masonry columns confined either with external FRP sheets or internal FRP bars.

$$f_{mcd} = f_{md}\left(1 + \frac{f_l}{f_{md}}\right)$$ <div align="right">Eq. 2-18</div>

2.6.5 Di Ludovico et al. (2010)

Di Ludovico et al. (2010) experimentally tested tuff and clay masonry. Test results with data available in the literature were used to assess confinement analytical models.

Two refined equations proposed by Di Ludovico et al. (2010) to predict the strength of confined masonry columns constructed from tuff and clay. The refined theoretical expressions for clay masonry was calibrated to minimize the scattering between theoretical predictions and experimental available data.

$$f_{mcd} = f_{md} + \left(1 + k'.\frac{f_{l,eff}}{f_{md}}\right)$$ <div align="right">Eq. 2-19</div>

$$where\ k' = 1.53 .\left(\frac{f_{l,eff}}{f_{md}}\right)^{-0.10}$$ <div align="right">Eq. 2-20</div>

The refined theoretical expressions for tuff masonry are:

$$f_{mcd} = f_{md} + \left(1 + k'.\frac{f_{l,eff}}{f_{md}}\right)$$ <div align="right">Eq. 2-21</div>

$$where\ k' = 1.09 .\left(\frac{f_{l,eff}}{f_{md}}\right)^{-0.24}$$ <div align="right">Eq. 2-22</div>

2.6.6 Faella et al. (2011a)

Faella et al. (2011a) collected a database from scientific literature to assess the available confinement models for FRP-confined masonry columns. Using experimental database, three different of design formulas for FRP-confined masonry columns are proposed with different level of accuracy and simplicity. The Italian Guideline CNR-DT 200 R1 (2004) expressions were adopted and calibrated as.

Model #1: the most general calibration:

$$f_{mcd} = f_{md} \cdot \left(1.618 + 0.013 \left(\frac{g_m}{1000} \right)^{6.324} \cdot \left(\frac{f_{l,eff}}{f_{md}} \right)^{2.119} \right) \qquad \text{Eq. 2-23}$$

Model #2: The best distributed relationship:

$$f_{mcd} = f_{md} \cdot \left(1 + 0.416 \left(\frac{g_m}{1000} \right)^{2.064} \cdot \left(\frac{f_{l,eff}}{f_{md}} \right)^{0.507} \right) \qquad \text{Eq. 2-24}$$

Model #3: The simplest expression:

$$f_{mcd} = f_{md} \cdot \left(1 + \left(\frac{g_m}{1000} \right) \cdot \left(\frac{f_{l,eff}}{f_{md}} \right)^{0.662} \right) \qquad \text{Eq. 2-25}$$

2.6.7 CNR-DT 200 R1 (2013)

The Italian National Research Council (CNR) updated the confinement model for masonry columns confined with FRP composites which published in the Technical Document 200/2004. The revision tried to improve the accuracy of the confinement model by limiting the increase in strength with the increase of FRP confinement. The new expression is a nonlinear confinement model:

$$\frac{f_{mcd}}{f_{md}} = 1 + k' \cdot \left(\frac{f_{l,eff}}{f_{md}} \right)^{\alpha_1} \qquad \text{Eq. 2-26}$$

$$where \ k' = \alpha_2 \cdot \left(\frac{g_m}{1000} \right)^{\alpha_3} \qquad \text{Eq. 2-27}$$

The coefficients α_1, α_2, α_3 can be taken as 0.50, 1.0 and 1.0, respectively, in case of experimental data is absent. Also, it can be calibrated with the result of experimental tests.

2.6.8 Nanjunda Rao and Pavan (2015)

Nanjunda Rao and Pavan (2015) investigated compression behaviour of FRP confined clay bricks masonry columns and assessed various confinement models available in the literature for prediction the gain in axial capacity of FRP-confined masonry. New calibrations are proposed using available experimental data. The authors proposed expressions for compressive strength of FRP-confined masonry with loading axis normal to bed joint (90°):

$$\frac{f_{mcd}}{f_{md}} = 1 + 1.53 \left(\frac{f_{l,eff}}{f_{md}}\right)^{0.92} \qquad \text{Eq. 2-28}$$

Expression for masonry with loading axis at various inclinations to bed joint (0, 30, 45, 60 and 90°):

$$\frac{f_{mcd}}{f_{md}} = 1 + 4.96 \left(\frac{f_{l,eff}}{f_{md}}\right)^{0.87} \qquad \text{Eq. 2-29}$$

2.6.9 Minafò et al. (2017)

Minafò et al. (2017) conducted a comparative analysis of available confinement models to predict the compressive stress-strain curve of FRP confined clay brick masonry. The models are evaluated in terms of effective confinement pressure, ultimate stress, ultimate strain, and the stress-strain curve.

From the comparative analysis, Minafò et al. (2017) found the following main conclusions:

- The expression proposed by Di Ludovico et al. (2010) is the most reliable because it is calibrated with a large database of experimental tests.
- The Italian CNR-DT 200 R1 (2013) guideline is conservative, because it is limiting the maximum strain in the FRP wrap to 0.004 mm/mm.
- For predicting the ultimate strain, there are two expressions; only the expression proposed by Krevaikas and Triantafillou (2005) was specific for masonry, whereas the expressions proposed by Campione and Miraglia (2003) was adopted for concrete.
- The approach of Di Ludovico et al. (2010) gives a low error with significant dispersion compared to the experimental data.
- Krevaikas and Triantafillou (2005) model gives the best prediction when the peak axial strain of unconfined masonry is assumed to be 0.002 mm/mm.

2.7 Closing remarks

Developing axial force-moment interaction diagrams is based on detailed section analysis. There are fundamental parameters that are controlling the detailed section analysis for FRP confined masonry such as; the compressive strength, ultimate strain, and the equivalent stress block parameters. The value of the compressive strength of FRP-confined masonry is essential for performing detailed section analysis. A reliable analytical confinement model to predict strength gains is needed. According to the experimental and analytical studies that were reviewed in this chapter, most of the work was conducted on clay, tuff, and limestone masonry columns. The ability of available expressions in the literature to predict the strength gain in concrete block masonry columns should be evaluated before using the available expressions in developing axial force-moment interaction diagrams, especially that the models were calibrated with experimental tests conducted on different materials of masonry.

Determining the ultimate usable strain that can be reached in the extreme compression fibre of FRP confined concrete masonry is essential for performing detailed section analysis. For integrating the stresses over the cross section, a stress-strain curve for FRP confined concrete masonry is needed. However, instead of using the nonlinear stress-strain curve, the equivalent stress block parameters can be used to integrate the stresses over the cross section.

Considering the limited information and tests conducted on concrete masonry columns confined with FRP, developing an experimental program is necessary to obtain the missing information and assess the available confinement models to predict the compressive strength gain of FRP confined concrete block masonry. The experimental data obtained from this work is useful in validating the proposed methodology to compute the axial force-moment interaction diagram of fully grouted reinforced concrete masonry column confined with FRP jacket for a short prismatic concrete masonry column failing in a compression-controlled manner.

Chapter 3

Axial Compressive Behaviour of Grouted Concrete Block Masonry Columns Confined by CFRP Jackets

Abstract

Confining existing concrete and masonry columns by Carbon Fibre Reinforced Polymers (CFRP) is a beneficial method for enhancing the column axial capacity and ductility. This paper presents an experimental investigation of the CFRP confinement influence on the uniaxial compression stress-strain behaviour of concrete block masonry columns. Scaled fully grouted concrete block masonry columns, with a square cross section, were confined by continuous CFRP jackets and tested under concentric axial loading up to failure. The results indicate that CFRP enhances the ultimate axial strain and the axial load capacity by up to 281% and 79%, respectively compared to unreinforced columns. In this study, the effect of corner radius and the thickness of CFRP jackets are investigated. Special attention was also given to the effective tensile strain in the CFRP jackets. Finally, the CNR-DT 200 R1 confinement model, the only guide addressing strengthening masonry columns with external FRP composites, was assessed and refined equation is proposed.

3.1 Introduction

Rehabilitation or upgrading of existing structures is often more economical and preferable solution than demolishing the entire structures or reconstructing some members. Many existing masonry buildings are structurally deficient or in need of seismic upgrade. On the other hand, many concrete masonry columns are not capable of meeting the increase in axial loading demand in case of a change in building occupancy. In addition, factors such as poor construction practices, low quality materials, and environmental deterioration may cause strength degradation. Also, reinforced concrete masonry columns that are part of the lateral force resisting system or designed to sway under lateral seismic load may need more ductility for better performance or to meet new seismic design requirements. All of the above create a need to develop effective strengthening method for increasing the ductility and bearing capacity of concrete masonry columns.

Fibre Reinforced Polymers (FRP) materials have been commonly used in recent decades to confine concrete columns. The popularity of using FRP for strengthening and upgrading concrete columns is mainly attributed to the high strength and lightweight characteristics of the FRP materials (Seible et al., 1997). Using FRP composites reduces additional dead load associated with traditional strengthening solutions and simplify the application in areas with limited access. Numerous researchers have taken advantage of FRP characteristics and see the potential of using FRP materials to externally confining concrete columns by aligning the fibres along the direction of hoop stresses perpendicular to the vertical axis of the columns, as will be presented in the following paragraphs.

In the last few decades, experimental, numerical and analytical works have been conducted to better understand the behaviour of FRP confined concrete columns. Ozbakkaloglu and Lim (2013) assembled a database of circular FRP-confined concrete tests contains 3042 results from 253 studies published between 1991 and 2013. Ozbakkaloglu et al. (2013) reviewed and assessed 88 stress-strain models developed to predict the stress-strain behaviour of circular FRP-confined concrete columns. The extensive researches of FRP confined concrete columns have explored many different parameters in order to determine main factors affecting the behaviour of confined sections including fibres type, the volumetric ratio of FRP or thickness of jacket, tensile strength and ultimate strain of the FRP, unconfined concrete strength, the shape and dimensions of column section, the aspect ratio and corner radius for prismatic sections, and the presence of steel

reinforcement in confined columns. A significant effort has been invested in field of strengthening reinforced concrete columns with externally bonded FRP. This has led to developing several design codes and guidelines (ISIS Canada, 2001; Concrete Society, 2004; FIB, 2007; ACI 440.2R-08, 2008).

Compared to the extensive research conducted in the field of confinement concrete columns with FRP, much less effort has been invested in retrofitting masonry columns. Few researchers have investigated the application of carbon, glass and basalt FRP to confine masonry columns constructed with clay, tuff, limestone, or concrete blocks.

In the experimental studies (Masia and Shrive, 2003; Alecci et al., 2009; Di Ludovico et al., 2010; Faella et al., 2011b), different types of masonry column confined with different FRP jackets were tested. Confinement models calibrated by experimental results were proposed in Refs. (Krevaikas and Triantafillou, 2005; Corradi et al., 2007; Faella et al., 2011a). Another technique has been considered by some researchers by internally confining masonry using FRP bars inserted in holes drilled through the column with or without FRP wrap (Aiello et al., 2007, 2009; Micelli et al., 2014b). Shaheen and Shrive (2007) explored a different technique for strengthen masonry columns by spraying the columns with glass FRP in different thicknesses. Recent studies focused on discontinuous confinement by FRP strips (Micelli et al., 2014a; Witzany et al., 2014; Witzany and Zigler, 2015). From the above it can be seen that there is a need for more research that contributes to the literature on FRP strengthening of concrete block masonry columns. Galal et al. (2012) tested reinforced concrete masonry columns strengthened with carbon FRP under combined axial load and cyclic quasi-static loading. Farnia (2011) proposed a confinement model for FRP wrapped concrete masonry columns calibrated based on an experimental investigation of continuous and discontinuous carbon FRP wrapped grouted concrete masonry columns.

In the failure mechanism of confined masonry columns with FRP wraps, the passive confinement provided by FRP composites is induced by increasing the lateral expansion of blocks and grout under axial force. The restraint of FRP composites to the expansion of core of column transforms into tension stress along the hoop direction of FRP composites. The FRP lateral confining pressure helps the masonry composite keep its integrity until the FRP composites reach the maximum tensile force, the system would fail due the rupture of FRP composites. Generally, confinement leads to axial strength increase and strain enhancement. Several experimental

research observed that FRP confinement is more effective in strengthening circular columns compared to other shapes (Lam and Teng, 2003). In the case of prismatic columns with a continuous FRP jacket, only the area contained by four second-degree parabolas is considered effectively confined. Rounding edges of the columns or increasing the corner radius plays a significant role in increasing the effectively confined area which leads to the increase of the compressive strength of the columns. The arch-effect for square cross section is shown in Figure 3.1. Also it has been noticed that confined plain concrete masonry prisms show similar behaviour under compression to the behaviour of confined prisms with vertical steel bars. Priestley and Elder (1983) indicated that presence of vertical steel bars in the columns does not significantly influence concrete masonry stress-strain curves when the contribution of vertical steel bars was subtracted from the total axial stress of masonry columns.
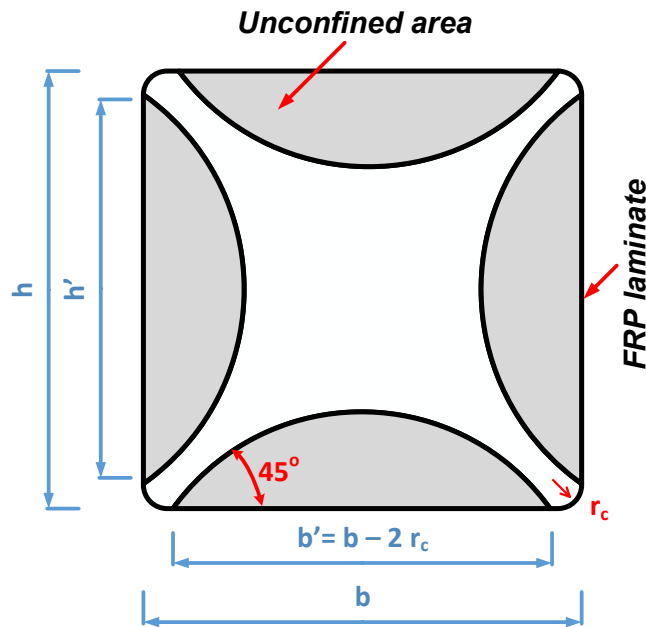
Figure 3.1 The arch-effect for square cross section.

The results of 19 half-scale unreinforced concrete block masonry prisms confined with Carbon Fibre Reinforced Polymers (CFRP) jackets are presented in this study. The main objective of this paper is to quantify the compressive strength and the ultimate axial strain capacity of concrete masonry columns under various CFRP confinement levels with different corner radius towards the development of the complete stress-strain curves. The thickness of CFRP jacket and the corner radius of section have been mainly chosen for their influence in changing the shape of stress-strain curve. Strain gages mounted along the faces of the prisms were used to obtain a precise

measurement of the effective tensile strain in the CFRP jackets. Finally, the analytical confinement model recommended by CNR-DT 200 R1 (2013), the only guide addressing strengthening masonry columns with external FRP composites, was assessed and refined.

3.2 Experimental tests

3.2.1 Prism construction and preparation

A total of 19 half-scale fully grouted concrete masonry prisms were constructed and tested under axial compression. All prisms were two blocks thick and five blocks high, bonded together with5mmmortar. Professional masons built prisms by placing blocks in running bond pattern. Prisms were grouted after a week of curing in laboratory environment. All half-scale masonry prisms had a cross section of 185 x 185 mm and height of 470 mm before rounding the corners, as shown in Figure 3.2. The primary variables in experimental tests were the number of composite layers and the corner radius of the cross section. The properties of the tested prisms are shown in Table 3.1. Seven sets of prisms consisted of three or two replicate prisms each, were tested in order to obtain average data. The sets varied with a corner radius of 0, 10 and 30 mm. Prisms were confined with one, two and three layers of CFRP composite jackets. Each prism is given a notation as RX-LN-#, where R stands for a corner radius, X is the corner radius, L stands for a composite layer, N is the number of composite layers, and the final number represents the number of replicate prism in the set. The prisms without wrapping and no rounded corners were used as control specimens and were denoted by R0-L0.

Table 3.1 Properties of the prisms.

Set	Corner radius (mm)	Number of CFRP layers	Number of specimens	Cross-sectional area (mm²)
R0-L0	-	-	3	34225
R10-L1	10	1	3	34139
R10-L2	10	2	3	
R10-L3	10	3	2	
R30-L1	30	1	3	33452
R30-L2	30	2	3	
R30-L3	30	3	2	
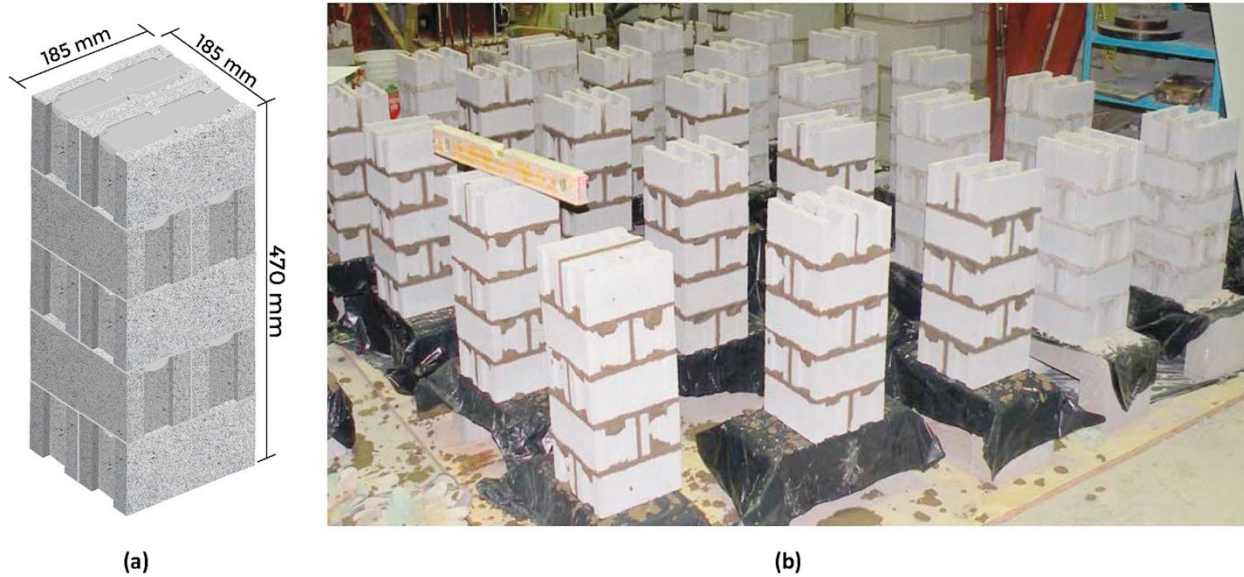
Figure 3.2 (a) Dimensions of half-scale fully grouted prism; (b) prisms construction before grouting.

The surface of all prisms was prepared before wrapping CFRP sheets. The flanged ends of the concrete block units were filled with a repair mortar, as shown in Figure 3.3. The recommended repair mortar according to the manufacturer's specifications is Sikadur® 30 epoxy extended with dried silica sand at a 1:1 volume mix ratio. Before jacketing the prisms, the corners were rounded with a radius of 10or 30 mm by using an electric grinder. After patching the repair mortar, a grinder was used to sand and remove any irregularity or protrusion that comes from the bed joint or the repair mortar. After that, the dust and loose particles coming from grinding process were removed by a vacuum, and then the surface was cleaned by water. The prepared masonry prisms before wrapping CFRP sheets are shown in Figure 3.4.
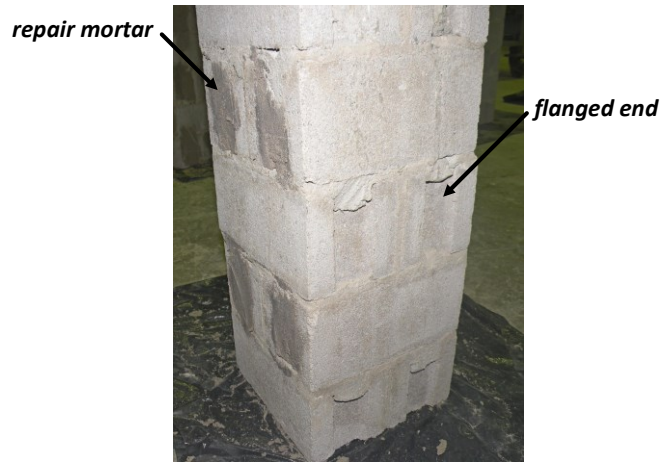
Figure 3.3 Filling the flanged ends of the concrete block units with a repair mortar.
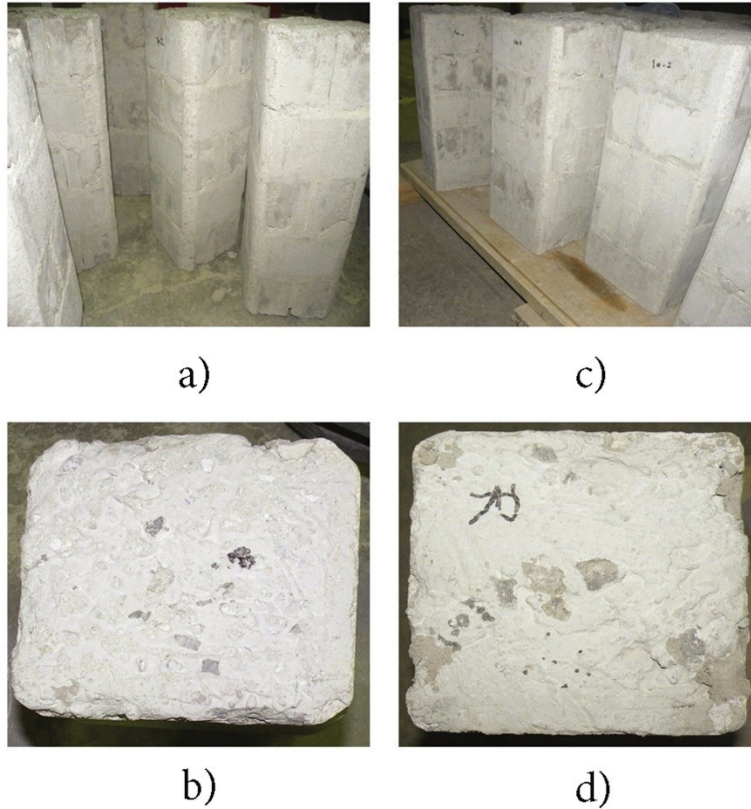
Figure 3.4 (a) Prisms with corner radius of 30 mm; (b) cross section of prism rounded with 30 mm; (c) prisms with corner radius of 10 mm; and (d) cross section of prism rounded with 10 mm.

The steps taken to wrap the masonry prisms are summarized in Figure 3.5. In order to ensure the effectiveness of the wrapping, the overlapping of the sheet in the direction of the fibres was 150 and 125 mm for prisms with corner radius of 10 and 30 mm, respectively. The overlapping is more than the recommended length of 100 mm by the manufacturer's specifications, as shown in Figure 3.6. The CFRP sheet was wrapped around the prisms by the dry lay-up procedure approximately six months after the prisms were constructed. First, the fibre sheet was cut to the desired length. Then, Sikadur® 330 epoxy resin was combined by adding contents of component A to component B and mixed thoroughly for 3 min with a mixing drill on a low speed until resin and hardener were uniform in colour. The mixed epoxy resin was applied directly onto the prepared prisms using a paint roller. The fibre sheet was carefully placed onto the resin coating and smoothed out. The resin was squeezed out between the fibres and any irregularities or air pockets were worked out with a plastic laminating roller. If more than one layer of fibre sheets was needed, additional epoxy resin was applied on the previous layer without stopping the lay-up process. The

overlapping area is always placed at one face of the prism. The wrapped prisms were cured in the laboratory environment for at least one week before testing.
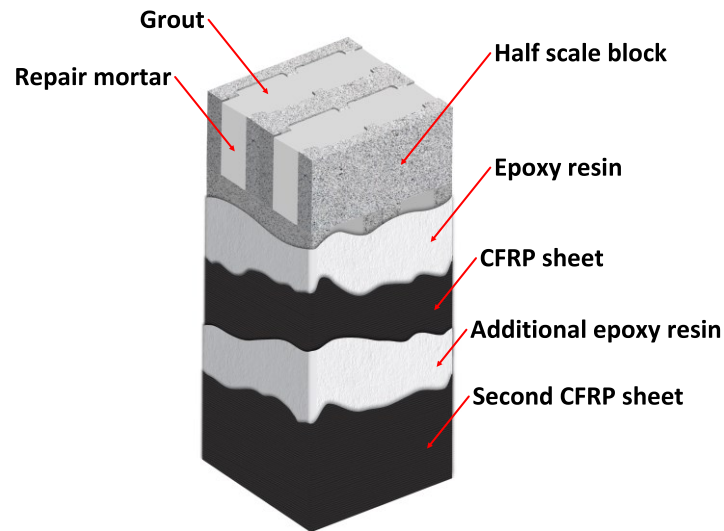
Figure 3.5 Steps taken to wrap prisms.
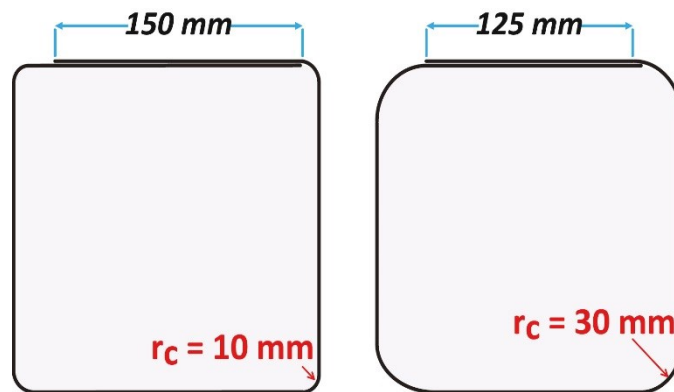
Figure 3.6 The overlapping for prisms with corner radius of 10 and 30 mm.

3.2.2 The mechanical properties of materials

The half-scale concrete blocks used in prisms construction were similar to the blocks proposed by Long (2006). The model units resemble the hollow stretcher type of 200 mm nominal size concrete masonry blocks. Typical dimensions of the half-scale block compared to the full-scale block are shown in Figure 3.7. Three half-scale masonry units were tested according to ASTM C140/C140M-15ae1 (2015) to determine the compressive strength of block. After cutting the top part of the block to remove the depressed webs, high strength gypsum capping compound was used to distribute the load uniformly to the blocks. The average compressive strength for half-scale concrete blocks was 22.88 MPa with coefficient of variation (COV) equals to 4.4% considering

average net area equals to 8424 mm^2 (COV = 1.5%). The average density of half-scale blocks was 2181 kg/m^3 (COV = 0.5%) and absorption was 108.5 kg/m^3 (COV = 2.1%). The moisture content of blocks averaged around 7.9% (COV = 4.6%). A coarse grout, according to ASTM C476-10 (2010), was designed for grouting the prisms. The grout was cast in 100 (diameter) x 200 (height) mm plastic moulds. The cylinder specimens of grout were cured for 28 days and tested after six months from construction in the same period of testing prisms. The average compressive strength of 3 cylinders of grout was 31.39 MPa (COV = 8.5%). Ready-to-use mortar mix, blend of sand and cements, commercially available used throughout the construction process in order to achieve more consistency. The mortar meets Type S requirements as specified in ASTM C270e14a (2014). Compression tests were conducted according to ASTM C780e15a (2015) on 51 mm mortar cubes resulted in average 13.12 MPa (COV = 5.0%).
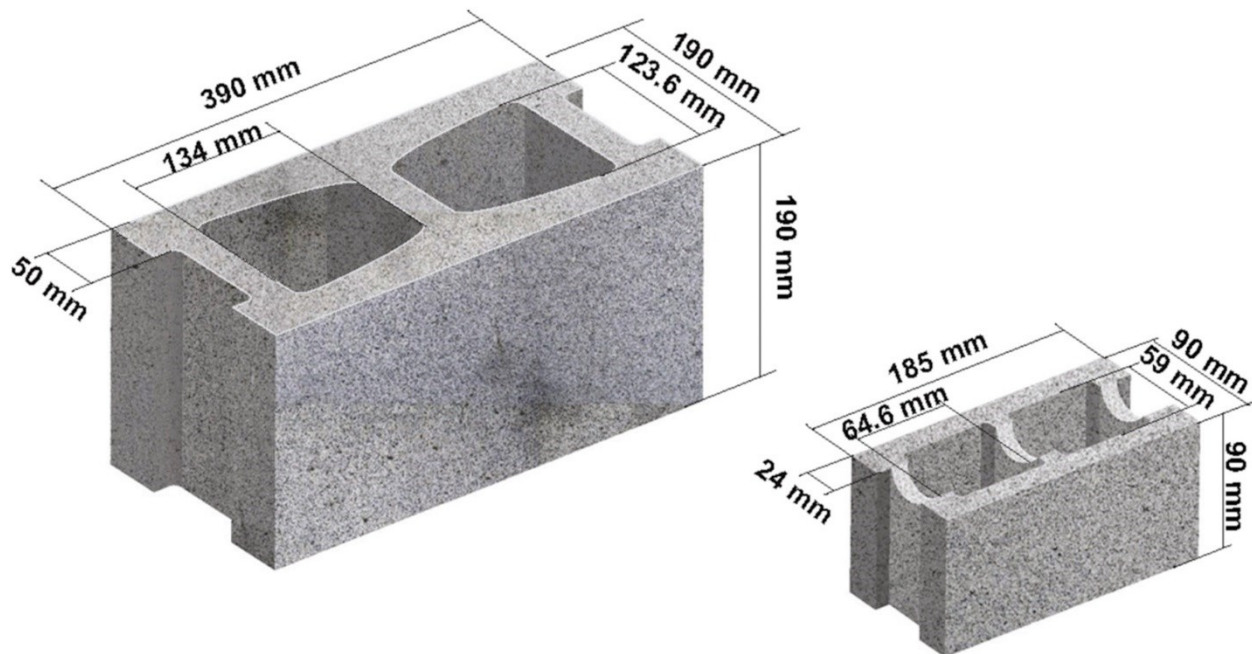
Figure 3.7 Typical dimensions of the half-scale block comparing to the full-scale block.

The unidirectional carbon fibre sheet SikaWrap® Hex 230C with Sikadur® 330 epoxy resin (Sikawrap Hex 230C) were used for wrapping the concrete block masonry prisms. The mechanical properties of the CFRP laminate were obtained experimentally from tensile testing of flat coupons and compared to the manufacturer's datasheet in Table 3.2. Five coupons of CFRP from the same roll used for wrapping the prisms were fabricated to perform tension tests according to ASTM D3039/D3039M-14 (2014) and ASTM D7565/D7565M-10 (2010). Large laminates were prepared with two layers by the regular dry layup process and then allowed to cure in the laboratory

environment for at least one week. The cured laminates were cut to 15 mm nominal wide strips by a diamond saw. The nominal thickness of the carbon fibre cured laminate is 0.381 mm. The flat coupons were fabricated with thick GFRP tabs at the ends to avoid premature failure caused by the jaws of the testing machine. Two strain gages with 5 mm gauge length were attached to each coupon to measure the ultimate tensile strain of the laminate. The test was conducted at a constant crosshead movement rate of 2 mm/min. The ultimate tensile strength and the modulus of elasticity were calculated according to ASTM D3039/D3039M-14 (2014) based on the actual composite laminate thickness and actual width rather than the nominal dimensions of cured laminate. The nominal dimensions of flat coupon specimen are shown in Figure 3.8.
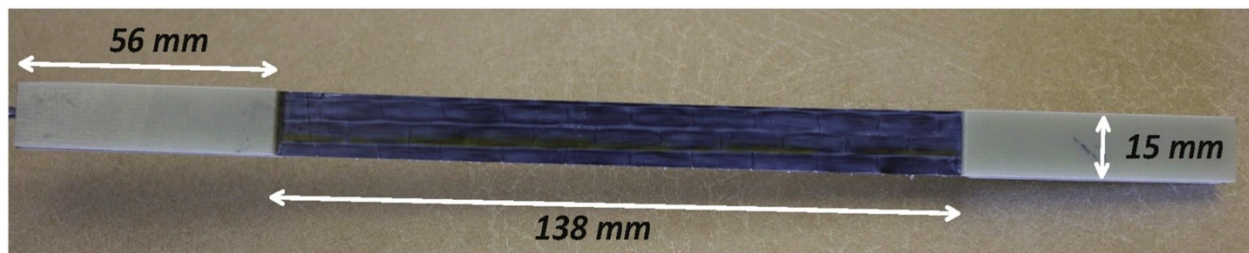
Figure 3.8 Nominal dimensions of flat coupon specimen.

Table 3.2 Comparison of CFRP coupon test and manufacturer's datasheet.

Mechanical properties of CFRP	Manufacturer	Average coupon test (COV)	Coupon test / Manufacturer
Tensile strength (MPa)	894	984 (3.4%)	1.10
Elastic modulus (GPa)	65.40	69.36 (8.3%)	1.06
Ultimate tensile strain (%)	1.33	1.34 (2.2%)	1.01

3.2.3 Test procedure and instrumentation

All prisms were instrumented to capture the complete stress-strain behaviour. A hydraulic loading cylinder connected to a manually controlled motor pump was used to apply the axial compression force on tested prisms. The applied compression load was measured by a load cell attached to the loading cylinder and recorded by a data acquisition system with high recording speed to be able to capture the descending branch of stress-strain curves. Before testing, the prism was placed inside the testing frame and both ends of prism were capped with a layer of high strength gypsum to level the steel bearing plates. A steel spherical head was placed above the upper

bearing plate and centred with respect to the centre of the prism to maintain uniform distribution of stress and avoid any eccentricity. Four draw wire displacement sensors, with 0.05% linearity, were attached between the lower and upper bearing plates at the centres of the four sides to measure the vertical displacement of tested prism. A total of 16 strain gages with 5 mm gauge length, four on each side of the prism, were installed on the outer layer of CFRP composite jacket to measure the tensile hoop strains within the fibre laminates. The strain gages were placed near the rounded corners at mid height of the second and the fourth courses of the prism. There were no strain gages on unwrapped control specimens. Test setup and instrumentation are shown in Figure 3.9. A monotonic uniaxial compressive load was applied up to prism failure by rupture of the entire CFRP jacket. The test was conducted at an approximate rate of 15 kN/min.
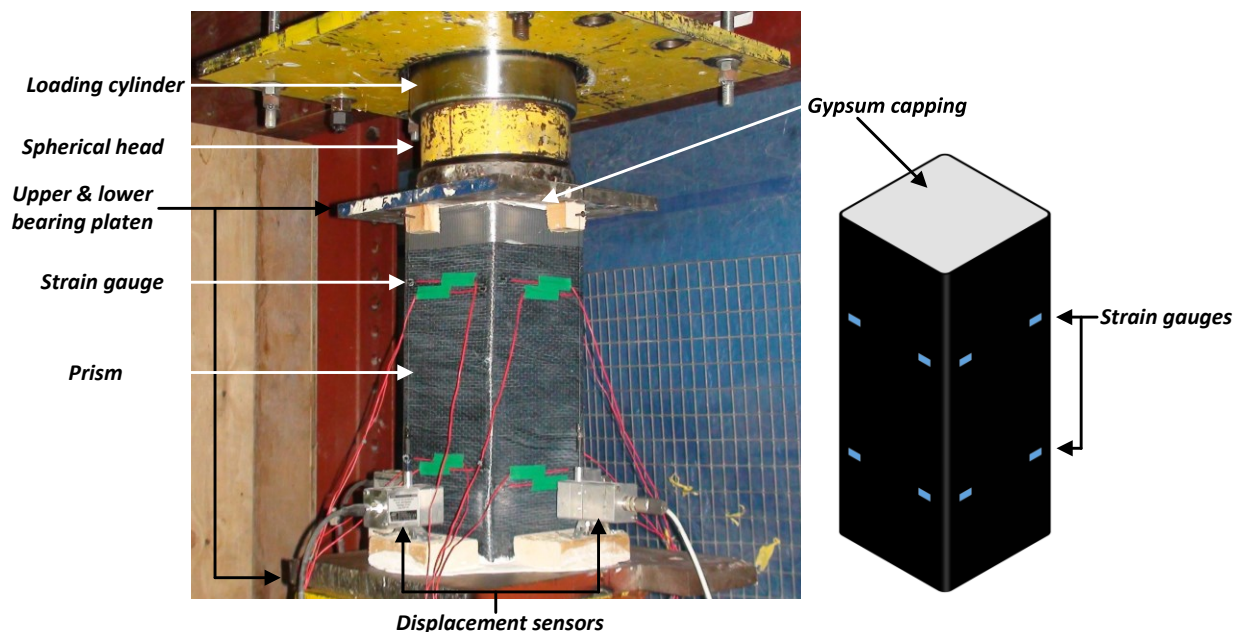
Figure 3.9 Typical test setup and instrumentation for wrapped prims.

3.3 Experimental results and discussions

3.3.1 Failure modes

The three unwrapped control specimens showed vertical cracks at maximum load followed by separation between the faces of the masonry blocks, leading to spalling of the face shells and end webs. Figure 3.10 shows failure modes of unwrapped prisms at the end of the compression tests. The failure of CFRP wrapped prisms was always by tensile rupture of the CFRP jacket. The damage of CFRP confined prisms at the end of the tests can be seen in Figure 3.11. Axial stress-

strain curves in Figure 3.12 show that when the load reached the peak and the descending branch of stress-strain curves started, the failure was initiated by local CFRP snapping near the prism corners due to local stress concentration in the jacket. The local rupture of CFRP straps subsequently decreased the load. The prism continued carrying load until a sudden rupture of the entire CFRP jacket with a loud sound followed by an abrupt load drop. The failure of composite jackets occurred near the corners in the medium portion of the confined prisms. After the test, a close visual examination of the prism revealed a strong bond between the CFRP jacket and the external masonry substrate (Figure 3.11(g)). The separation was mainly between the face shell of block and the grouted core or was in the mid of the face shell. No debonding between CFRP layers at the overlapping zone was noticed. Mainly this premature failure was avoided by providing the sufficient overlap length. Also, it was observed that the cores of CFRP wrapped prisms were severely crushed more than unconfined concrete masonry prisms (Figure 3.11(h)).

(a)   *(b)*   *(c)*   *(d)*   *(e)*
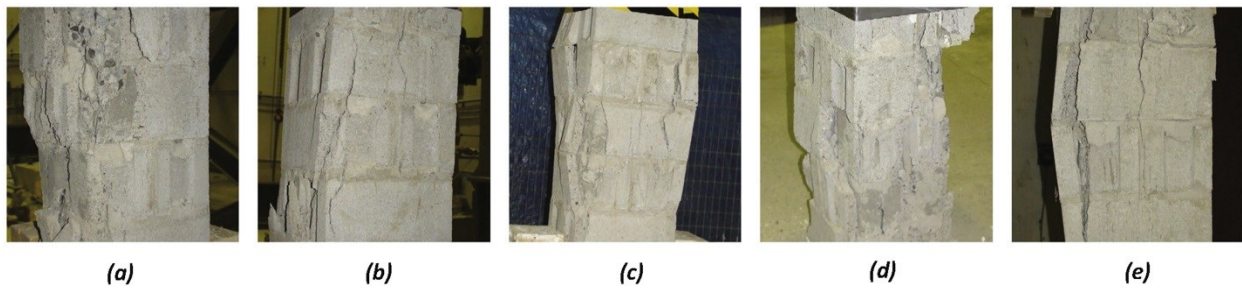
Figure 3.10 Failure modes of unwrapped prisms at the end of the compression tests: (a) R0-L0-1; (b), (c) R0-L0-2; (d), (e) R0-L0-3.
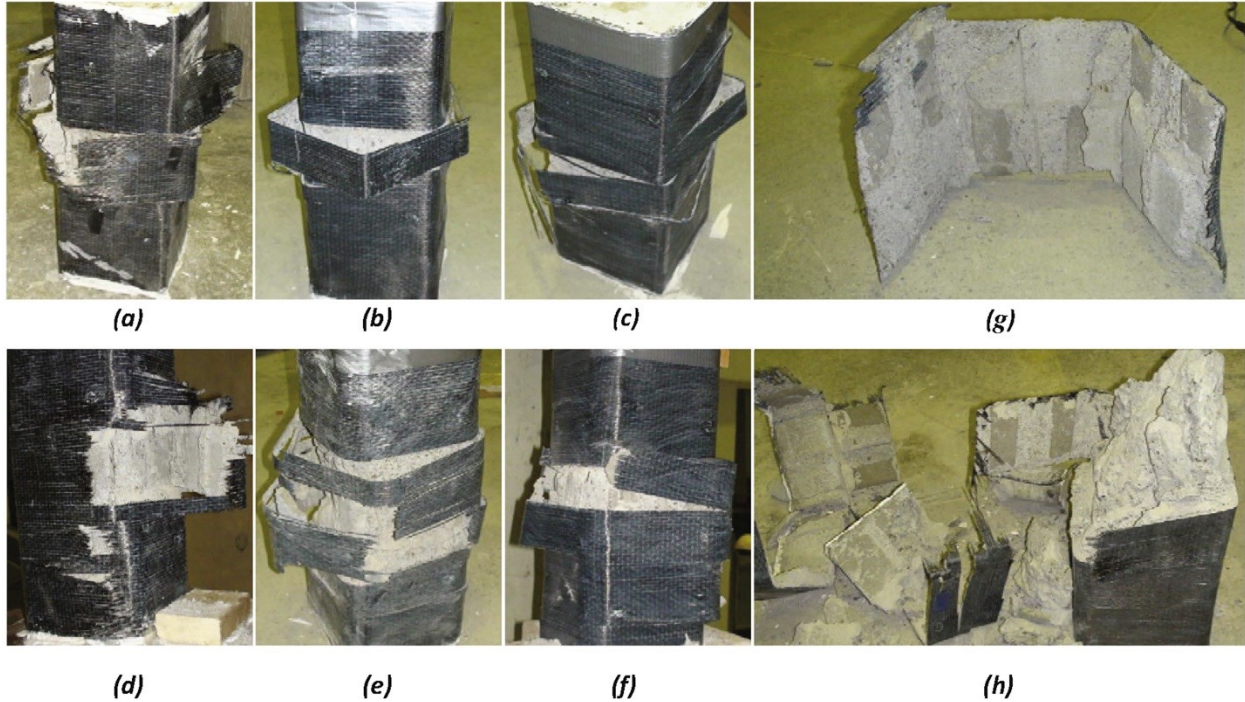
Figure 3.11 Failure modes of CFRP confined prisms at the end of the compression tests: (a) R10-L1; (b) R10-L2; (c) R10-L3; (d) R30-L1; (e) R30-L2; (f) R30-L3; (g) strong bond between CFRP and masonry; (h) severely crushed core.

3.3.2 Axial stress-strain curve

The axial stress-strain curves of all test prisms are shown in Figure 3.12. The axial stress is calculated as the force measured by the load cell divided by the area of the cross section considering the respective corner radius of the prism. The axial strain is the average reading of the four displacement sensors divided by gauge length equal to the prism height. The experimental results from axial compression tests with the average and (COV) are summarized in Table 3.3 and Table 3.4, where f_{md} is unconfined masonry strength; ε_m and ε_{mu} are axial strains at peak and ultimate axial strain of unconfined masonry corresponding to 0.85 f_{md} along the descending branch of the stress-strain curve, respectively. Also f_{mcd} is peak strength of confined masonry. ε_{mc} and ε_{mcu} are axial strains at peak and the axial strain at 15% strength degradation for confined masonry, respectively. The definition of the usable ultimate axial strain of confined or unconfined masonry at 15% strength degradation is arbitrary, although being consistent with ACI 440.2R-08 (2008) guideline.
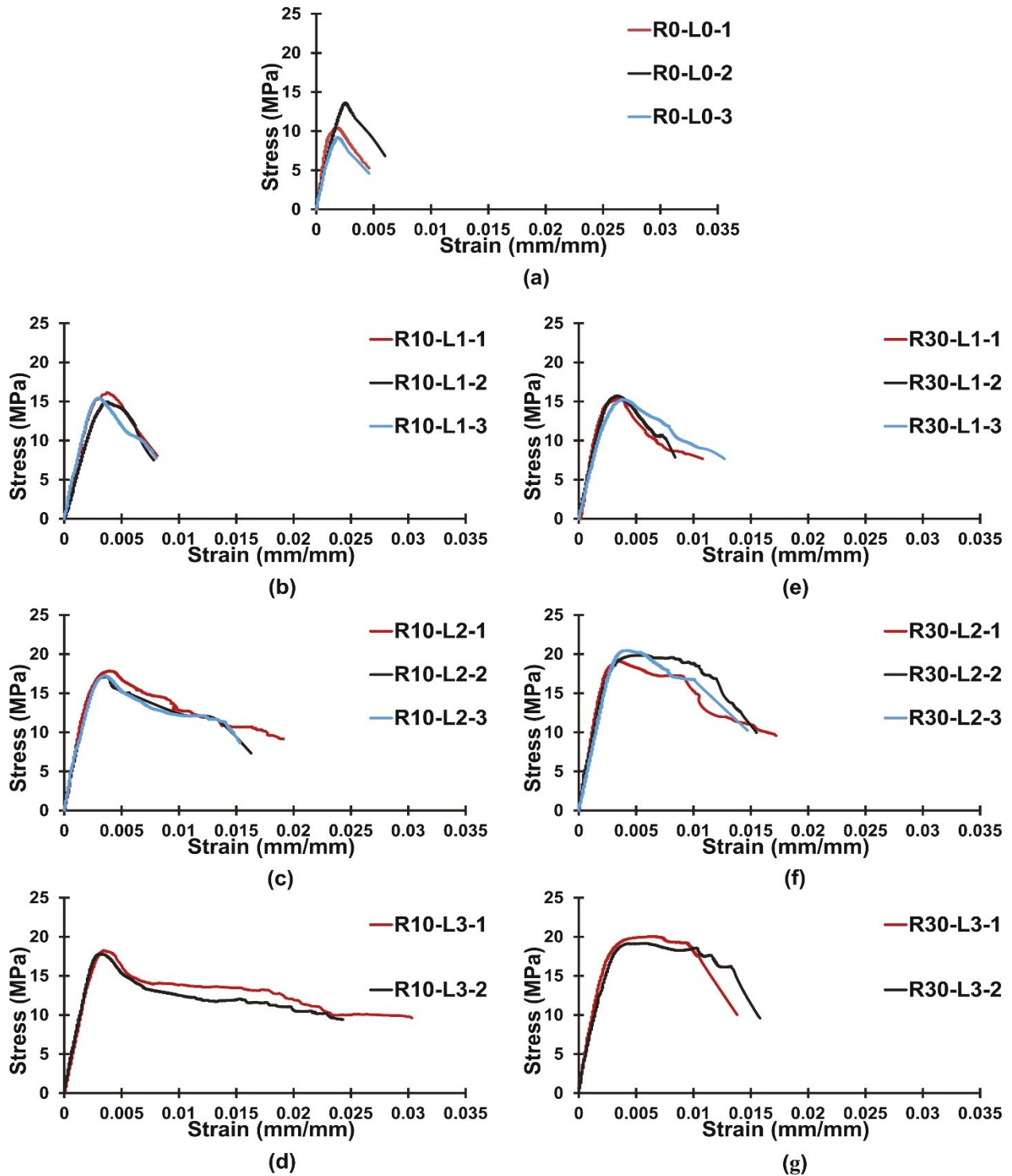
Figure 3.12 Axial stress-strain curves of all test sets: (a) R0-L0; (b) R10-L1; (c) R10-L2; (d) R10-L3; (e) R30-L1; (f) R30-L2; (g) R30-L3.

Table 3.3 Compressive strengths and ultimate axial strains of the unconfined prisms.

Prism	f_{md} (MPa)	Average and COV (%)	ε_m (mm/mm)	Average and COV (%) (%)	ε_{mu} (mm/mm)	Average and COV (%)
R0-L0-1	10.47		0.0018		0.0027	
R0-L0-2	13.63	11.10 20.6	0.0026	0.0021 20.8	0.0035	0.0030 15.6
R0-L0-3	9.19		0.0019		0.0027	

Table 3.4 Compressive strengths and ultimate axial strains of the CFRP confined prisms.

Prism	f_{mcd} (MPa)	Average and COV (%)	ε_{mc} (mm/mm)	Average and COV (%)	ε_{mcu} (mm/mm)	Average and COV (%)
R10-L1-1	16.15		0.0038		0.0054	
R10-L1-2	14.98	15.54 3.8	0.0037	0.0035 12.5	0.0059	0.0052 13.5
R10-L1-3	15.48		0.0030		0.0045	
R10-L2-1	17.85		0.0040		0.0068	
R10-L2-2	17.05	17.39 2.4	0.0039	0.0038 5.4	0.0063	0.0063 7.9
R10-L2-3	17.25		0.0036		0.0058	
R10-L3-1	18.26	18.03 1.8	0.0035	0.0033 8.6	0.0054	0.0053 2.7
R10-L3-2	17.80		0.0031		0.0052	
R30-L1-1	15.35		0.0034		0.0048	
R30-L1-2	15.75	15.46 1.6	0.0033	0.0035 7.6	0.0052	0.0055 16.2
R30-L1-3	15.29		0.0038		0.0065	
R30-L2-1	19.13		0.0034		0.0095	
R30-L2-2	19.90	19.84 3.4	0.0052	0.0043 20.9	0.0118	0.0098 19.6
R30-L2-3	20.49		0.0043		0.0080	
R30-L3-1	20.07	19.63 3.2	0.0063	0.0061 5.8	0.0107	0.0114 9.3
R30-L3-2	19.19		0.0058		0.0122	

All tested prisms exhibited a parabolic ascending portion of stress-strain curves followed by a descending branch, instead of featuring bi-linear stress-strain curves reported for FRP confined concrete prisms. However, the average peak stresses and ultimate axial strains at 15% strength degradation in confined prisms are much higher than the corresponding average stress and ultimate axial strain in unconfined prisms. It can be concluded that confining by CFRP jackets is an effective method for strengthening concrete block masonry columns. The unreinforced prisms possess the steeper descending branch and the R30-L2 and R30-L3 sets showed almost a plateau

region near the peak strength followed by a sudden drop. It is observed that the increase in CFRP jacket thickness makes the slope of the descending branch less steep.

The axial stress-strain curves for one prism from each set of tested prisms are shown in Figure 3.13 for a convenient comparison between sets. The unconfined control specimens exhibited a brittle behaviour with a steep drop in strength after reaching the peak load. It was observed from stress-strain curves for the one-layer specimens that all six prisms exhibited enhancement in the post peak behaviour by softening the descending branches of the stress-strain relationships compared to unreinforced prisms. For the two-layer prisms, the descending branches of the stress-strain curves showed more ductile behaviour than the one-layer sets. Also, the slope of the descending branches of the stress-strain curve of R30-L2 set is flatter than R10-L2 set which is related to the corner radius increasing. For the three-layer prisms, the higher confinement increased the ductility of prisms. The R30-L3 set almost demonstrates a plateau region near the peak strength. On the other hand, the R10-L3 showed more ductile behaviour after a slight drop in strength.
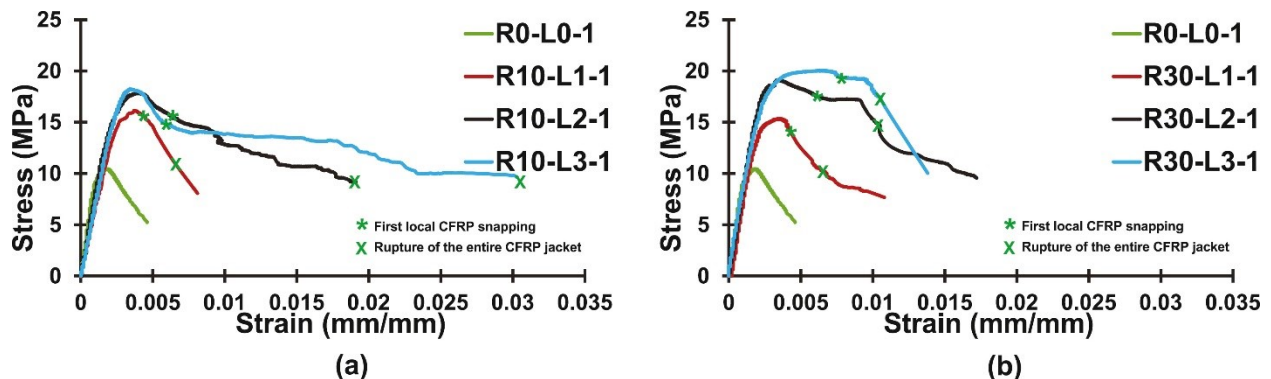
Figure 3.13 Axial stress–strain curves for one specimen from each set: (a) prisms rounded with 10 mm; (b) prisms rounded with 30 mm.

To assess the effect of confinement provided by CFRP jackets, strength and strain gains of confined masonry are presented in Table 3.5. The strength gain is defined as the peak stress of confined prisms divided by the average compressive strength of the unconfined control specimens and the strain gain is defined as the ultimate axial strain of confined masonry divided by the average ultimate axial strain of unconfined masonry at 15% strength degradation.

Table 3.5 Strength and strain gains of CFRP confined concrete prisms.

10 mm corner radius					30 mm corner radius					Average R30 / R10	
PRISM	$\dfrac{f_{mcd}}{f_{md}}$	Average	$\dfrac{\varepsilon_{mcu}}{\varepsilon_{mu}}$	Average	Prism	$\dfrac{f_{mcd}}{f_{md}}$	Average	$\dfrac{\varepsilon_{mcu}}{\varepsilon_{mu}}$	Average	f_{mcd}	ε_{mcu}
R10-L1-1	1.46		1.80		R30-L1-1	1.38		1.60			
R10-L1-2	1.35	1.40	1.95	1.74	R30-L1-2	1.42	1.39	1.72	1.82	0.99	1.05
R10-L1-3	1.39		1.49		R30-L1-3	1.38		2.16			
R10-L2-1	1.61		2.28		R30-L2-1	1.72		3.18			
R10-L2-2	1.54	1.57	2.10	2.10	R30-L2-2	1.79	1.79	3.94	3.26	1.14	1.55
R10-L2-3	1.55		1.92		R30-L2-3	1.85		2.67			
R10-L3-1	1.64	1.62	1.80	1.77	R30-L3-1	1.81	1.77	3.56	3.81	1.09	2.15
R10-L3-2	1.60		1.74		R30-L3-2	1.73		4.07			

The average strength gain for 10 mm rounded corner prisms with one, two, three layers were 40%, 57%, and 62% higher than the strength of control specimens, respectively. On the other hand, the strength increased by 39%, 79%, and 77% for 30 mm rounded corner prisms with one, two, three layers, compared to control specimens, respectively. All prisms showed a significant increase in term of peak strength if compared to control specimens. Therefore, CFRP jacketing is clearly an effective method to confine concrete block masonry columns. In general, providing CFRP jackets reduced the scatter of test results, which usually found in the axial stress of concrete block masonry prisms. The axial stresses of confined prisms showed low COV compared to control specimens in Table 3.3 and Table 3.4. The average strength gains for sets R10-L1 and R30-L1 are almost identical. This is mainly due to the low confinement effect eliminates the positive effect of rounding the corner radius. The average strength gain were 12% and 29% for 10 mm and 30 mm rounded corner prisms with two-layer compared to the one-layer prisms, respectively. It can be observed that increasing the thickness of jackets by a second layer of CFRP provided a noticeable gain in the axial strength compared to the one-layer prisms. The average change in strength gain was about 3% between R10-L3 and R10-L2. In case of R30-L3, the average axial strength gain dropped 1% compared to R30-L2. It can be concluded that adding a third layer of CFRP did not lead to a significant gain in the axial strength compared to the two-layer prisms. However, adding a third layer of CFRP improved significantly the ultimate strain compared to two-layer prisms.

This observation indicates a polynomial relationship between confinement levels and the strength gain of concrete masonry prisms. This is in agreement with the model proposed by Farnia (2011). However, considering the natural variability typically found in testing masonry and considering that only two prisms with three layers have been tested and compared against three prisms with two layers which expected to produce less reliable average and COV data. The authors suggest further experimental work by testing concrete masonry prism confined with much higher levels of confinement to validate this observation. In fact, the high level of confinement would eliminate the uncertainties due to the natural variability of masonry. Based on experimental data obtained by this work and Farnia (2011), assuming a polynomial relationship between confinement levels and the strength gain of concrete masonry columns seems to be reasonable.

On the other hand, the R30-L2 reached, on average, 14% higher strength compared to the R10-L2. In the case of three layers, the difference decreased to 9% between R30-L3 and R10-L3. That is attributed to the increasing in corner radius of cross section, which increased the effectively confined area.

For one layer prisms with 10 mm corner radius, R10-L1, the average increase of ultimate axial strain were 74% higher than unreinforced prisms. The R10-L2 and R10-L3 prism sets gave an average ultimate axial strain increase of 110% and 77%, compared to control specimens, respectively. The reduction in ultimate axial strain at 15% degradation between R10-L3 and R10-L2 are mainly caused by the sharp drop of stress-strain curve after the peak in the R10-L3 set. However, R10-L3 prisms showed 67% increase in average ultimate axial strain at 50% degradation compared to R10- L2. Large increment of ultimate axial strain compared to control specimens have been observed for prisms rounded with 30 mm. The prisms gave an average ultimate axial strain increase of 82%, 226%, and 281% for R30-L1, R30-L2, and R30-L3, respectively. It can be observed that increasing the jacket thickness increased the strain ductility of prisms. The ultimate axial strain of R30-L1 reached 5% higher than R10-L1 due the deference in corner radius. In case of two layers, the difference in the ultimate axial strain between R30-L2 and R10-L2 were 55%. R30-L3 and R10-L3 prisms exhibited higher difference equal to 115%.

3.3.3 Effective tensile strain in CFRP jackets

For accurate estimation of the confinement pressure due to CFRP jacketing, a precise measurement for the effective tensile strain in CFRP jackets is required. The average readings of the effective tensile strain of CFRP jackets at the peak strength along the faces of the prism are shown in Figure 3.14. Each value represents average of six or four measurements on CFRP jacket. Two longitudinal strain gages, one at the top and one at the bottom of prism, multiplied by three, or two replicate specimens. The erroneous readings are excluded from the average in case the strain gauge debonded during the preparation or the test. Figure 3.14 demonstrates that the strains at CFRP laminate at maximum loads are very low. R30-L2 set reached maximum average value at one face equal to 2838 µstrain. Figure 3.15 shows average effective tensile strain in CFRP jackets at 15% strength degradation. It can be clearly seen that the CFRP strain significantly increased up to 5541 µstrain in R30-L2 set.

R10-L1

1399	1090
1371	1038
1041	1145
1296	1450

R30-L1

1756	1710
1535	1487
1200	1797
1236	1410

R10-L2

1933	2464
1343	2010
1161	1943
1558	1504

R30-L2

1709	2518
2838	1520
1607	1663
2552	2102

R10-L3

1272	1756
1526	1003
1454	2810
1138	1034

R30-L3

2307	1816
2071	1984
1909	1252
1944	1534
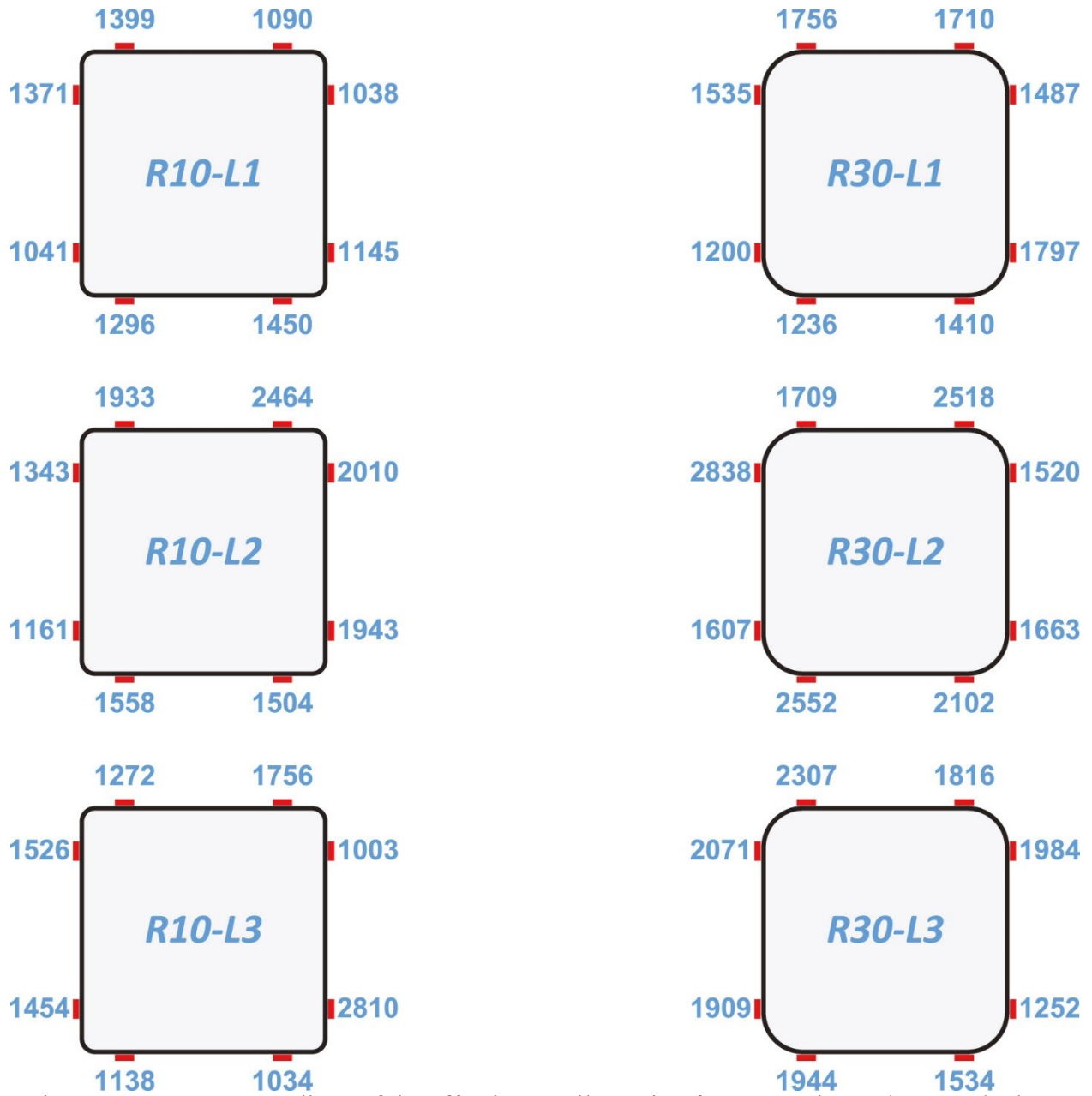
Figure 3.14 Average readings of the effective tensile strain of CFRP at the peak strength along the faces of the prism (all readings in μstrain).
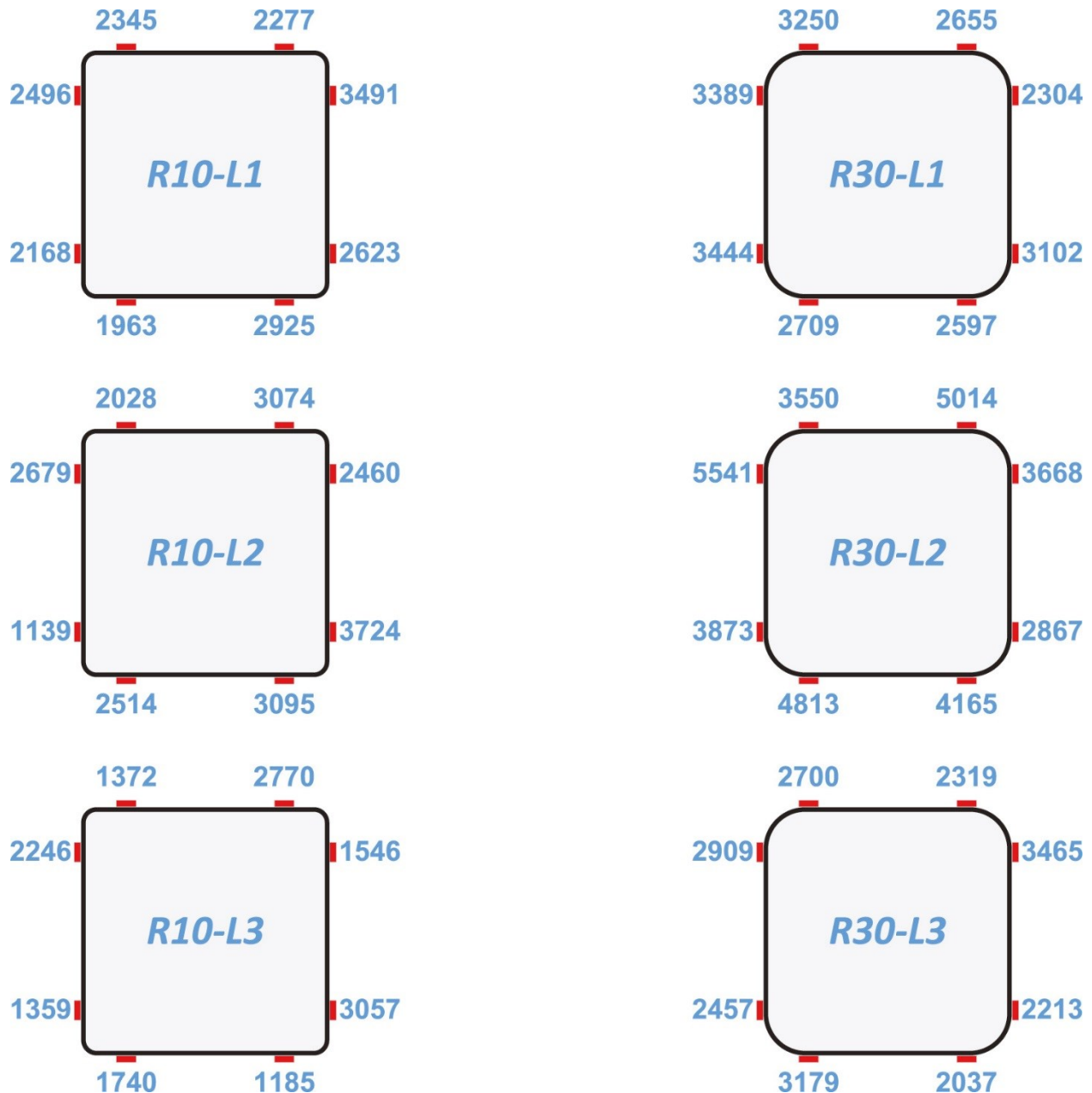
Figure 3.15 Average readings of the effective tensile strain of CFRP at 15% strength degradation along the faces of the prism (all readings in μstrain).

Table 3.6 presents the normalized effective tensile strain in CFRP jackets at peak strength and at 15% strength degradation to the ultimate strain of CFRP laminate obtained by tensile flat coupon tests. Each value represents the average readings of all strain gages applied on the set of prisms. Average 48 strain gages reading in case of the set consists three replicate prisms and average readings of 32 strain gages when the set has only two replicate prisms. The strain ε_p is the effective tensile strains within the CFRP jackets at peak strength, whereas ε_u is the effective tensile strains

of CFRP jackets at 15% strength degradation, and ε_{fu} is average of the maximum ultimate strain of CFRP laminates provided by tensile flat coupon tests.

Table 3.6 The comparison of the CFRP effective tensile strains at peak strength, at 15% strength degradation and the ultimate strain of CFRP flat coupon tests.

Set	At maximum strength			At 15% strength degradation			Gain ratio
	ε_p (µstrain)	COV (%)	$\varepsilon_p/\varepsilon_{fu}$ (%)	ε_u (µstrain)	COV (%)	$\varepsilon_u/\varepsilon_{fu}$ (%)	$\varepsilon_u/\varepsilon_p$
R10-L1	1330	76	10	2559	71	19	1.92
R10-L2	1767	75	13	2550	70	19	1.44
R10-L3	1499	56	11	1909	66	14	1.27
R30-L1	1526	58	11	2963	57	22	1.94
R30-L2	2077	58	16	4210	41	32	2.03
R30-L3	1852	52	14	2714	58	20	1.47

From Table 3.6, it is clearly seen that the strain profile in CFRP jackets at peak load and at 15% strength degradation along the perimeter of the prisms was highly non-uniform. This is confirmed by the high coefficient of variation values. The phenomenon of non-uniform strain distribution in CFRP jacket is believed to be due that the heterogeneous combination of grout, concrete masonry blocks, and mortar promotes the formation of localized deformation and cracks since the deformation compatibility between the composite jacket and concrete masonry prism is assumed. Furthermore, hand lay-up method creates fibre misalignment and produces variable thickness in the epoxy layer which influences the strain in the CFRP jackets.

Table 3.6 illustrates that the CFRP strains of 30 mm rounded prisms are greater than those of 10 mm corner radius with the same confinement level. Generally, the strain in CFRP jacket increases when the corner radius increases because the sharp edge effect has been reduced. One important observation is that the effective tensile strains in CFRP jacket at 15% strength degradation is much higher than CFRP strain at maximum load carrying capacity. The increase ranges between 27 and 103%. This indicates jacketing does not provide enough confinement pressure at maximum strength of prisms compared to that provided at the ultimate failure. The increase of confinement during the descending branch of the stress-strain curve mainly affects the axial strain of the prims, which explains the higher gain in the strain comparing to the gain in strength.

The ratios of the measured tensile strain in CFRP jacket to the ultimate tensile strain of the flat coupon test for peak loading and 15% strength degradation are reported in Table 3.6. At peak strength, the ratio fell between 10% and 16%. At 15% strength degradation, this ratio increases to range between 14% and 32%. Only 18 out of 256 strain gages instrumented on the CFRP jackets captured strain values higher than 10000 µstrain at around 50% strength degradation which is lower than the ultimate strain of CFFR material 13400 µstrain. The difference between the measured strain in the CFRP jacket and the ultimate strain of coupon test has been well researched in different works related to concrete confined by FRP (e.g. Refs. (Mirmiran et al., 1998; Shahawy et al., 2000; Harries and Carey, 2003; Lam and Teng, 2003, 2004; Cui, 2009; Zinno et al., 2010; Lignola et al., 2012; Wu and Jiang, 2013b; Alecci et al., 2014)). Various reasons have been proposed for this phenomena, including: stress concentration in FRP jacket produced by cracked concrete, which is expected to be more in masonry considering the heterogeneity of masonry; the curvature of the FRP jacket, especially in non-rounded corner columns; overlap regions in the FRP jacket; multiaxial stress condition generated on the FRP jacket; accidental load eccentricity caused by imperfections in the specimen or in the test setup; imperfections in manufacturing process or the laying-up process of fibre sheets; and uniformity of the resin in FRP laminate.

3.4 Comparison of analytical predictions with experimental results

The confinement model, recommended by the Italian design guideline CNR-DT 200 R1 (2013), will be assessed in this section. The experimental results are compared with the last updated version of the technical document for the use of FRP systems for strengthening existing structures published by the Italian National Research Council (CNR) in May 2014. The technical document provides an analytical confinement model to predict strength gains of masonry columns confined with FRP composites. The nonlinear confinement model suggests expressing the compressive strength of masonry columns confined with FRP as follows:

$$f_{mcd} = f_{md} \cdot \left(1 + k' \cdot \left(\frac{f_{l,eff}}{f_{md}}\right)^{\alpha_1}\right) \qquad \text{Eq. 3-1}$$

where f_{mcd} is characteristic compressive strength of FRP-confined masonry, f_{md} is compressive strength of masonry, $f_{l,eff}$ represents the effective confining pressure, and α_1 is a coefficient equal to 0.5 if further experimental data is not available. Unless a more detailed analysis is performed, the non-dimensional coefficient k' is indicated as the masonry mass density in kg/m^3 divided by

1000. The effective confining pressure, f_{leff} is a function of the cross section shape and the FRP system as follows:

$$f_{l,eff} = k_{eff} \cdot f_l = k_H \cdot k_V \cdot f_l$$ <div align="right">Eq. 3-2</div>

where k_{eff} is the coefficient of efficiency expressed as the product of a horizontal and vertical coefficient of efficiency, k_H and k_V , respectively, and f_l is the lateral confining pressure. For square or rectangular cross sections with continuous FRP wrapping, the confinement lateral pressure can be calculated as follows:

$$f_l = 2 \cdot \frac{t_f \cdot E_f}{\max\{b, h\}} \cdot \varepsilon_{fd,rid}$$ <div align="right">Eq. 3-3</div>

where E_f and t_f , are the tensile modulus of elasticity of FRP jacket and the FRP thickness. The calculation of the theoretical prediction in this section is based on nominal thickness of cured laminate at 0.381 mm for one layer and 69.36 GPa tensile modulus of elasticity of CFRP jacket obtained by flat coupon test. The width b and the thickness h are the cross section dimensions. The reduced design value of the FRP strain, $\varepsilon_{fd,rid}$, can be computed as follows:

$$\varepsilon_{fd,rid} = \min\left\{n_a \cdot \frac{\varepsilon_{fk}}{\gamma_f}; 0.004\right\}$$ <div align="right">Eq. 3-4</div>

where n_a is the environmental conversion factor, ε_{fk} and γ_f represent characteristic rupture strain and the partial factors of FRP sheets, respectively, and 0.004 is the maximum allowed strain. The environmental and safety coefficients n_a and γ_f were taken equal to one. Value of $\varepsilon_{fd,rid}$ equals to 0.004 was adopted while calculating the effective confining pressure for theoretical predictions. The coefficient of efficiency of square or rectangular columns confined by external FRP wrapping is:

$$k_{eff} = k_H \cdot k_V$$ <div align="right">Eq. 3-5</div>

$$k_H = \left(1 - \frac{b'^2 + d'^2}{3A_m}\right)$$ <div align="right">Eq. 3-6</div>

with $b' = b' - 2r_c$ and $h' = bh' - 2r_c$, r_c is cross section corner radius, and A_m masonry column area, as shown in Figure 3.1. For a continuous FRP wrapping, the vertical coefficient of efficiency k_V is equal to one. The confinement model suggests different formulas to calculate the lateral

confining pressure for circular and rectangular masonry columns in case of non-continuous FRP wrapping and in case of installing FRP sheets with fibre bars running in the orthogonal direction of the strengthened column. However, these formulas are out of scope of this work. The comparison between the experimental results and CNR-DT 200 R1 theoretical predictions can be seen in Figure 3.16. Strength gains f_{mcd}/f_{md} are plotted against $f_{l,eff}/f_{md}$. Differences between experimental results and theoretical predictions are calculated in Table 3.7. The absolute error is equal to the absolute value of experimental value minus theoretical prediction divided by the experimental value. The performance of confinement model was evaluated by using three statistical metrics: The mean absolute percentage error (MAPE), the mean square error (MSE) and the absolute fraction of variance (R^2).

$$MAPE = \frac{\sum_{i=1}^{n} \left| \frac{\exp_i - theo_i}{exp_i} \right|}{n} \qquad \text{Eq. 3-7}$$

$$MSE = \frac{\sum_{i=1}^{n}(\exp_i - theo_i)^2}{n} \qquad \text{Eq. 3-8}$$

$$R^2 = 1 - \left(\frac{\sum_{i=1}^{n}(exp_i - theo_i)^2}{\sum_{i=1}^{n} theo_i} \right) \qquad \text{Eq. 3-9}$$

where $theo$ is the theoretical prediction, exp is the experimental data, and n is the total number of data.

$$\frac{f_{mcd}(exp)}{f_{mcd}(theo)} = 0.992 \qquad COV = 4.90\% \qquad \begin{aligned} MPAE &= 8.87\% \\ MSE &= 0.025 \\ R^2 &= 0.986 \end{aligned}$$
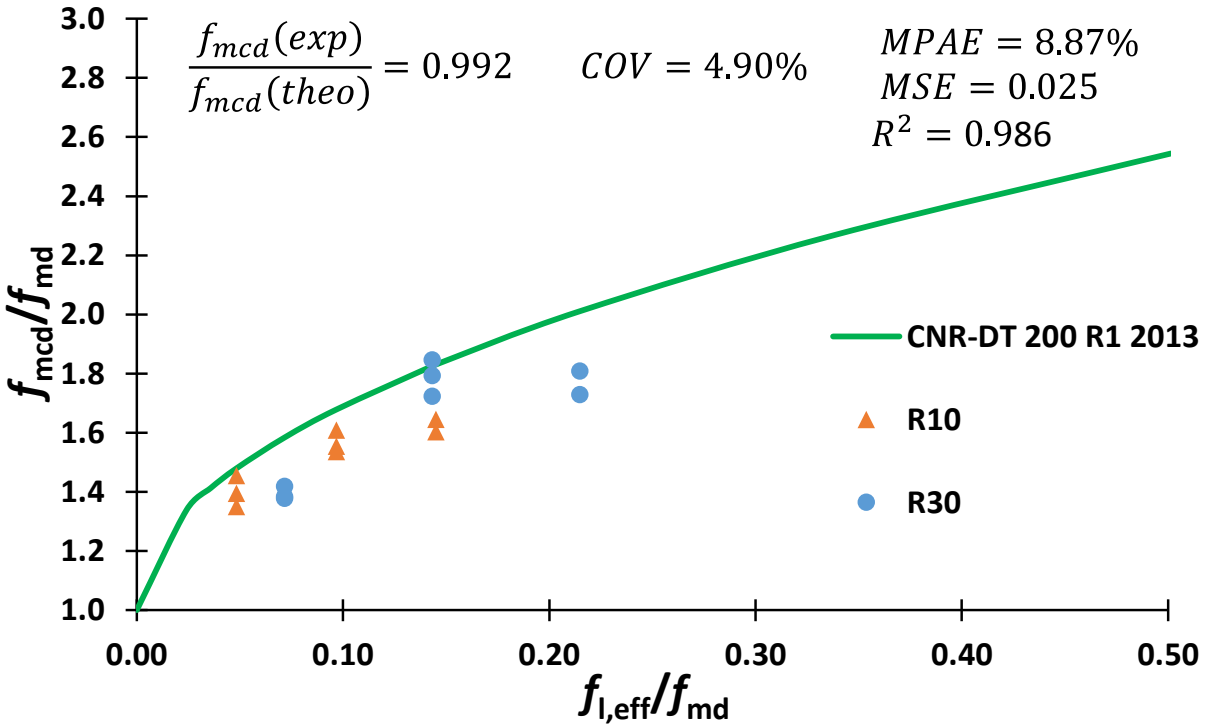
Figure 3.16 Comparison between the experimental results and the theoretical predictions by CNR-DT 200 R1.

From both Figure 3.16 and Table 3.7, It can clearly concluded that theoretical model (CNR-DT 200 R1 (2013)) can provide a good correlation between experimental data and theoretical prediction. Figure 3.16 points out that the mean absolute percentage error is 8.87%. However, the model generally gives non-conservative predictions for concrete masonry columns confined with CFRP composite. The accuracy of the model could be improve by refining the theoretical expression against the experimental data.

The main difference between the experimental data and theoretical prediction comes from that the CNR-DT 200 R1 model overestimates the effective strain in CFRP jacket which lead to overestimate the effective confining pressure. According to the experimental test data, the maximum average strain in the CFRP jackets at peak strength was 2077 µstrain which is 48% lower than the strain limit 4000 µstrain set by the theoretical model. Reducing the maximum allowed strain to 2000 µstrain would improve the accuracy of the model and reduce the mean absolute percentage error (MAPE) to 4.92% with absolute fraction of variance (R^2) equal to 0.992. The refined model gives conservative predictions with average ratio of experimental data to

theoretical predictions around 1.05. The comparison between the experimental results and refined CNR-DT 200 R1 theoretical predictions are shown in Figure 3.17.

Table 3.7 Comparison between theoretical predictions and experimental results.

Prism	Experimental results	Theoretical predictions CNR-DT 200 R1/2013		Difference between experimental result and theoretical predictions		
	f_{mcd}/f_{md}	$f_{l,eff}/f_{md}$	f_{mcd}/f_{md}	$\dfrac{f_{mcd}\,(exp)}{f_{mcd}\,(theo)}$	Absolute error (%)	Average absolute error (%)
R10-L1-1	1.46			0.98	1.67	
R10-L1-2	1.35	0.05	1.48	0.91	9.61	5.79
R10-L1-3	1.39			0.94	6.10	
R10-L2-1	1.61			0.96	4.33	
R10-L2-2	1.54	0.10	1.68	0.92	9.25	7.19
R10-L2-3	1.55			0.93	7.98	
R10-L3-1	1.64	0.15	1.83	0.90	11.31	12.75
R10-L3-2	1.60			0.88	14.19	
R30-L1-1	1.38			0.87	14.51	
R30-L1-2	1.42	0.07	1.58	0.90	11.62	13.70
R30-L1-3	1.38			0.87	14.96	
R30-L2-1	1.72			0.94	5.94	
R30-L2-2	1.79	0.14	1.83	0.98	1.83	2.96
R30-L2-3	1.85			1.01	1.11	
R30-L3-1	1.81	0.21	2.01	0.90	11.24	13.79
R30-L3-2	1.73			0.86	16.34	
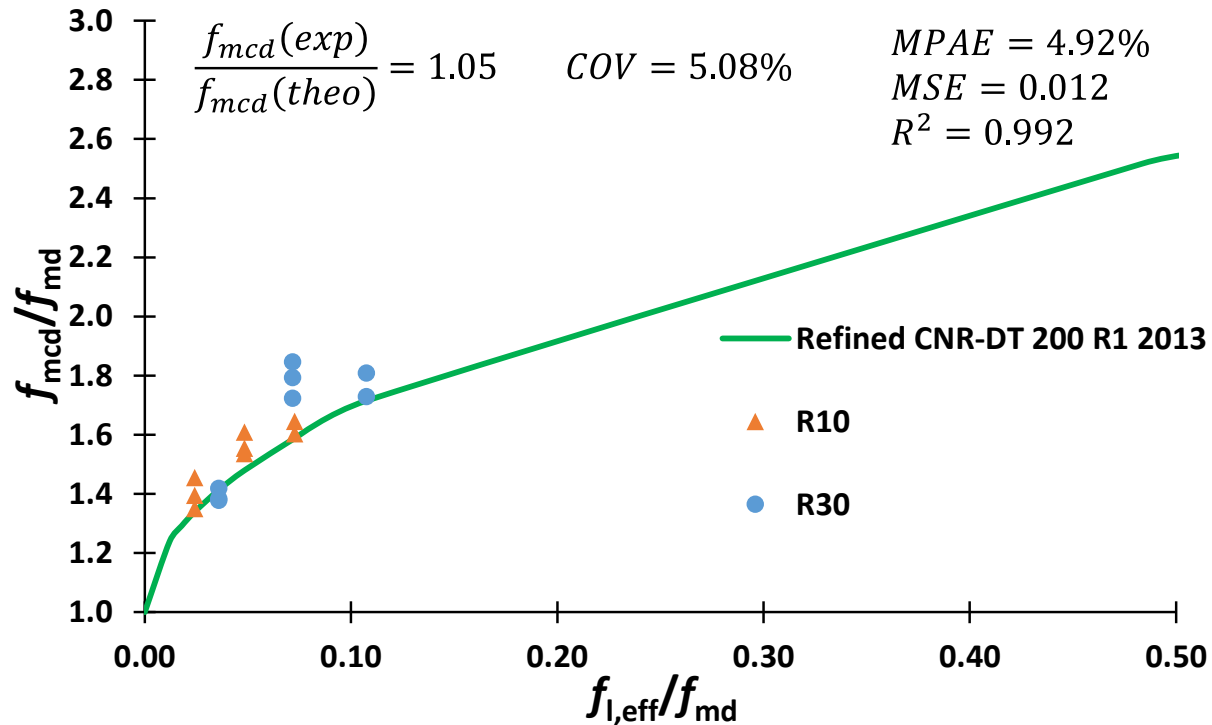
Figure 3.17 Comparison between the experimental results and refined CNR-DT 200 R1 theoretical predictions.

3.5 Conclusions

This paper presents an experimental investigation on the influence of CFRP confinement on the axial stress-strain behaviour of concrete block masonry columns. Scaled fully grouted concrete masonry prisms with a square cross section were confined by continuous CFRP jackets to upgrade their performance level by increasing the ductility and the axial load capacity. The experimental investigation studied the role of corner radius and the CFRP jackets thickness in increasing the axial load and the ultimate strain. The tensile strain in CFRP jacket was measured in order to identify the CFRP lateral confining pressure. The experimental results of testing CFRP concrete masonry prisms has been used to assess and calibrate the analytical model suggested by CNRDT 200 R1 to predict strength gain of masonry column confined by FRP composites.

The following conclusions are drawn from the test results of 19 half-scale concrete block masonry prisms confined with CFRP:

- CFRP jacketing proved to be an effective method for confining concrete block masonry columns. CFRP jacket significantly increased the peak strength and ultimate axial strain of the confined prisms compared to unreinforced prisms.

- Concrete masonry columns confined with CFRP sheets exhibits enhancement in the post peak behaviour by softening the descending branches of the stress-strain relationships compared to unreinforced prisms.

- A higher corner radius provides a higher ultimate axial strain for prisms with the same level of confinement.

- The CFRP strain profile at peak load and 15% strength degradation along the perimeter of the prisms are highly non-uniform.

- The tensile strains measured on the CFRP Jackets are lower than the average ultimate tensile strain obtained by flat coupons test.

- The tensile strain in CFRP jacket increases when the corner radius increases.

- CFRP jacketing provides higher confinement pressure at 15% strength degradation compared to that provided at the maximum strength of prisms.

- The refined CNR-DT 200 R1 theoretical model can provide a good correlation with the experimental data with mean absolute percentage error around 4.92%.

Experimental tests were conducted on CFRP confined concrete masonry columns to collect necessary data to assess the CNR-DT 200 R1 theoretical model. The refined theoretical expression shows low mean absolute percentage error. However, further experimental works investigating different FRP materials and considering various geometries of concrete masonry unites are required to generalize the findings.

Chapter 4

Experimental Study of CFRP-Confined Reinforced Concrete Masonry Columns Tested Under Concentric and Eccentric Loading

Abstract

Using Carbon Fibre Reinforced Polymers (CFRP) jackets to confine existing concrete masonry columns for capacity and ductility enhancement has been approved in axial compression applications. Considering that the majority of columns in practice are loaded under a combination of axial compression load and bending moment, experimental work for testing reinforced concrete masonry columns confined by CFRP jackets under eccentric loading is needed. This paper presents the results of testing 28 half-scale fully grouted reinforced concrete masonry columns under different concentric and eccentric loading conditions as well as variations in CFRP jacketing. The ability of CFRP jackets to improve the structural performance is evaluated. Axial force-bending moment interaction diagrams of confined reinforced concrete masonry columns are compared against the unconfined masonry columns to quantify the enhancement in axial and moment capacities. The results indicate that increasing the CFRP jacket thickness enhanced the performance of masonry columns regarding axial strain and strength; however, there was a noticeable reduction in strength gain under strain gradient condition upon increasing the eccentricity level. Also, axial force-bending moment interaction diagrams of confined masonry columns showed an increase in the load and the moment capacity compared to that of unconfined masonry columns.

4.1 Introduction

Rehabilitation is becoming an inevitable alternative for restoring deteriorated existing structures or for extending their service lives, especially that demolishing un-efficient structures and constructing new ones can be costly and time consuming, and in some cases not feasible. Confining existing reinforced concrete and masonry columns by steel jacketing used to be a common method for upgrading them in the past (Pantazopoulou et al., 2001). The confining effect of the jacket increases the axial capacity and improve the ductility of the strengthened columns. However, the steel jacketing system is often associated with difficulty in the assembly on the site and poor corrosion resistance on the long-term.

In the past two decades, Fiber Reinforced Polymers (FRP) materials started taking the place of traditional retrofit techniques due to their superior characteristics. High strength to lightweight ratio, durability, ease of handling and application, corrosion resistance, and minimal dead load added to the cross section are the main advantages that promoted the use of FRP materials in strengthening existing columns.

FRP sheets can be wrapped around the column to form FRP jacket where fibres are aligned along hoop direction and perpendicular to the load axis of the column. FRP sheets are bonded to the surface of the column using a high strength adhesive. The external confining would increase the axial capacity of the column to meet the additional loading demand or improve the ductility behaviour in order to satisfy the expected seismic performance.

Extensive research studies have been conducted to understand the behaviour of reinforced concrete columns confined with FRP composites. However, few researchers investigated the application of FRP composites in retrofitting masonry columns. Most of these studies focused on the behaviour of masonry columns strengthened with unidirectional fibres sheets and tested under concentric loads. Masonry columns constructed with clay, tuff, or limestone blocks and strengthened with different FRP jackets were experimentally studied in Masia and Shrive (2003), Di Ludovico et al. (2010) and Faella et al. (2011b). Recent studies have investigated the behaviour of masonry columns confined by FRP strips in Micelli et al. (2014b), Witzany et al. (2014) and Witzany and Zigler (2015). Several researchers tested concrete masonry columns strengthened with carbon FRP in (e.g., Farnia (2011); Galal et al. (2012); and Alotaibi and Galal (2017)). Milani

et al. (2017) carried out numerical analysis on FRP retrofitting of the columns and walls of three masonry churches to resist seismic action.

Despite the fact that the majority of columns in practice are loaded under a combination of axial compression load and bending moment, most of the previous studies focused on the behaviour of masonry columns under axial compression force only. Several design codes and guidelines (NZS 4230:2004, 2004; BS 5628, 2005; EN 1996-1-1, 2005; CSA S304-14, 2014; TMS 402/602-16, 2016) require masonry columns to resist the minimum bending moment which could be introduced by unintentional load eccentricity or non-straight construction of the masonry columns.

Shaheen and Shrive (2007) tested steel reinforced clay masonry columns under eccentric axial loading. The masonry columns were strengthened by sprayed GFRP laminate in two thicknesses. They concluded that eccentricity reduced the effect of the confinement and decreased the gain in strength caused by sprayed GFRP laminate on masonry columns if compared to concentrically loaded masonry columns. Further, Shaheen and Shrive (2007) tests on masonry columns as well as few eccentric tests reported for concrete columns in (Li and Hadi, 2003; Hadi, 2006, 2007; Maaddawy, 2009; Bisby and Ranger, 2010; Hadi and Widiarsa, 2012) appear to confirm that the eccentricity decreases the confinement effectiveness. However, no tests as of yet have been reported for reinforced concrete masonry columns wrapped with CFRP and tested under different levels of eccentricity.

This paper presents the results of an experimental program designed to improve the understanding of the axial and flexural performance of reinforced concrete masonry columns confined by CFRP jackets under eccentric loading. The ability of CFRP jackets to resist the axial strain gradient resulting from axial and flexural loading is evaluated. Axial force-bending moment interaction diagrams of reinforced concrete masonry columns confined with one and two layers of CFRP jackets are compared against non-strengthened concrete masonry columns to quantify the improvement in axial and moment capacities.

4.2 Experimental program

The experimental program consisted of testing 28 half-scale fully grouted reinforced concrete masonry columns under different loading conditions and variations in CFRP jacketing. All

masonry columns were constructed and tested in the Structures Laboratory at Concordia University.

4.2.1 Design of masonry columns

All masonry columns were constructed by professional masons using half-scale concrete "C" pilaster units. Each masonry column was fully grouted and had a square cross section with a side length of 190 mm. The masonry column was formed by laying ten concrete block layers in running bond pattern with 5 mm Type S mortar.

The masonry column was internally reinforced by four deformed steel bars of #4 with 12.7 mm nominal diameter. The bars were symmetrically placed in the grout at approximately 48 mm from the centreline of the cross section. D4 deformed cold drawn wires with 5.7 mm diameter were used as transverse ties. The 135° standard hook ties were spaced at 60 mm apart. All masonry columns have 1.4% longitudinal steel reinforcement ratio which is higher than the minimum ratios specified by the following standards: (NZS 4230:2004, 2004; BS 5628, 2005; EN 1996-1-1, 2005; CSA S304-14, 2014; TMS 402/602-16, 2016).

The 945 mm height masonry column was connected to a top and bottom high strength concrete footing with 200x200x250 mm dimensions. The longitudinal steel reinforcements were continuously extended from the bottom footing to the top footing without any lap splices. Ties formed from #4 reinforcement bars with 90° standard hook were used to confine the longitudinal reinforcements in the footings. Reduced spacing of 40 mm was maintained through high strength footings to increase the rigidity of ends. The concrete footings were introduced to prevent premature failure of the masonry columns ends and to distribute the load uniformly on masonry and the longitudinal steel reinforcements. Typical dimensions and construction details of reinforced masonry column are presented in Figure 4.1(a).
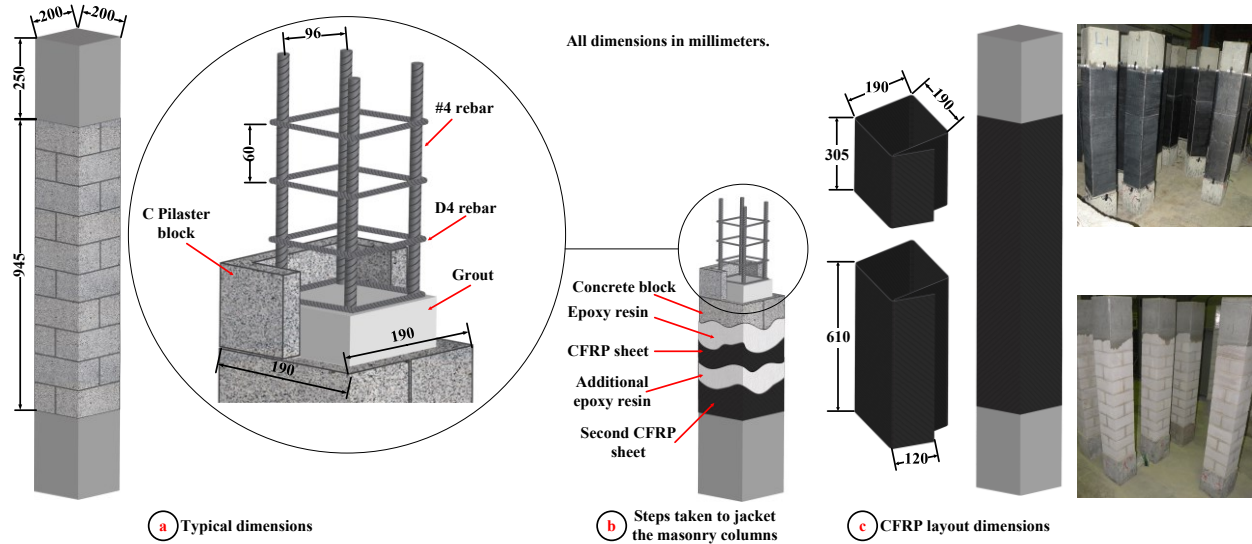
Figure 4.1 Typical dimensions and construction details of reinforced masonry column.

The general properties of the test matrix are given in Table 4.1. The essential variables in the testing program were the thickness of CFRP jacket and loading condition. The test columns varied from unwrapped masonry columns to wrapped masonry columns by one or two layers of CFRP composite jackets. Loading condition was varied between monotonic uniaxial compressive loading, small or large eccentric loading and flexural loading.

The masonry columns were divided into three major groups to investigate the influence of using CFRP jacketing and magnitude of load eccentricity on the compressive and flexural behaviour of reinforced concrete masonry columns. The first group is unwrapped reinforced concrete masonry columns to establish control data. The group consisted of four subgroups. The first subgroup is tested under pure monotonic uniaxial compressive loading, where second and third subgroups were tested under different monotonically increasing eccentric–compression loading. Two eccentricities of 20 and 40 mm were applied. Compared to the masonry column width of 190 mm, the 20 mm eccentricity can be assumed small eccentricity (e/t=0.11) and 40 mm eccentricity can be considered relatively large eccentricity (e/t=0.21). The last subgroup was tested as a beam under four-point-bending loading. The second and third group consisted of reinforced concrete masonry columns strengthened with CFRP composite jackets. These two groups are similar with the only difference being the number of composite layers where the second and third groups were strengthened with one and two layers of CFRP jackets, respectively. In wrapped masonry columns groups, no beam testing was conducted assuming no contribution of the CFRP-confinement for strengthening columns under pure bending moment without any axial force.

72

Each subgroup of columns consisted of three replicate masonry columns in order to generate average data. Each masonry column is given a notation as LN-eX-# or LN-B. The L, e and B letters stand for CFRP Layers, test eccentricity and Bending, respectively. The numbers N and X indicate the number of CFRP layers, and the magnitude of test eccentricity in millimetres, respectively. The symbol # is the replicate number in the subgroup. For example, masonry column L0-e40-1 is the first replicate of an unwrapped masonry column tested with 40 mm eccentricity.

Table 4.1 Test matrix.

Group	Subgroup	Number of replicates	Longitudinal reinforcement			Transverse reinforcement		Number of CFRP layers	Test eccentricity (mm)
			Number of bars	Bar. No	Reinforcement ratio (%)	Bar. No	Spacing (mm)		
1	L0-e0	3	4	#4	1.4	D4	60	-	0
	L0-e20	3							20
	L0-e40	3							40
	L0-B	1							Bending
2	L1-e0	3	4	#4	1.4	D4	60	1	0
	L1-e20	3							20
	L1-e40	3							40
3	L2-e0	3	4	#4	1.4	D4	60	2	0
	L2-e20	3							20
	L2-e40	3							40

The construction of reinforced concrete masonry columns started with assembling the reinforcement steel cages. Wooden formwork was used to shape the bottom concrete footing. After centring steel cages in the formwork and ensuring the verticality, high strength concrete mixes were poured in several batches to cast the bottom footings. Manual compaction by steel rods was preferred because the footings have relatively small dimensions. The surface of the footing was levelled and smoothed manually by trowels. After curing the concrete, the masons placed mortar on the top of the concrete footing and started laying concrete blocks by placing every two blocks together in alternating directions along the height. After five days of finishing the masonry work, fine grout was cast in the masonry columns using three-layered pouring procedure to ensure the uniformity of the grout and to reduce the lateral pressure on the masonry assembly. Wooden formworks were attached to the top of masonry columns to form the top concrete footings. Same

high concrete design mix was used to cast the top footings. The fresh concrete was compacted by steel rods and levelled manually.

Eighteen columns out of 28 reinforced concrete masonry columns were strengthened with CFRP jackets. The surface of masonry columns was prepared before wrapping CFRP sheets. All corners of the wrapped masonry columns were rounded to 10 mm radius using an electric grinder to reduce stress concentrations and to enhance the confining effect of the CFRP jackets on masonry section. Unsmoothed bed joints were sanded. After that, the masonry surface was vacuumed from dust.

The steps for wrapping the masonry columns are summarized in Figure 4.1(b). CFRP roll of 610 mm sheet width was used to wrap the masonry test region. There were no CFRP layers applied on the high strength concrete footings. Minimum of 120 mm overlapping in the direction of the fibres was always maintained to ensure the effectiveness of the wrapping and to avoid debonding premature failure. The overlapping area was always placed on the same face of the masonry columns. No overlapping in the axial direction of the masonry column was applied. The hoop and axial overlapping are consistent with recommended values by the manufacturer's specifications (Sikawrap Hex 230C). Considering the limited width of CFRP sheet rolls, the masonry columns were wrapped by two straps, with 610 and 305 mm width, in the axial direction of the column to form the CFRP composite jackets. Details about layout dimensions and CFRP jackets geometrical details are presented in Figure 4.1(c). Dry lay-up procedure was followed to wrap the CFRP sheets circumferentially around the masonry columns one month after columns construction. After cutting CFRP sheet to the desired lengths, the resin and hardener of Sikadur® 330 were combined and mixed slowly with low speed drill for 3 min until the components were uniform in colour. Paint rollers were used to directly apply the mixed epoxy resin onto the prepared masonry surfaces. Starting from the bottom of masonry column, the 610 mm width sheet of the first strap was placed onto epoxy resin. The air pockets were removed by pressing a roller on the laminate to squeeze out the resin between the fibres.

In order to apply second layers of CFRP sheets, the lay-up process continues by adding more epoxy on the previous layer without stopping. Then, a 305 mm wide CFRP sheet is placed higher than the lower strip in order to cover the whole column height, and the same dry lay-up procedure

was followed. The wrapped masonry columns were left to cure for seven days in the laboratory environment before being tested.

4.2.2 Material properties

The half-scale concrete pilaster units adopted in this study resemble the 8x8x16 inch concrete masonry "C" Pilaster units that could be used to construct concrete masonry columns and concrete masonry pilaster walls. The nominal dimensions of the half-scale and full-scale blocks are illustrated in Figure 4.2. Ten coupons were cut from half-scale pilaster units according to ASTM C140/C140M-15ae1 (2015) with 25x100x50 mm nominal dimensions to determine the compressive strength of the block. Gypsum material was used as high strength capping in order to distribute uniform loads to the ends of coupons. The average compressive strength of concrete block coupons was 21.73 MPa, based on net area equals to 2500 mm^2, with coefficient of variation (COV) around 9.4%. According to ASTM C140/C140M-15ae1 (2015), three half-scale concrete pilaster blocks were tested to obtain the density, absorption, and moisture content of blocks. The average density was 2171 kg/m^3 (COV = 0.7%) and the average absorption was 125.3 kg/m^3 (COV = 0.5%). The half-scale concrete pilaster blocks has moisture content about 11.7% (COV = 7.2%).
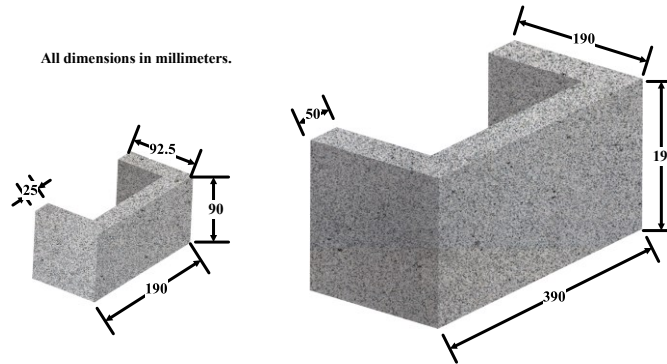
Figure 4.2 The nominal dimensions of the half-scale and full-scale blocks.

Ready-to-use grout and mortar mixes, commercially available, were used during the construction of masonry columns to achieve more consistency. The concrete masonry columns were grouted with a fine grout, according to ASTM C476-10 (2010). Each 30 kilogram ready to use grout bag was mixed with 5.4 litres of water to produce designed grout with 15 MPa strength. An initial grout slump of 280 mm was measured. For determining the compressive strength, the fine grout was cast in cylindrical moulds with 100 mm diameter and 200 mm height. The grout cylinders were tested in the same period of masonry columns testing after 28 days of curing. Ten grout cylinders have average compressive strength of 15.23 MPa (COV = 5.0%). Type S mortar

according to ASTM C270e14a (2014) was used to bond pilaster units. The mortar has 12.40 MPa (COV = 4.3%) as average compression strength for five compression tests conducted on 51 mm cubes of mortar according to ASTM C270e14a (2014).

Three unreinforced masonry prisms constructed with ten courses high were tested in order to obtain an average compressive strength of grouted concrete masonry (f_{md}). Even though ASTM C1314-16 (2016) specifies a height to thickness ratio of two, ten courses prism would give a better presentation of the actual behaviour of masonry columns tested in this paper. The average of tests was 10.96 MPa with (COV = 1.7%).

Deformed carbon-steel reinforcing bars with imperial bar size #4, also known as "No. 13" in the metric system, were used as grout reinforcement and ties in high strength concrete footings. Reinforcing bars meet the requirements of ASTM A615/A615M-16 (2016). The #4 reinforcement steel was designated as Grade 60 [420 MPa] with 129 mm^2 nominal area. Deformed carbon-steel reinforcing wire of D4 was used as ties to confine the vertical reinforcement steel in the grout of masonry columns. The wires were manufactured according to ASTM A1064/A1064M-17 (2017) and have a nominal area of 25.8 mm^2. For determining the characteristics of the reinforcing bars and obtaining typical tensile stress-strain curves, five tensile specimens for each bar size were tested according to ASTM A370-17 (2017) with 200 mm measured gauge length. The stress-strain curves of tensile specimens are shown in Figure 4.3. The average mechanical properties of reinforcement steel obtained from tension tests are summarized in Table 4.2.
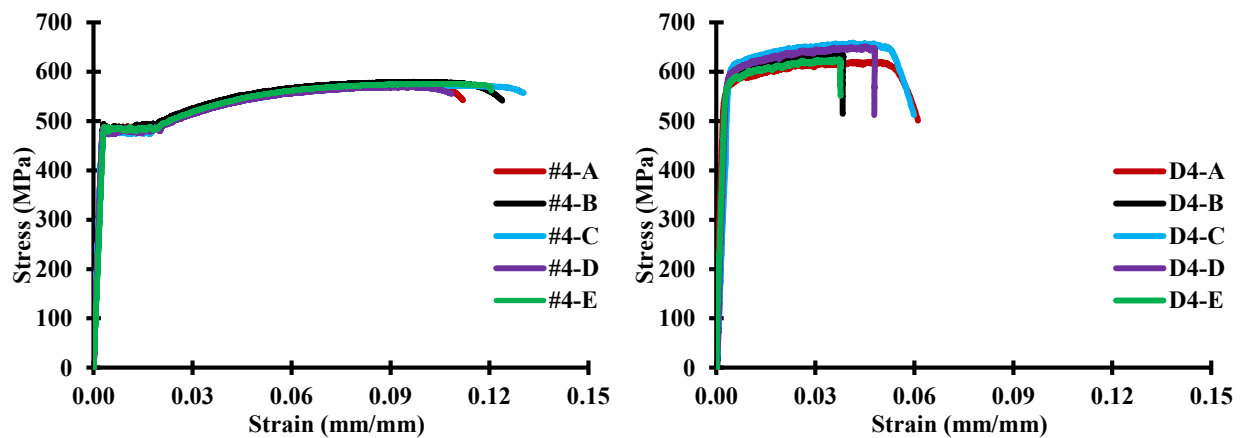
Figure 4.3 The stress-strain curves of reinforcement steel.

Table 4.2 Average mechanical properties of reinforcing bars.

Bar type	Nominal diameter (mm)	Nominal area (mm²)	Yield strength (MPa) and COV	Yield strain (mm/mm) and COV	Tensile strength (MPa) and COV	Ultimate strain (%) and COV
#4	12.7	129	483.0 (0.8%)	0.0024 (7.4%)	573.5 (0.8%)	10.9 (10.5%)
D4	5.7	25.8	588.3 (2.4%)	0.0031 (15.6%)	632.8 (2.5%)	4.5 (15.4%)

High strength concrete mix was used to cast the bottom and top footings of reinforced concrete masonry columns. The mix proportion of the materials used to produce high strength concrete is given in Table 4.3. Five 75x150 mm cylinders were cast from mix batches. The cylinders were tested under compression test in the same period of testing the masonry columns to determine the compressive strength of the concrete. The minimum strength of the cylinders was 79.61 MPa with an average around 83.66 MPa (COV = 5.4%).

Table 4.3 The mix proportion of high strength concrete.

Ratio to cement weight	Ordinary Portland cement	Water	Fine aggregate	Coarse aggregate	Superplasticizers
	1	0.3	1.1	2	390 ml for 100 kg cement

Reinforced concrete masonry columns were retrofitted with a structural strengthening system of CFRP composite. SikaWrap® Hex 230C, a unidirectional carbon fibre fabric, was used in conjunction with Sikadur® 330 epoxy laminating resin to give a dry lay-up composite strengthening system. According to the product's datasheet in (Sikawrap Hex 230C), the cured laminate has a nominal thickness of 0.381 mm, and the CFRP composite has 894 MPa ultimate tensile strength with 65.40 GPa modulus of elasticity. The ultimate tensile strain of CFRP laminate can reach 1.33%.

4.2.3 Test set-up and instrumentation

Twenty-eight fully grouted reinforced masonry columns built with half-scale concrete blocks were evaluated under different loading conditions. Nine tests were conducted with pure monotonic uniaxial compressive loading, where eighteen tests were conducted under monotonically increasing eccentric–compression loading with small and large eccentricity. One masonry columns was tested as a beam under four-point-bending loading.

A loading cylinder attached to a rigid steel frame and connected to an electro-hydraulic control testing system was utilized to generate the compression load on concentric and eccentric tested columns. A load cell between the frame and loading cylinder measured the applied force. All readings were recorded and monitored by a data acquisition connected to the instrumentations.

For masonry columns tested with concentric load, both ends of the tested column were capped with 50 mm thick steel bearing plates levelled by high strength gypsum materials. The eccentricity was eliminated by placing a steel spherical head on the top of tested masonry column. Two laser lines were used to ensure the masonry column and the spherical head were centred under the loading cylinder to avoid any eccentricity and maintain uniform load distribution. Four linear variable inductance transducer (LVIT) sensors were used to measure the axial deformation of tested columns. The LVITs were bonded to the rigid top concrete footing and linked to the bottom footing. The LVITs were placed at the centrelines of the four sides near the end of masonry work. In some selected masonry columns, four strain gages with gauge length of 5 mm were bonded on the mid-height of longitudinal steel reinforcements to monitor the compression strains. Test setup and instrumentation of tested column are presented in Figure 4.4(a).

Eccentric loading was applied to the masonry columns by means of specially designed loading mechanism. A two set of loading heads manufactured from steel plates and rods were placed at bottom and top of the masonry column. The loading heads composed of cylindrical steel rollers with 37 mm diameter passed between two 50 mm thick steel plates and welded to the bearing plates. This loading mechanism ensures hinged ends boundary condition of eccentrically tested masonry columns about one axis and fixed ends condition about the perpendicular axis. The bottom and top rollers were centred with the loading cylinder axis in both directions by means of two laser lines guide. The axis of tested masonry column was shifted from the loading cylinder axis to achieve the desirable initial eccentricity in one direction. The loading cylinder axis and the masonry column axis were centred in the perpendicular direction. High strength gypsum was used to bond and level the bearing plates. Four LVITs sensors were mounted on the top concrete footing to measure the axial deformation of masonry column, where two LVITs sensors at the compression face and two LVITs sensors at the tension face. For wrapped masonry columns, the overlap zones were always placed out of compression and tension faces to reduce the effect of overlapping on the results. Additional LVIT fixed to the wooden supporting frame was used to monitor the lateral displacement of the masonry column. The LVIT was levelled at the mid-height of the masonry

column on the tension face of the section. The lateral displacement was measured to account the second order moment effect. Selected masonry columns were instrumented with four strain gages at the mid-height of longitudinal steel reinforcements to capture the compression and tension strains. Test setup and loading heads are shown in Figure 4.4(b).

A monotonic uniaxial compressive load was applied in both concentric and eccentric tests until a significant reduction in column strength was achieved. Eccentric and concentric masonry columns were loaded using two loading protocols. For unwrapped masonry columns, the load was increased monotonically with a crosshead speed rate of 0.3 mm/min up to the peak load. After this, the crosshead speed was adjusted to 0.03 mm/min to help to capture the post peak behaviour. The test of wrapped masonry columns was preformed at 0.3 mm/min speed for the cross-head during the entire test period.

The typical setup of the masonry column tested as a beam under four-point-bending loading is shown in Figure 4.4(c). The beam was loaded with a pin and a roller supports at the ends with centre-to-centre distance of 700 mm. The distance between the middle loading rollers is 300 mm. A load cell integrated into the testing machine was used to record the load. Two LVITs sensors were placed under the beam to measure the mid-span deflection. The beam was instrumented with four strain gages bonded to the longitudinal steel reinforcements in order to capture strains at the mid-span.
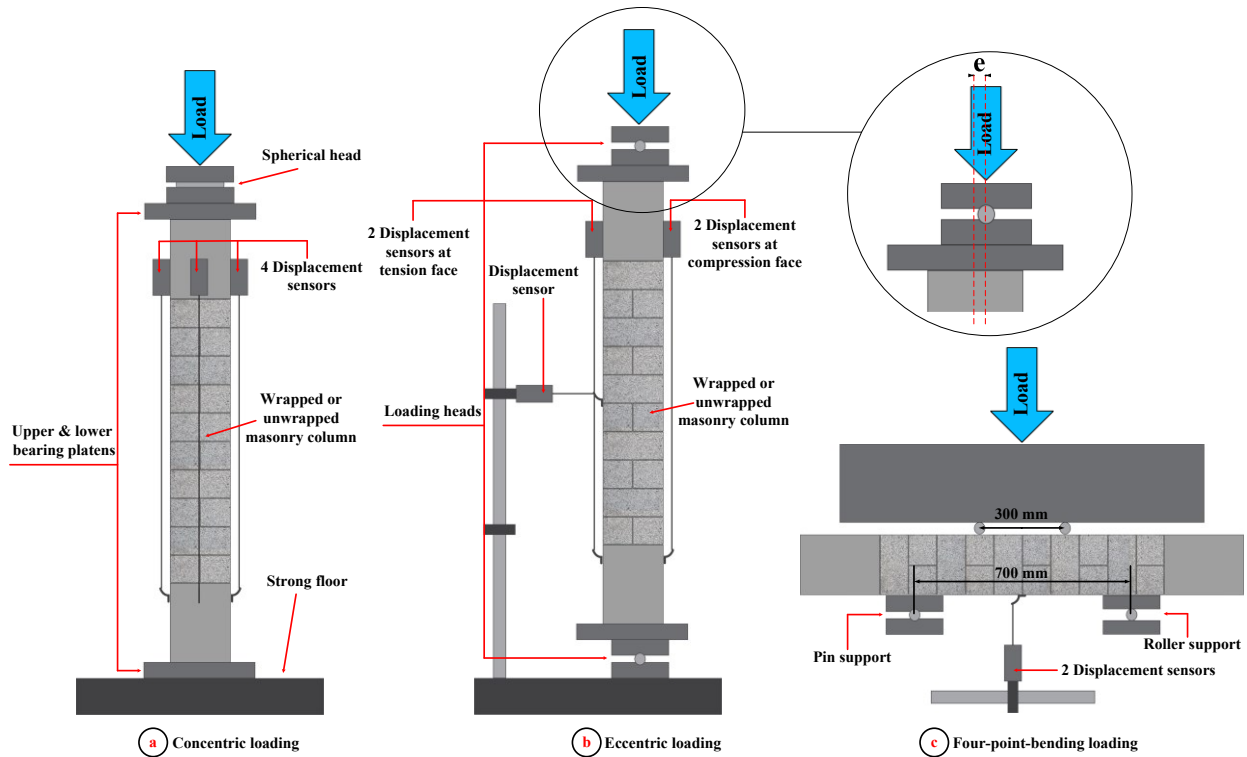
Figure 4.4 Test setup and instrumentation for masonry columns.

4.3 Experimental results and discussions

4.3.1 Behaviour under concentric and eccentric loading

4.3.1.1 Failure modes

The failure modes of the compression columns at the test end are shown in Figure 4.5. The unwrapped masonry columns showed vertical cracks at the peak load. During the post peak, mild buckling of the longitudinal steel reinforcements between the ties was accompanied by face shells spalling and separation between blocks and grout. The failure of strengthened masonry column was dominated by a tensile rupture of CFRP fibres. When the descending branch of axial load-deformation curves started, local stress concentrations near the masonry column corners induced local CFRP snapping and load decreasing. The opening of CFRP jacket caused an abrupt load drop. CFRP wrapped masonry columns exhibited severe steel reinforcement buckling between ties. The CFRP jackets did not show any debonding between CFRP layers at the overlapping zones or separation between the masonry substrates and the CFRP jackets. The failure of masonry columns always occurred in the test region between the footings. Unwrapped masonry columns showed damage at most of the column height where the masonry columns strengthened with CFRP

jackets sustained small damage zone. Also, it was observed that the damage in the grout of CFRP wrapped columns was severe compared to unwrapped masonry columns.

Crushing of concrete masonry   *Mild steel buckling*   *Rupture of the CFRP jacket*   *Severe steel buckling*
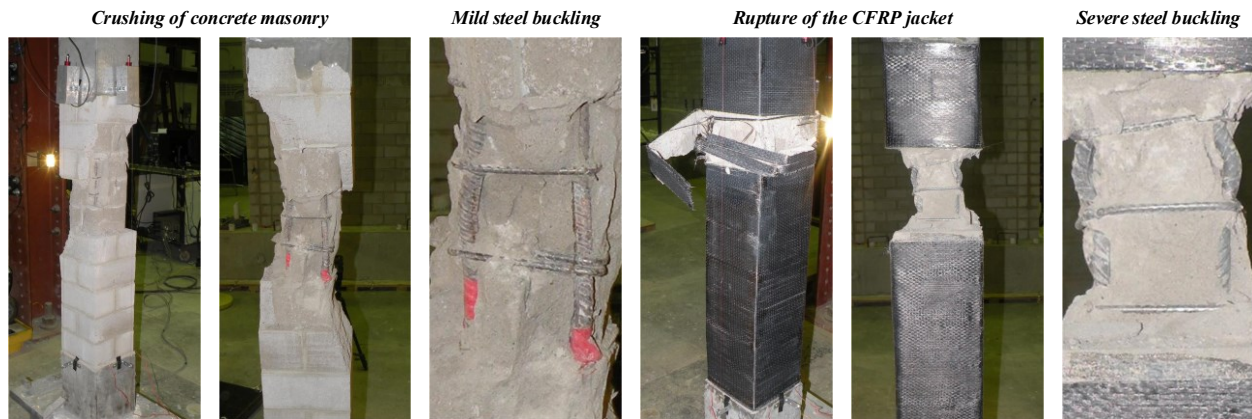
Figure 4.5 Failure modes of the compression columns at the end of the test.

Typical failure modes of masonry columns tested under eccentric loading are shown in Figure 4.6. The failure of non-strengthened masonry columns was grout crushing and spalling of large portions of concrete masonry in the compression face. The opening of mortar joints and vertical tensile cracks were noticed in the tension faces. For masonry column wrapped with CFRP jackets and tested under eccentric loading, the failure at the compression face was concrete blocks crushing with tensile CFRP snapping at the face corners. The mortar joints opened in the tension face. However, there was no tensile CFRP rupture at the compression face of the two-layer masonry columns tested with larger eccentricity. More discussions on the sequence of the failure are presented in the following sections.

Compression face   *Tension face*   *Compression face*   *Tension face*
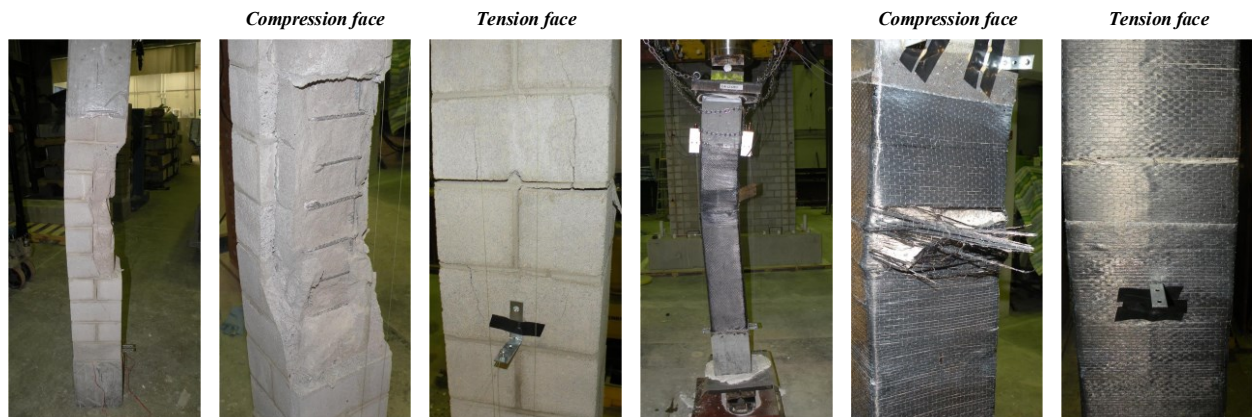
Figure 4.6 Typical failure modes of masonry columns tested under eccentric loading.

4.3.1.2 Load capacity versus axial and lateral deformations

The applied load versus axial deformation of concentric-loaded masonry columns are shown in Figure 4.7. The measured axial force was plotted versus the average reading of the four LVIT sensors over the masonry assembly height. For the masonry columns tested with initial axial load eccentricities, the average reading of the two LVIT sensors on compression faces and the reading of the lateral LVIT sensor were plotted against the load cell reading in Figure 4.8.
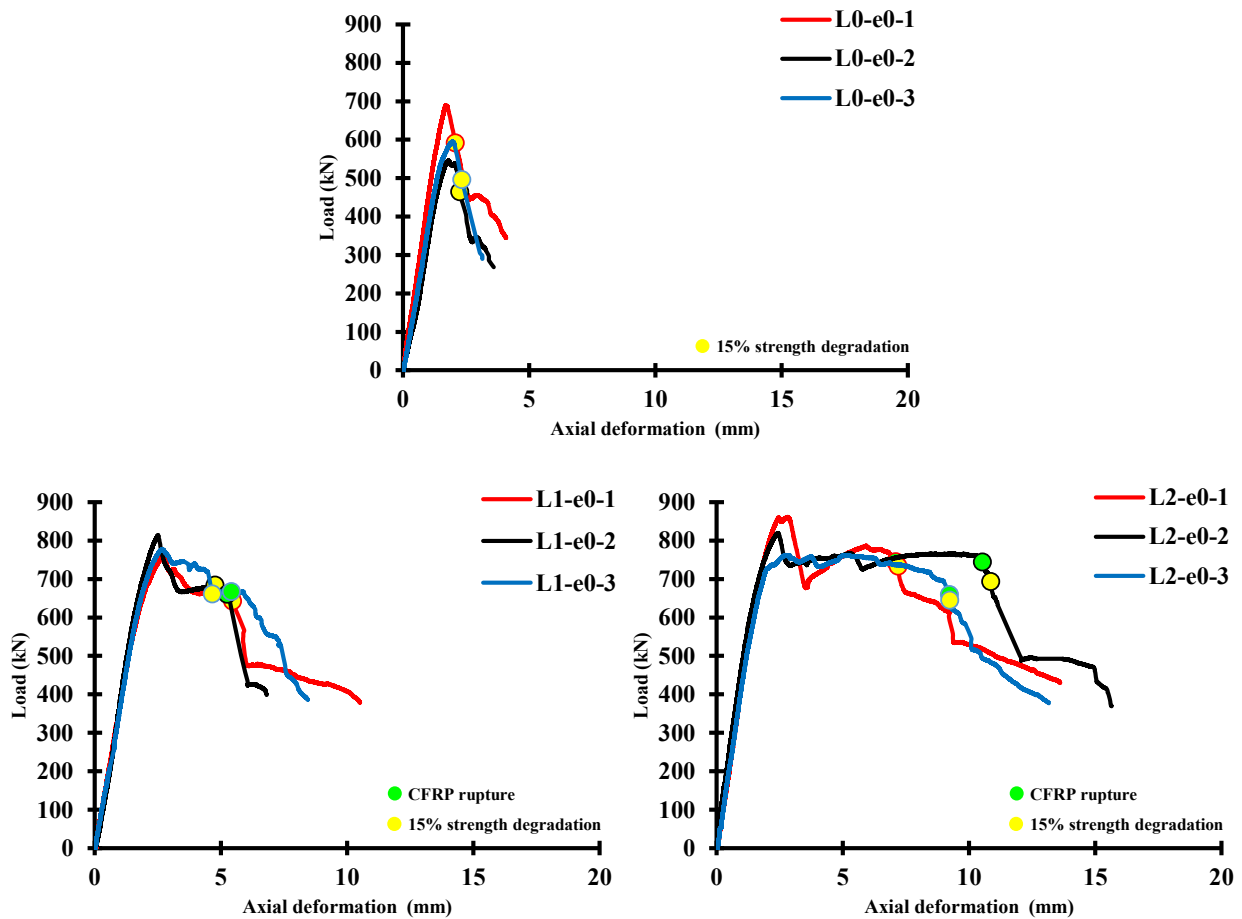
Figure 4.7 Axial load-deformation curves of concentric-loaded reinforced masonry columns.
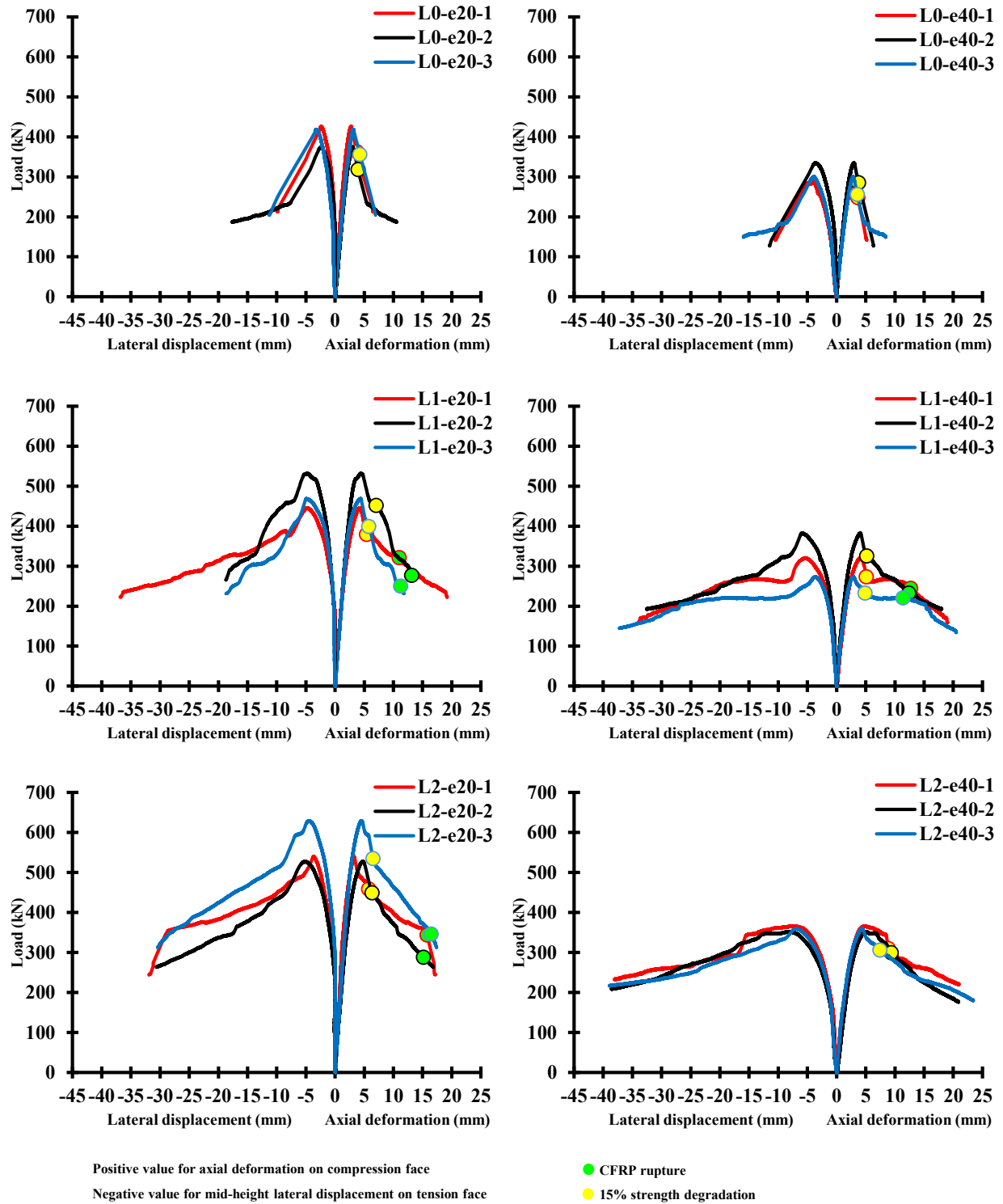
Figure 4.8 Axial deformations and lateral displacements of eccentric-loaded masonry columns.

The experimental results for unconfined and confined masonry columns with average values and (COV) are present in Table 4.4 and Table 4.5, respectively. All readings were reported in

absolute values for better presentation of the data. In these tables, P_{md} is the peak load of unconfined masonry; Δ_m is the axial deformation of unconfined masonry at peak load; and δ_m is the mid-height lateral displacement of masonry columns at peak load. Δ_{mu} and δ_{mu} are the ultimate axial deformation and the mid-height lateral displacement of unconfined masonry corresponding to 85% of peak load during the descending branch of the axial load-deformation curve, respectively. For confined masonry, different symbols were used: P_{mcd} is the peak load of confined masonry; Δ_{mc} and δ_{mc} are the axial deformation and the mid-height lateral displacement of confined masonry at peak load; Δ_{mcu} is the ultimate axial deformation of confined masonry at 15% strength degradation; and δ_{mcu} is the mid-height lateral displacement of confined masonry columns at 15% strength degradation. Two HD cameras were used to synchronize CFRP rupture moments with the load and the axial deformation. P_{ru} and Δ_{ru} represent the load and the axial deformation of confined masonry at first rupture of the CFRP jacket, respectively. Although the definition of the ultimate failure of columns is arbitrary, the authors preferred reporting ultimate values at 15% strength degradation to be in accordance with American design guideline ACI 440.2R-08 (2008).

Table 4.4 The experimental results for unconfined masonry columns.

Column	P_{md} (kN)	Average and COV	Δ_m (mm)	Average and COV	δ_m (mm)	Average and COV	Δ_{mu} (mm)	Average and COV	δ_{mu} (mm)	Average and COV
				At peak				**At 15% strength degradation**		
L0-e0-1	689.48		1.68		-		2.10		-	
L0-e0-2	546.18	610.27 (11.9%)	1.80	1.81 (7.1%)	-	- -	2.25	2.22 (4.7%)	-	- -
L0-e0-3	595.17		1.94		-		2.30		-	
L0-e20-1	426.23		2.70		2.33		3.75		4.44	
L0-e20-2	374.50	406.54 (6.9%)	2.93	2.93 (8.1%)	2.33	2.64 (20.5%)	3.95	3.99 (6.5%)	4.46	4.85 (14.3%)
L0-e20-3	418.90		3.17		3.26		4.27		5.65	
L0-e40-1	289.80		2.72		4.07		3.68		6.59	
L0-e40-2	335.12	308.57 (7.7%)	2.97	2.81 (4.7%)	3.64	3.83 (5.7%)	3.79	3.68 (3.0%)	5.63	5.99 (8.8%)
L0-e40-3	300.79		2.76		3.79		3.57		5.73	

Table 4.5 The experimental results for CFRP confined masonry columns.

Column	P_{mcd} (kN)	Average and COV	Δ_{mc} (mm)	Average and COV	δ_{mc} (mm)	Average and COV	Δ_{mcu} (mm)	Average and COV	δ_{mcu} (mm)	Average and COV	P_{ru} (kN)	Average and COV	Δ_{ru} (mm)	Average and COV
							At peak / **At 15% strength degradation** / **At CFRP rupture**							
L1-e0-1	759.06	783.48 (3.6%)	2.69	2.62 (3.9%)	-	- -	5.45	4.97 (8.6%)	-	- -	657.89	661.70 (0.7%)	5.40	5.35 (1.6%)
L1-e0-2	814.00		2.50		-		4.80		-		660.18		5.25	
L1-e0-3	777.38		2.66		-		4.65		-		667.04		5.41	
L1-e20-1	446.37	482.54 (9.2%)	4.20	4.30 (2.0%)	4.68	4.74 (2.6%)	5.41	6.08 (14.3%)	7.64	7.92 (10.1%)	320.93	282.63 (12.7%)	11.00	11.79 (9.9%)
L1-e20-2	531.99		4.33		4.65		7.06		8.82		276.98		13.13	
L1-e20-3	469.27		4.36		4.87		5.78		7.29		249.97		11.25	
L1-e40-1	321.39	325.97 (16.8%)	4.05	3.64 (19.5%)	5.39	4.94 (24.6%)	5.10	5.05 (3.1%)	7.63	7.63 (7.5%)	244.48	232.57 (5.0%)	12.70	12.13 (6.0%)
L1-e40-2	382.74		4.04		5.87		5.17		8.20		232.11		12.38	
L1-e40-3	273.78		2.82		3.57		4.87		7.05		221.13		11.31	
L2-e0-1	861.62	814.61 (6.1%)	2.79	2.65 (8.1%)	-	- -	7.18	9.09 (20.2%)	-	- -	744.87	716.06 (6.9%)	7.10	8.95 (19.3%)
L2-e0-2	819.50		2.40		-		10.85		-		743.96		10.53	
L2-e0-3	762.73		2.75		-		9.24		-		659.37		9.23	
L2-e20-1	540.23	565.86 (9.8%)	3.26	4.17 (19.0%)	3.68	4.44 (15.7%)	5.77	6.20 (6.3%)	8.88	8.62 (2.6%)	343.36	325.66 (10.0%)	15.77	15.81 (4.3%)
L2-e20-2	527.87		4.69		5.06		6.33		8.51		287.97		15.15	
L2-e20-3	629.50		4.56		4.57		6.51		8.47		345.65		16.50	
L2-e40-1	366.71	359.69 (2.0%)	4.91	4.72 (7.6%)	7.57	7.43 (7.5%)	8.87	8.56 (11.7%)	16.34	16.50 (14.1%)	-	- -	-	- -
L2-e40-2	352.52		4.95		7.91		9.38		18.91		-		-	
L2-e40-3	359.85		4.31		6.81		7.44		14.25		-		-	

According to Lam and Teng (2003), a monotonically ascending stress-strain curve can be expected when providing sufficient confinement level to strengthen reinforced concrete columns. However, all columns tested in this study showed a parabolic ascending portion of axial load-deformation curve then followed by a descending portion. This finding is in agreement with previous tests conducted on concrete masonry prisms strengthened with CFRP jackets by Alotaibi and Galal (2017). It should be noted that even though there is no monotonically ascending bi-linear load-deformation curves that were observed, strengthening concrete pilaster masonry columns by CFRP jackets is an effective retrofit method because the CFRP confined masonry columns showed higher strength and ductility more than unconfined masonry columns. Axial load-deformation curves for selected masonry columns are compared in Figure 4.9 to emphasize the effect of CFRP jacketing on strength and ductility of concrete masonry columns. The unconfined masonry columns showed a brittle behaviour in post peak where the strength steeply dropped after the peak. However, the confined masonry columns showed more ductile behaviour in descending branches of the axial load-deformation curves if they compared to unconfined masonry columns.
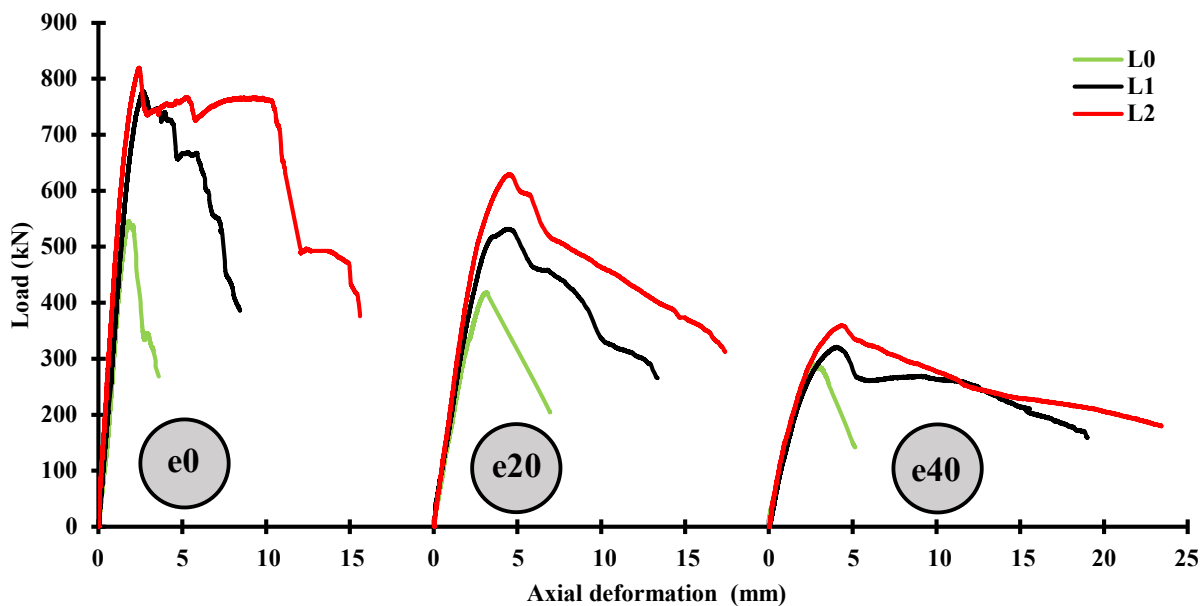
Figure 4.9 Axial load-deformation curves for selected masonry columns.

4.3.1.3 Effect of eccentricity

The effect of eccentricity on the behaviour of masonry columns can be seen in Figure 4.9. It is clear that the initial eccentricity of loading reduced the carrying capacity of masonry columns as expected. The masonry columns failed at a lower capacity because there was less portion of

cross section under compression. The reduction of the portion under compression increases with the increase of the strain gradient. The average peak load of the unconfined masonry columns decreased by about 33 and 49% under 20 and 40 mm eccentricities, when compared to unwrapped concentric columns, respectively. Considering the average peak load of L1-e0 subgroup as a reference point, the average strength drops were 38 and 58% for one-layer columns tested with 20 and 40 mm eccentricity, respectively. On the contrary, the average strength drops were 31 and 56% for L2-e20 and L2-e40 subgroups when compared with two-layer columns tested with zero eccentricity.

4.3.1.4 Strain in longitudinal steel reinforcements

The average strain obtained from the four strain gages bonded to longitudinal steel reinforcement at the mid-height of concentrically loaded masonry columns are shown in Figure 4.10, where positive values indicate compression strains and negative values present tension strains. The test results indicated that longitudinal steel reinforcement developed high compression strain at the peak and passed the yield value. The average compression strains at the peak were 3093, 3183, and 3184 μstrain for L0-e0, L1-e0, and L2-e0, respectively.
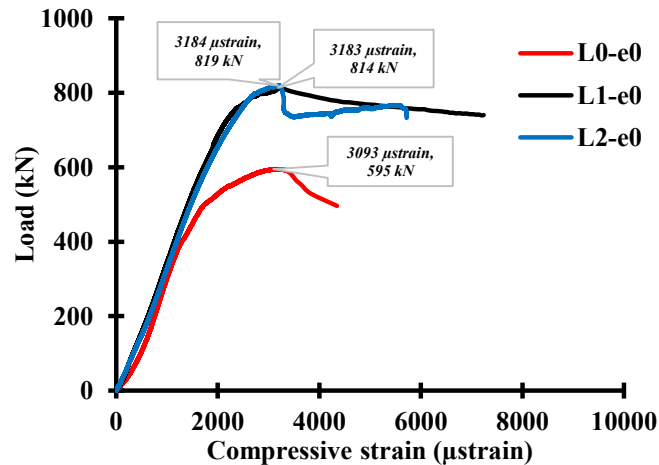
Figure 4.10 Average strain of longitudinal steel reinforcement in concentrically loaded masonry columns.

Average strain gages reading of longitudinal steel reinforcement at the compression and tension faces for masonry columns tested with eccentricities of 20 and 40 mm are shown in Figure 4.11 and Figure 4.12, respectively. For masonry columns confined with CFRP jacketing and tested with small and large eccentricities, the longitudinal steel reinforcements at the

compression face were yield or so close to yielding except L1-e20. On the contrary, the unconfined columns showed lower compressive strains at the compression face. Longitudinal steel reinforcements at tension face developed compression strain at the peak for the eccentricity of 20 mm. The compression strain increased with the increase of the confinement level. These measurements are evident that the lateral confining pressure produced by the CFRP jackets is providing additional support against buckling of longitudinal steel reinforcements. For masonry column tested with large eccentricity, the axial strain at longitudinal steel reinforcements at tension faces had a transition from compression to tension. During loading, the transition is led by the movement of the neutral axis into a higher position to account for second order moment induced by the increase of the lateral displacement.
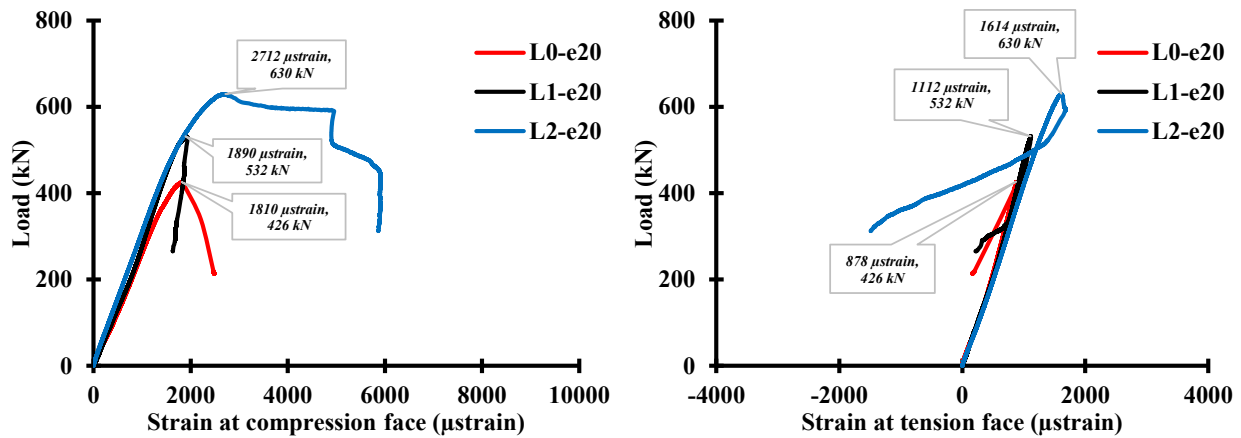
Figure 4.11 Average strain gages reading of longitudinal steel reinforcement at the compression and tension faces for 20 mm eccentricity.
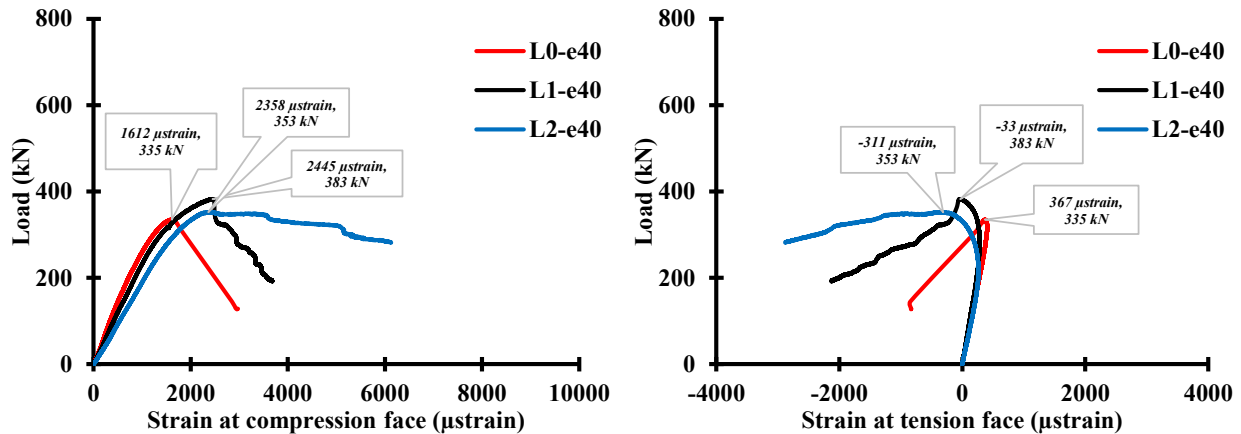
Figure 4.12 Average strain gages reading of longitudinal steel reinforcement at the compression and tension faces for 40 mm eccentricity.

88

4.3.1.5 Effect of confinement

Normalized load and deformation values of confined masonry columns are presented in Table 4.6. Average values of load and deformation for the three replicates were used to define the effect of CFRP jacketing on the strength and ductility of the concrete masonry columns. The performance of unconfined control specimens at the same level of eccentricity was considered as benchmarks to evaluate the performance of the confined column. The ductility of the columns is reported as the ratio of axial deformation of the column at 15% strength degradation to its axial deformation at peak load. Also, the average load at first rupture of the CFRP jackets of the subgroup was normalized to the average peak load to determine at which level of strength degradation the rupture of CFRP jackets occurred.

Table 4.6 Normalized load and deformation values of confined masonry columns.

Subgroup	P_{mcd}/P_{md}	Δ_{mc}/Δ_m	Δ_{mcu}/Δ_{mu}	Ductility Δ_{mcu}/Δ_{mc}	Δ_{ru}/Δ_{mu}	P_{ru}/P_{mcd}
L0-e0	1.00	1.00	1.00	1.23	-	-
L1-e0	1.28	1.45	2.24	1.90	2.41	0.85
L2-e0	1.33	1.46	4.10	3.48	4.04	0.88
L0-e20	1.00	1.00	1.00	1.36	-	-
L1-e20	1.19	1.46	1.52	1.41	2.96	0.59
L2-e20	1.39	1.42	1.56	1.52	3.96	0.58
L0-e40	1.00	1.00	1.00	1.31	-	-
L1-e40	1.14	1.44	1.40	1.27	3.41	0.68
L2-e40	1.17	1.68	2.33	1.81	-	-

All confined masonry columns, except L1-e40-3, showed an increase in terms of peak load when compared to the average load of unconfined columns with the same level of eccentricity. L1-e40-3 column showed the lowest performance in all tested masonry columns. The unsuccessful strength could be due to the variability of grout strength or human error in performing the test. The results of this masonry column were removed from the average in Table 4.6 in order not to mislead the findings.

The average strength gain for concentrically tested columns were 28% and 33% for one and two CFRP layers compared to unconfined masonry columns strength, respectively. It can be observed that the first layer of CFRP significantly increased the axial strength compared to control

specimens. However, no significant increment in peak force was noticed by adding second CFRP layer if compared to masonry columns strengthened with the one-layer. The masonry columns tested with concentric load had the highest gain in term of ultimate deformation when compared to unconfined columns, where L1-e0 and L2-e0 recorded 124% and 310% gain, respectively.

The reason that confined masonry columns showed a higher gain in the ultimate axial deformation more than the gain in strength could be attributed to the confinement mechanism. Hence, the restraint of CFRP jacket to the lateral expansion of masonry composite under axial stress transforms into tensile strain in CFRP jacket in the hoop direction. The passive pressure produced laterally by confining jacket keeps the integrity of blocks and grout until the CFRP jacket reaches its ultimate tensile rupture force. The amount of confining pressure provided by CFRP jacket depends on the stiffness of the CFRP composite and the lateral expansion of masonry composite if deformation compatibility is assumed between the CFRP jacket and concrete masonry. The lateral expansion of masonry composite is low at maximum load and increases within the descending branch of the axial load-deformation curve leading to increasing the confining pressure of CFRP jacket which mainly affects the ultimate axial deformation gain.

The eccentrically tested columns recorded lower gain in strength and the ultimate axial deformation compared to concentrically tested columns. This is mainly due to the effect of strain gradient and the increase of the second order moment due to the increase of the lateral displacements. Moreover, it is known that the FRP confining stress is nonuniformly distributed over the columns' cross sections under compression loading and it would be expected that the nonuniformity of confinement would increase with the increase of strain gradient. Also considering the complexity of masonry dilation, the shape of the effectively confined area could change under strain gradient. The gain in axial deformation of confined masonry columns at peak load for concentric tests with one and two CFRP layers were 45% and 46%, respectively. The average gain in axial deformation of confined masonry columns at peak load increased by about 44% and 56% under 20 and 40 mm eccentricity, respectively. As mentioned previously, the passive confinement requires significant lateral expansion of the masonry before activating the CFRP confinement. At the peak load, masonry has small dilation with limited microcracks. In the post peak behaviour, the cracks grow under compressive loading and dilation increase significantly.

The highest ductility ratios were recorded in masonry columns confined with CFRP jackets and tested under concentric load. The average ductility ratios of concentric columns were 1.90 and 3.48 for masonry columns with one and two CFRP layers, respectively. The eccentricity reduced the ductility ratios compared to concentrically tested columns. However, confined masonry columns, in general, showed higher ductility ratios than unconfined masonry columns. Since the reported ductility ratio in the table is a measure of the inelastic to elastic deformation of the column itself, the improvement in the structural performance due to confinement can be presented by the increase in the ultimate axial deformation of confined columns compared to unconfined columns. The later values allow better estimates of retrofit efficiency and better estimates of the ability of confined masonry columns to absorb external energy through its deformation capacity.

Axial deformation of confined masonry at the first rupture of the CFRP jacket was normalized to the average ultimate deformation of unconfined masonry at the same level of eccentricity and reported in Table 4.6 to present the ductility of columns. Even though the tensile rupture in the CFRP jacket is the main physical sign of column failure, considering that the axial deformation at first rupture in the CFRP jacket as the maximum usable strain is not a conservative assumption. This is especially true when the carrying capacity of confined masonry columns drops more than 30% from peak load and drop beyond the original capacity of unconfined masonry columns. For columns confined with CFRP and tested concentrically, the rupture of the CFRP occurred around 15% strength degradation. With the presence of eccentricity, the rupture of the CFRP jacket delayed until 41% and 32% strength degradation for 20 and 40 mm eccentricity, respectively. To explain that, it is important to recognize that the failure of masonry columns depends mainly on the global cross section behaviour, where the CFRP rupture is related to the stiffness of the CFRP jacket and the dilation of the masonry. Considering that CFRP confined masonry columns under eccentric loading has less portion of the cross section under compression which led to less overall dilation of the masonry. Specifically, the late is essential to active the confinement and case the rupture of CFRP jacket when there is enough dilation in the masonry to initiate the rupture.

The effect of confinement and the level of eccentricity on the enhancement in peak load is illustrated in Figure 4.13. The peak loads were normalized to the average peak load of unconfined masonry columns tested under concentric loading and plotted versus initial load eccentricity-to-width ratio. The trend lines were developed based on a linear regression analysis of the test results. As shown in Figure 4.13, the steeper slopes of the trend lines of confined masonry columns

illustrate more proportionally load capacity reductions in CFRP masonry columns compared to unconfined masonry columns. The strength of confined masonry columns under eccentric loading is substantially improved if compared with unconfined masonry columns with the same level of eccentricity. This would prove that CFRP confinement is able to strengthen reinforced concrete masonry columns by increasing their axial capacity to sustain the additional applied load. The trend lines of confined masonry columns are parallel, the columns wrapped with two CFRP layers are higher in strength gain than columns wrapped with one CFRP layer columns because the second layer of CFRP increased the lateral confining pressure.
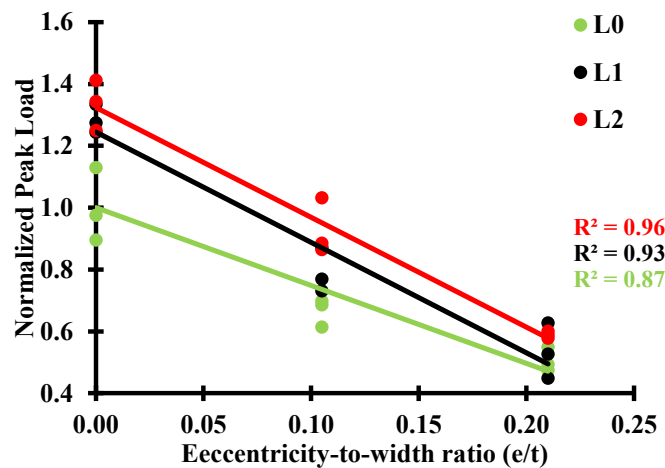
Figure 4.13 The effect of confinement and the level of eccentricity on the enhancement in peak load.

4.3.1.6 Mid-height lateral displacement

Figure 4.14 shows mid-height lateral displacement of masonry columns against the axial load for selected masonry columns tested with 20 and 40 mm eccentricity. Displacement measurements were reported in absolute values for better presentation of the data.

Strengthened masonry columns tested with 20 mm eccentricity showed lower lateral displacement in early loading when compared to control specimens. This may indicate better serviceability behaviour. In the post peak behaviour, the control specimens showed higher stiffness degradation than strengthened masonry columns. At any lateral displacement value, the axial strength of the strengthened masonry columns was higher than that of control specimens, which shows more ductile behaviour. The average lateral displacement increases at the peak load for 20 mm eccentricity columns with one and two CFRP layers were 79% and 68% compared to the

lateral displacements of unconfined columns, respectively, where the average lateral displacement increases around 15% strength degradation were 63% and 78% for masonry columns strengthened with one and two CFRP layers, respectively.

Masonry columns tested with 40 mm eccentricity showed similar behaviour trends up to maximum loads. However, the unwrapped masonry columns showed higher stiffness degradation after peak compared to the strengthened masonry columns. L1-e40 and L2-e40 subgroups showed 47% and 94% increase of lateral displacement at the peak load compared to unconfined masonry columns, while the increases at 15% strength degradation were 32% and 195%, respectively. This confirms that confinement provided by CFRP jackets is effective in enhancing the capacity of eccentrically loaded columns to withstand a higher level of second order moment.
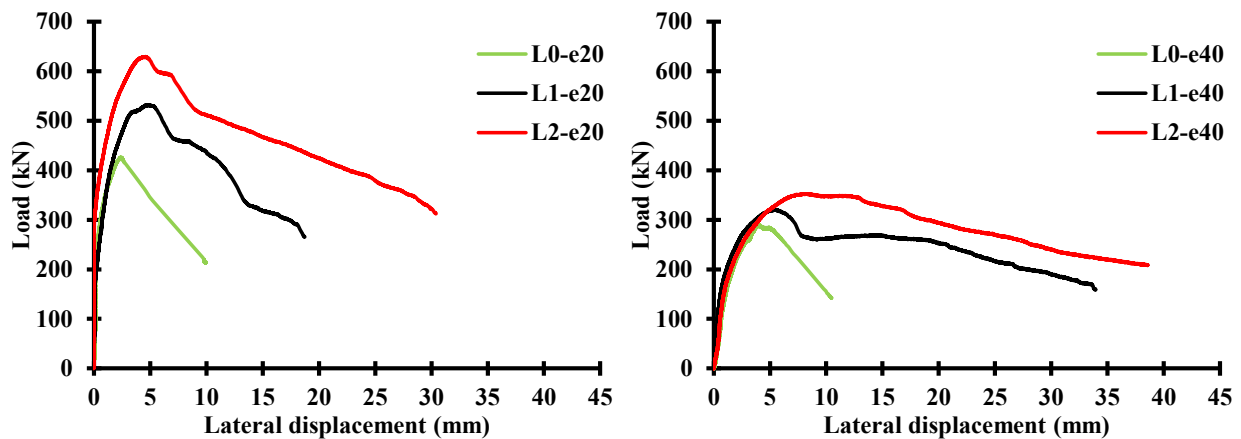
Figure 4.14 Load-Mid-height lateral displacement of selected masonry columns.

4.3.2 Behaviour under pure bending

The masonry column was tested under four-point-bending loading. The load-midspan deflection curve of the beam tested under flexure is shown in Figure 4.15. The beam failed at a maximum load of 157.92 kN with crushing of masonry concrete between the middle roller supports in the top part and tensile cracks with yielding of the tensile steel reinforcements in the bottom part of the beam. The failure mode of the beam at the end of the test is shown in Figure 4.16. The mid-span deflection at peak load was 4.83 mm which is the average reading of the two LVITs sensors placed under the beam. The average strain gages readings of steel reinforcement are shown in Figure 4.17, where positive values indicate compression strains and negative values present tension strains. The average tensile strains reached 3146 μstrain in lower steel reinforcements at the peak which is higher than the yielding point. The upper steel reinforcements transited from

compression to tension in early loading stage and reached 242 tensile μstrain at peak. The flexure capacity of the investigated beam is 15.79 kN.m and was calculated as:

$$M = \frac{P}{2}(a)$$

where P is the maximum load measured from the load cell, and the constant a is the shear span length, which is the distance between the roller support at the end and the middle loading roller.
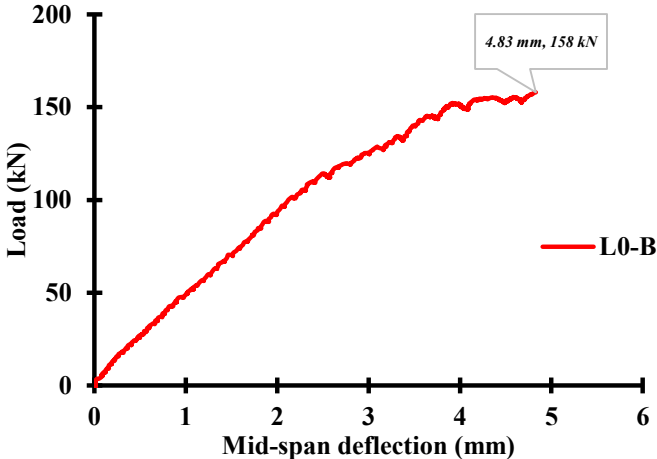
Figure 4.15 The load-midspan deflection curve of the beam tested under flexure.

Figure 4.16 The failure mode of the beam at the end of the test.
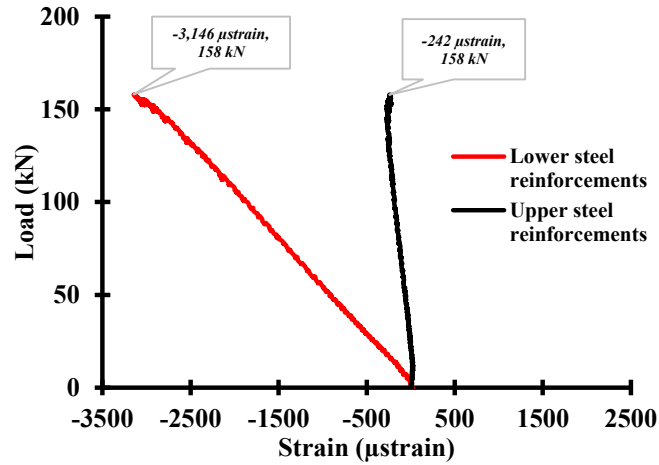
Figure 4.17 Average strain gages reading of steel reinforcement.

4.4 Axial-flexural interaction

4.4.1 Axial force-bending moment interaction diagrams

The bending moment capacity of eccentrically loaded masonry columns is reported in Table 4.7. The bending moment capacity (M_I) for 20 and 40 mm eccentrically loaded columns was calculated by multiplying the maximum axial load (P) and initial eccentricity (e). To consider the second order moment, bending moment capacity (M_{II}) was also calculated as follows:

$$M_{II} = P * (e + \delta)$$

Eq. 4-2

where (δ) is lateral displacement at the maximum load capacity.

Table 4.7 Experimental bending moment capacity of columns tested with eccentricity.

Column	P (kN)	δ (mm)	M_I (kN.m)	Average and COV	M_{II} (kN.m)	Average and COV
L0-e20-1	426.23	2.33	8.52		9.52	
L0-e20-2	374.50	2.33	7.49	8.13 (6.9%)	8.36	9.21 (8.1%)
L0-e20-3	418.90	3.26	8.38		9.74	
L0-e40-1	289.80	4.07	11.59		12.77	
L0-e40-2	335.12	3.64	13.40	12.34 (7.7%)	14.63	13.52 (7.2%)
L0-e40-3	300.79	3.79	12.03		13.17	
L1-e20-1	446.37	4.68	8.93		11.02	
L1-e20-2	531.99	4.65	10.64	9.65 (9.2%)	13.11	11.93 (9.0%)
L1-e20-3	469.27	4.87	9.39		11.67	
L1-e40-1	321.39	5.39	12.86		14.59	
L1-e40-2	382.74	5.87	15.31	13.04 (16.8%)	17.56	14.69 (19.2%)
L1-e40-3	273.78	3.57	10.95		11.93	
L2-e20-1	540.23	3.68	10.80		12.79	
L2-e20-2	527.87	5.06	10.56	11.32 (9.8%)	13.23	13.83 (10.4%)
L2-e20-3	629.50	4.57	12.59		15.46	
L2-e40-1	366.71	7.57	14.67		17.45	
L2-e40-2	352.52	7.91	14.10	14.39 (2.0%)	16.89	17.06 (2.0%)
L2-e40-3	359.85	6.81	14.39		16.85	

The experimental axial force-bending moment interaction diagrams of the masonry columns are shown in Figure 4.18. The interaction diagrams of tested masonry columns were constructed to describe the moment capacity at peak load with and without the effect of second order moments. Points on the diagrams represent the results of masonry columns tested under concentric loads, eccentric loads, or pure bending. The curves present the average values calculated from three replicates for each subgroup.

It can be seen that CFRP jackets significantly increased the bending moment capacity (M_{II}) of strengthened masonry columns. For example, a larger increment of 50% was obtained in bending moment capacity of masonry column wrapped with two layers of CFRP and tested with 20 mm eccentricity if compared to unwrapped masonry columns.
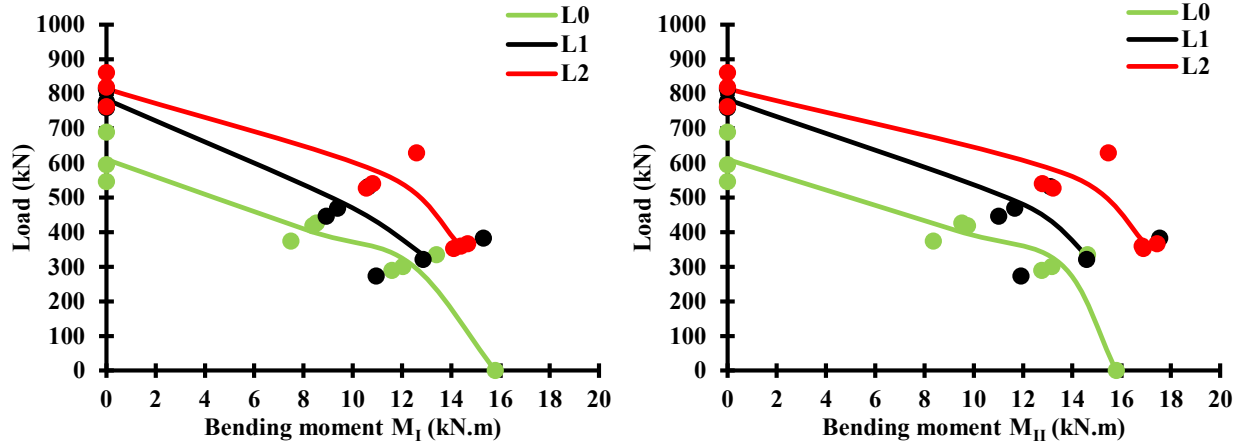
Figure 4.18 Experimental axial load-bending moment interaction diagrams.

A linear regression analysis of the experimental data is illustrated in Figure 4.19 to show the effect of confinement on the enhancements in axial load and bending moment. The axial loads were normalized to the average peak load of unwrapped masonry columns tested under concentric loads. The bending moment capacity M_I and M_{II} were normalized to the ultimate pure bending capacity of unwrapped masonry column. The ultimate bending moment was experimentally obtained by testing the masonry column as a beam under four-point-bending loading.

The figure demonstrates the clear benefits of CFRP confinement for masonry columns subjected to combined axial-flexural loading. Strengthened masonry columns showed an increase in axial load and moment capacity. The presence of the CFRP confinement contributed to the bending capacity of the masonry column when including the second order moments. Strengthened masonry columns were able to stand a moment higher than the ultimate bending moment of unwrapped masonry column. Strengthened masonry columns with one layer of CFRP jacket can carry 50% of the maximum axial load of unwrapped masonry columns loaded concentrically and withstanding the ultimate bending moment of unwrapped masonry column tested as a beam. In comparison, the masonry columns with two layers carried around 69% on average.
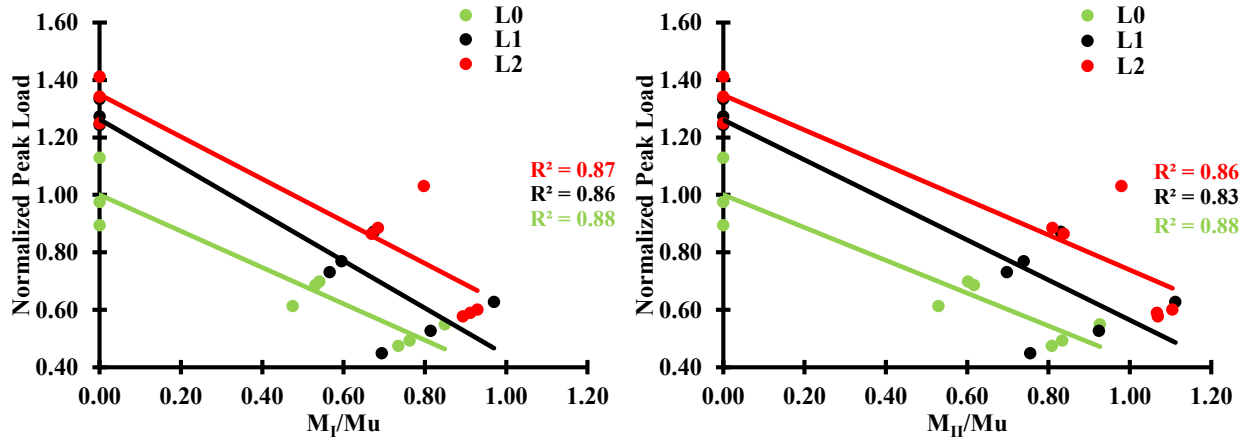
Figure 4.19 Normalized axial load and moment capacity of tested masonry columns.

4.4.2 Strain distribution in cross sections

Figure 4.20 shows the average strain distribution of cross section for masonry columns tested eccentrically at two different stages of loading. The values represent the average of three replicate masonry columns. The results of L1-e40-3 column was ignored when calculating the average of L1-e40 subgroup. The strain is calculated as the average axial deformation divided by the whole gage length (945 mm) which represents the average strain along column height. Figure 4.20 was produced assuming linear-strain distribution in elastic and plastic phases for simplicity.
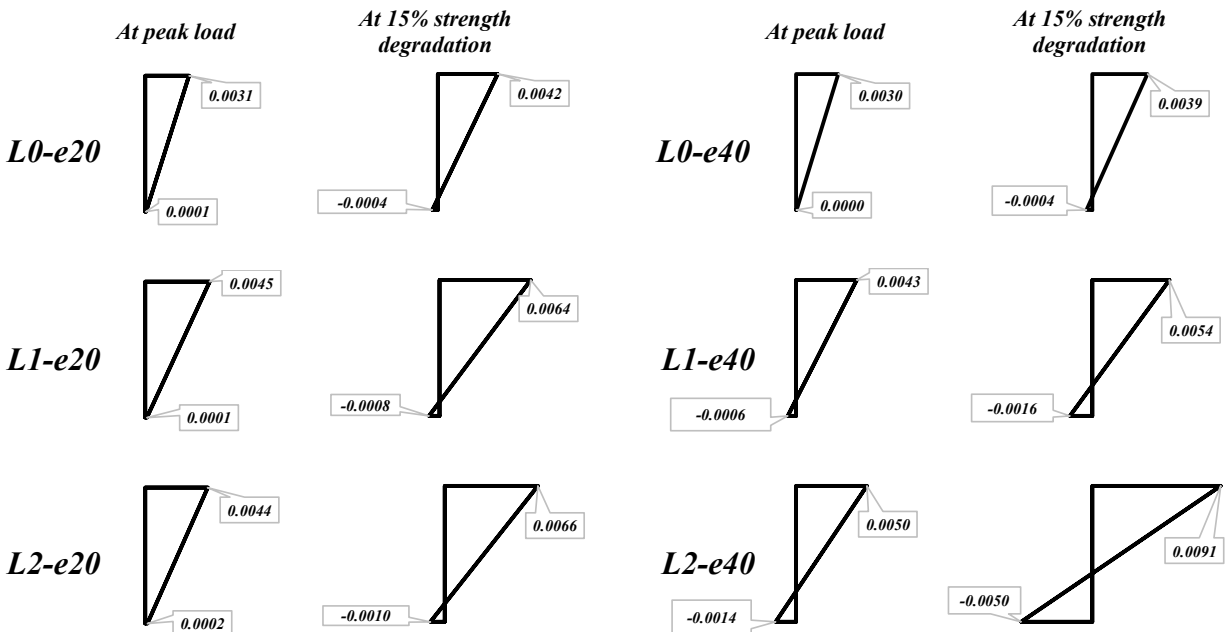
Figure 4.20 The average strain distribution of eccentric masonry columns at two stages of loading.

Unwrapped masonry columns tested with 20 mm eccentricity failed in a compression controlled manner due to a sudden crushing of the concrete masonry at the compression face. The extreme compression masonry fibre reached maximum strain equals to 0.0031 (mm/mm) at the peak. All longitudinal steel reinforcements were under compression without yielding. At 15% strength degradation, a limited tensile strain developed at the tension face with an increase in compressive strain of masonry to 0.0042 (mm/mm).

Unwrapped masonry columns tested with larger eccentricity (40 mm) showed similar behaviour, where the maximum strain was 0.0030 (mm/mm) at extreme compression fibre and zero strain at the tension face when the masonry columns started failing at maximum load. At 15% strength degradation, compressive strain of masonry reached to 0.0039 (mm/mm), and the longitudinal steel reinforcements near the tension face showed less compressive value. The masonry columns were able to develop 0.0004 (mm/mm) tensile strain at the tension face.

For masonry columns strengthened with one or two layers of CFRP and tested under 20 mm eccentricity, the effect of CFRP confinement was able to enhance the maximum strain at the extreme compression masonry fibre to 0.0044 (mm/mm) at the peak and 0.0064 (mm/mm) at 15% strength degradation. The wrapped masonry columns failed in a compression controlled manner due to CFRP snapping at the corners of the compression face. L1-e20 subgroup showed the ability to resist 0.0008 (mm/mm) tensile strain at the tension face at 15% strength degradation which was about two times greater than the tensile strain of L0-e20. Adding a second layer of CFRP increased the tensile strain at the tension face at 15% strength degradation to 0.0010 (mm/mm) and increased the compressive strain at the tension face at maximum load from 0.0001 (mm/mm) for L1-e20 to 0.0002 (mm/mm) for L2-e20. All longitudinal steel reinforcements of confined masonry columns tested with 20 mm eccentricity were under compression at maximum loading. For L2-e20 subgroup, the longitudinal steel reinforcements near the compression face were yield with 2712 μstrain. After the peak, the strain in the longitudinal steel reinforcements of L2-e20 at the tension face transferred from compression to tension in late loading stage.

For 40 mm eccentric masonry columns strengthened with one and two layers of CFRP, the confinement of the jacketing at the peak load increased the maximum strain at the extreme compression masonry fibre to 0.0043 and 0.0050 (mm/mm) for one or two layers, respectively. L1-e40 columns failed in a compression controlled manner due to reaching the ultimate confined

masonry strain at peak load. The tensile strain was rapidly developed at the extreme tension fibre after the peak to reach 0.0016 (mm/mm) at 15% strength degradation due to the increase of moment. The longitudinal steel reinforcements of L1-e40 near the tension face were under tension at maximum loading. The tension increased during the post peak behaviour. L2-e40 columns failed in a compression controlled manner at peak load since the ultimate confined masonry strain reached 0.0050 (mm/mm) at the extreme compression fibre. Around 15% strength degradation, L2-e40 columns were failing in a tension controlled manner due to the yielding of the longitudinal steel reinforcements near the tension face and opening of the mortar joints at the tension face which led to a large lateral displacement and higher second order moment. The tensile strain at the extreme tension fibre reached 0.0050 (mm/mm) at 15% strength degradation. The absence of CFRP rupture at the compression face of the two-layer masonry columns tested with 40 mm eccentricity could be explained by that the application of two layers changed the columns' mode of failure to a tension controlled manner around 15% strength degradation before reaching the CFRP rupture level which is 32% strength degradation for confined masonry columns tested with 40 mm eccentricity.

4.5 Conclusions

The results of the experimental program for testing reinforced concrete masonry columns confined by CFRP jackets under axial and flexural loading are presented in this paper. The effect of axial strain gradient resulting from axial and flexural loading on confinement level provided by CFRP jackets was experimentally measured. Axial force-bending moment interaction diagrams of reinforced concrete masonry columns confined with two different level of jacketing are compared against non-strengthened concrete masonry columns to quantify the enhancement in the load and moment capacities.

The following observations are highlighted from the experimental testing of 28 concrete masonry columns under concentric and eccentric axial load:

- CFRP jackets significantly increased the maximum axial load and axial deformation of the confined masonry columns compared to unconfined columns.
- The eccentrically tested columns recorded lower gain in strength and the ultimate axial deformation compared to concentrically tested columns.

- CFRP jackets enhanced the post peak behaviour of confined masonry columns by softening the descending branches of axial load-deformation curve compared to unconfined columns.

- The initial eccentricity of loading reduced the axial load carrying capacity of masonry columns.

- The confined masonry columns showed a higher gain in the ultimate axial deformation more than the gain in strength.

- The rupture of the CFRP jackets happened around 15% strength degradation in concentric tests. The onset of rupture was delayed with the eccentricity.

- The unwrapped masonry columns showed higher stiffness degradation after peak compared to the wrapped masonry columns.

- Confinement can change the columns' mode of failure to a tension controlled manner during post peak behaviour.

The experimental results proved that CFRP jacketing is an efficient technique for strengthening of reinforced concrete masonry columns by increasing the axial load and improving the axial deformation. However, additional tests using different types of FRP materials and taking into account various cross sections of columns are recommended before generalizing the findings of this study.

Chapter 5

Axial-Flexural Interaction for FRP-wrapped Reinforced Concrete Masonry Columns:
Design Methodology and Design Variables

Abstract

This paper proposes a simplified methodology to construct the axial force-moment interaction diagram of fully grouted reinforced concrete masonry column strengthened with Fibre Reinforced Polymers (FRP) jackets. The methodology considers short prismatic reinforced concrete masonry columns failing in a compression-controlled manner and it complies with equilibrium and strain compatibility principles. The proposed procedure is designed to predict the nominal capacity of reinforced concrete masonry columns for practical design applications, where the columns will be subjected to both axial load and bending moment. The essential parameters to perform detailed section analysis are established, and suggested expressions are proposed to obtain the parameters' values. Practical values for the equivalent rectangular stress block parameters are proposed, which represent the actual stress distribution in the compression zone of FRP-confined concrete masonry section. The theoretical axial force-moment interaction diagrams obtained by the proposed procedure were compared with the available experimental data. The experimental test results are in good agreement with the analytical predictions by a good margin. Constant value of 0.80 for the parameters α and β of the equivalent rectangular stress block are recommended for simplicity. The mean absolute percentage error was less than 6% between the experimental data and analytical predictions. The paper further investigates the effect of the design variables on the axial-flexural interaction of FRP-wrapped reinforced concrete masonry columns. The variables considered in the parametric study are the number of FRP layers, the corners radius, the stiffness of the FRP composite, the cross section aspect ratio, and the masonry compressive strength.

5.1 Introduction

Most reinforced concrete masonry columns in real masonry structures are subjected to combinations of axial force and flexure moment. The flexure can be expected from unintentional eccentricities, unsymmetrical loading, or lateral loads.

Some existing reinforced concrete masonry columns need to be strengthened in terms of their capacity or ductility. The need for additional bearing capacity could arise from a change in the structure use, insufficient design, errors in construction, and deterioration of materials, whereas the ductility enhancement is needed for seismic upgrading in case of changing the seismic codes requirements and also to account for poor reinforcement detailing.

Using fibre reinforced polymers (FRP) jackets to confine reinforced concrete masonry columns is seen to be an effective technique to strengthen masonry columns with insufficient capacity or ductility. FRP jacket can be formed by wrapping FRP sheets around the columns where the fibres are aligned along hoop direction and perpendicular to the vertical axis of the column.

Several studies investigated the application of FRP jackets to retrofit masonry columns built from different materials (tuff, clay, and limestone units) (Campione and Miraglia, 2003; Alecci et al., 2009; Di Ludovico et al., 2010; Faella et al., 2011b). Recent studies focused on the experimental behaviour of concrete masonry columns strengthened by carbon FRP jackets (Galal et al., 2012; Alotaibi and Galal, 2017, 2018; Ashour et al., 2018).

This paper proposes a simplified methodology to compute the axial force-moment interaction diagram of fully grouted reinforced concrete masonry column confined with FRP jacket. The proposed procedure follows the equilibrium and strain compatibility principles. The methodology only considers short prismatic reinforced concrete masonry columns that are subjected to large axial loads and small moments, i.e., axial-moment pairs that fall in the compression-controlled region of the axial force-moment interaction diagram.

The proposed procedure is designed to predict the nominal capacity of reinforced concrete masonry columns for practical design applications. However, no specific design guideline has been adopted in developing the proposed procedure. Hence, structural engineers shall explicitly consider load factors, resistance reductions and ultimate axial strain limits consistent with a

compatible design code to ensure the safety of structures and to consider material variability and uncertainties in properties of material during the construction and manufacture.

The theoretical axial force-moment interaction diagrams obtained by the procedure proposed in this paper are compared to experimental data presented in Alotaibi and Galal (2018). The results of the experimental tests correlate well with the analytical predictions with an acceptable margin of error. A parametric study is conducted to evaluate the effect of design variables on the axial-flexural interaction of fully grouted reinforced concrete masonry column strengthened by FRP jackets.

5.2 Experimental data of FRP-confined concrete masonry columns

There is limited experimental work conducted on FRP-confined concrete masonry columns. In this paper, the experimental data of 28 tests reported by Alotaibi and Galal (2018) is used for validating the proposed interaction diagram methodology. The study featured 18 reinforced FRP-confined concrete masonry columns tested with pure monotonic compressive force or monotonic eccentric compressive force. The concrete masonry columns tested in that study were constructed from half scale concrete "C" pilaster units. The square cross section is fully grouted and has four longitudinal steel reinforcements with 12.7 mm nominal diameter. The masonry column has a length to cross section thickness ratio (L/t) of 4.97. The column with such slenderness ratio is considered as a short column. The general properties of the masonry columns, longitudinal steel reinforcement and composite jacket are summarized in Table 5.1. The maximum axial load capacity and maximum moment of a total of 17 concrete masonry columns strengthened with CFRP jackets are presented in Table 5.2. Columns with unsuccessful strength or without FRP jackets are excluded from the table. The symbols used in the tables are defined in the notations section. More details of the tests and the columns construction can be found in Alotaibi and Galal (2018).

Table 5.1 Properties of tested columns in the literature (Alotaibi and Galal, 2018).

	f_{md} (MPa)	g_m (kg/m³)	b (mm)	h (mm)	f_y (MPa)	E_s (GPa)	ε_y (mm/mm)
Columns	10.96	2171	190	190	483.0	200	0.0024
	E_f (GPa)	t_f (mm)	ε_{fk} (%)	A_s (mm²)	ρ_g (%)	L (mm)	r_c (mm)
	65.40	0.381	1.33	516	1.4	945	10

Table 5.2 Test data in the literature (Alotaibi and Galal, 2018).

Column label	t_f (mm)	P_{max} (kN)	M_{max} (kN.m)	e (mm)
L1-e0-1	0.381	759.06	0.00	0.00
L1-e0-2	0.381	814.00	0.00	0.00
L1-e0-3	0.381	777.38	0.00	0.00
L1-e20-1	0.381	446.37	11.02	24.69
L1-e20-2	0.381	531.99	13.11	24.64
L1-e20-3	0.381	469.27	11.67	24.87
L1-e40-1	0.381	321.39	14.59	45.40
L1-e40-2	0.381	382.74	17.56	45.88
L1-e40-3	0.381	273.78	11.93	43.58
L2-e0-1	0.762	861.62	0.00	0.00
L2-e0-2	0.762	819.50	0.00	0.00
L2-e0-3	0.762	762.73	0.00	0.00
L2-e20-1	0.762	540.23	12.79	23.68
L2-e20-2	0.762	527.87	13.23	25.06
L2-e20-3	0.762	629.50	15.46	24.56
L2-e40-1	0.762	366.71	17.45	47.59
L2-e40-2	0.762	352.52	16.89	47.91
L2-e40-3	0.762	359.85	16.85	46.83

5.3 Axial force-moment interaction diagrams

According to MacGregor (1997), Bank (2006), and Rocca et al. (2009), the main difference of analysis FRP confined concrete and conventional concrete is the choice of stress-strain curve that presents the new confined material in the compression zone. Hence, assuming that the same concept applies for concrete masonry is considered to be acceptable and valid.

Construction of axial force-moment interaction diagrams is essential to evaluate the flexural capacity of an axially loaded masonry column. The shape of the interaction diagram is characterised by four fundamental points. Determining at least the axial load and moment values of fundamental points allows drawing simple interaction diagram. The points with the strain distributions in the cross section are illustrated in Figure 5.1.
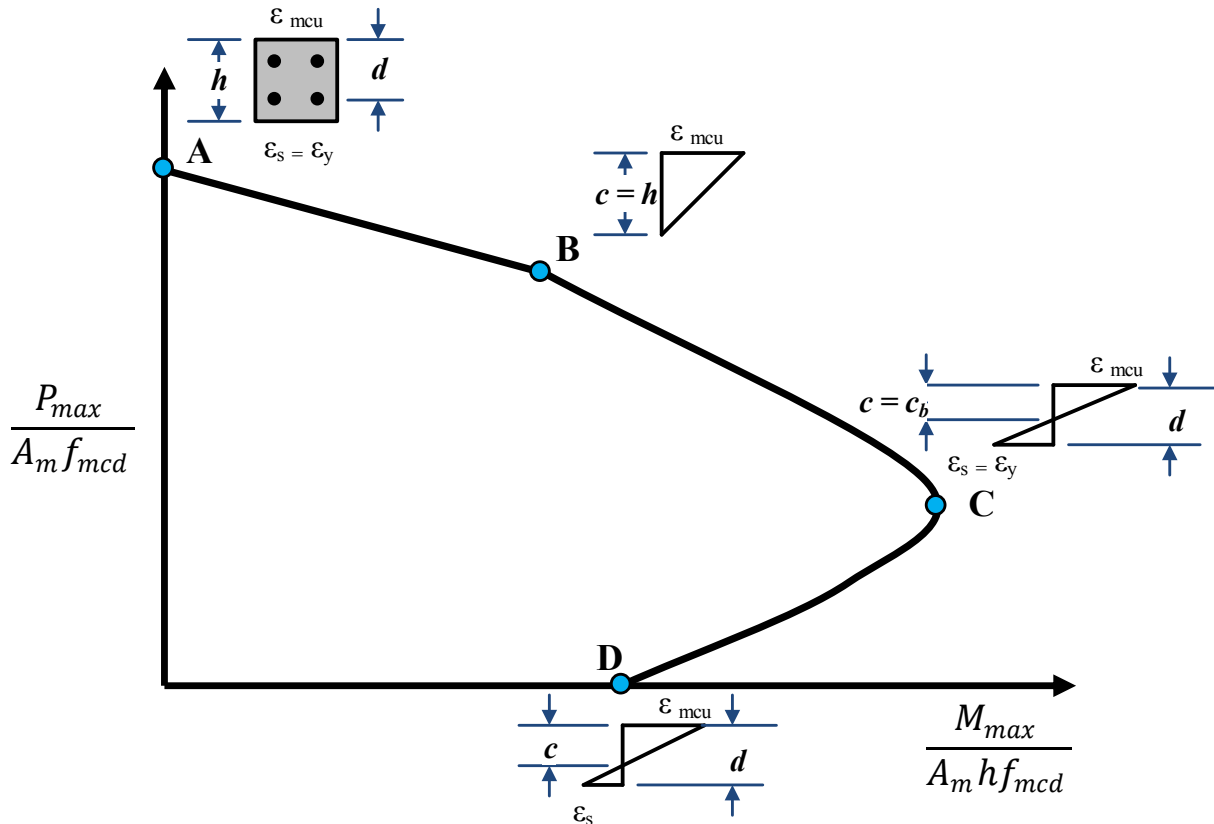
Figure 5.1 Axial force-moment interaction diagram.

Point A: Pure axial loading case with zero moment which represents the maximum axial load limit. The masonry column, in this case, experiences uniform compressive strain in entire the cross section with reaching the ultimate axial strain of confined masonry (ε_{mcu}), and the longitudinal steel reinforcements are yielded with compressive strain equals to (ε_y).

Point B: The loading case when extreme compression fibre reaches the ultimate axial strain of confined masonry with zero strain in the tension side of the masonry column.

Point C: The balanced loading case is the condition when the ultimate compressive strain in extreme compression fibre of confined masonry simultaneously occurs with the yielding of the layer of longitudinal steel reinforcements the nearest to the tension face of the masonry column.

Point D: Pure bending case with zero axial load which represents the ultimate bending moment capacity.

Developing axial force-moment interaction diagrams is based on the well-known procedure of section analysis adopted for conventional reinforced concrete columns. The following

assumptions are considered while performing the analysis of the FRP confined concrete masonry section:

a) Plane sections remain plane during bending.

b) The equilibrium of forces and strain compatibility must be satisfied.

c) Perfect composite action in masonry composite (grout, blocks, and mortar) is assumed.

d) The tensile strength of masonry composite is neglected.

e) There is a perfect bond between all of steel reinforcements, masonry composite, and FRP jacket.

f) The equivalent rectangular stress block can accurately describe the distribution of compressive stress in FRP confined concrete masonry.

g) The additional confinement provided by steel ties is neglected.

h) FRP jacket does not carry or under any direct axial loads.

i) No contribution of the transverse FRP confinement for columns failing in a tension controlled manner.

In the interaction diagram, the segment defined by the points A, B, and C, and the segment defined by the points C and D represent compression-controlled and tension-controlled failure, respectably. Point D denotes the maximum bending moment capacity of the masonry columns. The value of the point D can be obtained by determining the neutral axis position following the conventional reinforced concrete beam theory. This paper only addresses the segment of the axial force-moment interaction diagrams where the compression is considered the dominated failure mode. Assuming no contribution of the FRP confinement for strengthening columns failing in a tension controlled manner (Rocca et al., 2009).

Point A represents the condition of pure axial compression without any bending moment. The nominal axial load capacity of a short reinforced concrete masonry column can be taken as the contribution of the axial compressive strengths of FRP confined masonry and longitudinal steel

reinforcements. The maximum axial capacity of masonry column can be theoretically expressed as:

$$P_{max} = f_{mcd}(A_m - A_s) + f_y A_s$$

Eq. 5-1

The equation gives the force without considering the slenderness or accidental eccentricity present in most of the columns in the site. The structural engineers must consider these factors and apply reduction factors that are consistent with the applicable design code. The points B and C can be computed by determining the position of the neutral axis in the strain distribution using similar triangles for each loading case, then integrate the stresses over the cross section.

In order to perform detailed section analysis, fundamental parameters need to be established. Maximum usable FRP confined concrete masonry strain must be defined to determine the ultimate strain value that can be reached in the extreme compression fibre. In order to integrate the stresses over the cross section, a stress-strain curve represents the real behaviour of the material is needed. However, instead of using the nonlinear stress-strain curve, most of the design codes allow the use of equivalent stress block parameters to evaluate the capacity of the member in compression. Also, the value of the compressive strength of FRP-confined masonry is essential for performing detailed section analysis. Since the axial strength of FRP confined concrete masonry depends on both the compressive strength of masonry before strengthening and confinement pressure provided by FRP jacket, a reliable analytical confinement model to predict strength gains is needed.

The following subsections discuss the values of these fundamental parameters that control the section analysis which is necessary to predict the strength and moment capacity of FRP confined concrete masonry columns. Also, the computational methods to obtain these values are discussed.

5.3.1 Predicting the strength gain

Determining the axial capacity of FRP confined concrete masonry (f_{mcd}) is necessary to axial force-moment interaction diagram prediction. Suitable strength model that gives a reliable estimation of the effectiveness of FRP strengthening system can be used to quantify the enhancement in the strength as a result of FRP jacketing. The model provided in CNR-DT 200 R1 (2013) guide would be satisfactory for predicting the strength enhancement in masonry columns strengthened by FRP jackets. The model expresses the gain in strength as follows:

$$\frac{f_{mcd}}{f_{md}} = 1 + k'.\left(\frac{f_{l,eff}}{f_{md}}\right)^{\alpha_1} \qquad \text{Eq. 5-2}$$

f_{mcd} is the compressive strength of FRP-confined masonry, and f_{md} is the compressive strength of masonry before strengthening. The coefficient k' can be calculated as follows:

$$k' = \alpha_2.\left(\frac{g_m}{1000}\right)^{\alpha_3} \qquad \text{Eq. 5-3}$$

g_m is the density of masonry in kg/m^3. The coefficients α_1, α_2, α_3 can be taken as 0.50, 1.0 and 1.0, respectively, in case of experimental data is absent. The effective confining pressure, $f_{l,eff}$, is adjusted by a horizontal and vertical coefficient of efficiency as follows:

$$f_{l,eff} = k_H.k_V.f_l \qquad \text{Eq. 5-4}$$

where f_l is the lateral confining pressure produced by FRP jacket. For prismatic masonry columns continuously wrapped with FRP jacket, the lateral confining pressure can be estimated according to the following expression:

$$f_l = 2.\frac{t_f.E_f}{\max\{b,h\}}.\varepsilon_{fd,rid} \qquad \text{Eq. 5-5}$$

where b and h are the width and the height of cross section, and t_f and E_f are thickness and the tensile modulus of elasticity for of FRP jacket. The reduced value of the ultimate strain of FRP, $\varepsilon_{fd,rid}$, can be computed as follows:

$$\varepsilon_{fd,rid} = \min\left\{n_a.\frac{\varepsilon_{fk}}{\gamma_f}; 0.004\right\} \qquad \text{Eq. 5-6}$$

where n_a and γ_f are environmental and safety factors for FRP material, respectively. ε_{fk} is characteristic FRP ultimate tensile strain which can be obtained by testing FRP flat coupons.

It should be noted that the FRP jacket fails at lower hoop strain than the ultimate tensile strain of flat coupon tests in most cases. The CNR-DT 200 R1 model limits the value of strain in FRP jacket to be 0.004 (mm/mm). According to the experimental test conducted by Alotaibi and Galal (2017) on grouted concrete block masonry columns confined by CFRP jackets, the strain limit should be reduced to 0.002 (mm/mm) to improve the accuracy of the CNR-DT 200 R1 model in predicting the strength gain in concrete masonry columns.

For noncircular columns, the confinement of FRP jacket is less effective in strengthening the column. For the columns with prismatic cross section, only a portion of it is considered effectively confined by FRP jacket. Increasing the corner radius would increase the confined area leading to more gain in the axial capacity of columns. The effectively confined area for a square column is illustrated in Figure 5.2.

Effectively confined area
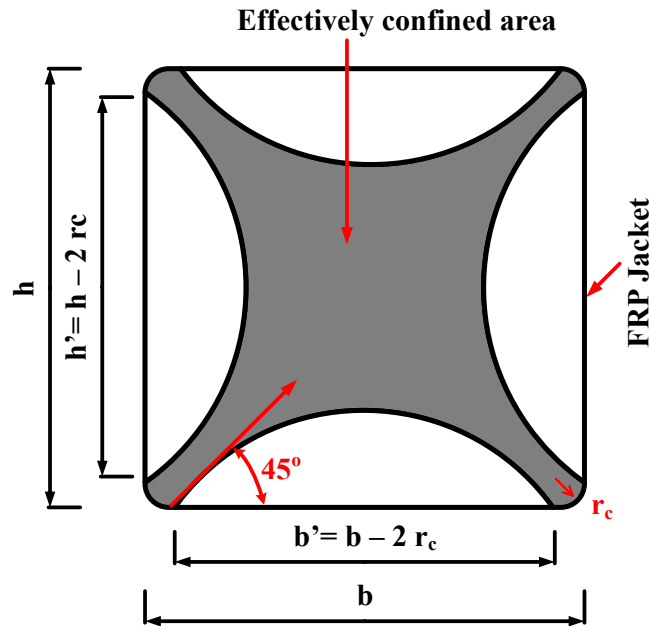
Figure 5.2 Effectively confined area in square cross section.

The CNR-DT 200 R1 model introduces a horizontal coefficient of efficiency, k_H, to account for the geometry of cross section.

$$k_H = \left(1 - \frac{b'^2 + d'^2}{3A_m}\right)$$

Eq. 5-7

A_m is masonry column area, $b' = b - 2r_c$, and $h' = h - 2r_c$, where r_c is cross section corner radius, as shown in Figure 5.2. The vertical coefficient of efficiency k_V can be considered as one for a continuous wrapped columns. The model provides mathematical expressions to predict the lateral confining pressure for masonry columns with circular cross sections and can predict the strength gain for prismatic masonry columns with FRP strips (non-continuous wrapping). However, discussing these expressions is out of scope of this paper.

Comparison between CNR-DT 200 R1 strength model and experimental data for fully grouted reinforced concrete masonry columns is carried out in terms of strength gain to ensure the reliability of strength model. Six stress-strain curves described in Alotaibi and Galal (2018) for

reinforced concrete masonry columns tested under pure compressive force and strengthened with one and two layers of CFRP jackets were used. The labels L1 and L2 were utilized for masonry columns strengthened with one and two layers of CFRP, respectively. In Figure 5.3, the stress-strain curves for each group were averaged to obtain a unified representation of the behaviour of the masonry columns confined with FRP jackets. The methodology that was used to obtain the average stress-strain curves is based on choosing one thousand strain values on the x-axis and averaging the three corresponding stress values for each strain value, then the average stress values plots against the chosen strain values.
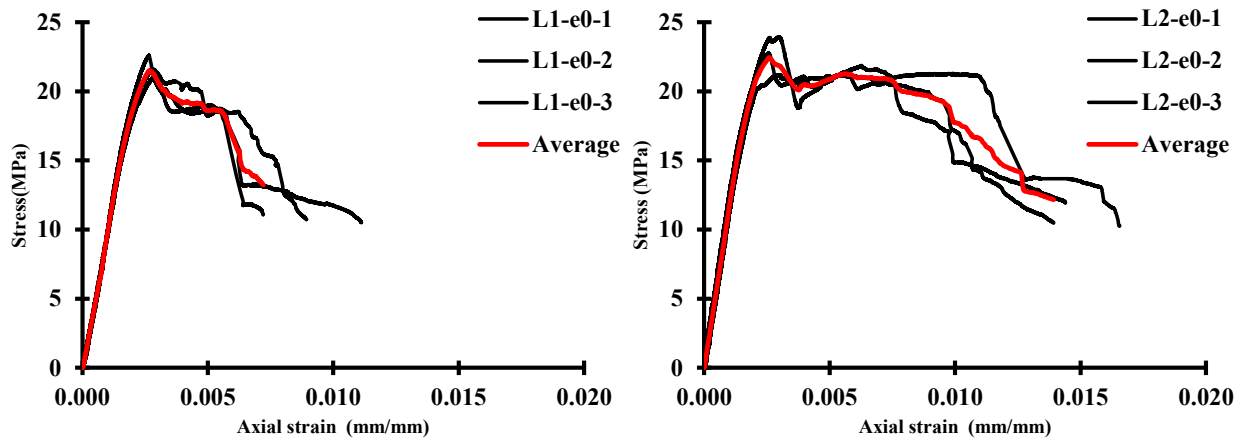
Figure 5.3 Averaged stress-strain curves for masonry columns strengthened with one and two layers of CFRP.

Averaged stress-strain curves for masonry columns strengthened with one, and two layers of CFRP jackets are presented in Figure 5.4 with and without longitudinal steel reinforcements' contribution. The strength provided by the longitudinal steel reinforcements was subtracted from the total strength capacity of the FRP confined concrete masonry column. An elastic-perfect plastic response of the longitudinal steel reinforcements was assumed. The values of elastic modulus, yield strain and yield stress for the longitudinal steel reinforcements were obtained from experimental tests conducted on steel bars are summarized in Table 5.1. Strain compatibility between longitudinal steel reinforcements and concrete masonry was assumed while producing stress-strain curves for FRP confined concrete masonry. The reduction by corner radius was considered when calculating stresses in the cross section.
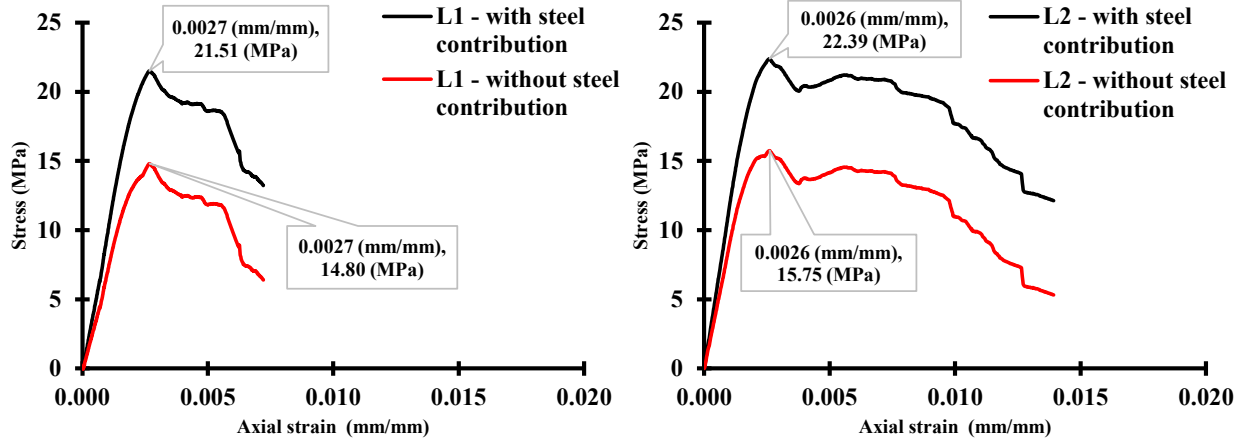
Figure 5.4 Averaged stress-strain curves of masonry columns for one and two layers of CFRP with and without longitudinal steel reinforcements' contribution.

The differences between the experimental tests and CNR-DT 200 R1/2013 predictions are summarized in Table 5.3, along with the absolute error percentage. The absolute error is calculated as the difference between experimental strength and theoretical strength over the experimental strength multiplied by 100.

For calculating CNR-DT 200 R1/2013 prediction, the environmental and safety coefficients were taken equal to one in order to represent the nominal capacity. The maximum allowed strain in FRP jacket was limited to 0.002 (mm/mm) while calculating theoretical predictions. CFRP material properties which used to calculate the theoretical strengths of reinforced concrete masonry columns confined with CFRP jackets are summarized in Table 5.1.

Table 5.3 Comparison between theoretical predictions and experimental data.

Column	Experimental value (MPa)	CNR-DT 200 R1/2013 prediction (MPa)	Absolute error (%)
L1-e0	14.80	14.51	1.9
L2-e0	15.75	15.99	1.5

It can be seen from the table that CNRDT 200 R1 model can give a close prediction for FRP confined concrete masonry columns. The absolute errors between the experimental data and theoretical prediction are low. The absolute errors are 1.9, and 1.5% for concrete masonry columns strengthened with one and two layers of CFRP jackets, respectively. This is in support of the suggestion proposed by Alotaibi and Galal (2017) to limit the strain in FRP to 0.002 (mm/mm) to

improve the accuracy of CNRDT 200 R1 model in predicting the strength of concrete masonry columns confined by FRP jackets.

5.3.2 Predicting ultimate strain gain

The ultimate axial strain of FRP confined masonry columns must be defined in order to perform the detailed section analysis. The main issue that needs to be addressed before determining the ultimate strain is defining the stress-strain curve that accurately represents the stress distribution of FRP confined masonry in the compression zone. Studies reported in the literature about FRP confined concrete still have no consensus on whether concentric stress-strain models are appropriate for predicting the behaviour of eccentrically loaded columns or not (Wu and Jiang, 2013a).

More than 88 stress-strain models of FRP confined concrete were reported in Ozbakkaloglu et al. (2013). Most of these models were developed for columns under concentric loading. Lam and Teng (2003) proposed widely used stress-strain model calibrated with concentrically tested concrete columns. The model was adopted by ACI 440.2R-08 (2008) design guideline. Carrazedo and Hanai (2017) constructed axial force-moment interaction diagrams for noncircular FRP-confined concrete columns loaded in compression with small eccentricities following the procedure proposed by Rocca et al. (2009) based on the stress-strain curves obtained from Lam and Teng (2003) model. The study concluded that the overall performance of the procedure proposed by Rocca et al. (2009) with Lam and Teng (2003) model was satisfactory.

In contrast, research conducted on FRP confined concrete columns (Fam et al., 2003; Maaddawy, 2009; Hu et al., 2011; Wu and Jiang, 2013a) found that the eccentric stress-strain curve is different from the concentric stress-strain curve. Parvin and Wang (2001) and Parvin and Schroeder (2008) showed that nonlinear finite element analyses could satisfactorily capture the column behaviour if the effect of strain gradient on confining stress is considered. According to Wu and Jiang (2013a) the FRP confined stress-strain models derived from concentric tests are not applicable to concrete columns tested under eccentric loading. Wu and Jiang (2013a) proposed FRP confined concrete stress-strain model under increasing axial loading with constant eccentricity. Recently a new stress-strain model for FRP confined circular concrete columns under constant axial force, and increasing load eccentricity was proposed by Cao et al. (2018).

The tests reported for concrete masonry columns in Alotaibi and Galal (2018) showed an increase in strain under eccentric loading. From the above, it can be seen that there is no unified approach for quantifying the effect of strain gradient on the FRP confined concrete stress-strain curve.

Maaddawy (2009) proposed using a stress-strain curve that was obtained for concentrically loaded columns for predicting the capacity of eccentrically loaded columns with only one change to account for the strain gradient resulted from the eccentricity. Maaddawy (2009) suggested changing the final point of the ultimate failure of concentric the stress–strain curve based on the level of eccentricity.

In this paper, the expression proposed for predicting the ultimate axial strain of FRP confined concrete masonry is calibrated using empirical constants from regression analysis of ten eccentric tests of reinforced concrete masonry columns strengthened with CFRP jackets reported in Alotaibi and Galal (2018).

Considering the suggestion of Maaddawy (2009), the axial strain of eccentrically loaded columns corresponding to the peak load is assumed to be the ultimate strain can be reached in the extreme compression fibre of confined masonry. Furthermore, concentric stress-strain curve end with ultimate axial strain equals to axial strain corresponding to the peak load of eccentrically loaded columns can accurately represent the stress distribution of FRP confined masonry in the compression zone in eccentrically loaded columns.

Figure 5.5 shows the ultimate axial strain gain of confined masonry ($\varepsilon_{mcu}/\varepsilon_{mu}$) versus the ratio of effective confining pressure to unconfined masonry strength ($f_{l,eff}/f_{md}$). The ultimate axial strain gains were calculated by considering the ultimate axial strain of unconfined concrete masonry equals 0.0025 mm/mm. The effective confining pressure is obtained by adopting the predictions of CNR-DT 200 R1/201 model.
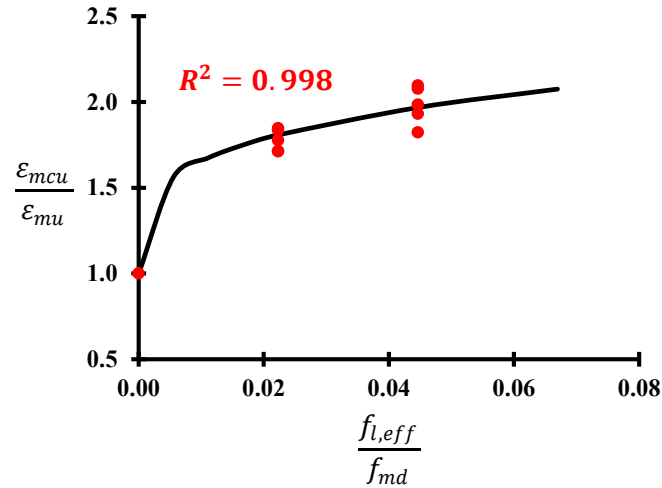
Figure 5.5 Ultimate axial strain of confined concrete masonry in terms of effective confining pressure.

A similar function used by (CNR-DT 200 R1, 2013) guide for strength gain was utilized to establish the best-fit representation of the experimental data for the ultimate strain gain of confined masonry. The expression obtained from the regression analysis can be written as follows:

$$\frac{\varepsilon_{mcu}}{\varepsilon_{mu}} = 1 + \left(\frac{g_m}{1000}\right) \cdot \left(\frac{f_{l,eff}}{f_{md}}\right)^{0.26} \qquad \text{Eq. 5-8}$$

Note that by using the same function for both strength gain (f_{mcd}/f_{md}) and ultimate axial strain gain ($\varepsilon_{mcu}/\varepsilon_{mu}$), the shapes of the output curves are assumed to be similar.

From the proposed expression, the ultimate axial strains for concrete masonry columns confined with effective confining pressures of 0.245 and 0.489 MPa are equal to 0.0045 and 0.0049 (mm/mm), respectively.

5.3.3 Equivalent stress block parameters

For performing the analysis of sections subjected to axial and flexure combinations, the stress distribution in the compression zone should be determined for the section at the ultimate strain. The strain distribution over the section depth is linear when assuming the plane section remains plane after bending. The actual stress distribution is non-linear and can be obtained by testing the material to determine the uniaxial stress-strain curve. Considering the complexity of using non-linear stress distribution in practical design, the non-linear stress distribution of the material can be replaced by an equivalent rectangular stress block to analysis a member under flexural loading. Realistic equivalent rectangular stress block must have the same area and centroid of the original

uniaxial stress-strain curve of the material to match the magnitude and location of the resultant compressive force, as shown in Figure 5.6. The equivalent rectangular stress block is controlled by α and β parameters. The average stress, $\alpha\, f_{mcd}$, and the distance βc should be determined to give a stress block with equivalent centroid and area similar to that of the actual non-linear stress-strain curve.
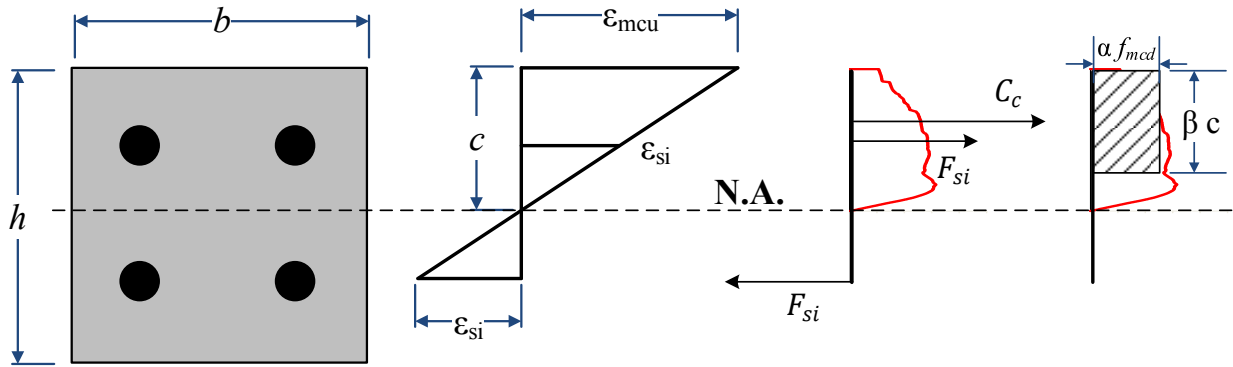
Figure 5.6 Equivalent rectangular stress block.

By assuming the maximum compressive strength and the ultimate axial strain of FRP-confined masonry, the equivalent rectangular stress block can be calculated by:

$$\int_{0}^{\varepsilon_{mcu}} \sigma_m\, d\varepsilon_m = \alpha\, f_{mcd} \cdot \beta\, \varepsilon_{mcu} \qquad \text{Eq. 5-9}$$

$$\int_{0}^{\varepsilon_{mcu}} \sigma_m\, \varepsilon_m\, d\varepsilon_m = \alpha\, f_{mcd} \cdot \beta\, \varepsilon_{mcu}\, . (1 - 0.5\beta)\, \varepsilon_{mcu} \qquad \text{Eq. 5-10}$$

where σ_m is the nonlinear stress of masonry confined by FRP as a function of axial strain ε_m. The stress in compression zone can be expressed as:

$$\sigma_m = f(\varepsilon_m) \qquad \text{Eq. 5-11}$$

The area under the stress-strain curve of FRP confined masonry A_{crv} is equal to the integration of stress function.

$$A_{crv} = \int_{0}^{\varepsilon_{mcu}} \sigma_m\, d\varepsilon_m \qquad \text{Eq. 5-12}$$

The first moment of area for the nonlinear stress function S_{crv} can be described as follows:

$$S_{crv} = A_{crv} \cdot x_{crv} = \int_{0}^{\varepsilon_{mcu}} \sigma_m \, \varepsilon_m \, d\varepsilon_m \qquad \text{Eq. 5-13}$$

where x_{crv} is the centroid of the FRP confined masonry stress-strain curve.

The two parameters of the equivalent rectangular stress block (α and β) can be found by solving the two equations:

$$A_{crv} = \alpha \, f_{mcd} \cdot \beta \, \varepsilon_{mcu} \qquad \text{Eq. 5-14}$$

$$A_{crv} \cdot x_{crv} = \alpha \, f_{mcd} \cdot \beta \, \varepsilon_{mcu} \cdot (1 - 0.5\beta) \, \varepsilon_{mcu} \qquad \text{Eq. 5-15}$$

For finding the α and β parameters of the equivalent rectangular stress block, the calculation of the area and centroid of averaged stress-strain curves for masonry columns confined with one and two layers of CFRP is presented in Figure 5.7.
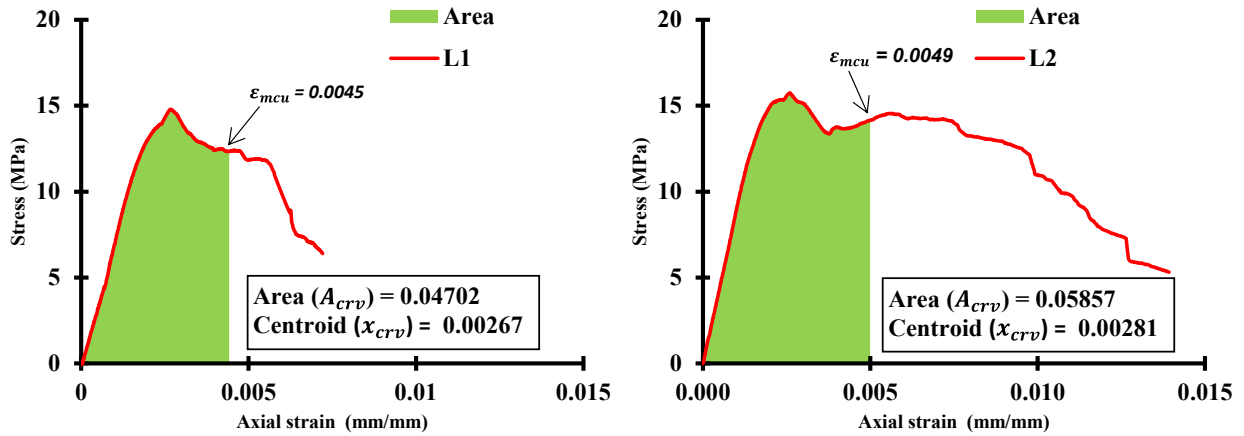
Figure 5.7 The area and centroid of averaged stress-strain curves for masonry columns confined with one and two layers of CFRP.

The area under the stress-strain curve was calculated by dividing the curve into multiple trapezoid pieces where the total area equals the sum of each trapezoid area. The centroid can be founded by the following relationship:

$$x_{crv} = \frac{Total \ moments}{A_{crv}} \qquad \text{Eq. 5-16}$$

where the total moment is the sum of each trapezoid area multiplied by the distance of its centroid in the x-axis. The solutions of Eq. 5-14 and Eq. 5-15 are summarized in Table 5.4.

Table 5.4 The equivalent rectangular stress block parameters values.

Parameters	L1	L2	Selected value
α	0.87	0.89	0.85
β	0.81	0.85	0.85

The effect of strain gradient on the equivalent rectangular stress block parameters is related to the effect of strain gradient on the actual stress-strain curve. An alternative approach can be developed to account for strain gradient by calibrating the force and moment equilibriums in the confined section for each eccentrically tested column by changing the values of parameters α and β.

The axial force and moment capacities of the column can be written as following where compression is taken as positive:

$$P_{\max} = \alpha\, f_{mcd} \cdot \beta\, c \cdot b + \sum_{i=1}^{n} f_{si} A_{si} \qquad \text{Eq. 5-17}$$

$$M_{\max} = (\alpha\, f_{mcd} \cdot \beta\, c \cdot b)\left(\frac{h}{2} - \beta \frac{c}{2}\right) + \sum_{i=1}^{n} f_{si} A_{si}\left(d_i - \frac{h}{2}\right) \qquad \text{Eq. 5-18}$$

$P_{\max}$ is the measured axial load and $M_{\max}$ the measured moment of FRP confined masonry column tested eccentrically. f_{mcd} is the maximum FRP confined stress predicted base on concentrically tested masonry prisms. n is the total longitudinal steel reinforcements number. The stress and area of the ith steel reinforcement denoted by f_{si} and A_{si}, respectively. d_i represents the distance of the ith steel reinforcement from the extreme compression fibre of confined masonry. The strain of the ith steel reinforcement ε_{si} can be determined by using similar triangles of the strain distribution as follows:

$$\varepsilon_{si} = \frac{x}{c}\, \varepsilon_{mcu} \qquad \text{Eq. 5-19}$$

where x is the distance between the centre of ith steel reinforcement to the neutral axis.

Beside the parameters α and β, the neutral axis depth c is treated as an unknown to find the axial force and moment values that satisfies the equilibrium for each eccentrically tested column. Although the average strain distribution of cross section is reported in Alotaibi and Galal (2018), these values was not adopted. The reported values represent the average of three replicate masonry

columns and also represent the average strain along the height of column. This would underestimate the actual strain in critical section of the column at the mid-height. Instead of using the neutral axis depth linearly interpolated from measured displacements on the compression and tension faces, the calculated values based on force and moment equilibriums are used and considered to be more representative. The values of α, β and c calculated for each eccentrically tested concrete masonry columns are summarized in Table 5.5.

Table 5.5 Values of α, β, and c for the eccentrically tested columns.

columns	f_{mcd} (MPa)	t_f (mm)	α	Average (St. Dev.)	β	Average (St. Dev.)	c
L1	14.80	0.381	0.72	0.81 (0.12)	0.80	0.78 (0.02)	175.2
			0.94		0.80		175.0
			0.78		0.78		177.5
			0.68		0.78		139.2
			0.91		0.75		139.0
L2	15.75	0.762	0.89	0.82 (0.06)	0.83	0.82 (0.02)	172.2
			0.88		0.79		175.3
			0.81		0.81		133.3
			0.77		0.82		132.9
			0.78		0.82		133.9
SELECTED VALUE				0.80		0.80	

Considering solving equations that involve three variables α, β and c, the values of neutral axis depth linearly interpolated from experimental tests and stress block values obtained from concentric stress-strain curve were used as initial guess values, where the solution is sensitive to initial guess. The solutions were achieved by adjusting values of variables until experimental values of force, moment and eccentricity were satisfied.

For two approaches, practical values were selected to simplify the design procedure. The validation of selected equivalent rectangular stress block parameters values will be presented in section 5.5.

5.4 Proposed design methodology

Enhancement in the performance of concrete masonry columns due to the confinement by FRP jackets can only be expected when the coordinates of the applied axial force and flexural moment falls above the balance line; Where the balance line is a straight line between the origin

point and the balanced point (Point C) in the axial force-moment interaction diagrams of unconfined columns. In other words, the contribution of the FRP confinement for strengthening columns is considered only when the control failure mode is the compression.

The proposed design methodology only addresses the segment defined by the points A, B, and C correspond to compression-controlled region in the axial force-moment interaction diagram.

The first step in the construction of the axial force-moment interaction diagram is predicting the strength gain in axial force as a result of using FRP jackets to retrofit the concrete masonry column. The strength gain can be determined by solving Eq. 5-2 proposed by CNR-DT 200 R1 design guideline. The ultimate axial strain of concrete masonry confined by FRP can be defined by the expression proposed in this paper by Eq. 5-8.

After determining the compressive strength (f_{mcd}) and the ultimate strain (ε_{mcu}) of FRP-confined masonry, the curve of the interaction diagram can be drawn by generating many points on the curve where the coordinates of any point indicate axial load and bending moment of FRP confined concrete masonry column. However, a simpler multi-linear interaction diagram can be drawn if the values of the points A, B, and C were determined.

The pure nominal axial strength, point A, can be calculated by Eq. 5-1. The nominal strength and moment capacities for the points B and C would be found by Eq. 5-17 and Eq. 5-18, where the depth of neutral axis c can be determined by Eq. 5-20 for the points B and C.

$$c = \begin{cases} h \\ c_b = d \dfrac{\varepsilon_{mcu}}{\varepsilon_{mcu} + \varepsilon_y} \end{cases} \qquad \text{Eq. 5-20}$$

The segment of the interaction diagram curve between the points A and B is assumed to be linear. On the other hand, the segment BC of the curve can be drawn by selecting arbitrary values of c in the range $h \geq c \geq c_b$ and solving Eq. 5-17and Eq. 5-18.

5.5 Accuracy of the proposed design equations

The experimental data reported in Table 5.2 were compared to theoretical axial force-moment interaction diagrams generated by the proposed procedure to evaluate the accuracy of the design equations. Figure 5.8 and Figure 5.9 show comparisons of the experimental data against the theoretical predictions of the nominal capacities using the proposed approach by changing the position of neutral axis and using different values of the stress block parameters. The parameters

α and β are taken according to the suggested values in this paper considering the two alternative approaches discussed in Section 5.3.3. In the figures, green dashed lines connecting the balanced points to the origin points were depicted to distinguish between compression-controlled failure and tension-controlled failure.
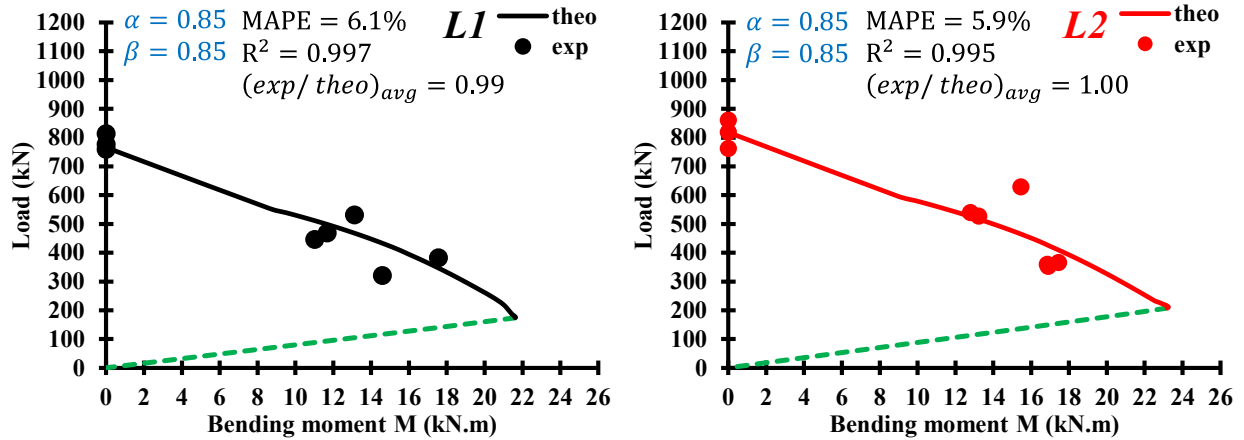
Figure 5.8 The comparisons of the experimental tests against the theoretical predictions $(\alpha = 0.85, \beta = 0.85)$.
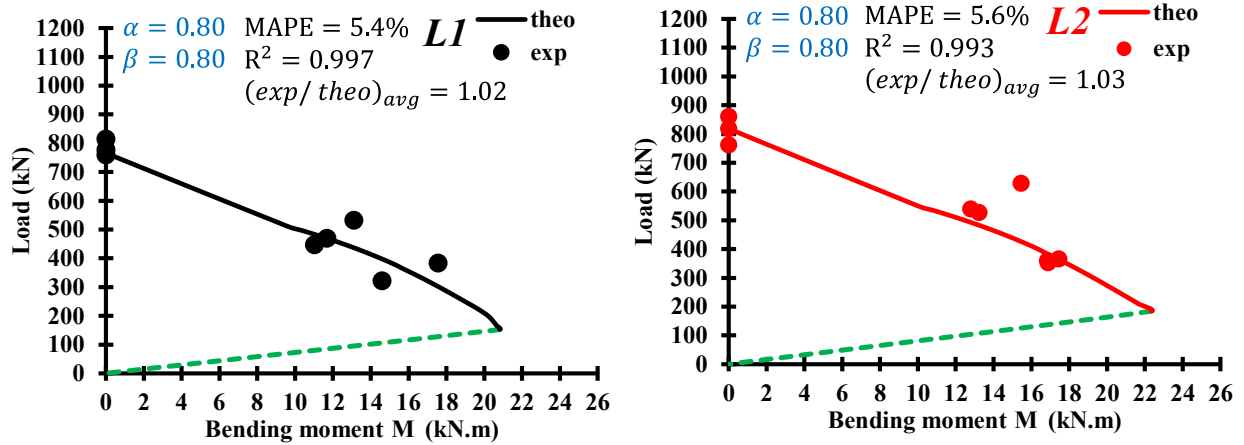
Figure 5.9 The comparisons of the experimental tests against the theoretical predictions $(\alpha = 0.80, \beta = 0.80)$.

The parameter δ is defined to quantify the absolute error percentage between experimental result and theoretical predictions. The intersection points between the radial origin line and both experimental point and the theoretical point on interaction curve were used to calculate the absolute error percentage (δ), as shown in Figure 5.10. Both the points $E\left(M_{exp}, P_{exp}\right)$ and $T\left(M_{theo}, P_{theo}\right)$ have the same slope which is simply the inverse of eccentricity.

121
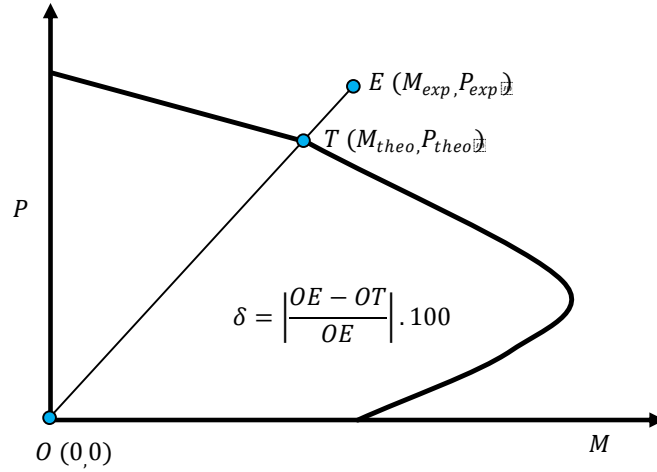
Figure 5.10 The definition of the absolute error percentage between experimental test and theoretical prediction.

The calculated differences between theoretical predictions and tests are reported in Table 5.6 and Table 5.7, where the mean absolute percentage error (MAPE) is the average of the absolute error. The definitions of the statistical metrics reported in figures are:

$$APE = \frac{\sum_{i=1}^{n} \left| \frac{\exp_i - theo_i}{\exp_i} \right|}{n} \qquad \text{Eq. 5-21}$$

$$R^2 = 1 - \left(\frac{\sum_{i=1}^{n}(\exp_i - theo_i)^2}{\sum_{i=1}^{n} theo_i^2} \right) \qquad \text{Eq. 5-22}$$

$$(exp/\, theo)_{avg} = \frac{\sum_{i=1}^{n}(\exp_i /theo_i)}{n} \qquad \text{Eq. 5-23}$$

where R^2 and $(exp/\, theo)_{avg}$ are the absolute fraction of variance and average the experimental test to theoretical prediction ratios, respectively. The term $theo$ represents theoretical and the term exp represents experimental test. n is the total number of tests.

Table 5.6 The calculated differences between theoretical predictions and tests for $(\alpha = 0.85, \beta = 0.85)$.

Column label	Experimental data		Theoretical predictions		δ (%)	MAPE (%)	$(exp_i / theo_i)$	Average and COV (%)
	P_{max} (kN)	M_{max} (kN.m)	P (kN)	M (kN.m)				
L1-e0-1	759.06	0.00	765.57	0.00	0.9		0.99	
L1-e0-2	814.00	0.00	765.57	0.00	6.0		1.06	
L1-e0-3	777.38	0.00	765.57	0.00	1.5		1.02	
L1-e20-1	446.37	11.02	490.03	12.10	9.8	6.1	0.91	0.99 (7.6)
L1-e20-2	531.99	13.11	490.28	12.08	7.8		1.09	
L1-e20-3	469.27	11.67	488.77	12.16	4.2		0.96	
L1-e40-1	321.39	14.59	370.36	16.81	15.2		0.87	
L1-e40-2	382.74	17.56	368.10	16.89	3.8		1.04	
L2-e0-1	861.62	0.00	818.23	0.00	5.0		1.05	
L2-e0-2	819.50	0.00	818.23	0.00	0.2		1.00	
L2-e0-3	762.73	0.00	818.23	0.00	7.3		0.93	
L2-e20-1	540.23	12.79	530.56	12.56	1.8		1.02	
L2-e20-2	527.87	13.23	520.50	13.05	1.4	5.9	1.01	1.00 (8.8)
L2-e20-3	629.50	15.46	524.13	12.87	16.7		1.20	
L2-e40-1	366.71	17.45	384.10	18.28	4.7		0.95	
L2-e40-2	352.52	16.89	382.53	18.33	8.5		0.92	
L2-e40-3	359.85	16.85	387.81	18.16	7.8		0.93	

Table 5.7 The calculated differences between theoretical predictions and tests for
$(\alpha = 0.80, \beta = 0.80)$.

Column label	Experimental data		Theoretical predictions		δ (%)	MAPE (%)	$(exp_i/theo_i)$	Average and COV (%)
	P_{max} (kN)	M_{max} (kN.m)	P (kN)	M (kN.m)				
L1-e0-1	759.06	0.00	765.57	0.00	0.9		0.99	
L1-e0-2	814.00	0.00	765.57	0.00	6.0		1.06	
L1-e0-3	777.38	0.00	765.57	0.00	1.5		1.02	
L1-e20-1	446.37	11.02	470.78	11.62	5.5		0.95	1.02 (7.1)
L1-e20-2	531.99	13.11	471.02	11.61	11.5	5.4	1.13	
L1-e20-3	469.27	11.67	469.53	11.68	0.1		1.00	
L1-e40-1	321.39	14.59	353.33	16.04	9.9		0.91	
L1-e40-2	382.74	17.56	351.13	16.11	8.3		1.09	
L2-e0-1	861.62	0.00	818.23	0.00	5.0		1.05	
L2-e0-2	819.50	0.00	818.23	0.00	0.2		1.00	
L2-e0-3	762.73	0.00	818.23	0.00	7.3		0.93	
L2-e20-1	540.23	12.79	509.15	12.05	5.8		1.06	
L2-e20-2	527.87	13.23	499.22	12.51	5.4	5.6	1.06	1.03 (9.0)
L2-e20-3	629.50	15.46	502.80	12.35	20.1		1.25	
L2-e40-1	366.71	17.45	365.68	17.40	0.3		1.00	
L2-e40-2	352.52	16.89	364.15	17.45	3.3		0.97	
L2-e40-3	359.85	16.85	369.27	17.29	2.6		0.97	

The theoretical axial force-moment interaction diagrams obtained by the proposed procedure has a good correlation with tests results with an acceptable margin of error.

Figure 5.8 indicates that the mean absolute percentage errors are 6.1 and 5.9 for concrete masonry columns strengthened with one and two layers of CFRP jackets, respectively. However, using the equivalent rectangular stress block parameters α and β with value of 0.85 has given non-conservative predictions where the average the experimental test to theoretical prediction ratios is equal to one or less.

As Figure 5.9, using 0.80 for the values of the equivalent rectangular stress block parameters would give lower mean absolute percentage error with 5.4, and 5.6% for columns strengthened

with one and two layers of CFRP jackets, respectively. The predictions now are more conservative with the average experimental test to theoretical prediction ratios higher than one.

The authors recommend using the value of 0.80 for the parameters α and β. The equivalent rectangular stress block parameters were kept constant with different confinement levels for the simplicity. The lower value 0.80 was selected because a lower value of β would lead to slightly a longer lever arm that increase the moment capacity of the section. Taking the parameter α with 0.80, would reduce the axial force capacity. The suggested value provides a good correlation with conservative predictions when compared to experimental tests.

5.6 Parametric study

The proposed design equations showed a good accuracy with the available experimental data. The validated proposed procedure can be extended to study the effect of design variables on the axial-flexural interaction of fully grouted reinforced concrete masonry columns strengthened by FRP jackets. The outcome of the parametric study is seen as a quick useful tool for engineers to determine the effect of design variables and to be able to choose between strengthening alternatives in terms of costs and benefits. The design variables could be divided into two categories as variables related to FRP strengthening system and variables related to the original masonry column. The variables related to FRP jacket were emphasized in the parametric study considering that these variables are chosen by the retrofit engineer to find the most affordable and effective strengthening strategy. The variables related to the original concrete masonry column are more restricted to the existing properties. However, these variables would affect the outcomes of strengthening technique.

The design variables considered for strengthening system are the number of FRP layers, radius of the corners, and the stiffness of the FRP composite. The number of FRP layers (1-5 layers, with notation L) and corners radius (10 and 70 mm, with notation R) were investigated. The stiffness of the FRP composite is mainly controlled by modulus of elasticity and the thickness of the FRP laminate. Three different unidirectional FRP strengthening systems available in the market were used in this parametric study. The strengthening systems were chosen for their wide range of thickness and elastic modulus. The mechanical properties of the chosen FRP strengthening systems are summarized in Table 5.8, where the W letter stand for FRP wrap.

Table 5.8 Mechanical properties of the cured laminate.

Properties in primary fibre direction	W1	W2	W3
Ultimate tensile strength (MPa)	504	715	414
Thickness (mm)	0.508	1.3	0.51
Elastic modulus (MPa)	24591	18800	82000
Elongation at break (%)	1.93	1.09	1.6

The critical variables considered for the original masonry column are cross section aspect ratio and the masonry compressive strength (10 and 15 MPa). Two cross section of 390 x 390 mm and 190 x 390 mm with different aspect ratios (h/b) (1 for square and 2 rectangular cross section, with notations Sq and Rect, respectively) were investigated. According to the CNR-DT 200 R1 confinement model, the effect of FRP confinement shall not be considered for rectangular cross sections having aspect ratio more than two. However, considering that the aspect ratio for cross section of 190 x 390 mm is 2.05 and it is slightly off the range, the effect of FRP confinement was assumed to be existed in this parametric study and the confinement model was used to predict the gain in strength according to the proposed design methodology.

From the different combinations of variables, 124 axial force-moment interaction diagrams were constructed. Figure 5.11 and Figure 5.12 show P_{mcd}/P_{md} ratios against number of FRP layers, where P_{mcd} and P_{md} are the axial capacity of the columns at $0.15h$ level of eccentricity for FRP strengthened column and original masonry column, respectively.

Due to the difference in the original capacities of unconfined concrete masonry columns, a direct comparison between the results of masonry columns with different aspect ratios and masonry compressive strengths is not possible. However, the comparison was made between the axial capacity gain ratios at $0.15h$ level of eccentricity (i.e. e/h=0.15) to quantify the effect of design variables on the axial capacity.
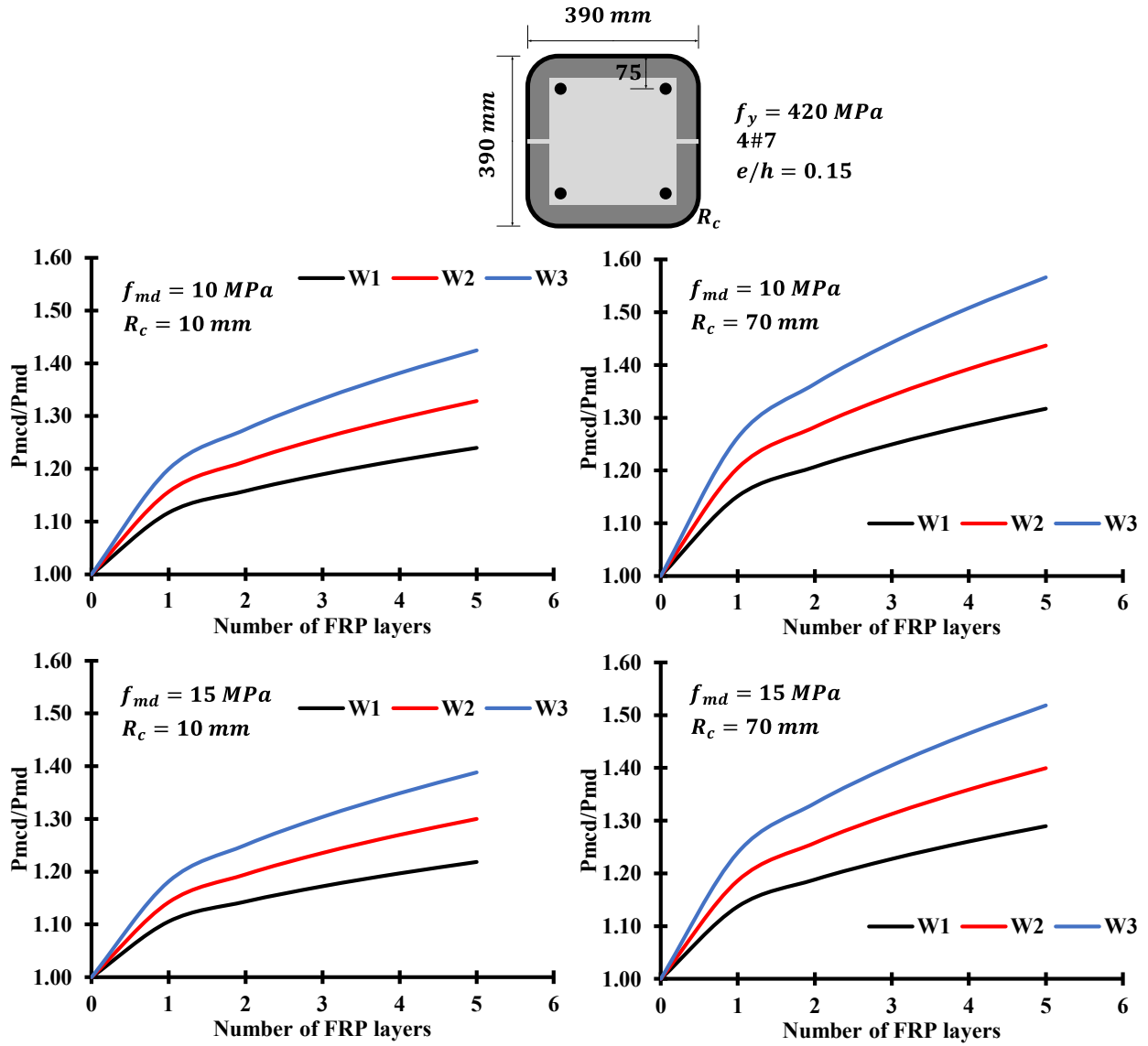
Figure 5.11 Axial load gains versus number of FRP layers for square reinforced masonry columns with f_{md} 10 and 15 MPa, R_c 10 and 70 mm for FRP systems W1, W2 and W3.
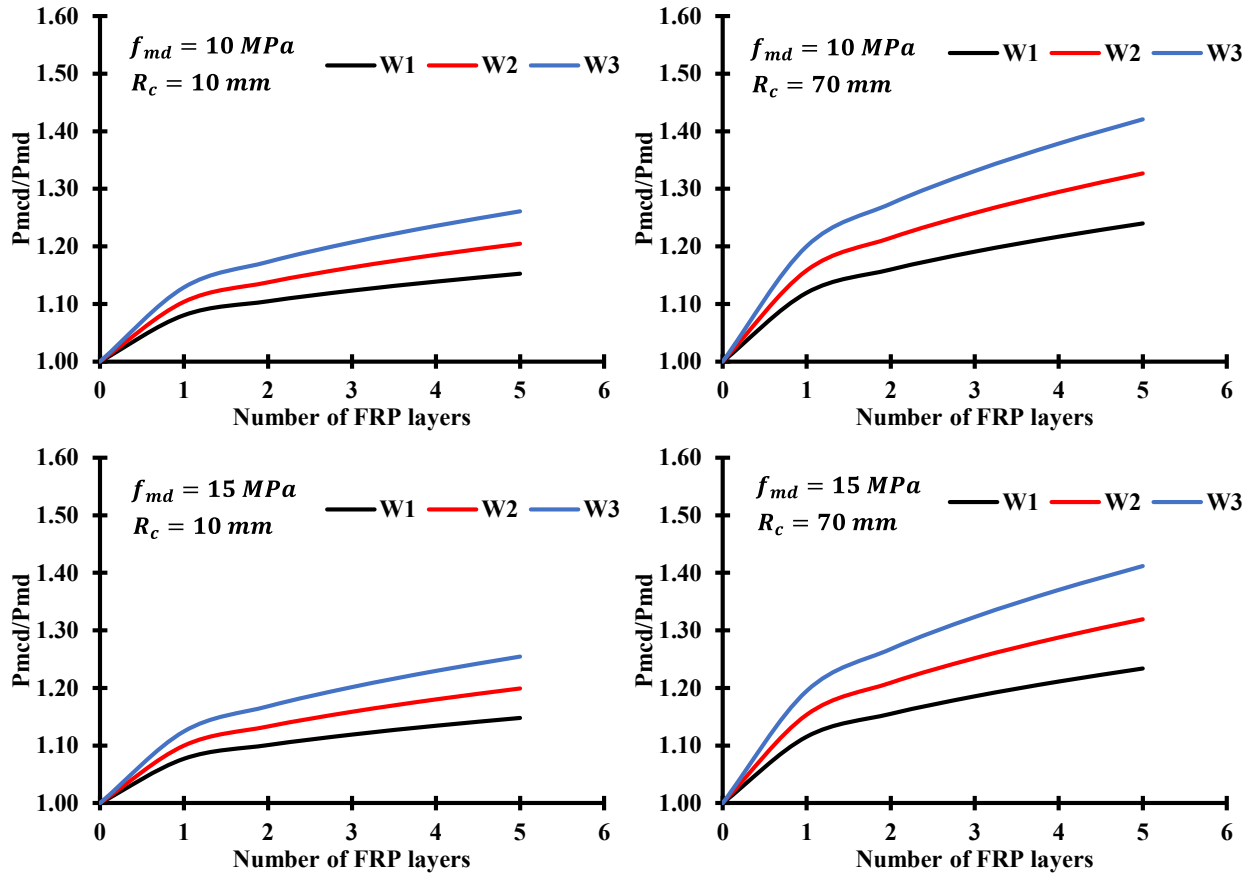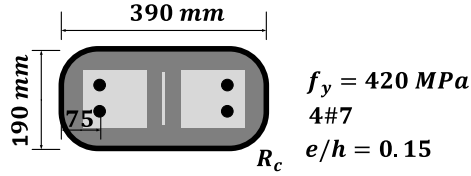
Figure 5.12 Axial load gains versus number of FRP layers for rectangular reinforced masonry columns with f_{md} 10 and 15 MPa, R_c 10 and 70 mm for FRP systems W1, W2 and W3.

The effect of increasing the number of FRP layers for a square column subjected to an eccentric axial load with e/h=0.15 can be quantified from Figure 5.11 when comparing L1-R10-W1-10MPa-Sq with L5-R10-W1-10MPa-Sq. Masonry column with one layer has 1.12 gain ratio of axial capacity whereas the gain ratio is 1.24 for masonry column with five layers of FRP.

Comparing L5-R10-W1-10MPa-Sq curve with L5-R70-W1-10MPa-Sq curve shows the effect of the corner radius. Increasing corner radius from 10 mm to 70 mm increased the gain ratio from 1.24 to 1.32 which is 8% increase in the axial capacity of original masonry column. This further increases to 15% with the stiffer jacket W3.

The effect of increasing the stiffness of FRP jacket can be seen in L5-R10-15MPa-Sq curve. The masonry column strengthened with W1 jacket has 1.22 gain ratio in axial capacity, whereas strengthening the masonry column with W3 jacket would lead to 1.39 gain ratio. This denotes a 17% increment in the axial capacity of original masonry column.

The effect of increasing the compressive strength of concrete masonry can be seen when comparing L5-R70-W1-10MPa-Sq curve with L5-R70-W1-15MPa-Sq curve. The gain ratio for masonry column with 10 MPa compressive strength is 1.32, where the gain ratio drops by 2% to 1.29 in case the column with 15MPa compressive strength. When using the W3 jacket, the reduction increases to 3%.

The effect of the aspect ratio of cross section can be concluded from comparing L5-R10-W1-10MPa-Sq curve with L5-R10-W1-10MPa-Rect curve. The square masonry column can reach 1.24 gain ratio comparing to 1.15 for rectangular cross section which around 7% reduction. This reduction increases to 11% with the stiffer W3 jacket.

From Figure 5.11, it can be observed concrete masonry column with a square shape and 10 MPa compressive strength can achieve 1.12 gain ratio if it is strengthened with one layer of W1 composite and the corner is rounded with 10 mm. The retrofit engineer could increase the gain in the axial capacity to 1.57 if five layers of W3 composite were used with rounding the corner to 70 mm.

It can be concluded from the comparison of Figure 5.11 and Figure 5.12 that applying the same level of strengthening on rectangular masonry column would lead to a reduction in the axial capacity gain ratio if compared to square masonry column. This is attributed to the reduction of the horizontal coefficient of efficiency (k_H) from 0.4 to 0.3 for square and rectangular cross section, respectably. Also, it can be concluded from the figures that the increase in f_{md} of the original masonry column would lead to a slight reduction in the strength gain of the strengthening system. Obviously, increasing the number of FRP layers and applying stiffer FRP jacket would increase the FRP confinement pressure and increase the efficiency of the retrofitting system. Also, increasing the corner radius would lead to more effective strengthening system by minimizing arch-effect illustrated in Figure 5.2.

Axial force-moment interaction diagrams for selected concrete masonry columns are demonstrated in Figure 5.13 for comparing the actual values of axial and moment capacities. For

distinguishing between compression-controlled failure and tension-controlled failure zones in the interaction diagrams, green solid lines connecting the balanced points to the origin points were drawn.

The effect of increasing the ratio of the corner radius from 10 to 70 mm for L5-W3-15MPa-Sq increased the pure axial capacities of columns by 394 kN. Retrofitting masonry column of L5-R70-15MPa-Sq with FRP jacket of W3 provides it with 692 kN higher in terms of pure axial capacity when compared to the same column with W1 jacket, considering that W3 jacket is 2.35 times stiffer than W1 jacket if the stiffness represented by $E_f.t_f$.
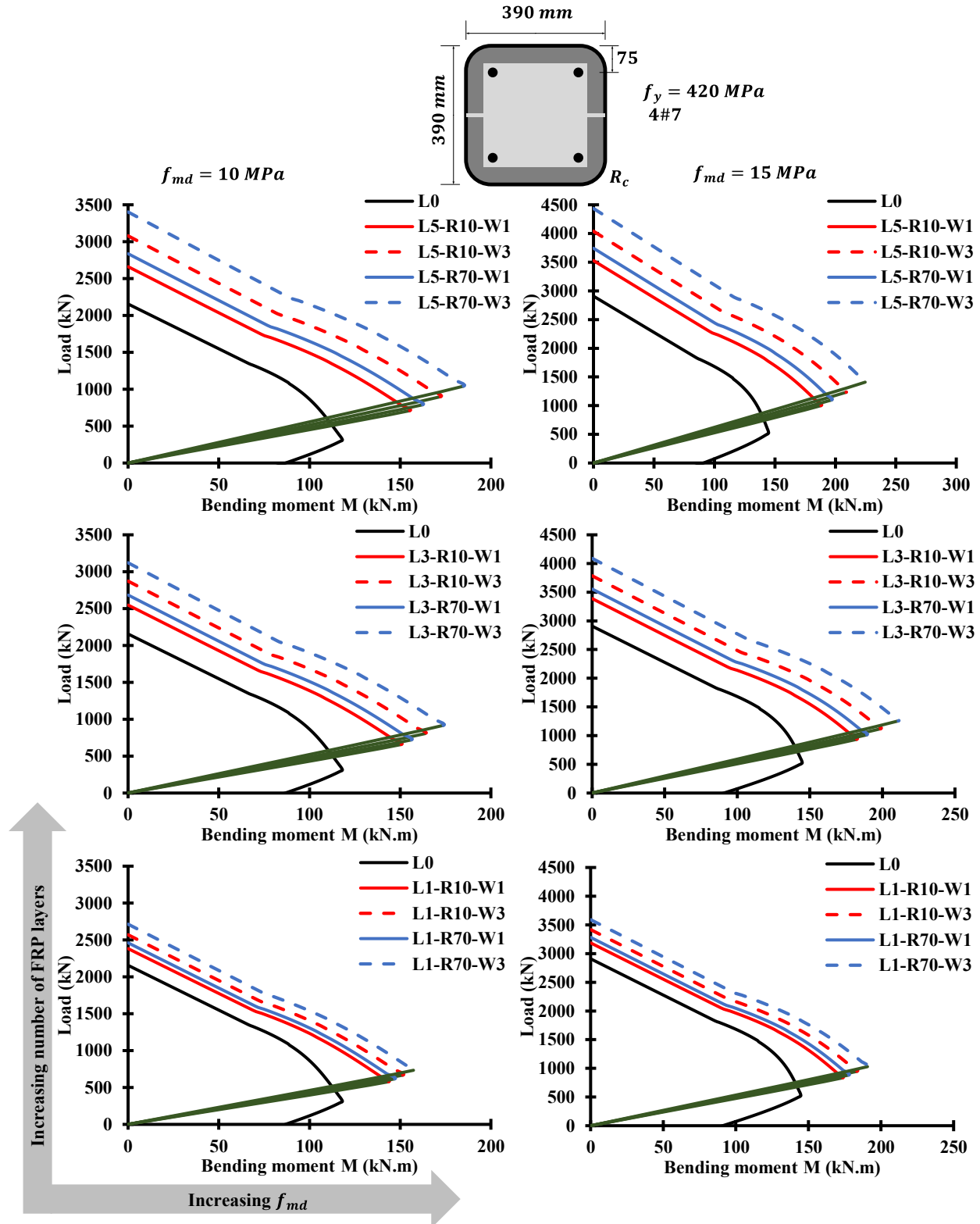
Figure 5.13 Axial force-moment interaction diagrams for selected square reinforced concrete masonry columns with various FRP retrofit configurations.

5.7 Conclusions

This paper proposes a simplified methodology that predicts the axial force-moment interaction diagram of fully grouted reinforced concrete masonry column strengthened with FRP jackets. Complying with force equilibrium and strain compatibility principles, the proposed methodology aims to predict the nominal capacity of FRP-confined concrete masonry columns for design purposes.

The fundamental parameters to perform detailed section analysis were established, and computational expressions were proposed to determine the values of these parameters. First, the strength model of CNR-DT 200 R1 design guideline was used to quantify the enhancement in the axial strength and determine the value of f_{mcd} parameter. An equation calibrated using available experimental data in Alotaibi and Galal (2018) was proposed for predicting maximum usable FRP confined concrete masonry strain in the extreme compression fibre. The values of the two parameters α and β that define the equivalent rectangular stress block were determined to simplify the design procedure. Two approaches were adopted to find the effect of strain gradient on the equivalent rectangular stress block parameters.

The segment of the interaction diagram curve represents the region controlled by compression failure can be generated by selecting arbitrary neutral axis positions then calculating the nominal axial strengths and moments capacities for these positions. The practical values that were selected for the equivalent rectangular stress block parameters and the proposed procedure were validated against experimental tests in Alotaibi and Galal (2018). It should be mentioned that more extensive experimental data on concrete masonry columns built with various geometries and strengthened with different FRP materials are required to increase the confidence in the proposed methodology.

The effect of design variables on the axial-flexural interaction of fully grouted reinforced concrete masonry column strengthened by FRP jackets was quantified in the parametric study.

Increasing FRP layers, corner radius, and FRP jacket stiffness has a positive impact on the axial capacity of the FRP-confined concrete masonry column. However, the increase in compressive strength of masonry and the aspect ratio of cross section would limit the benefit sought from FRP strengthening.

Chapter 6

Conclusions

This chapter covers summary, conclusions, contributions, limitations, and recommendations for future work on the main research topic carried out in this thesis.

6.1 Summary

The goal of this research is to develop a simplified methodology to construct the axial force-moment interaction diagram of fully grouted reinforced concrete masonry column strengthened with FRP jackets. The methodology only considers short prismatic reinforced concrete masonry columns that fail in a compression-controlled manner. The simplified methodology complies with equilibrium and strain compatibility principles. The proposed procedure is designed to predict the nominal capacity of reinforced concrete masonry column for practical design applications, where the columns will be subjected to both axial load and bending moment. The essential parameters to perform detailed section analysis are established. Suggested expressions are proposed to obtain the parameters values computationally. Two phases of the experimental program were adopted to provide experimental data to develop and validate the proposed methodology.

In the first phase of the experimental program, a total of nineteen half-scale fully grouted concrete masonry prisms were constructed and tested under axial compression to quantify the strength and strain capacity towards validating the available models for predicting the strength gain which is necessary to perform detailed section analysis. In the first phase, the effect of the thickness of CFRP jacket and the corner radius of section on the strength gain was investigated. Special attention was also given to the effective tensile strain in the CFRP jackets to accurately estimate the confinement pressure provided by CFRP jacketing. In this phase, it is concluded that the CNR-DT 200 R1 confinement model, the Italian guide addressing strengthening masonry columns with external FRP composites, needs to be refined to give a good correlation with the experimental data.

The second phase of the experimental program consists of testing 28 half-scale fully grouted reinforced concrete masonry columns under different loading conditions, and variations in CFRP

jacketing. The ultimate axial strains of eccentrically tested FRP confined columns are used to calibrate the empirical constants of the proposed expression for predicting the ultimate strain in extreme compression fibre of confined masonry. Also, the experimental data in this phase were used to calculate the parameters of the equivalent rectangular stress block considering the effect of the strain gradient resulted from the eccentricity.

Finally, theoretical axial force-moment interaction diagrams obtained by a proposed procedure were compared with experimental data. The result of the proposed procedure is in a good agreement with experimental data with an acceptable margin of error. The proposed procedure was extended to study the effect of design variables on the axial-flexural interaction of fully grouted reinforced concrete masonry column confined by FRP jackets.

6.2 Conclusions

The effectiveness of CFRP jackets to strengthen concrete masonry columns is investigated in this thesis. Experimental program was adopted to experimentally quantify the strength and strain capacity of confined concrete masonry columns under concentric and eccentric loading. The experimental observations were adopted to determine the values of fundamental parameters that controlling the section analysis procedure for predicting axial force-moment interaction diagrams of FRP confined concrete masonry columns.

The following points were concluded based on the two phases of experimental tests and the proposed methodology to construct the axial force-moment interaction diagram:

6.2.1 Conclusions based on axial compressive behaviour

This section presents the conclusions drawn from the experimental results covered in Chapter 3 on the axial compressive behaviour of grouted concrete block masonry columns confined by CFRP jackets. This experimental research on 19 half-scale C-shaped concrete block masonry prisms confined with CFRP led to the following findings:

- CFRP jacket significantly increased the axial strength and ultimate strain of concrete masonry prisms compared to non-strengthened prisms.
- Concrete masonry columns confined with CFRP sheets exhibit an enhancement in the post peak behaviour by softening the descending branches of the stress-strain relationships compared to unreinforced prisms.

- Increasing the corner radius of the section with the same level of confinement leads to a higher ultimate strain gain.
- The CFRP strain profile at peak load and 15% strength degradation along the perimeter of the prisms are highly non-uniform.
- The average ultimate tensile strain of flat coupons tests is higher than the average tensile strains recorded in the surface of CFRP jackets.
- The tensile strain in CFRP jacket increases when the corner radius of the section increases.
- CFRP jacketing provides higher confinement pressure at 15% strength degradation compared to that provided at the maximum strength of prisms.
- The refined CNR-DT 200 R1 theoretical model has 4.92% mean absolute error compared to the experimental data.

6.2.2 Conclusions based on combined axial and flexural behaviour

This section presents the conclusions drawn from the experimental results covered in Chapter 4 on CFRP-confined reinforced concrete masonry columns tested under concentric and eccentric loading. This experimental test of 28 half-scale reinforced concrete masonry columns led to the following findings:

- CFRP jackets significantly increased both the axial load and deformation of strengthened masonry columns compared to non-strengthened columns.
- The eccentrically tested columns recorded lower gain in strength and the ultimate axial deformation compared to concentrically tested columns.
- CFRP jackets enhanced the post peak behaviour of confined masonry columns by softening the descending branches of axial load-deformation curve compared to unconfined columns.
- The confined masonry columns showed a higher gain in the ultimate axial deformation more than the gain in strength.
- The rupture of the CFRP jackets in concentric tests occurs around 15% strength degradation, where the onset of rupture delays with the eccentricity.
- The non-strengthened masonry columns showed higher stiffness degradation in post peak behaviour compared to strengthened columns.

- The effect of confinement can change the columns' mode of failure from compression to tension controlled manner during the post peak behaviour.

6.2.3 Conclusions based on the proposed methodology for axial-flexure interaction

This section presents the conclusions drawn in Chapter 5 on axial-flexural interaction for FRP-wrapped reinforced concrete masonry columns: design methodology and design variables:

- The refined strength model of CNR-DT 200 R1 design guideline can be used to quantify the enhancement in the axial strength of FRP confined reinforced concrete masonry columns.

- Ultimate axial strain equation calibrated by experimental tests can predict the maximum usable strain in the extreme compression fibre of FRP confined concrete masonry columns.

- Concentric stress-strain curve end with ultimate axial strain equals to axial strain corresponding to the peak load of eccentrically loaded columns can accurately represent the stress distribution of FRP confined masonry in the compression zone in eccentrically loaded columns.

- The constant value of 0.80 for the parameters α and β of the equivalent rectangular stress block are recommended for the simplicity.

- The proposed procedure is in good agreement with the experimental results with an acceptable margin where the mean absolute percentage error was less than 6%.

- The parametric study finds that increasing FRP layers, corner radius, and FRP jacket stiffness has a positive impact on the axial capacity of the FRP-confined concrete masonry column. However, the increment in compressive strength of masonry and the aspect ratio of cross section would limit the benefit from FRP strengthening.

6.3 Contributions

The contributions achieved in this thesis can be summarized as follows:

- Proving experimentally that CFRP jacketing can be effective for confining concrete block masonry columns by increasing the peak strength and ultimate axial strain.

- Quantifying experimentally the enhancement provided by CFRP jacket on strength and ductility of concrete block masonry columns under concentric and eccentric load.

- Quantifying experimentally the effect of corner radius of cross section on CFRP jacket level of confinement.

- Quantifying experimentally the CFRP strain profile at peak load and 15% strength degradation along the perimeter of concrete block masonry prisms.

- Assessment of CNR-DT 200 R1 theoretical model ability to predict the strength gain for concrete block masonry columns by comparing the theoretical predictions with the experimental data.

- Refining CNR-DT 200 R1 theoretical model based on experimental tests to increase the accuracy of the model to predict the strength gain for concrete block masonry columns.

- Providing first experimental data on axial force-bending moment interaction diagrams of FRP confined concrete masonry columns.

- Proposing a simplified methodology validated with experimental tests to construct the axial force-moment interaction diagram of fully grouted reinforced concrete masonry column strengthened with FRP jackets.

- Proposing ultimate axial strain equation to predict the maximum usable strain in the extreme compression fibre of FRP confined concrete masonry.

- Proposing constant value for the parameters α and β of the equivalent rectangular stress block for FRP confined concrete masonry considering the effect of the strain gradient on the stress-strain curve.

- Conducting a parametric study to quantify the effect of the design variables on the axial-flexural interaction of FRP-wrapped reinforced concrete masonry columns.

6.4 Limitations

The following are the limitations of the work conducted in this thesis:

- Even though 47 reinforced and unreinforced concrete masonry columns strengthened with FRP jackets were tested in this experimental work, more tests would lead to more confidence in the proposed methodology and the refined model.

- Different FRP materials and considering various geometries of concrete masonry units are required to generalize the findings.

- The results of the concrete masonry columns are limited to square cross section.

- The effect of steel ties confinement is not considered.

- The effect of location of masonry column in the structure (i.e., pilaster column, in-wall column, or between two openings) has not been considered in this study.

- The simplified methodology to construct the axial force-moment interaction diagram of fully grouted reinforced concrete masonry column strengthened with FRP jackets only considers concrete masonry column is failing in a compression controlled manner.

- The methodology only considers short prismatic concrete masonry column. The effect of slenderness is out of the scope of this work.

6.5 Recommendations for future work

The effectiveness of CFRP jackets to strengthen concrete masonry columns is investigated in this thesis. The goal of this research is to develop a simplified methodology to construct the axial force-moment interaction diagram of FRP confined fully grouted reinforced concrete masonry column. The conclusions of this study were concluded based on the two phases of experimental tests and limited to the parameters that were tested. However, in order to further expand the knowledge in this field, other parameters may be considered. Therefore, the following is a list of several potential research topics and some recommendations for future research:

- Additional experimental tests are needed to consider some parameters which not covered in this investigation. It is recommended to perform experimental tests on concrete masonry columns considering the variation of:
  - Cross-sectional aspect ratio.

- Carbon, glass and basalt FRP with different properties and applying different techniques of FRP confinement (FRP strips, spraying, internally confining by FRP bars).

- Height to thickness ratio.

- Vertical reinforcement ratio and transversal ties reinforcement ratio.

- Validation of the proposed models can be further confirmed or refined with more tests that consider the above parameters.

- Testing full-scale columns can be conducted to insure eliminating the size effect.

- Conducting analytical and experimental studies on the effect of location of masonry column in the structure (i.e., pilaster column, in-wall column, or between two openings) on the effective of FRP confinement.

- Conducting experimental tests to develop methodologies to consider the effect of slenderness.

- The rich experimental data provided in this thesis is valuable for future calibrating and validating of numerical and analytical models.

- The current study focused on the behaviour of a single FRP-confined concrete masonry column. The design model and the experimental results can be a part of experimental or numerical study for upgrading reinforced masonry building to evaluate the influence of strengthened columns on the overall behaviour of the structure. The models would be used to quantify the gain in axial and flexural capacities of the original columns after applying FRP strengthening system.

References

Abo El Ezz, A., Eldin, H., and Galal, K. (2015). Influence of confinement reinforcement on the compression stress–strain of grouted reinforced concrete block masonry boundary elements. *Structures, 2*(32-43).

ACI 440.2R-08. (2008). Guide for the design and construction of externally bonded FRP systems for strengthening concrete structures. Farmington Hills, MI, U.S.A: ACI Committee 440.

Aiello, M. A., Micelli, F., and Valente, L. (2007). Structural upgrading of masonry columns by using composite reinforcements. *ASCE Journal of Composites for Construction, 11*(6), 650-658.

Aiello, M. A., Micelli, F., and Valente, L. (2009). FRP confinement of square masonry columns. *ASCE Journal of Composites for Construction, 13*(2), 148-158.

Alecci, V., Bati, S. B., and Ranocchiai, G. (2009). Study of brick masonry columns confined with CFRP composite. *ASCE Journal of Composites for Construction, 13*(3), 179-187.

Alecci, V., Bati, S. B., and Ranocchiai, G. (2014). Concrete columns confined with CFRP wraps. *Materials and Structures, 47*(3), 397-410.

Alotaibi, K. S., and Galal, K. (2017). Axial compressive behavior of grouted concrete block masonry columns confined by CFRP jackets. *Composites Part B: Engineering, 114*(4), 467-479.

Alotaibi, K. S., and Galal, K. (2018). Experimental study of CFRP-confined reinforced concrete masonry columns tested under concentric and eccentric loading. *Composites Part B: Engineering, 155*(12), 257-271.

Ashour, A., Galal, K., and Farnia, N. (2018). Analytical and experimental study on upgrading the seismic performance of reinforced masonry columns using GFRP and CFRP wraps. *ASCE Journal of Composites for Construction, 22*(4).

ASTM A370-17. (2017). Standard test methods and definitions for mechanical testing of steel products. West Conshohocken, PA: ASTM International.

ASTM A615/A615M-16. (2016). Standard specification for deformed and plain carbon-steel bars for concrete reinforcement. West Conshohocken, PA: ASTM International.

ASTM A1064/A1064M-17. (2017). Standard specification for carbon-steel wire and welded wire reinforcement, plain and deformed, for concrete. West Conshohocken, PA: ASTM International.

ASTM C140/C140M-15ae1. (2015). Standard test methods for sampling and testing concrete masonry units and related units. West Conshohocken, PA: ASTM International.

ASTM C270e14a. (2014). Standard specification for mortar for unit masonry. West Conshohocken, PA: ASTM International.

ASTM C476-10. (2010). Standard specification for grout for masonry. West Conshohocken, PA: ASTM International.

ASTM C780e15a. (2015). Standard test method for preconstruction and construction evaluation of mortars for plain and reinforced unit masonry. West Conshohocken, PA: ASTM International.

ASTM C1314-16. (2016). Standard test method for compressive strength of masonry prisms. West Conshohocken, PA: ASTM International.

ASTM D3039/D3039M-14. (2014). Standard test method for tensile properties of polymer matrix composite materials. West Conshohocken, PA: ASTM International.

ASTM D7565/D7565M-10. (2010). Standard test method for tensile properties of polymer matrix composite materials. West Conshohocken, PA: ASTM International.

Bank, L. C. (2006). *Composites for construction: structural design with FRP materials*. Hoboken, NJ, USA: John Wiley and Sons.

Bisby, L., and Ranger, M. (2010). Axial–flexural interaction in circular FRP-confined reinforced concrete columns. *Construction and Building Materials, 24*, 1672-1681.

Borri, A., Castori, G., and Corradi, M. (2013). Masonry confinement using steel cords. *ASCE Journal of Materials in Civil Engineering, 25*(12), 1910-1919.

BS 5628. (2005). Code of practice for structural use of masonry. London, U.K: British Standards Institution.

Campione, G., and Miraglia, N. (2003). Strength and strain capacities of concrete compression members reinforced with FRP. *Cement and Concrete Composites, 23*, 31-41.

Cao, Y. G., Wu, Y. F., and Jiang, C. (2018). Stress-strain relationship of FRP confined concrete columns under combined axial load and bending moment. *Composites Part B: Engineering, 134*, 207-217.

Carrazedo, R., and Hanai, J. (2017). Concrete prisms and cylinders wrapped by FRP loaded in compression with small eccentricities. . *ASCE Journal of Composites for Construction, 21*(4), 04016115.

CNR-DT 200 R1. (2004). Guide for the design and construction of externally bonded FRP systems for strengthening existing structures. Rome, Italy.

CNR-DT 200 R1. (2013). Guide for the design and construction of externally bonded FRP systems for strengthening existing structures. Rome, Italy.

Concrete Society. (2004). Design guidance on strengthening concrete structures using fibre composite materials *Technical Rep. No. 55*. London, U.K.

Corradi, M., Grazini, A., and Borri, A. (2007). Confinement of brick masonry columns with CFRP materials. *Composites Science and Technology, 67*(9), 1772-1783.

CSA S304-14. (2014). Design of masonry structures. Mississauga, Ontario, Canada: Canadian Standards Association.

Cui, C. (2009). *Behaviour of normal and high strength concrete confined with fibre reinforced polymers (FRP).* (Ph.D. Dissertation), University of Toronto.

De Lorenzis, L., and Tepfers, R. (2003). Comparative study of models on confinement of concrete cylinders with fiber-reinforced polymer composites. *ASCE Journal of Composites for Construction, 7*(3), 219-237.

Di Ludovico, M., D'Ambra, C., Prota, A., and Manfredi, G. (2010). FRP confinement of tuff and clay brick columns: experimental study and assessment of analytical models. *ASCE Journal of Composites for Construction, 14*(5), 583-596.

EN 1996-1-1. (2005). Eurocode 6-design of masonry structures-Part 1-1: general rules for reinforced and unreinforced masonry structures. London, U.K: British Standards Institution.

Ewing, B. D., and Kowalsky, M. J. (2004). Compressive Behavior of unconfined and confined clay brick masonry. *ASCE Journal of Structural Engineering, 130*(4), 650-661.

Faella, C., Martinelli, E., Camorani, G., Aiello, M. A., Micelli, F., and Nigro, E. (2011a). Masonry columns confined by composite materials: design formulae. *Composites Part B: Engineering, 42*(4), 705-716.

Faella, C., Martinelli, E., Paciello, S., Camorani, G., Aiello, M. A., Micelli, F., and Nigro, E. (2011b). Masonry columns confined by composite materials: experimental investigation. *Composites Part B: Engineering, 42*(4), 692-704.

Fam, A., Flisak, B., and Rizkalla, S. (2003). Experimental and analytical modeling of concrete filled fiber-reinforced polymer tubes subjected to combined bending and axial loads. *ACI Structural Journal, 100*(4), 499-509.

Farnia, N. (2011). *Seismic rehabilitation of reinforced masonry columns using CFRP and GFRP wraps*. (Ph.D. Dissertation), Concordia University.

Feeg, C., Longworth, J., and Warwaruk, J. (1979). *Effects of reinforcement detailing for concrete masonry columns*. (Technical report), University of Alberta.

FIB. (2007). FRP reinforcement in RC structures *Fib task group 9.3*. lausanne, Switzerland: fib Bull.

Galal, K., Farnia, N., and Pekau, O. A. (2012). Upgrading the seismic performance of reinforced masonry columns using CFRP wraps. *ASCE Journal of Composites for Construction, 16*(2), 196-206.

Hadi, M. N. S. (2006). Behaviour of FRP wrapped normal strength concrete columns under eccentric loading. *Composite Structures, 72*, 503-511.

Hadi, M. N. S. (2007). Behaviour of FRP strengthened concrete columns under eccentric compression loading. *Composite Structures, 77*, 92-96.

Hadi, M. N. S., and Widiarsa, I. B. R. (2012). Axial and flexural performance of square RC columns wrapped with CFRP under eccentric loading. *ASCE Journal of Composites for Construction, 16*, 640-649.

Harries, K. A., and Carey, S. A. (2003). Shape and "gap" effects on the behavior of variably confined concrete. *Cement and Concrete Research, 33*(6), 881-890.

Hart, G., Noland, J., Kingsley, G., Englekirk, R., and Sajjad, N. A. (1988). The use of confinement steel to increase the ductility in reinforced concrete masonry shear walls. *TMS Journal, 7*(2), 19-42.

Hart, G., Sajjad, N., Kingsley, G. R., and Noland, J. L. (1989). Analytical stress-strain curves for grouted concrete masonry. *The Masonry Society Journal, 8*(1), 21-34.

Hatzinikolas, M. A., and Korany, Y. (2005). *Masonry design for engineers and architects*. Edmonton, AB, Canada: Canadian Masonry Publications.

143

Hu, B., Wang, J. G., and Li, G. Q. (2011). Numerical simulation and strength models of FRP wrapped reinforced concrete columns under eccentric loading. *Construction and Building Materials, 25*(5), 2751-2763.

Ilyas, M., Farooq, S. H., Qazi, A. U., and Umair, R. (2009). Masonry confinement using steel strips. *Pakistan Journal of Engineering and Applied Sciences, 5*, 1-9.

ISIS Canada. (2001). Strengthening reinforced concrete structures with externally bonded fibre reinforced polymers *ISIS Canada design manual no. 4*. Canada.

Khalaf, F., Hendry, A., and Fairbairn, D. (1993). Reinforced blockwork masonry columns. *ACI Structural Journal, 90*(5), 496-504.

Kog, Y. C., Ong, K. C. G., Yu, C. H., and Sreekanth, A. P. V. (2001). Reinforced concrete jacketing for masonry columns with axial loads. *ACI Structural Journal, 98*(2), 105-115.

Krevaikas, T. D., and Triantafillou, T. C. (2005). Masonry confinement with fiber-reinforced polymers. *ASCE Journal of Composites for Construction, 9*(2), 128-135.

Lam, L., and Teng, J. (2003). Design-oriented stress-strain model for FRP-confined concrete in rectangular columns. *Journal of Reinforced Plastics and Composites, 22*(13), 1149-1186.

Lam, L., and Teng, J. (2004). Ultimate condition of fiber reinforced polymer-confined concrete. *ASCE Journal of Composites for Construction, 8*(6), 539-548.

Li, J., and Hadi, M. N. S. (2003). Behaviour of externally confined high-strength concrete columns under eccentric loading. *Composite Structures, 62*, 145-153.

Lignola, G. P., Nardone, F., Prota, A., and Manfredi, G. (2012). Analytical model for the effective strain in FRP-wrapped circular RC columns. *Composites Part B: Engineering, 43*(8), 3208-3218.

Long, L. M. (2006). *Behaviour of half-scale reinforced concrete masonry shear walls.* (MSc Dissertation), McMaster University.

Maaddawy, T. E. (2009). Strengthening of eccentrically loaded reinforced concrete columns with fiberreinforced polymer wrapping system: experimental investigation and analytical modeling. *ASCE Journal of Composites for Construction, 13*, 13-24.

MacGregor, J. (1997). *Reinforced concrete: mechanics and design* (3 ed.). Upper Saddle River, NJ, USA: Prentice Hall Inc.

144

Malmquist, K. J. (2004). *Influence of confinement reinforcement on the compressive behavior of concrete block masonry and clay brick masonry prisms.* (MSc Dissertation), Washington State University.

Masia, M. J., and Shrive, N. G. (2003). Carbon fibre reinforced polymer wrapping for the rehabilitation of masonry columns. *Canadian Journal of Civil Engineering, 30*(4), 734-744.

Micelli, F., De Lorenzis, L., and La Tegola, A. (2004). FRP-confined masonry columns under axial loads: experimental results and analytical model. *Masonry International Journal, 17*, 95-108.

Micelli, F., Angiuli, R., Corvaglia, P., and Aiello, M. A. (2014a). Passive and SMA-activated confinement of circular masonry columns with basalt and glass fibers composites. *Composites Part B: Engineering, 67*, 348-362.

Micelli, F., Di Ludovico, M., Balsamo, A., and Manfredi, G. (2014b). Mechanical behaviour of FRP-confined masonry by testing of full-scale columns. *Materials and Structures, 47*(12), 2081-2100.

Milani, G., Shehu, R., and Valente, M. (2017). Possibilities and limitations of innovative retrofitting for masonry churches: advanced computations on three case studies. *Construction and Building Materials, 47*, 239-263.

Minafò, G., D'Anna, J., Cucchiara, C., Monaco, A., and La Mendola, L. (2017). Analytical stress-strain law of FRP confined masonry in compression: literature review and design provisions. *Composites Part B: Engineering, 115*, 160-169.

Mirmiran, A., Shahawy, M., Samaan, M., Echary, H. E., Mastrapa, J. C., and Pico, O. (1998). Effect of column parameters on FRP-confined concrete. *ASCE Journal of Composites for Construction, 2*(4), 175-185.

Nanjunda Rao, K. S., and Pavan, G. S. (2015). FRP-confined clay brick masonry assemblages under axial compression: experimental and analytical investigations. *ASCE Journal of Composites for Construction, 19*(4), 04014068.

NZS 4230:2004. (2004). Design of reinforced concrete masonry structures: New Zealand Concrete Masonry Association.

Obaidat, A., Ashour, A., and Galal, K. Stress-strain behavior of C-shaped confined concrete masonry boundary elements of RM shear walls. *ASCE Journal of Structural Engineering*.

Obaidat, A., Abo El Ezz, A., and Galal, K. (2017). Compression behavior of confined concrete masonry boundary elements. *Engineering Structures, 132*, 562-575.

Ozbakkaloglu, T., and Lim, J. C. (2013). Axial compressive behavior of FRP-confined concrete: experimental test database and a new design-oriented model. *Composites Part B: Engineering, 55*, 607-634.

Ozbakkaloglu, T., Lim, J. C., and Vincent, T. (2013). FRP-confined concrete in circular sections: review and assessment of stress-strain models. *Engineering Structures, 49*, 1068-1088.

Pantazopoulou, S. J., Bonacci, J. F., Thomas, M. D. A., and Hearn, N. (2001). Repair of corrosion-damaged columns with FRP wraps. *ASCE Journal of Composites for Construction, 5*, 3-11.

Parvin, A., and Wang, W. (2001). Behavior of FRP jacketed concrete columns under eccentric loading. *ASCE Journal of Composites for Construction, 5*, 146-152.

Parvin, A., and Schroeder, J. M. (2008). Investigation of eccentrically loaded CFRP-confined elliptical concrete columns. *ASCE Journal of Composites for Construction, 12*(93-101).

Priestley, M., and Bridgeman, D. O. (1974). Seismic resistance of brick masonry walls. *Bulletin of the New Zealand National Society for Earthquake Engineering, 7*(4), 167-187.

Priestley, M., and Elder, D. (1983). Stress-strain curves for unconfined and confined concrete masonry. *ACI Journal Proceedings, 80*(3), 192-201.

Reitherman, R., and Perry, S. C. (2009). *Unreinforced masonry buildings and earthquakes: developing successful risk reduction programs*. (Technical report), Federal Emergency Management Agency.

Rocca, S., Galati, N., and Nanni, A. (2009). Interaction diagram methodology for design of FRP-confined reinforced concrete columns. *Construction and Building Materials, 23*(4), 1508-1520.

Seible, F., Priestley, M. J. N., Hegemier, G., and Innamorato, D. (1997). Seismic retrofit of RC columns with continuous carbon fiber jackets. *ASCE Journal of Composites for Construction, 1*(2), 52-62.

Shahawy, M., Mirmiran, A., and Beitelman, T. (2000). Tests and modeling of carbon-wrapped concrete columns. *Composites Part B: Engineering, 31*(6), 471-480.

Shaheen, E., and Shrive, N. (2007). Sprayed glass fibre reinforced polymer masonry columns under concentric and eccentric loading. . *Canadian Journal of Civil Engineering, 34*(11), 1495-1505.

Shedid, M., El-Dakhakhni, W., and Drysdale, R. (2010). Alternative strategies to enhance the seismic performance of reinforced concrete-block shear wall Systems. *ASCE Journal of Structural Engineering, 136*(4), 676-689.

Sikawrap Hex 230C. Product data sheet: carbon fibre fabric for structural strengthening system (Edition 05.2013/v1). 2013. https://can.sika.com/dms/ getdocument.get/3e96623c-3e8e-3d4d-b95e-813eb7f9f87d/ SikaWrapHex230C_pds.pdf. Retrieved 28.12.2016.

Singh, H., and Cooke, N. (1994). Ductile behaviour of reinforced masonry columns. *Bulletin of the New Zealand National Society for Earthquake Engineering, 7*(2), 83-95.

Sturgeon, G., Longworth, J., and Warwaruk, J. (1980). *An investigation of reinforced concrete block masonry columns.* (Technical report), University of Alberta.

Taly, N. (2010). *Design of reinforced masonry structures*. Columbus, OH, USA: McGraw-Hill Companies.

TMS 402/602-16. (2016). Building code requirements and specifications for masonry structures. Longmont, CO, U.S.A: The Masonry Society.

Witzany, J., Cejka, T., and Zigler, R. (2014). Failure mechanism of compressed short brick masonry columns confined with FRP strips. *Construction and Building Materials, 63*, 180-188.

Witzany, J., and Zigler, R. (2015). Failure mechanism of compressed reinforced and nonreinforced stone columns. *Materials and Structures, 48*(5), 1603-1613.

Wu, Y. F., and Jiang, C. (2013a). Effect of load eccentricity on the stress-strain relationship of FRP-confined concrete columns. *Composite Structures, 98*, 228-241.

Wu, Y. F., and Jiang, J. F. (2013b). Effective strain of FRP for confined circular concrete columns. *Composite Structures, 95*, 479-491.

Zinno, A., Lignola, G., Prota, A., Manfredi, G., and Cosenza, E. (2010). Influence of free edge stress concentration on effectiveness of FRP confinement. *Composites Part B: Engineering, 41*(7), 523-532.

Appendices

In the Appendices, detailed and additional information with diagrams and images were provided to assist the reader in visualizing the content of thesis. Clear and concise information is already available in the main body of the thesis.

Appendix A Experimental Works

A.1 Experimental work of concrete masonry prisms

Additional images and information for the experimental work of the plain (without steel reinforcement) concrete masonry prisms are covered in this section. The primary information is discussed in Chapter 3 of the main body of the thesis.

A.1.1 Construction of concrete masonry prisms

Figure A.1 Construction of concrete masonry prisms.

Figure A.2 Ungrouted concrete masonry prisms.

Figure A.3 Construction of concrete masonry prisms.

A.1.2 Testing the mechanical properties of materials

Figure A.4 Testing Type S mortar.

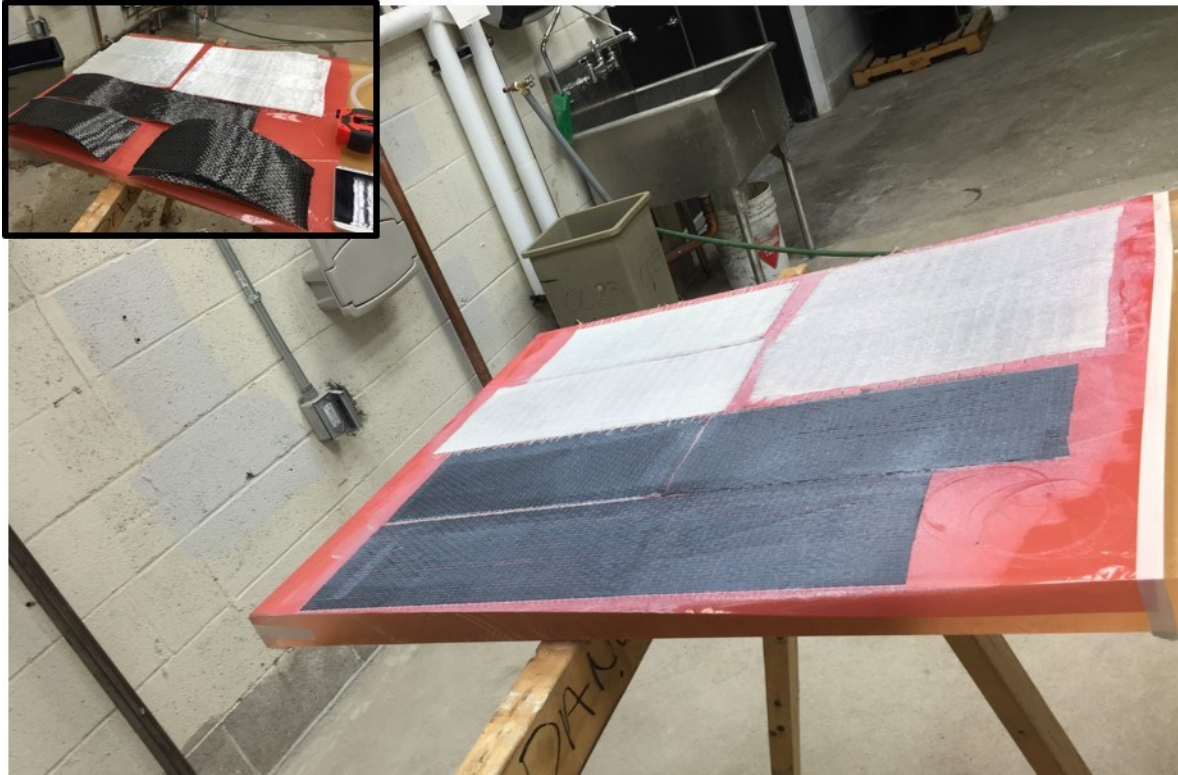Figure A.5 Testing grout cylinder and half-scale block.
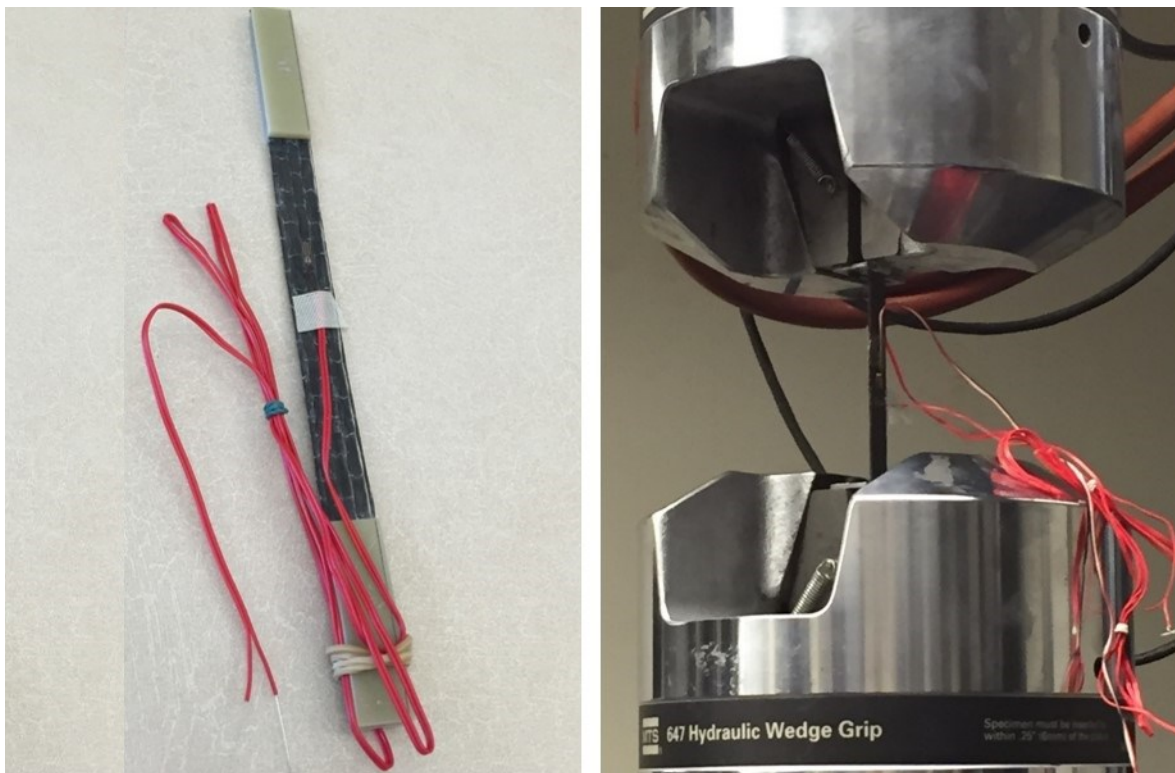
Figure A.6 Manufacturing FRP flat coupons.

Figure A.7 Tensile testing of flat coupon.

A.1.3 Preparing the masonry prisms for CFRP jacketing

Figure A.8 Prisms with corners radius of 10 and 30 mm.

Figure A.9 Filling the flanged ends of the concrete block units with a repair mortar.

A.1.4 Wrapping masonry prisms with CFRP

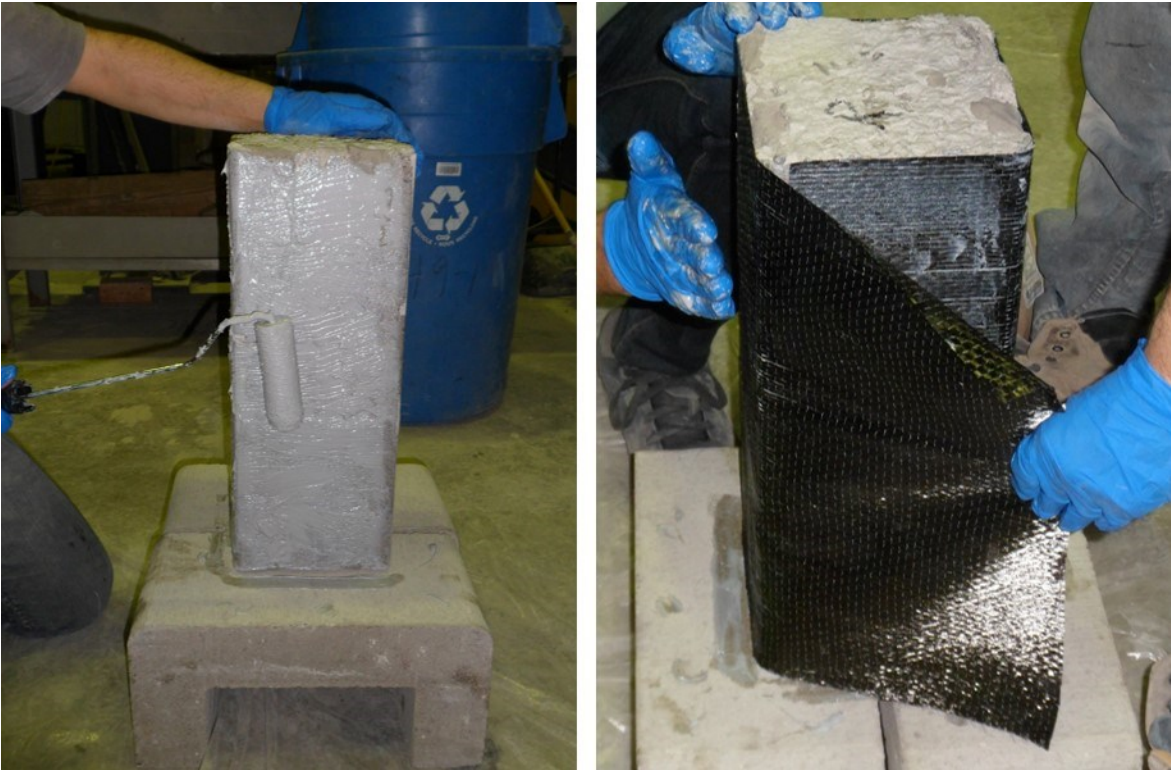Figure A.10 CFRF sheet cutting and mixing component A to component B.

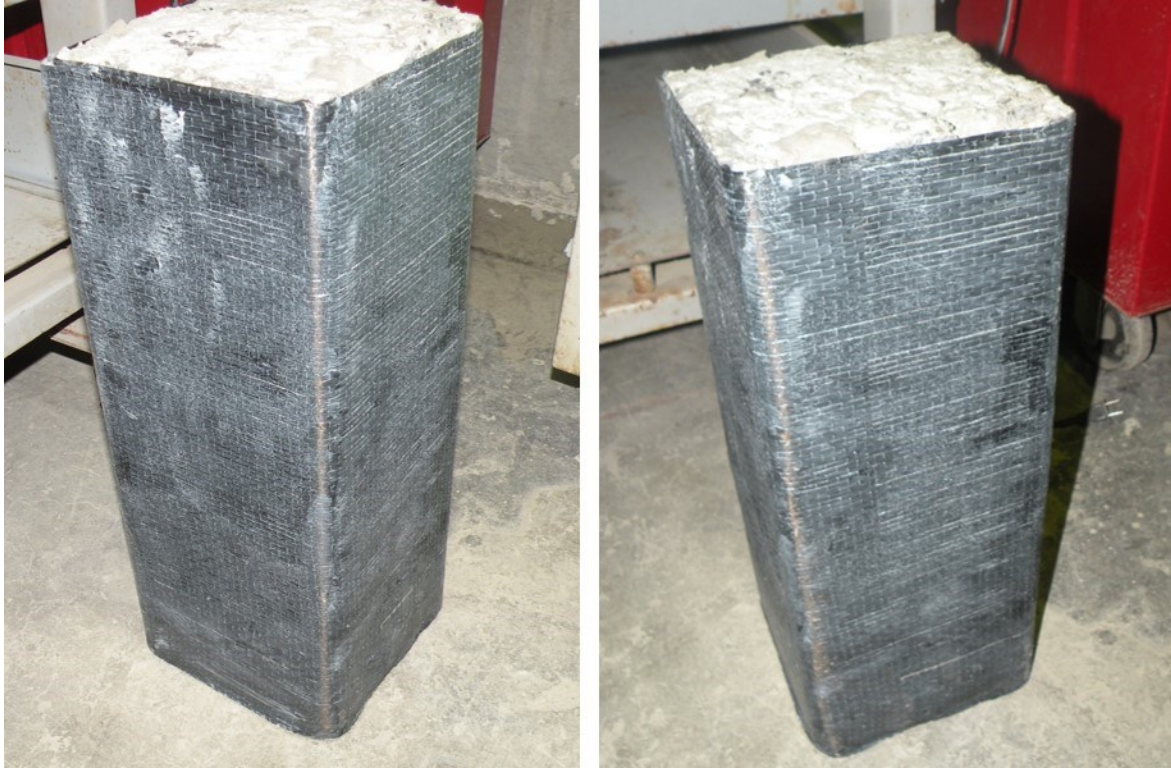Figure A.11 Applying epoxy and wrapping prisms.

Figure A.12 Wrapped prisms.

Figure A.13 Attaching strain gage to CFRP jacket.
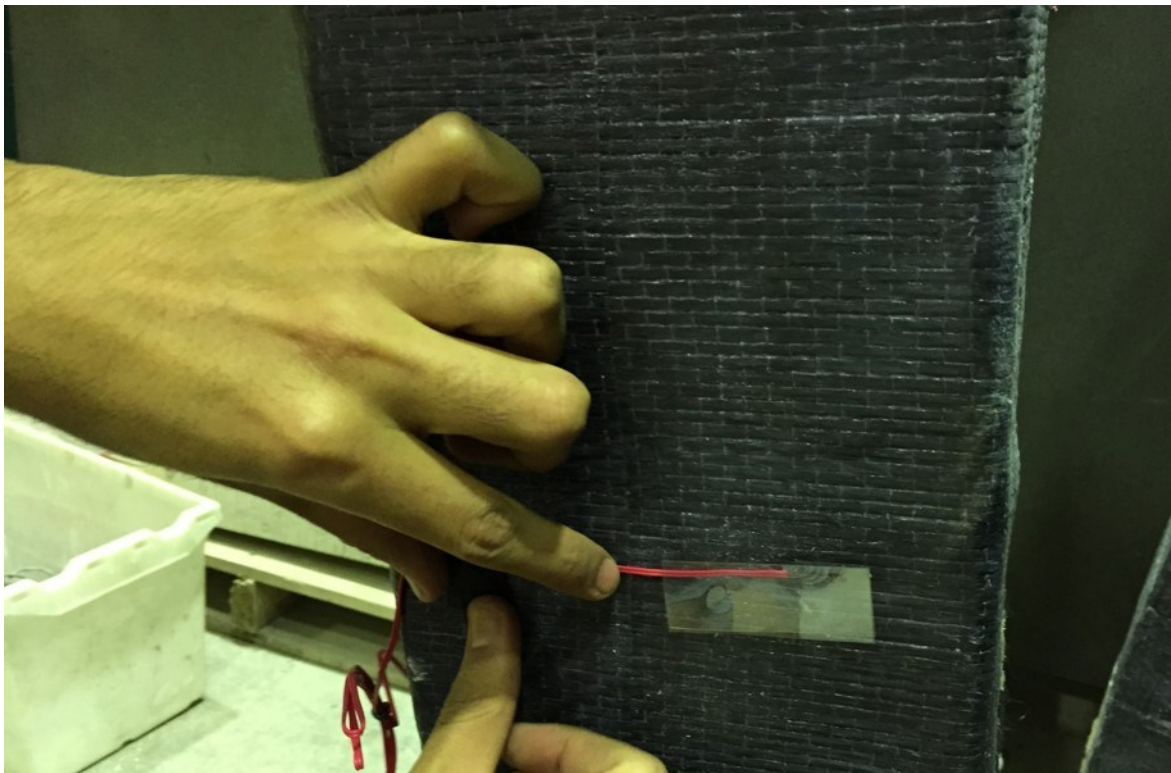
A.2 Experimental work of concrete masonry columns

Additional images and information for the experimental work of reinforced concrete masonry columns are covered in this section. The primary information is discussed in Chapter 4 of the main body of the thesis.

A.2.1 Construction of reinforced concrete masonry columns

Figure A.14 Assembling the reinforcement steel cages.

Figure A.15 Wooden formwork for the bottom concrete footings.
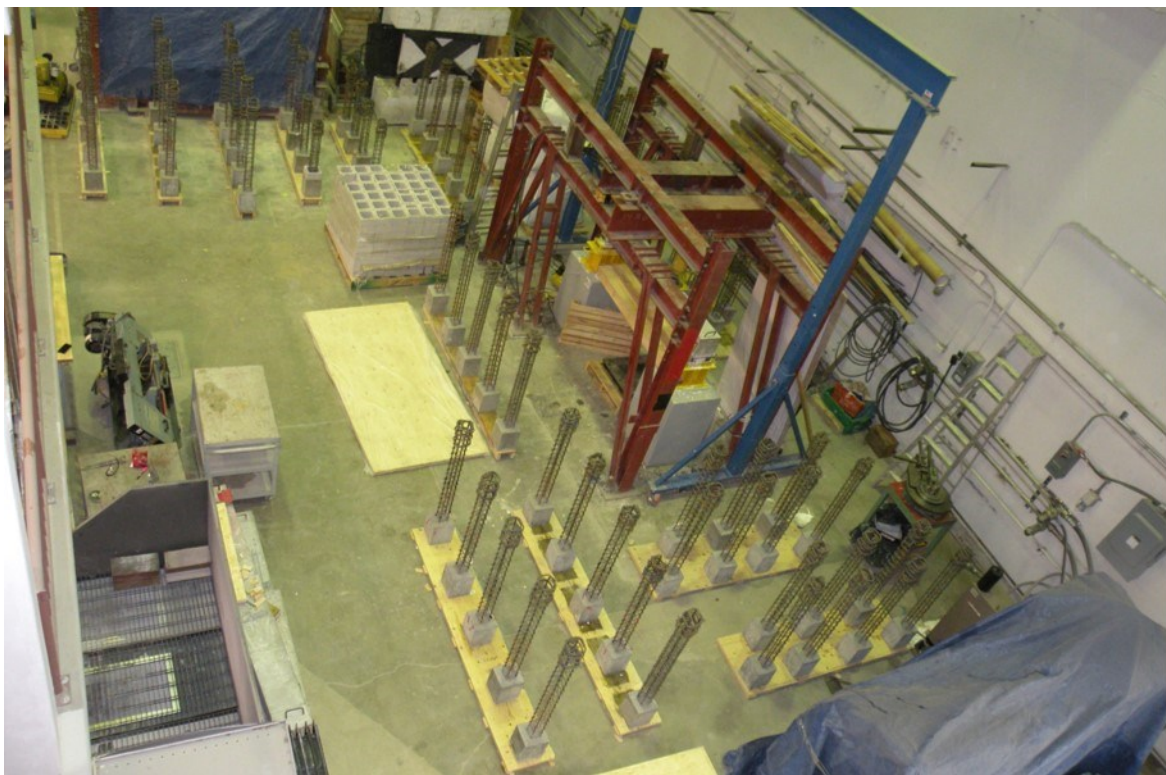
Figure A.16 Construction of reinforced concrete masonry columns.

Figure A.17 Cutting half scale concrete masonry blocks.
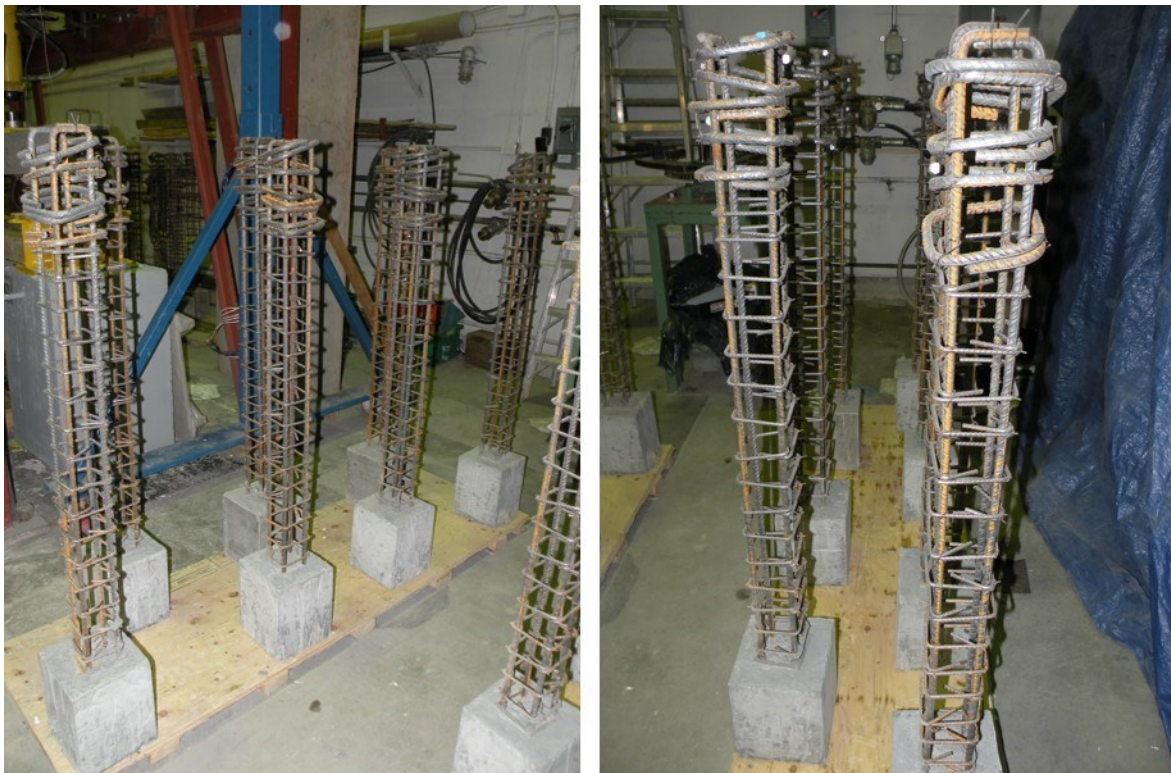
Figure A.18 Reinforcement steel cages with bottom footings.

Figure A.19 Attaching strain gage to reinforcement steel.
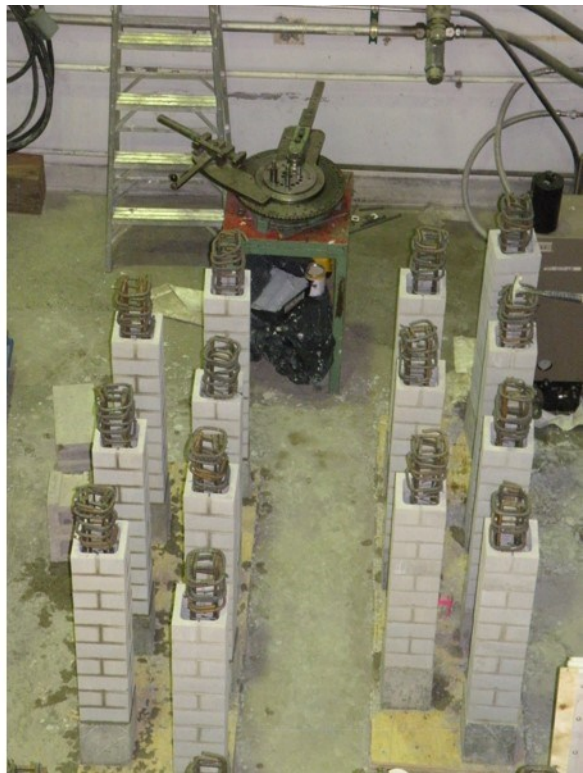
Figure A.20 Reinforced concrete masonry columns before grouting.
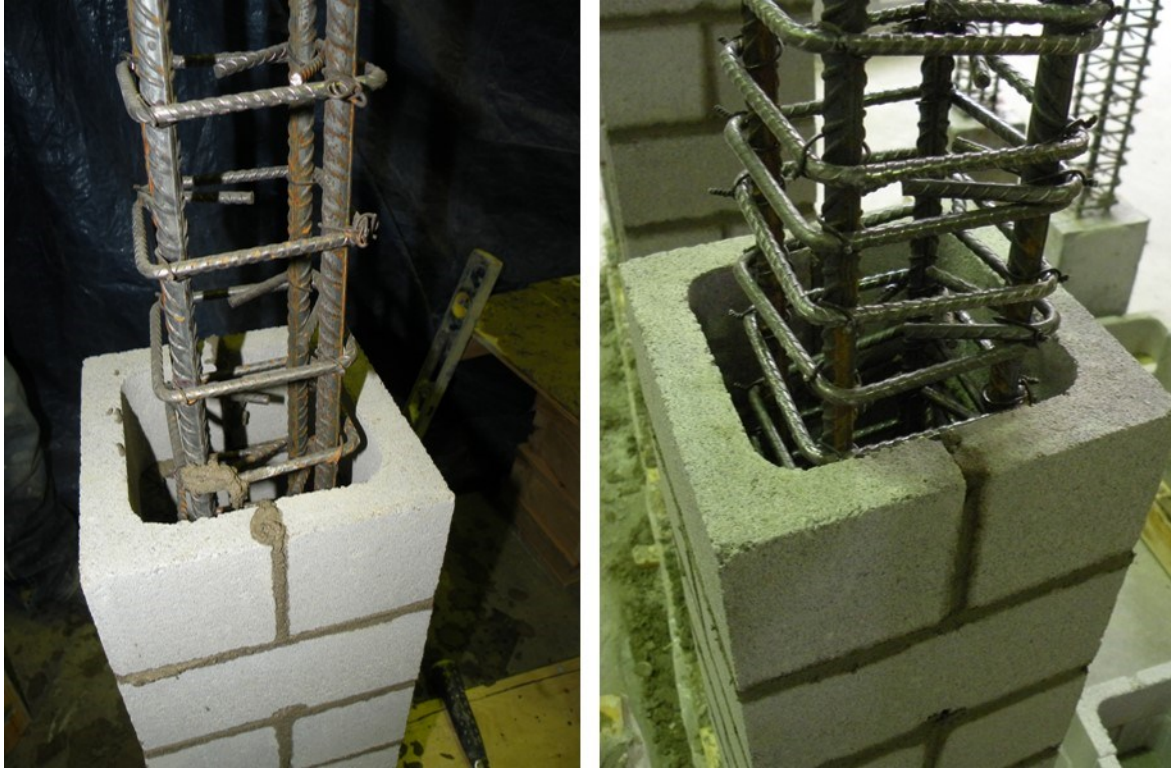
Figure A.21 Reinforced concrete masonry columns during the construction.

Figure A.22 Reinforced concrete masonry columns and ten course concrete masonry prisms.

Figure A.23 Wrapped reinforced concrete masonry columns.

A.2.2 Testing the mechanical properties of materials

Figure A.24 Testing coupons of half-scale pilaster units.
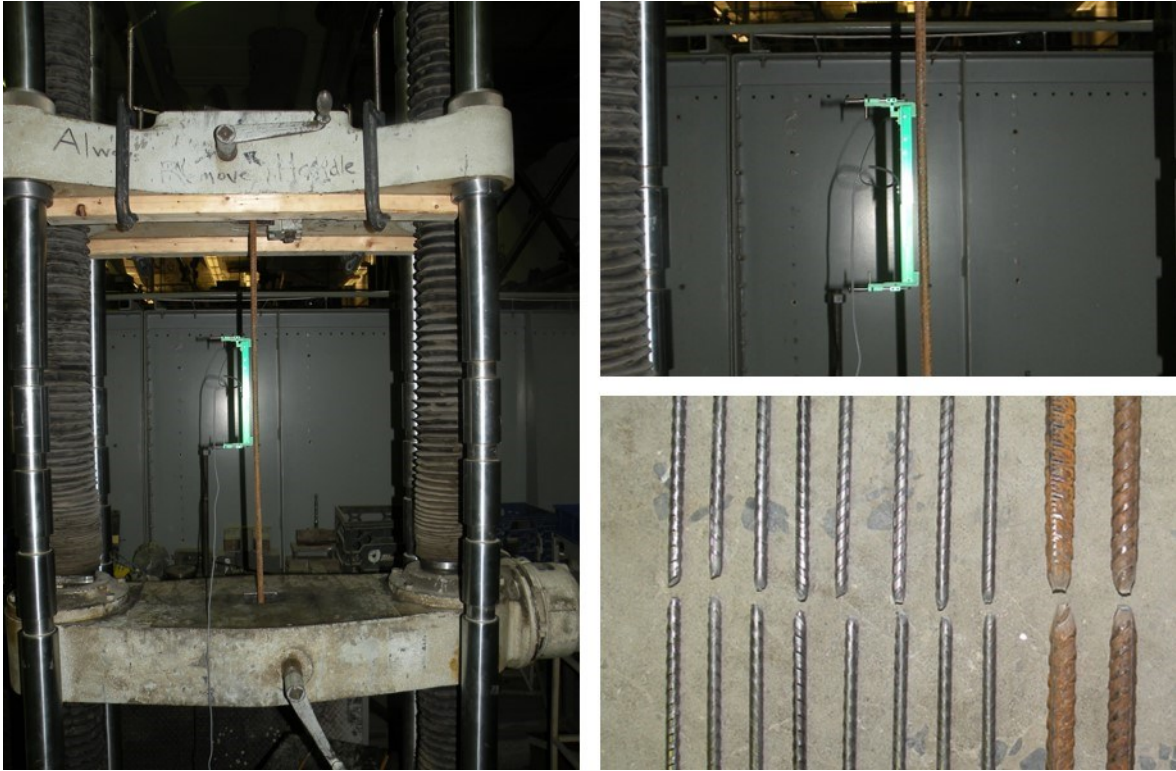
Figure A.25 Tensile tests of reinforcement steel.
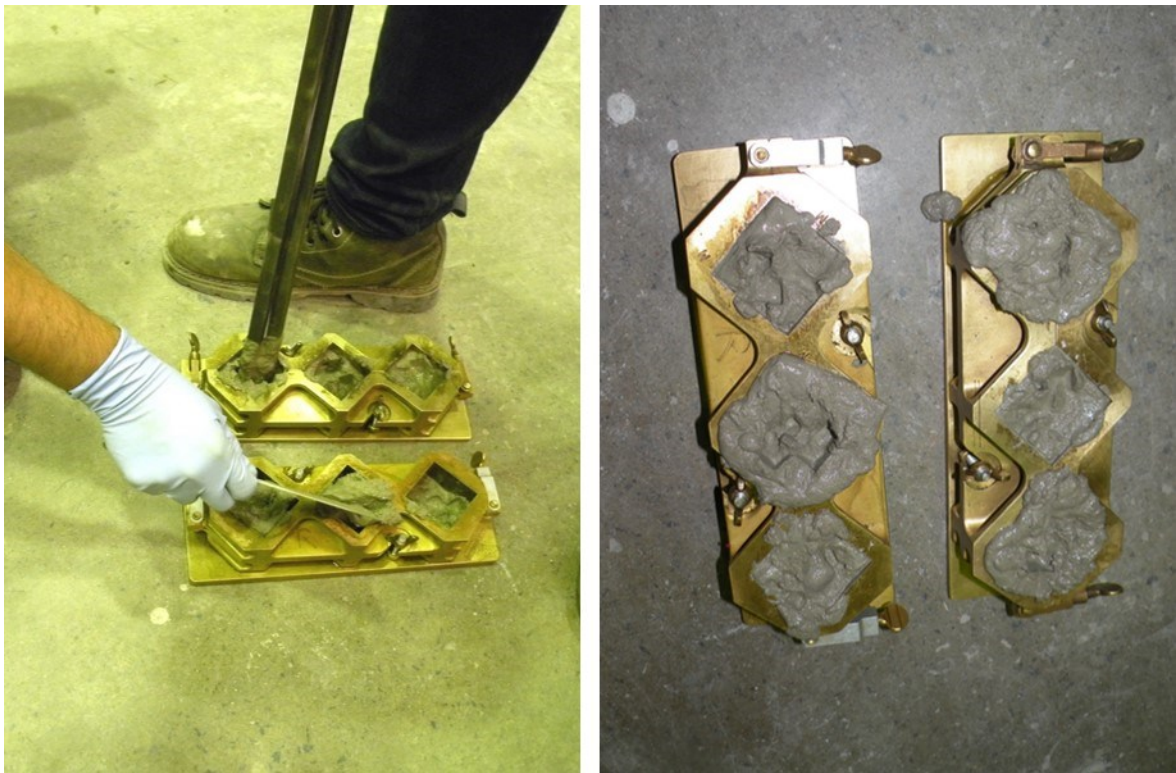
Figure A.26 Manufacturing Type S mortar cubes.

Figure A.27 Slump test.

A.2.3 Testing the masonry columns

Figure A.28 Test setup for concentric load.
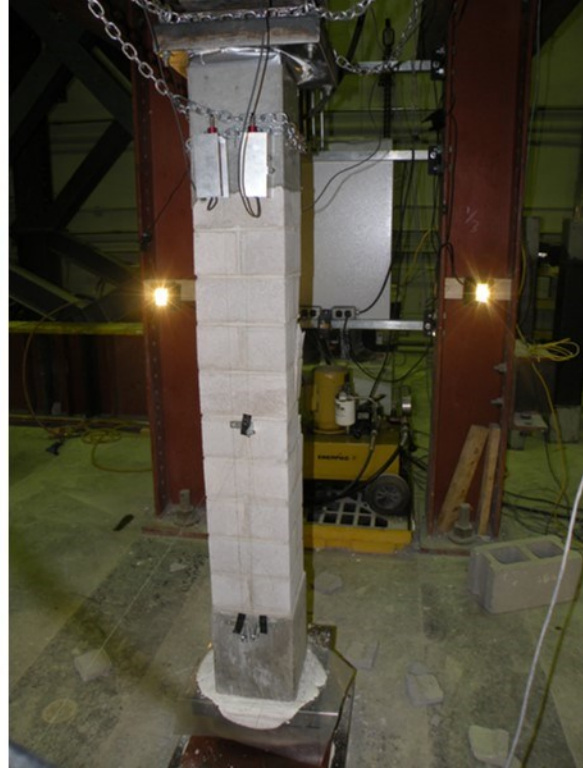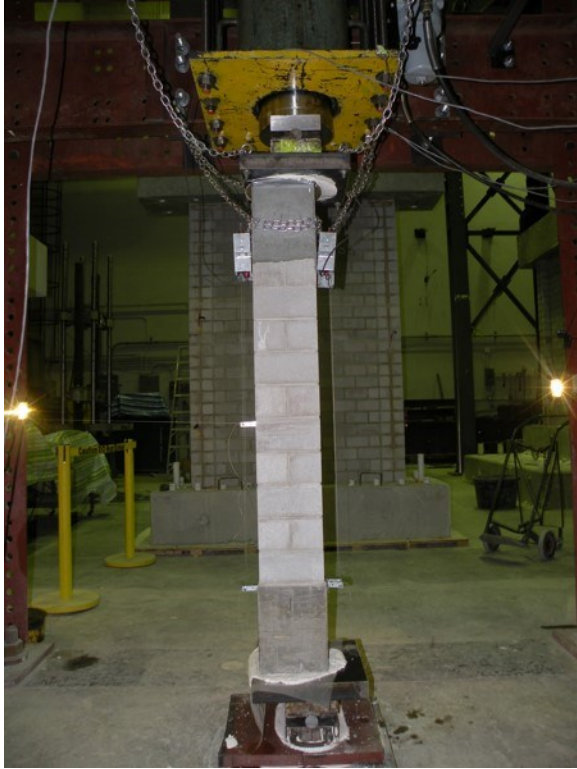
Figure A.29 Test setup for unwrapped columns under eccentric load.

Figure A.30 Test setup for wrapped columns under eccentric load.
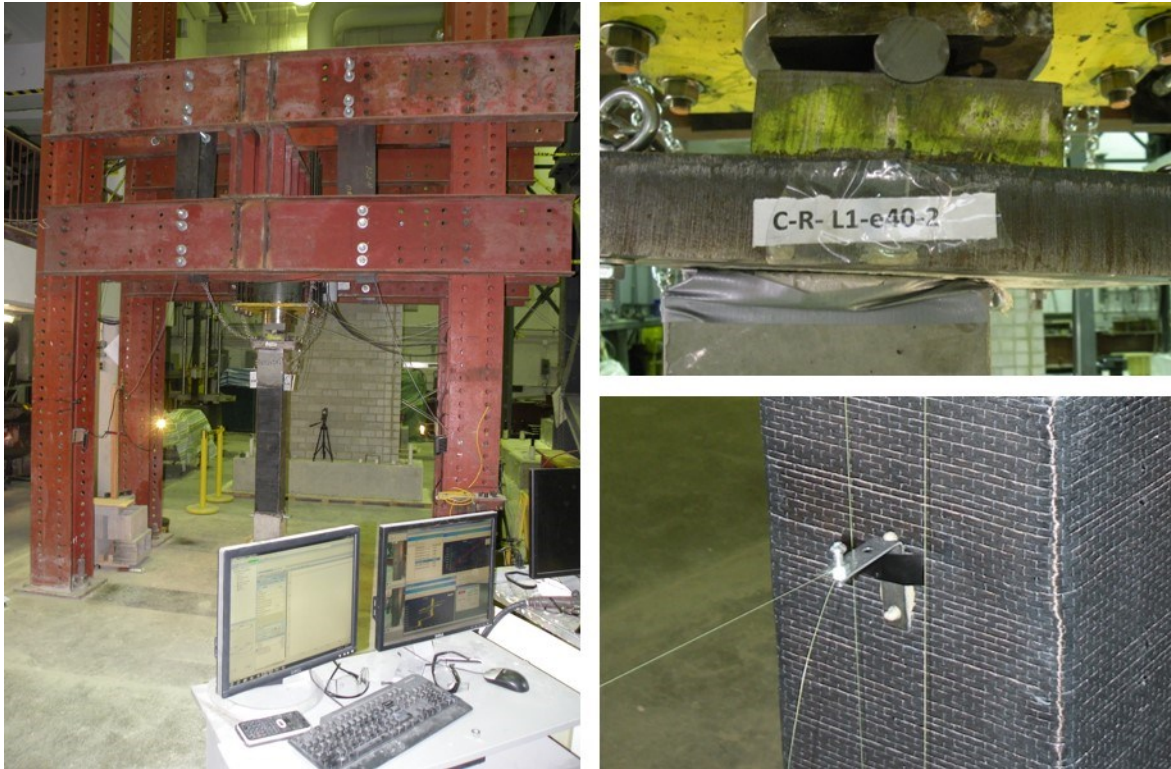
Figure A.31 Test setup frame and instrumentations.
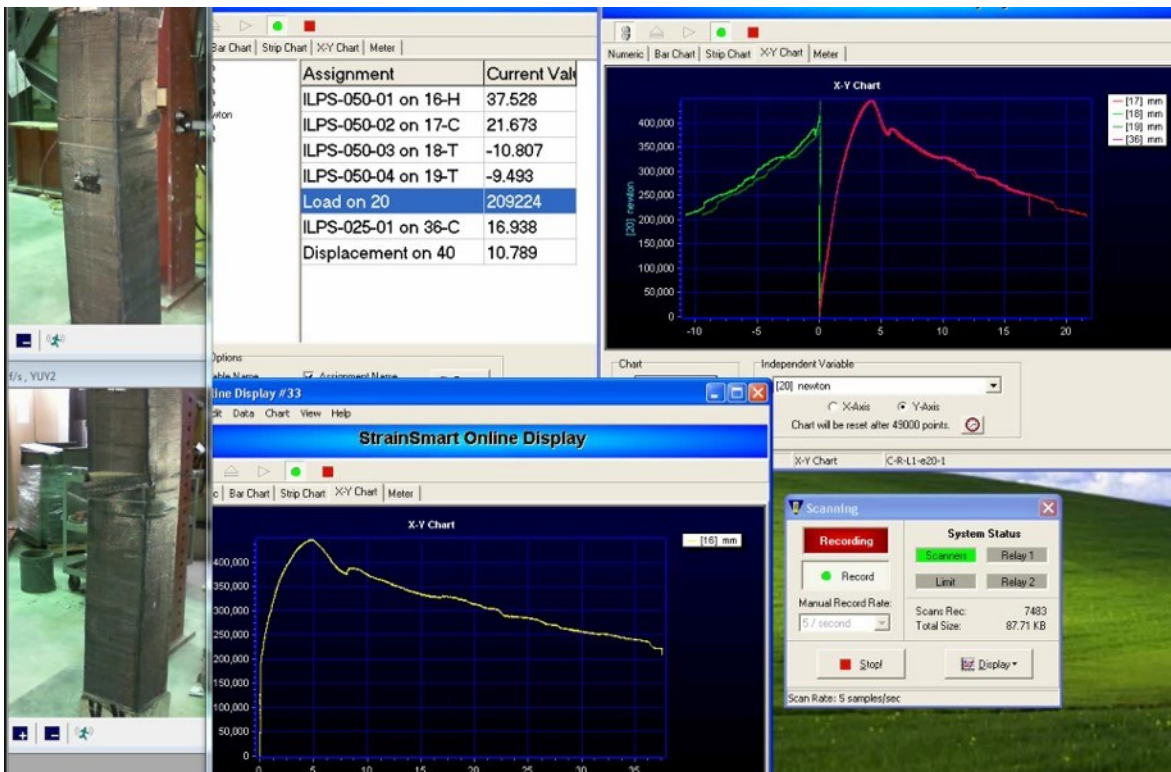
Figure A.32 Screenshot of the data acquisition system with the two HD cameras recording the instrumentations readings.

Appendix B Analysis of the Experimental Results

B.1 VBA macro

Considering the huge number of measurements obtained from more than 47 tests, VBA (Visual Basic for Applications) macros for Excel were developed to automate tasks and avoid human errors. Excel VBA macros were written to draw charts, find values, and perform calculations.

B.2 Processing the experimental measurements

The displacements measurements in the experimental tests were obtained by draw wire displacement sensors and linear variable inductance transducer (LVIT) sensors mounted on the specimens. During the tests, the wires of these sensors were affected by the impact of ejected pieces of concrete blocks or snapped CFRP materials, resulting in cutting the wire or moving the wire backward or forward. In case of cutting the wire, the forward readings of the sensor were removed from the average. In case of moving the wire, only the affected readings were removed, as shown in Figure B.1.
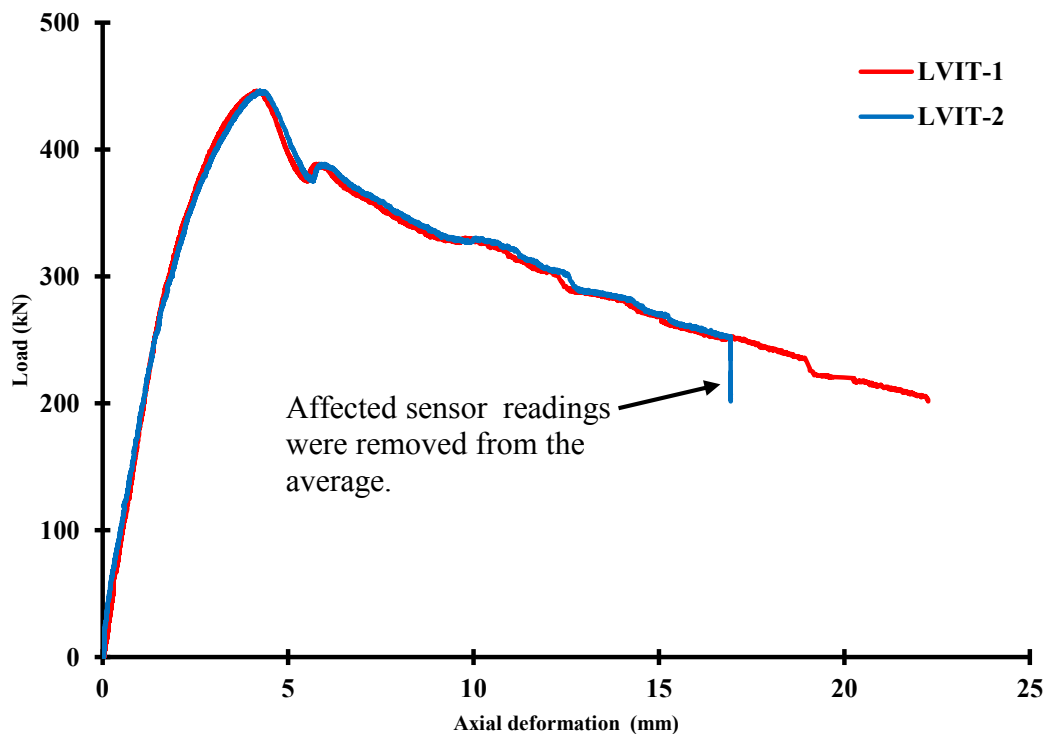
Figure B.1 Processing the displacements measurements.

B.3 Slenderness effect

The effect of slenderness was calculated based on TMS 402/602 Building Code Requirements and Specification for Masonry Structures.

$slenderness - dependent\ modification\ factors\ are$

$$1 - \left(\frac{h}{140.r}\right)^2 \quad for\ \frac{h}{r} \leq 99 \quad and \quad \left(\frac{70.r}{h}\right)^2 \quad for\ \frac{h}{r} > 99$$

$h = effective\ height\ of\ column \qquad r = radius\ of\ gyration$

$$r = \sqrt{\frac{I}{A}} \quad I = \frac{b^4}{12} \quad A = b^2$$

Given values for masonry columns with b=195 mm and considering only the masonry work height where h=945 mm.

$Solution:$

$$I = \frac{195^4}{12} = 120491718.8\ mm^4 \qquad A = 195^2 = 38025\ mm^2$$

$$r = \sqrt{\frac{120491718.8}{38025}} = 56.29\ mm$$

$$\frac{h}{r} = \frac{945}{56.29} = 16.79 < 99$$

$The\ slenderness - dependent\ modification\ factor$

$$= 1 - \left(\frac{h}{140.r}\right)^2 = 1 - \left(\frac{945}{140 * 56.29}\right)^2 = 0.986$$

Given values for masonry columns with b=195 mm and considering the two high strength footings, steel bearing plates, and the masonry work heights where h=1585 mm.

Solution:

$$\frac{h}{r} = \frac{1585}{56.29} = 28.16 < 99$$

The slenderness − dependent modification factor

$$= 1 - \left(\frac{h}{140.r}\right)^2 = 1 - \left(\frac{1585}{140 * 56.29}\right)^2 = 0.960$$

From the two calculations, it can be concluded that the slenderness effect is small (1.5% and 4%) and can be neglected in concentric tests. Furthermore, considering that the strength of high strength footings is more than four times the strength of masonry work and steel bearing plates have high strength, it is more reasonable to consider the height of masonry work only.

B.4 Section Analysis
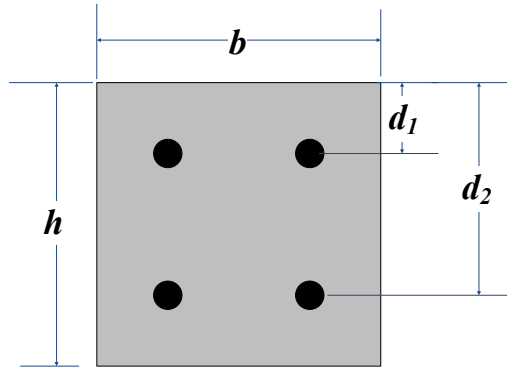
Solving Equations for proposed theoretical axial force-moment interaction diagram:

$$c = assumed\ value,$$
$$where\ h \geq c \geq c_b$$

<div style="text-align:right">Eq. B-1</div>

$$\varepsilon_{s1} = \frac{(c - d_1)}{c} \varepsilon_{mcu}$$

<div style="text-align:right">Eq. B-2</div>

$$\varepsilon_{s2} = \frac{(c - d_2)}{c} \varepsilon_{mcu}$$

<div style="text-align:right">Eq. B-3</div>

$$if\ \varepsilon_{s1} > \varepsilon_y\ \ f_{s1} = f_y\ not\ f_{s1} = \varepsilon_{s1}.E_s$$

<div style="text-align:right">Eq. B-4</div>

$$if\ \varepsilon_{s2} > \varepsilon_y\ \ f_{s2} = f_y\ not\ f_{s2} = \varepsilon_{s2}.E_s$$

<div style="text-align:right">Eq. B-5</div>

$$C_c = \alpha\ f_{mcd}\ .\beta\ c\ .b$$

<div style="text-align:right">Eq. B-6</div>

$$if\ c > d_1\ \ F_{s1} = A_{s1}.(f_{s1} - \alpha\ f_{mcd})\ not\ F_{s1} = A_{s1}.f_{s1}$$

<div style="text-align:right">Eq. B-7</div>

$$if\ c > d_2\ \ F_{s2} = A_{s2}.(f_{s2} - \alpha\ f_{mcd})\ not\ F_{s2} = A_{s2}.f_{s2}$$

<div style="text-align:right">Eq. B-8</div>

$$P = C_c + F_{s1} + F_{s2}$$

<div style="text-align:right">Eq. B-9</div>

$$M = C_c \left(\frac{h}{2} - \beta \frac{c}{2}\right) + F_{s1}.\left(\frac{h}{2} - d_1\right) - F_{s2}.\left(\frac{h}{2} - d_1\right)$$

<div style="text-align:right">Eq. B-10</div>

$$c_b = d_2 \frac{\varepsilon_{mcu}}{\varepsilon_{mcu} + \varepsilon_y}$$

<div style="text-align:right">Eq. B-11</div>

Given Values for one layer with α and β equal 0.85:

$f_{mcd}(MPa)$	$b\ (mm)$	$h\ (mm)$	$\varepsilon_{mcu}\ (mm/mm)$	α	β	$f_y\ (MPa)$	$C_b\ (mm)$
14.51	190	190	0.0045	0.85	0.85	483.03	93.26

$\varepsilon_y\ (mm/mm)$	$E_s\ (MPa)$	$As_1(mm^2)$	$d_1(mm)$	$As_2(mm^2)$	$d_2(mm)$	$A_m\ (mm^2)$	$A_s\ (mm^2)$
0.0024	200000	258	47	258	143	36100	516

Solutions for theoretical axial force-moment interaction diagram obtained by the proposed procedure:

c (mm)	ε_{s1} (mm/mm)	ε_{s2} (mm/mm)	f_{s1} (MPa)	f_{s2} (MPa)	C_{c1} (kN)	F_{s1} (kN)	F_{s2} (kN)	P (kN)	M $(kN.m)$	e (mm)
190	0.0034	0.0011	483	223	378.45	121.44	54.26	554.15	8.62	15.6
185	0.0034	0.0010	483	204	368.49	121.44	49.53	539.47	9.49	17.6
180	0.0033	0.0009	483	185	358.53	121.44	44.55	524.52	10.32	19.7
175	0.0033	0.0008	483	165	348.58	121.44	39.28	509.29	11.13	21.9
170	0.0033	0.0007	483	143	338.62	121.44	33.70	493.75	11.92	24.1
165	0.0032	0.0006	483	120	328.66	121.44	27.78	477.87	12.67	26.5
160	0.0032	0.0005	483	96	318.70	121.44	21.49	461.63	13.40	29.0
155	0.0031	0.0003	483	70	308.74	121.44	14.79	444.97	14.11	31.7
150	0.0031	0.0002	483	42	298.78	121.44	7.65	427.87	14.80	34.6
145	0.0030	0.0001	483	12	288.82	121.44	0.02	410.28	15.47	37.7
140	0.0030	-0.0001	483	-19	278.86	121.44	-4.98	395.32	15.97	40.4
135	0.0029	-0.0003	483	-53	268.90	121.44	-13.76	376.58	16.61	44.1
130	0.0029	-0.0005	483	-90	258.94	121.44	-23.22	357.16	17.24	48.3
125	0.0028	-0.0006	483	-130	248.98	121.44	-33.44	336.99	17.86	53.0
120	0.0027	-0.0009	483	-173	239.02	121.44	-44.51	315.96	18.48	58.5
115	0.0027	-0.0011	483	-219	229.06	121.44	-56.54	293.97	19.11	65.0
110	0.0026	-0.0014	483	-270	219.10	121.44	-69.66	270.88	19.74	72.9
105	0.0025	-0.0016	483	-326	209.15	121.44	-84.03	246.55	20.40	82.7
100	0.0024	-0.0019	477	-387	199.19	119.88	-99.85	219.22	21.00	95.8
95	0.0023	-0.0023	455	-455	189.23	114.14	-117.32	186.04	21.45	115.3
93.26	0.0022	-0.0024	446	-480	185.76	112.00	-123.84	173.92	21.60	124.2

Assuming c that gives the same level of eccentricity in experimental tests:

c (mm)	ε_{s1} (mm/mm)	ε_{s2} (mm/mm)	f_{s1} (MPa)	f_{s2} (MPa)	C_{c1} (kN)	F_{s1} (kN)	F_{s2} (kN)	P (kN)	M $(kN.m)$	e (mm)
168.82	0.0032	0.0007	483	138	336.26	121.44	32.33	490.03	12.10	24.68
168.90	0.0032	0.0007	483	138	336.42	121.44	32.42	490.28	12.08	24.65
168.42	0.0032	0.0007	483	136	335.47	121.44	31.86	488.77	12.16	24.87
133.38	0.0029	-0.0003	483	-65	265.67	121.44	-16.75	370.36	16.81	45.39
132.79	0.0029	-0.0003	483	-69	264.51	121.44	-17.85	368.10	16.89	45.87

Given Values for two layer with α and β equal 0.85:

$f_{mcd}(MPa)$	$b\ (mm)$	$h\ (mm)$	$\varepsilon_{mcu}\ (mm/mm)$	α	β	$f_y\ (MPa)$	$C_b\ (mm)$
15.99	190	190	0.0049	0.85	0.85	483.03	95.99

$\varepsilon_y\ (mm/mm)$	$E_s\ (MPa)$	$As_1(mm^2)$	$d_1(mm)$	$As_2(mm^2)$	$d_2(mm)$	$A_m\ (mm^2)$	$A_s\ (mm^2)$
0.0024	200000	258	47	258	143	36100	516

Solutions for theoretical axial force-moment interaction diagram obtained by the proposed procedure:

c (mm)	ε_{s1} (mm/mm)	ε_{s2} (mm/mm)	f_{s1} (MPa)	f_{s2} (MPa)	C_{c1} (kN)	F_{s1} (kN)	F_{s2} (kN)	P (kN)	M (kN.m)	e (mm)
190	0.0037	0.0012	483	242	417.06	121.12	59.04	597.21	8.92	14.94
185	0.0037	0.0011	483	222	406.08	121.12	53.89	581.09	9.88	17.00
180	0.0036	0.0010	483	201	395.10	121.12	48.47	564.69	10.80	19.12
175	0.0036	0.0009	483	179	384.13	121.12	42.73	547.97	11.69	21.32
170	0.0035	0.0008	483	156	373.15	121.12	36.65	530.92	12.54	23.63
165	0.0035	0.0007	483	131	362.18	121.12	30.21	513.50	13.37	26.04
160	0.0035	0.0005	483	104	351.20	121.12	23.36	495.68	14.17	28.60
155	0.0034	0.0004	483	76	340.23	121.12	16.07	477.41	14.95	31.32
150	0.0034	0.0002	483	46	329.25	121.12	8.29	458.66	15.70	34.24
145	0.0033	0.0001	483	14	318.28	121.12	-0.02	439.37	16.44	37.41
140	0.0033	-0.0001	483	-21	307.30	121.12	-5.42	423.00	16.98	40.15
135	0.0032	-0.0003	483	-58	296.33	121.12	-14.98	402.46	17.68	43.93
130	0.0031	-0.0005	483	-98	285.35	121.12	-25.28	381.18	18.37	48.19
125	0.0031	-0.0007	483	-141	274.38	121.12	-36.41	359.08	19.05	53.05
120	0.0030	-0.0009	483	-188	263.40	121.12	-48.46	336.06	19.73	58.71
115	0.0029	-0.0012	483	-239	252.43	121.12	-61.56	311.98	20.41	65.43
110	0.0028	-0.0015	483	-294	241.45	121.12	-75.85	286.72	21.10	73.61
105	0.0027	-0.0018	483	-355	230.48	121.12	-91.50	260.09	21.82	83.88
100	0.0026	-0.0021	483	-421	219.50	121.12	-108.72	231.90	22.56	97.27
95.99	0.0025	-0.0024	483	-480	210.69	121.12	-123.84	207.97	23.18	111.45

Assuming c that gives the same level of eccentricity in experimental tests:

c (mm)	ε_{s1} (mm/mm)	ε_{s2} (mm/mm)	f_{s1} (MPa)	f_{s2} (MPa)	C_{c1} (kN)	F_{s1} (kN)	F_{s2} (kN)	P (kN)	M (kN.m)	e (mm)
169.90	0.0035	0.0008	483	155	372.93	121.12	36.52	530.56	12.56	23.68
167.00	0.0035	0.0007	483	141	366.56	121.12	32.82	520.50	13.05	25.06
168.04	0.0035	0.0007	483	146	368.85	121.12	34.17	524.13	12.87	24.56
130.67	0.0031	-0.0005	483	-92	286.83	121.12	-23.85	384.10	18.28	47.59
130.31	0.0031	-0.0005	483	-95	286.03	121.12	-24.62	382.53	18.33	47.91
131.54	0.0031	-0.0004	483	-85	288.73	121.12	-22.03	387.81	18.16	46.83

Given Values for one layer with α and β equal 0.80:

$f_{mcd}(MPa)$	$b\ (mm)$	$h\ (mm)$	$\varepsilon_{mcu}\ (mm/mm)$	α	β	$f_y\ (MPa)$	$C_b\ (mm)$
14.51	190	190	0.0045	0.80	0.80	483.03	93.26

$\varepsilon_y\ (mm/mm)$	$E_s\ (MPa)$	$As_1(mm^2)$	$d_1(mm)$	$As_2(mm^2)$	$d_2(mm)$	$A_m\ (mm^2)$	$A_s\ (mm^2)$
0.0024	200000	258	47	258	143	36100	516

Solutions for theoretical axial force-moment interaction diagram obtained by the proposed procedure:

c (mm)	ε_{s1} (mm/mm)	ε_{s2} (mm/mm)	f_{s1} (MPa)	f_{s2} (MPa)	C_{c1} (kN)	F_{s1} (kN)	F_{s2} (kN)	P (kN)	M (kN.m)	e (mm)
190	0.0034	0.0011	483	223	335.24	121.63	54.44	511.31	9.59	18.76
185	0.0034	0.0010	483	204	326.42	121.63	49.72	497.76	10.31	20.71
180	0.0033	0.0009	483	185	317.59	121.63	44.74	483.96	11.00	22.72
175	0.0033	0.0008	483	165	308.77	121.63	39.46	469.86	11.66	24.82
170	0.0033	0.0007	483	143	299.95	121.63	33.88	455.46	12.31	27.03
165	0.0032	0.0006	483	120	291.13	121.63	27.97	440.72	12.94	29.36
160	0.0032	0.0005	483	96	282.31	121.63	21.68	425.61	13.55	31.83
155	0.0031	0.0003	483	70	273.48	121.63	14.98	410.09	14.14	34.49
150	0.0031	0.0002	483	42	264.66	121.63	7.84	394.13	14.72	37.36
145	0.0030	0.0001	483	12	255.84	121.63	0.21	377.68	15.29	40.50
140	0.0030	-0.0001	483	-19	247.02	121.63	-4.98	363.67	15.71	43.20
135	0.0029	-0.0003	483	-53	238.20	121.63	-13.76	346.06	16.26	47.00
130	0.0029	-0.0005	483	-90	229.37	121.63	-23.22	327.78	16.82	51.30
125	0.0028	-0.0006	483	-130	220.55	121.63	-33.44	308.74	17.37	56.25
120	0.0027	-0.0009	483	-173	211.73	121.63	-44.51	288.85	17.93	62.06
115	0.0027	-0.0011	483	-219	202.91	121.63	-56.54	268.00	18.49	69.01
110	0.0026	-0.0014	483	-270	194.09	121.63	-69.66	246.05	19.08	77.54
105	0.0025	-0.0016	483	-326	185.26	121.63	-84.03	222.86	19.69	88.36
100	0.0024	-0.0019	477	-387	176.44	120.07	-99.85	196.67	20.26	103.02
95	0.0023	-0.0023	455	-455	167.62	114.33	-117.32	164.62	20.67	125.58
93.26	0.0022	-0.0024	446	-480	164.55	112.18	-123.84	152.90	20.82	136.19

Assuming c that gives the same level of eccentricity in experimental tests:

c (mm)	ε_{s1} (mm/mm)	ε_{s2} (mm/mm)	f_{s1} (MPa)	f_{s2} (MPa)	C_{c1} (kN)	F_{s1} (kN)	F_{s2} (kN)	P (kN)	M (kN.m)	e (mm)
175.32	0.0033	0.0008	483	166	309.34	121.63	39.81	470.78	11.62	24.68
175.41	0.0033	0.0008	483	166	309.49	121.63	39.90	471.02	11.61	24.65
174.88	0.0033	0.0008	483	164	308.56	121.63	39.34	469.53	11.68	24.87
137.04	0.0030	-0.0002	483	-39	241.80	121.63	-10.10	353.33	16.04	45.39
136.42	0.0029	-0.0002	483	-43	240.70	121.63	-11.20	351.13	16.11	45.87

Given Values for Two layer with α and β equal 0.80:

$f_{mcd}(MPa)$	$b\ (mm)$	$h\ (mm)$	$\varepsilon_{mcu}\ (mm/mm)$	α	β	$f_y\ (MPa)$	$C_b\ (mm)$
15.99	190	190	0.0049	0.80	0.80	483.03	95.99

$\varepsilon_y\ (mm/mm)$	$E_s\ (MPa)$	$As_1(mm^2)$	$d_1(mm)$	$As_2(mm^2)$	$d_2(mm)$	$A_m\ (mm^2)$	$A_s\ (mm^2)$
0.0024	200000	258	47	258	143	36100	516

Solutions for theoretical axial force-moment interaction diagram obtained by the proposed procedure:

c (mm)	ε_{s1} (mm/mm)	ε_{s2} (mm/mm)	f_{s1} (MPa)	f_{s2} (MPa)	C_{c1} (kN)	F_{s1} (kN)	F_{s2} (kN)	P (kN)	M (kN.m)	e (mm)
190	0.0037	0.0012	483	242	369.43	121.32	59.24	550.00	10.00	18.18
185	0.0037	0.0011	483	222	359.71	121.32	54.10	535.13	10.78	20.15
180	0.0036	0.0010	483	201	349.99	121.32	48.67	519.98	11.54	22.19
175	0.0036	0.0009	483	179	340.27	121.32	42.93	504.52	12.27	24.32
170	0.0035	0.0008	483	156	330.55	121.32	36.86	488.72	12.98	26.56
165	0.0035	0.0007	483	131	320.82	121.32	30.41	472.56	13.67	28.92
160	0.0035	0.0005	483	104	311.10	121.32	23.56	455.99	14.34	31.44
155	0.0034	0.0004	483	76	301.38	121.32	16.27	438.98	14.99	34.14
150	0.0034	0.0002	483	46	291.66	121.32	8.50	421.48	15.62	37.07
145	0.0033	0.0001	483	14	281.94	121.32	0.19	403.44	16.25	40.27
140	0.0033	-0.0001	483	-21	272.21	121.32	-5.42	388.12	16.70	43.03
135	0.0032	-0.0003	483	-58	262.49	121.32	-14.98	368.83	17.30	46.92
130	0.0031	-0.0005	483	-98	252.77	121.32	-25.28	348.81	17.91	51.34
125	0.0031	-0.0007	483	-141	243.05	121.32	-36.41	327.96	18.51	56.43
120	0.0030	-0.0009	483	-188	233.33	121.32	-48.46	306.19	19.12	62.43
115	0.0029	-0.0012	483	-239	223.60	121.32	-61.56	283.36	19.73	69.65
110	0.0028	-0.0015	483	-294	213.88	121.32	-75.85	259.35	20.37	78.55
105	0.0027	-0.0018	483	-355	204.16	121.32	-91.50	233.98	21.04	89.91
100	0.0026	-0.0021	483	-421	194.44	121.32	-108.72	207.04	21.74	104.99
95.99	0.0025	-0.0024	483	-480	186.63	121.32	-123.84	184.12	22.33	121.29

Assuming c that gives the same level of eccentricity in experimental tests:

c (mm)	ε_{s1} (mm/mm)	ε_{s2} (mm/mm)	f_{s1} (MPa)	f_{s2} (MPa)	C_{c1} (kN)	F_{s1} (kN)	F_{s2} (kN)	P (kN)	M (kN.m)	e (mm)
176.49	0.0036	0.0009	483	186	343.16	121.32	44.67	509.15	12.05	23.68
173.31	0.0036	0.0009	483	171	336.98	121.32	40.92	499.22	12.51	25.06
174.45	0.0036	0.0009	483	177	339.20	121.32	42.28	502.80	12.35	24.56
134.20	0.0032	-0.0003	483	-64	260.94	121.32	-16.58	365.68	17.40	47.59
133.82	0.0032	-0.0003	483	-67	260.19	121.32	-17.35	364.15	17.45	47.91
135.11	0.0032	-0.0003	483	-57	262.71	121.32	-14.76	369.27	17.29	46.83

Appendix C Results

C.1 Concrete masonry prisms

Additional images and results of concrete masonry prisms tested in Chapter 3 of the main body of the thesis are presented in this section.
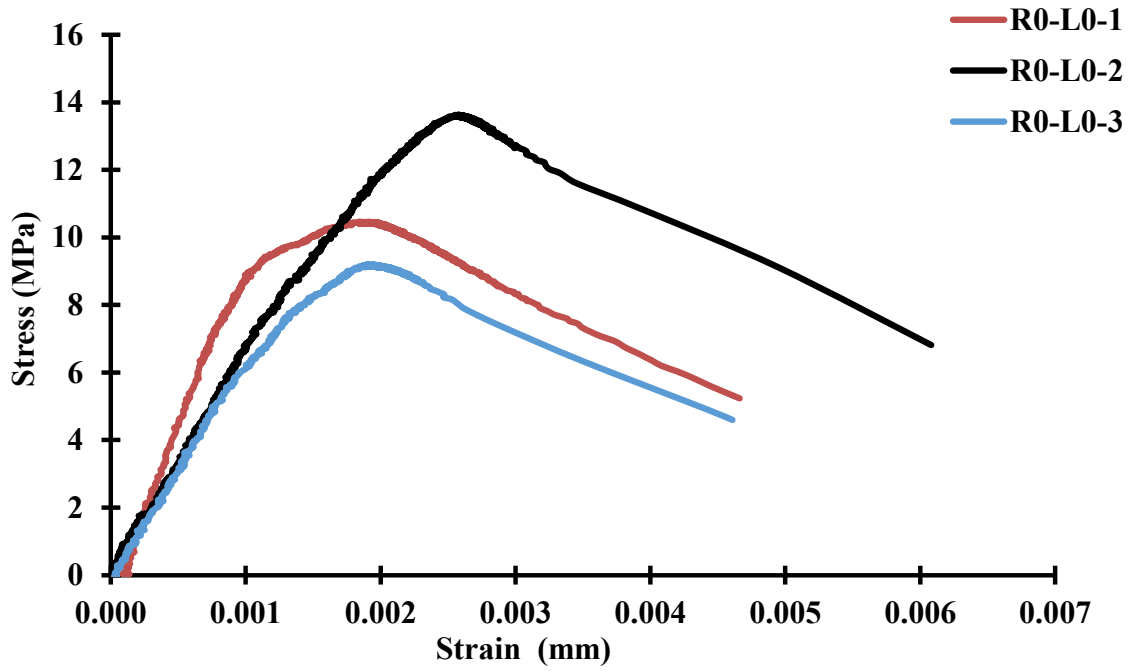
Group R0-L0

Figure C.1 Axial stress-strain curves of R0-L0.

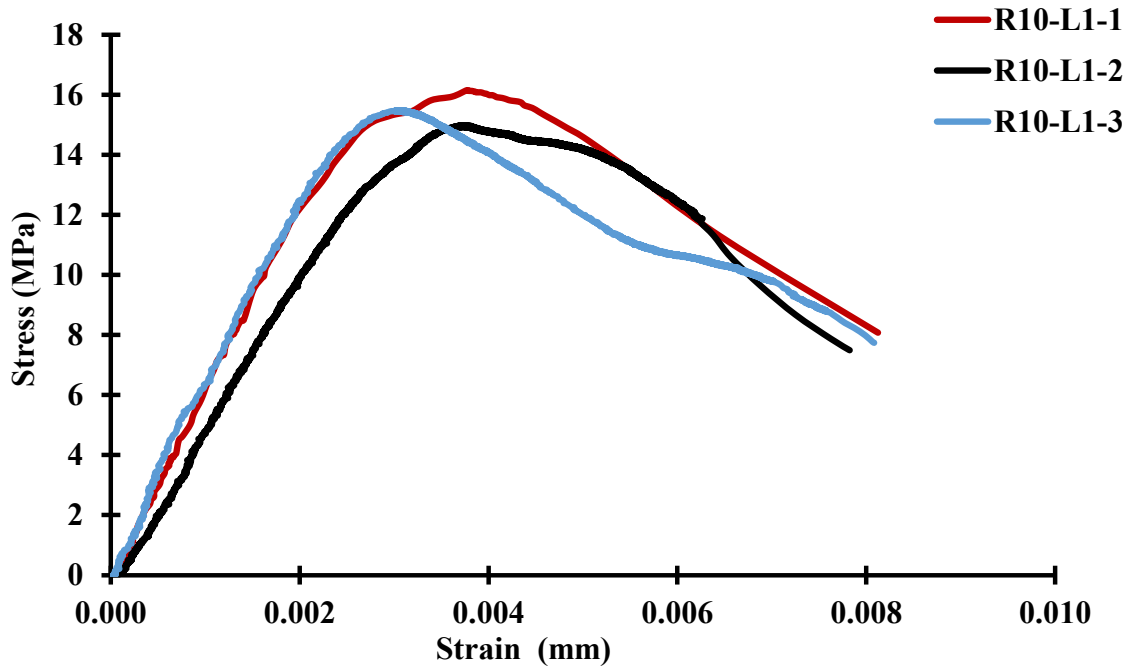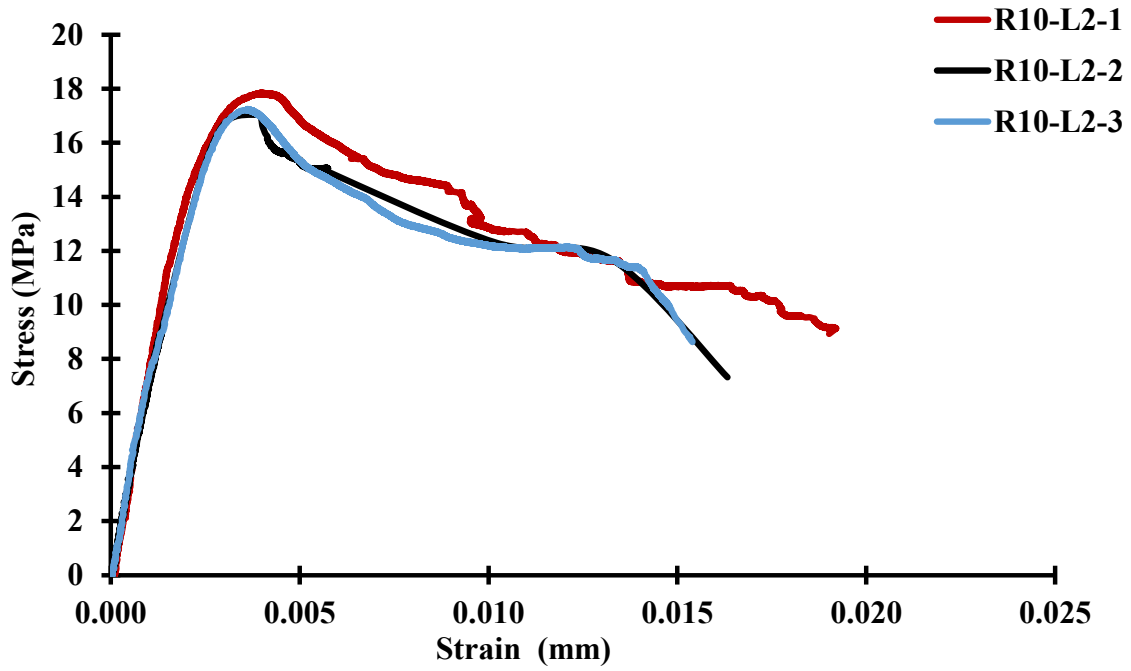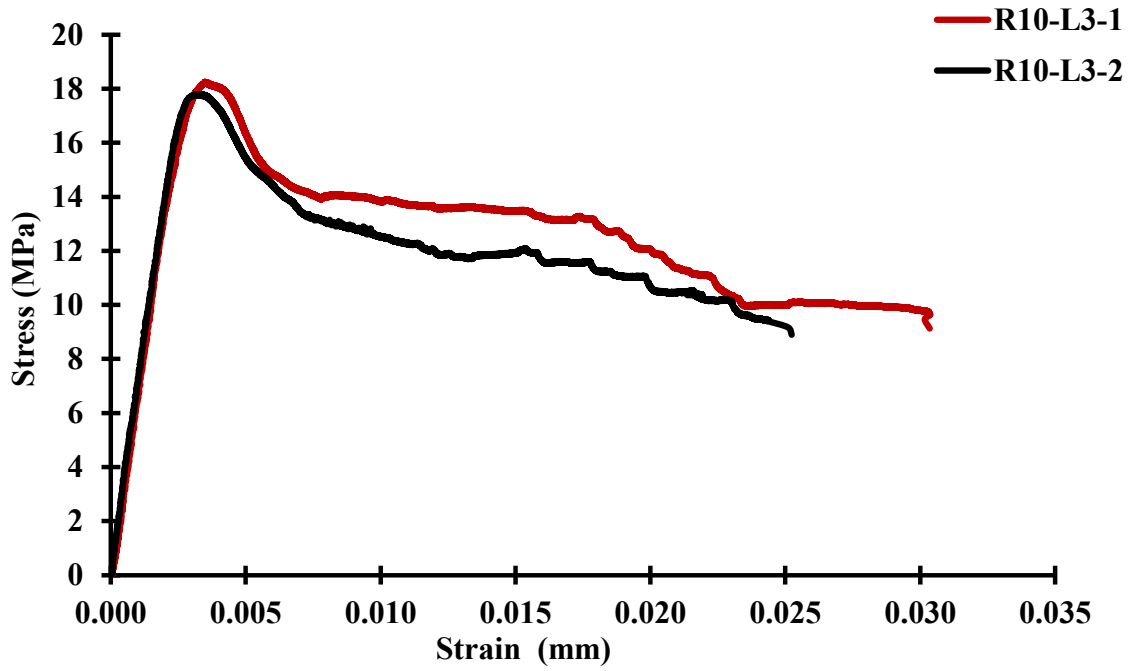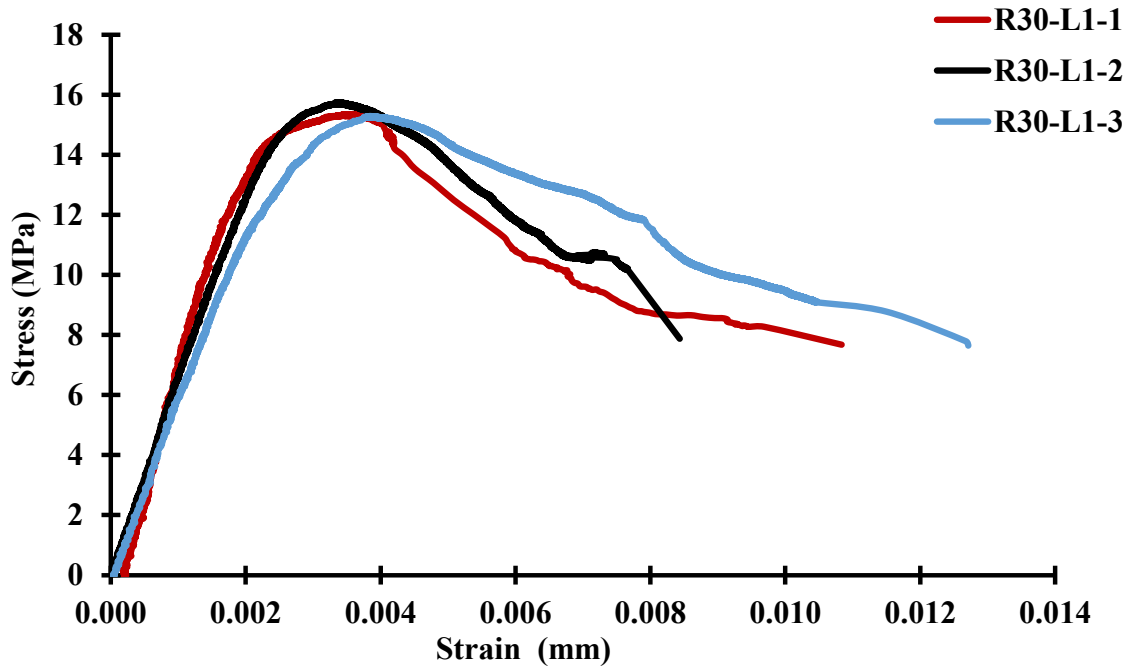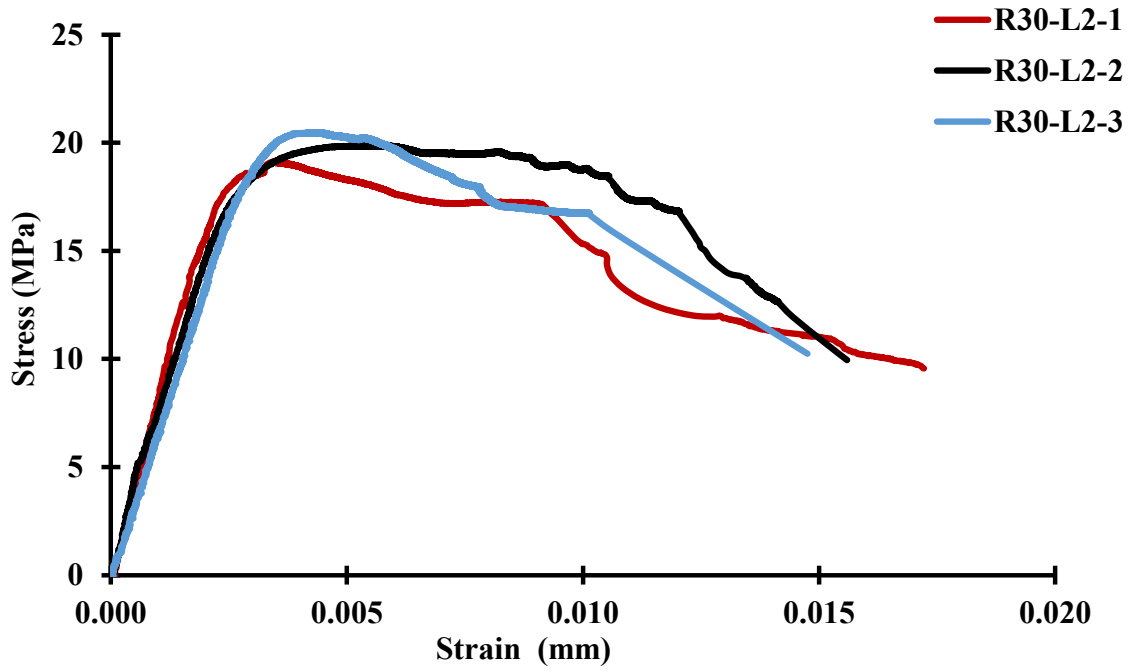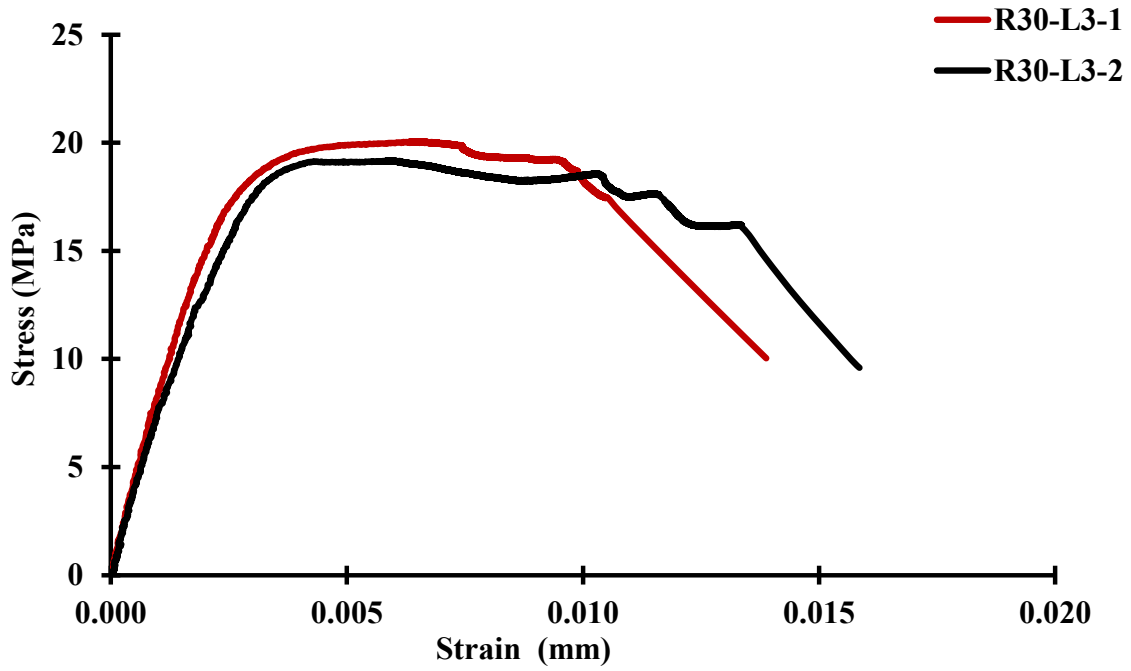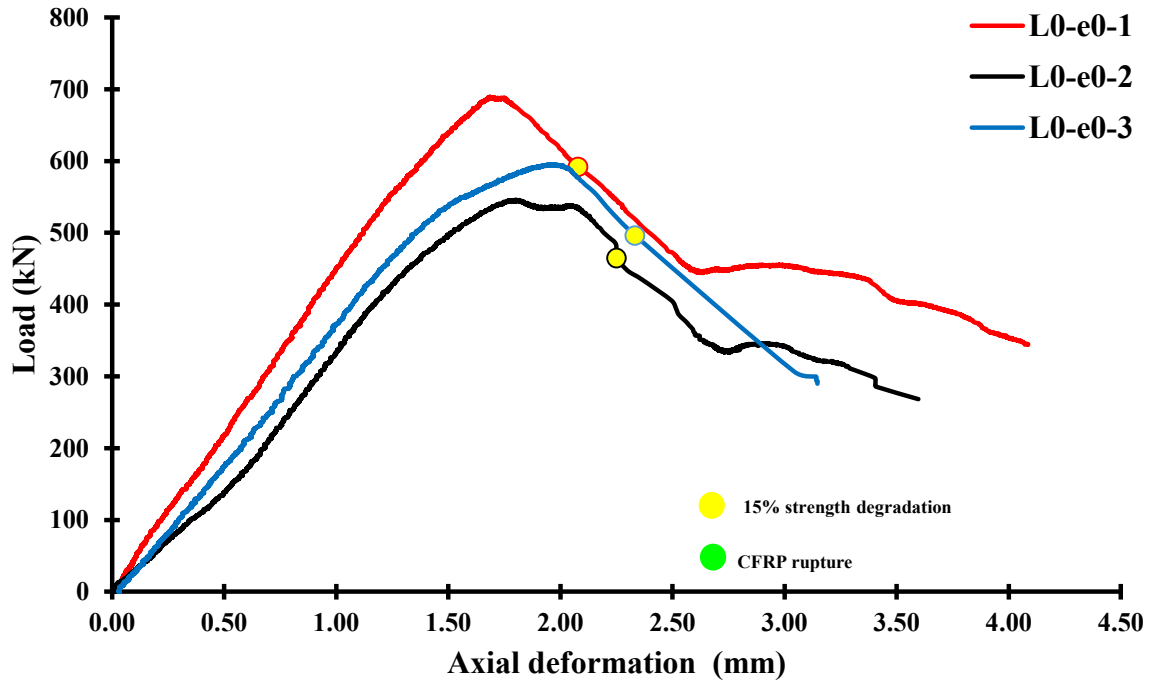Figure C.2 Failure modes at the end of the compression tests for R0-L0.

Group R10-L1

Figure C.3 Axial stress-strain curves of R10-L1.

Figure C.4 Failure modes at the end of the compression tests for R10-L1.

Group R10-L2

Figure C.5 Axial stress-strain curves of R10-L2.

Figure C.6 Failure modes at the end of the compression tests for R10-L2.

Group R10-L3

Figure C.7 Axial stress-strain curves of R10-L3.

Figure C.8 Failure modes at the end of the compression tests for R10-L3.

Figure C.9 Axial stress-strain curves of R30-L1.

Figure C.10 Failure modes at the end of the compression tests for R30-L1.

Group R30-L2

Figure C.11 Axial stress-strain curves of R30-L2.

Figure C.12 Failure modes at the end of the compression tests for R30-L2.

Figure C.13 Axial stress-strain curves of R30-L3.

Figure C.14 Failure modes at the end of the compression tests for R30-L3.

C.2 Concrete masonry columns

Additional images and results of reinforced concrete masonry columns tested in Chapter 4 of the main body of the thesis are presented in this section.

Group L0-e0

Figure C.15 Axial load-deformation curves of L0-e0.

Figure C.16 Failure modes at the end of the compression tests for L0-e0.

Group L1-e0
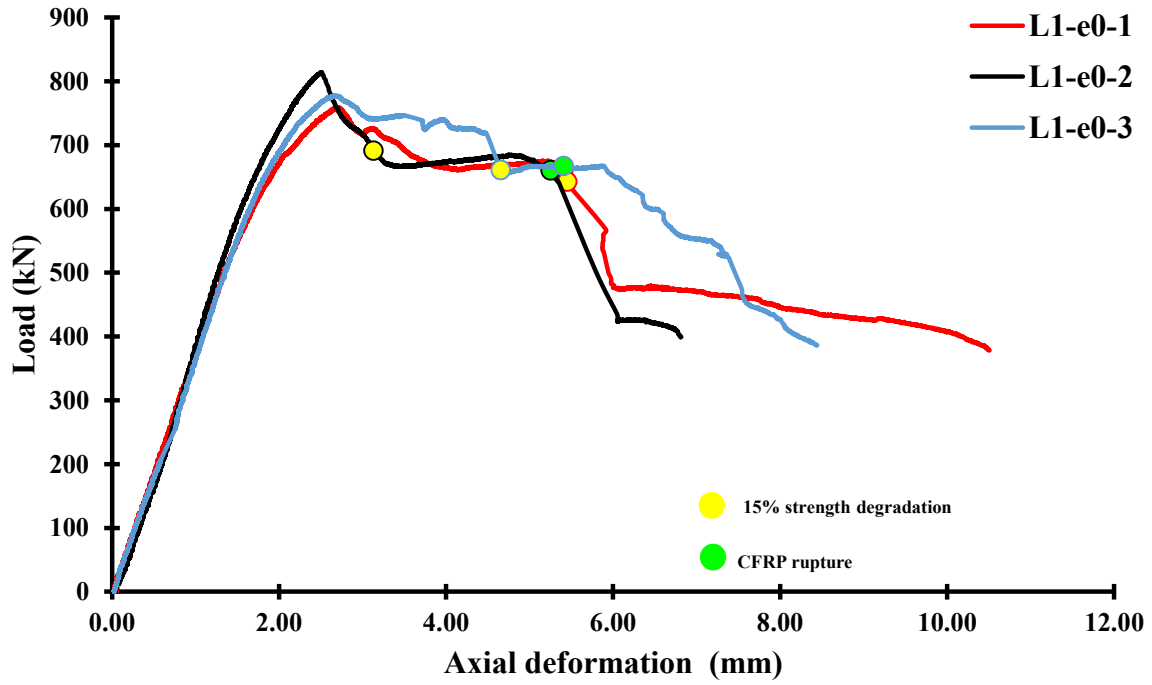
Figure C.17 Axial load-deformation curves of L1-e0.

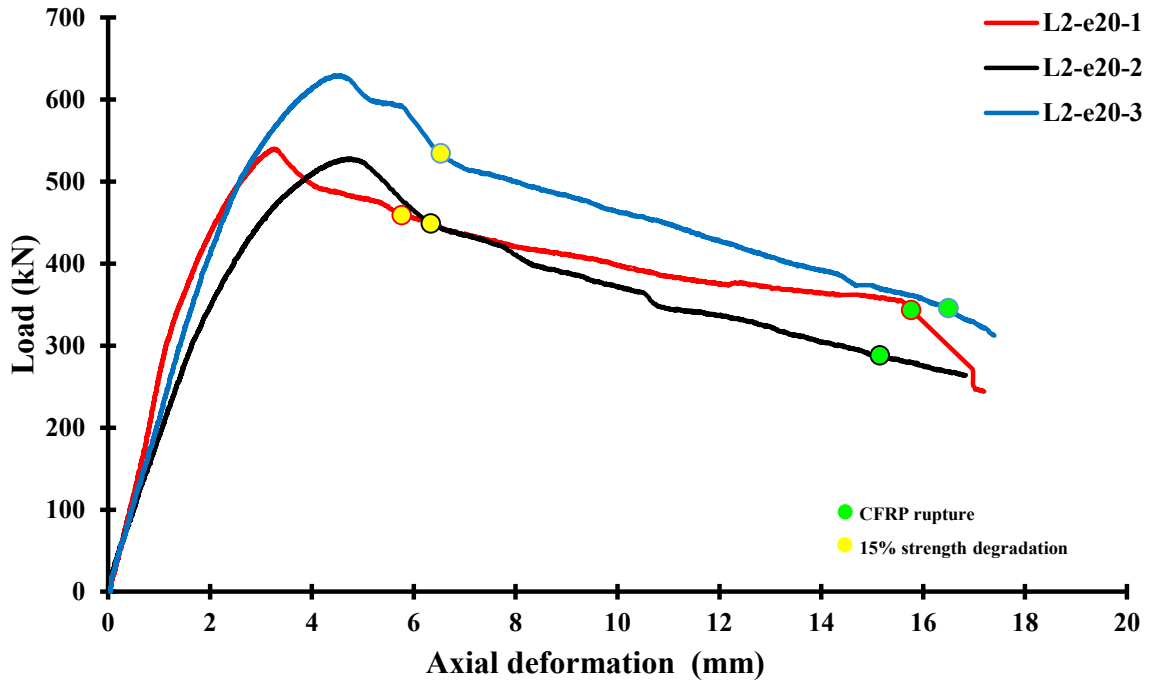Figure C.18 Failure modes at the end of the compression tests for L1-e0.

Group L2-e0
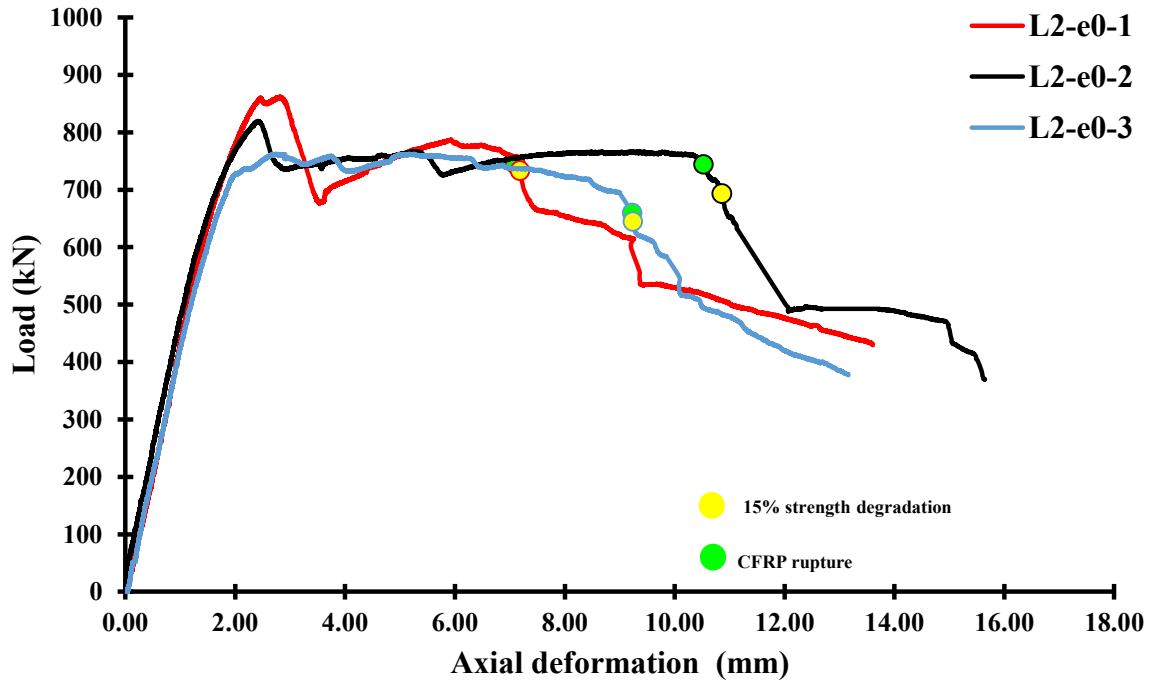
Figure C.19 Axial load-deformation curves of L2-e0.

Figure C.20 Failure modes at the end of the compression tests for L2-e0.

Group L0-e20
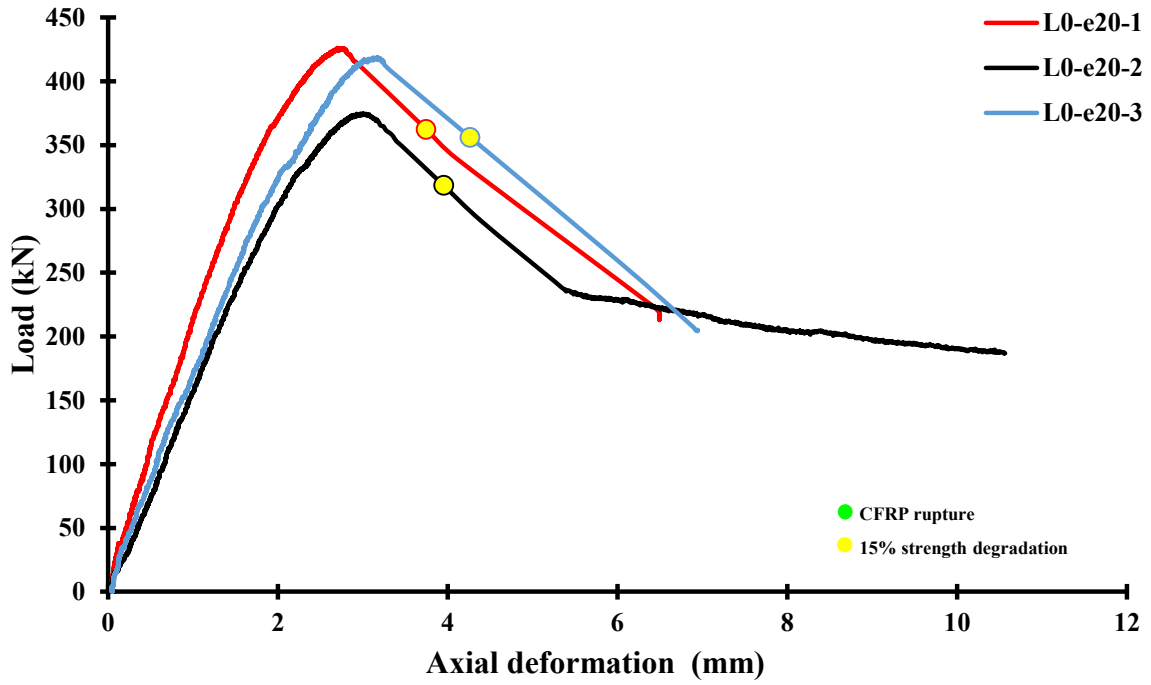
Figure C.21 Axial load-deformation curves of L0-e20.

Figure C.22 Failure modes at the end of the eccentric tests for L0-e20.
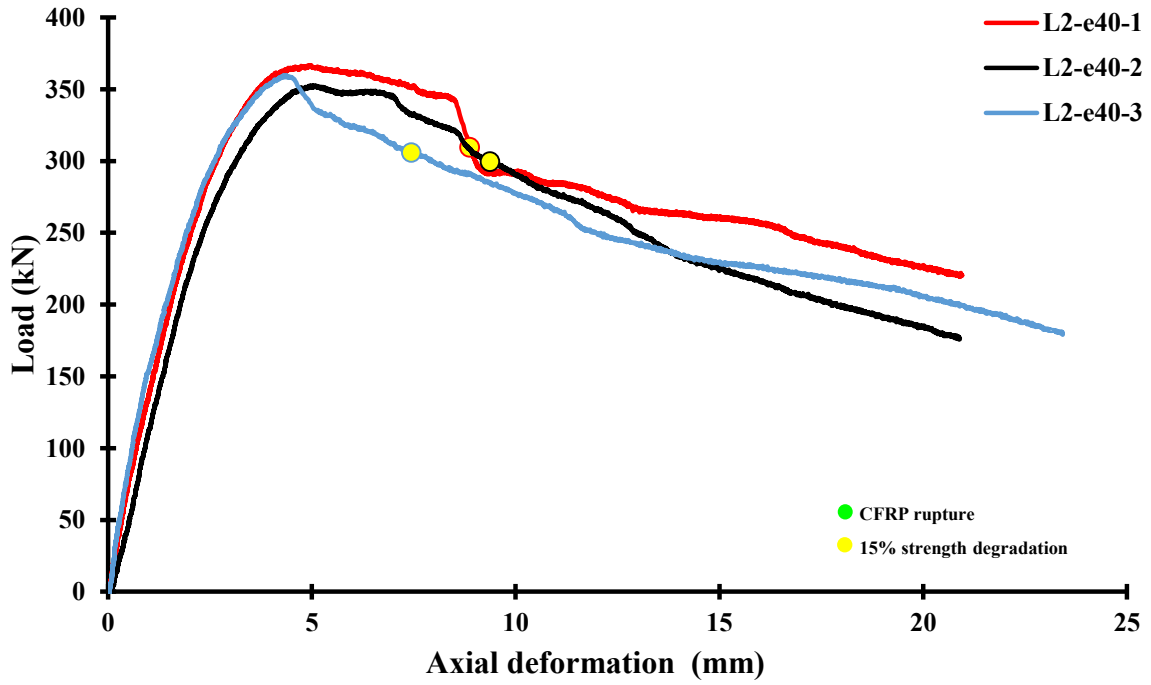
Group L0-e40
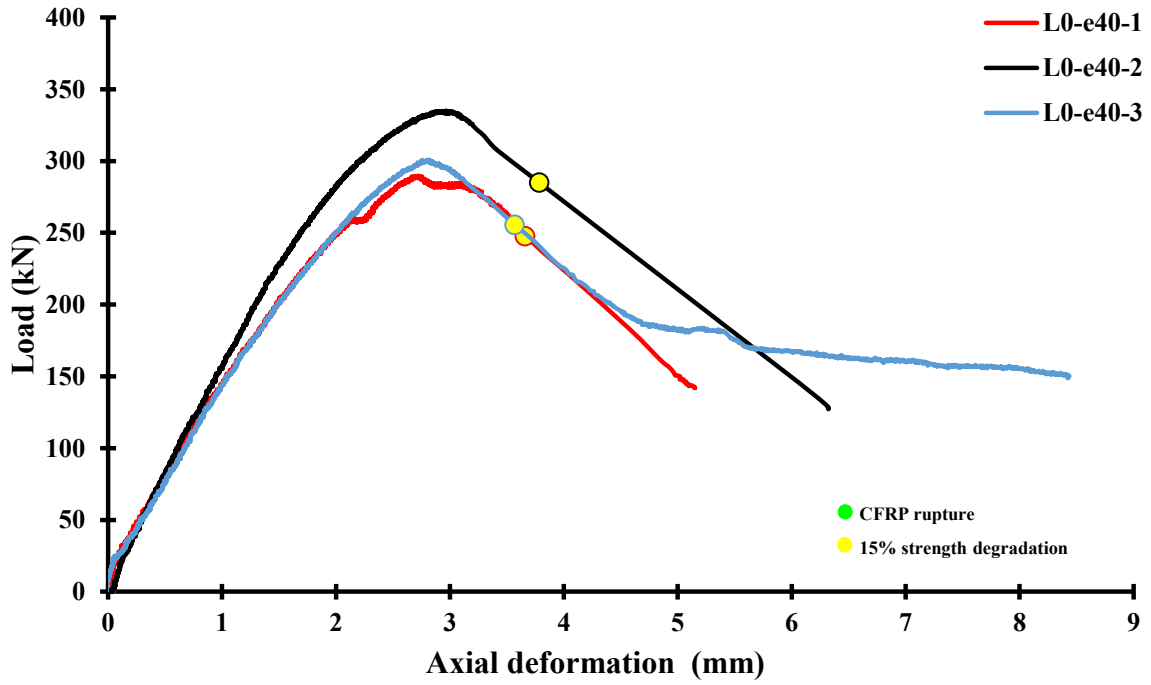
Figure C.23 Axial load-deformation curves of L0-e40.

Figure C.24 Failure modes at the end of the eccentric tests for L0-e40.

Group L1-e20
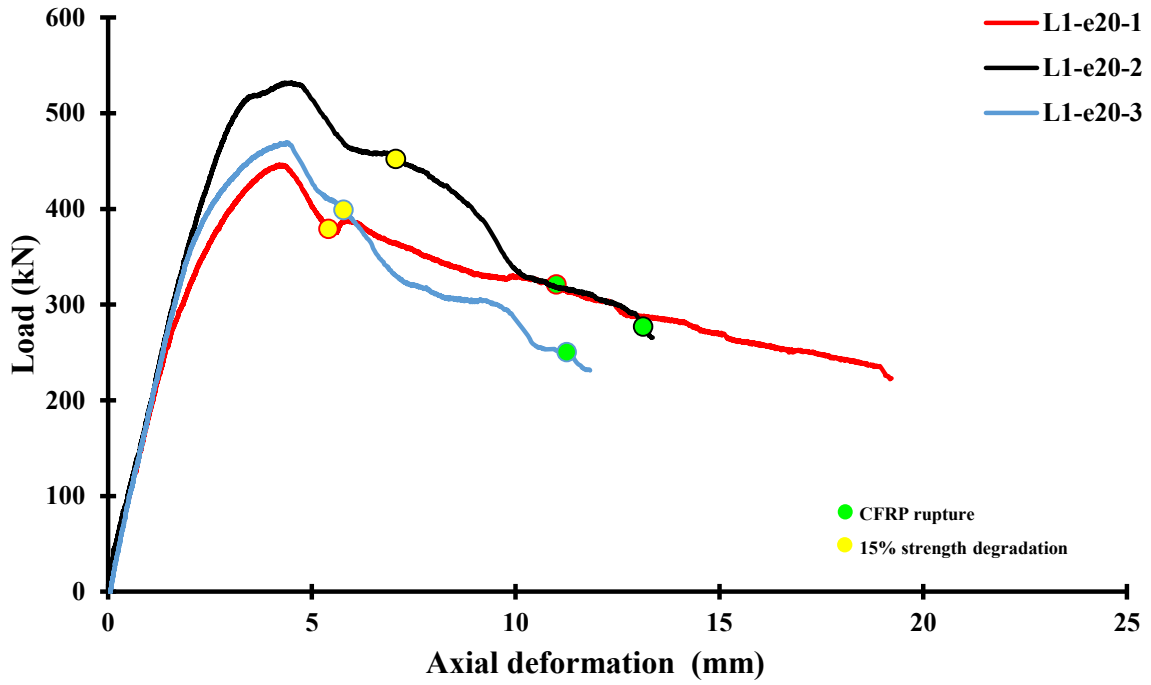

Figure C.25 Axial load-deformation curves of L1-e20.
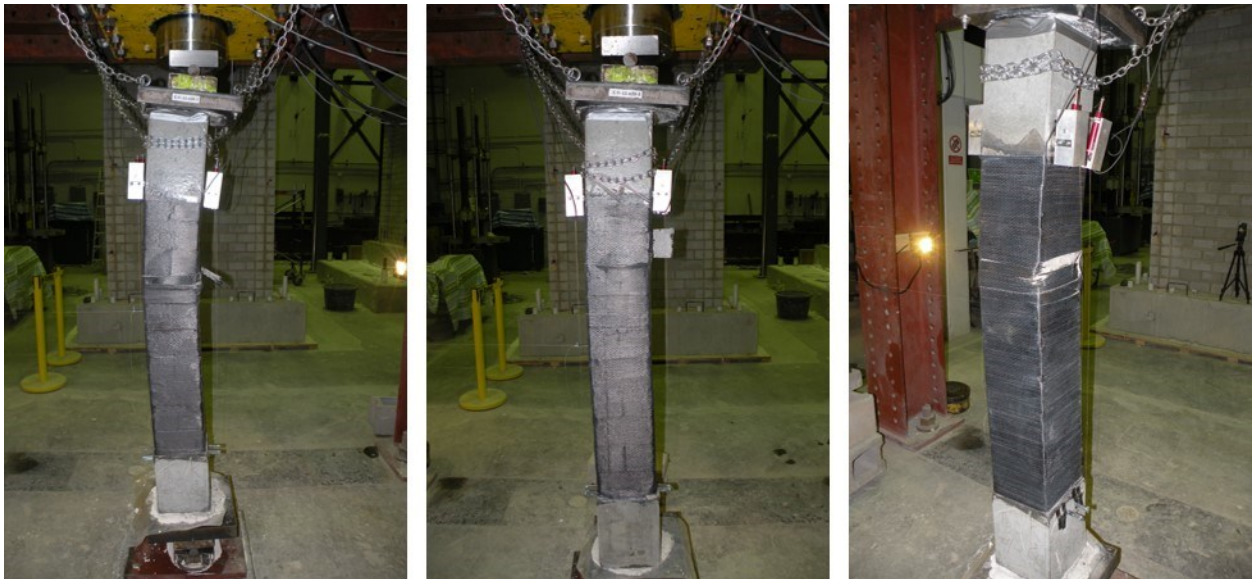
Figure C.26 Failure modes at the end of the eccentric tests for L1-e20.

Group L1-e40
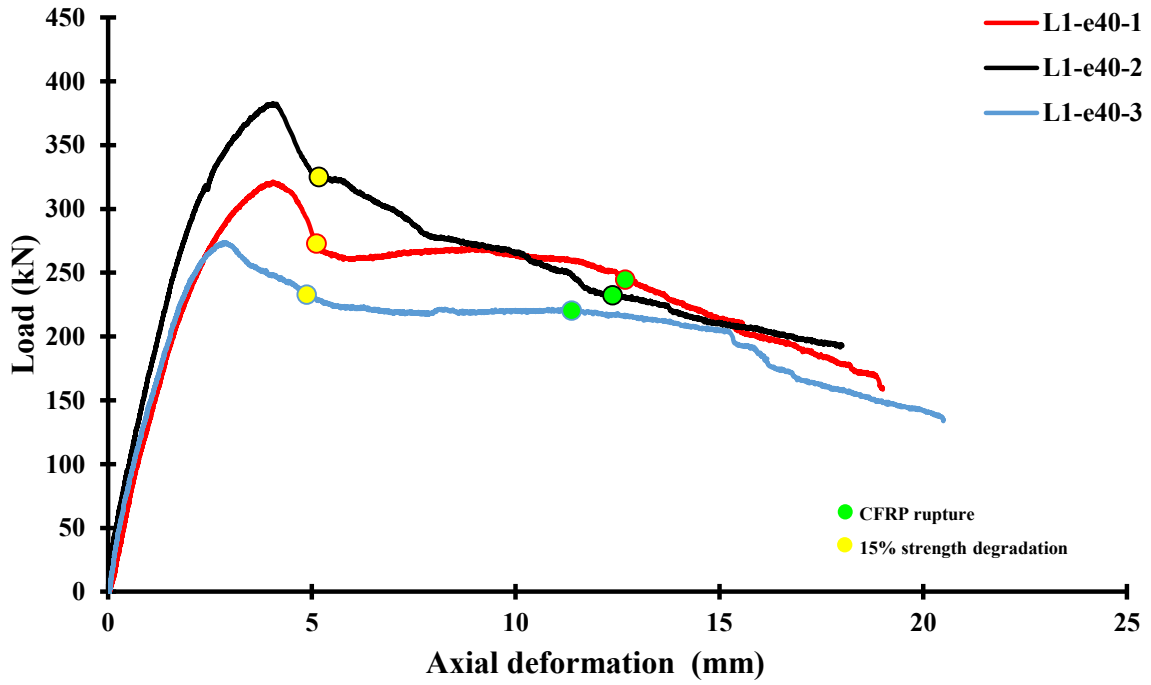
Figure C.27 Axial load-deformation curves of L1-e40.
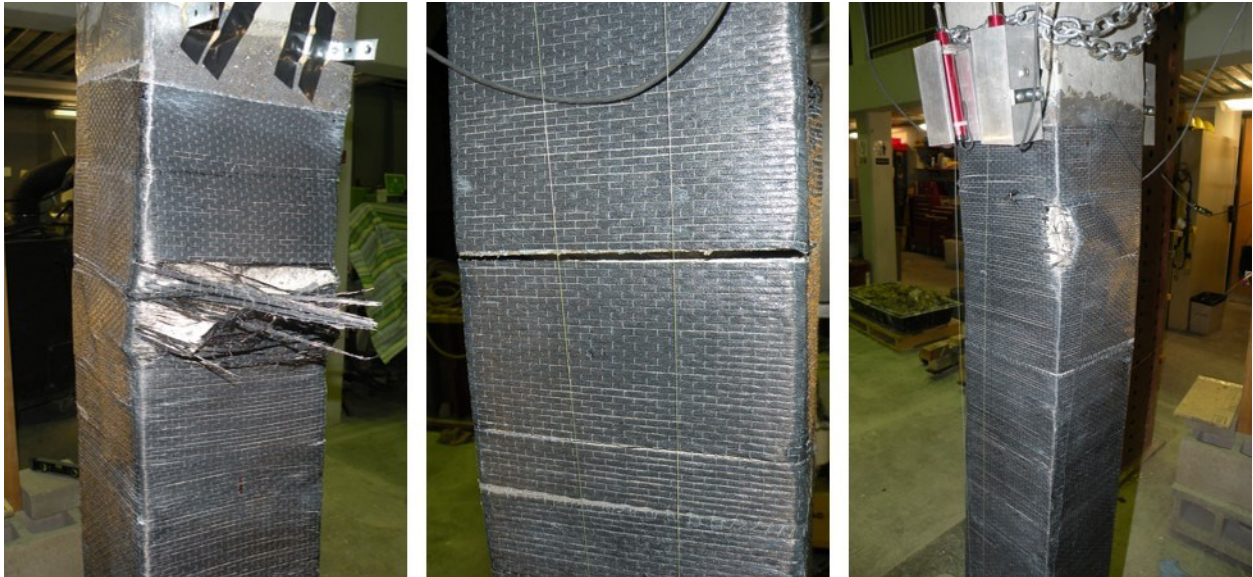
Figure C.28 Failure modes at the end of the eccentric tests for L1-e40.

Group L2-e20

Figure C.29 Axial load-deformation curves of L2-e20.

Figure C.30 Failure modes at the end of the eccentric tests for L2-e20.

Group L2-e40

Figure C.31 Axial load-deformation curves of L2-e40.

Figure C.32 Failure modes at the end of the eccentric tests for L2-e40.

Group L0
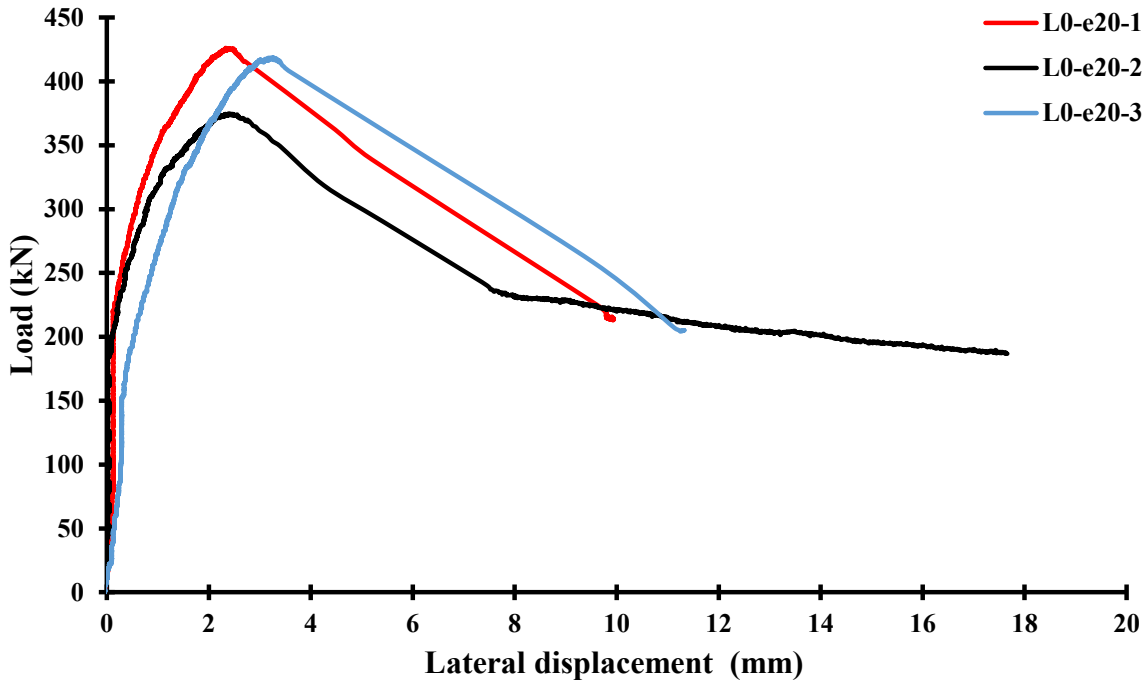
Figure C.33 Axial load- lateral displacements curves of L0-e20.
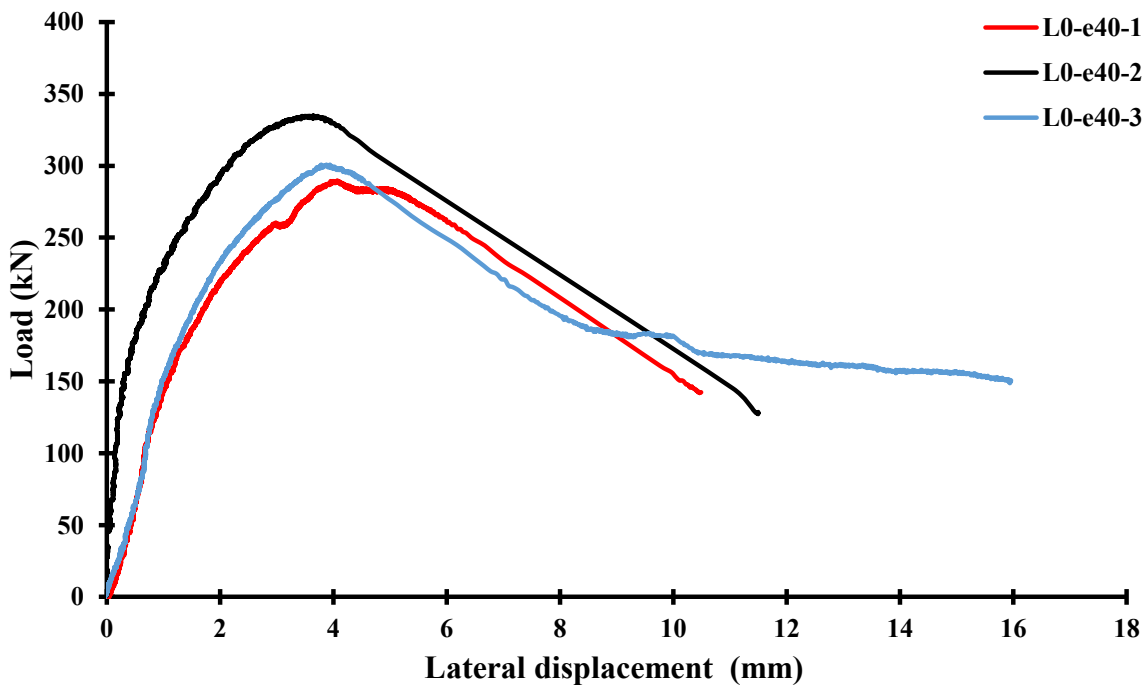
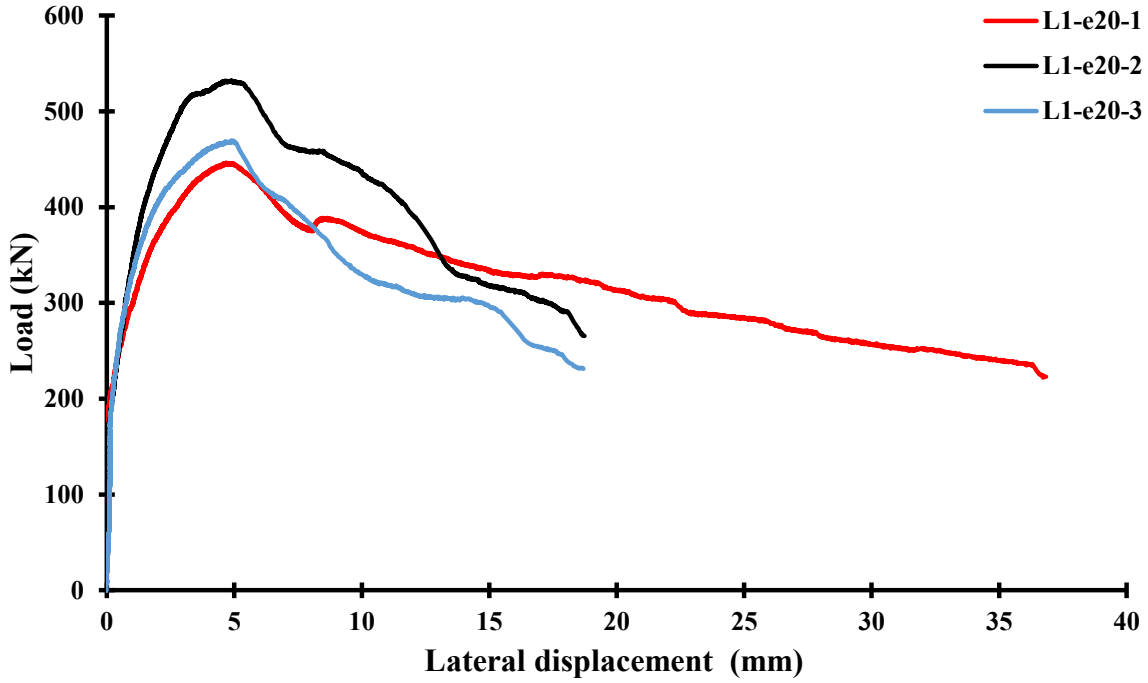Figure C.34 Axial load- lateral displacements curves of L0-e40.

Group L1

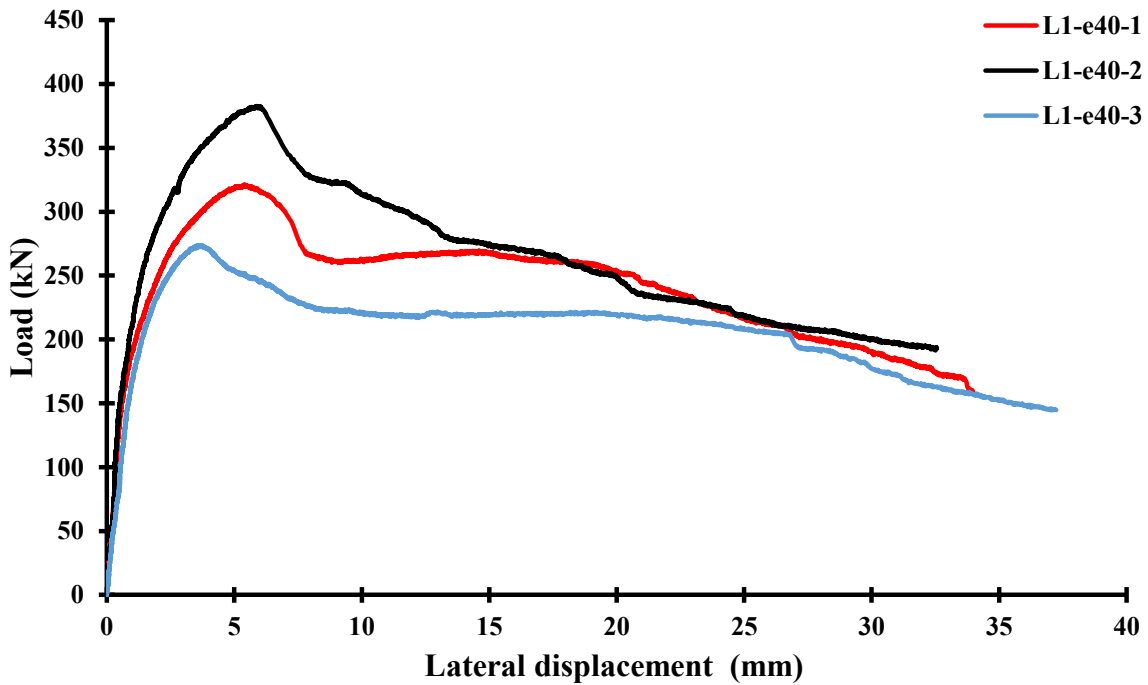Figure C.35 Axial load- lateral displacements curves of L1-e20.

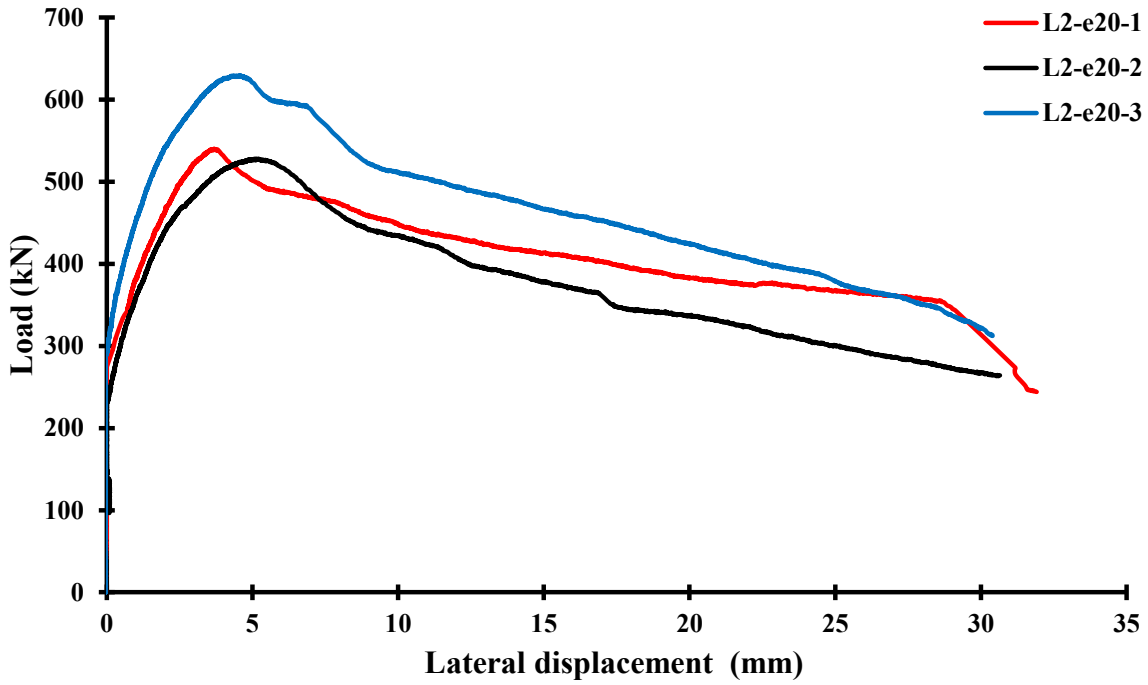Figure C.36 Axial load- lateral displacements curves of L1-e40.

Group L2

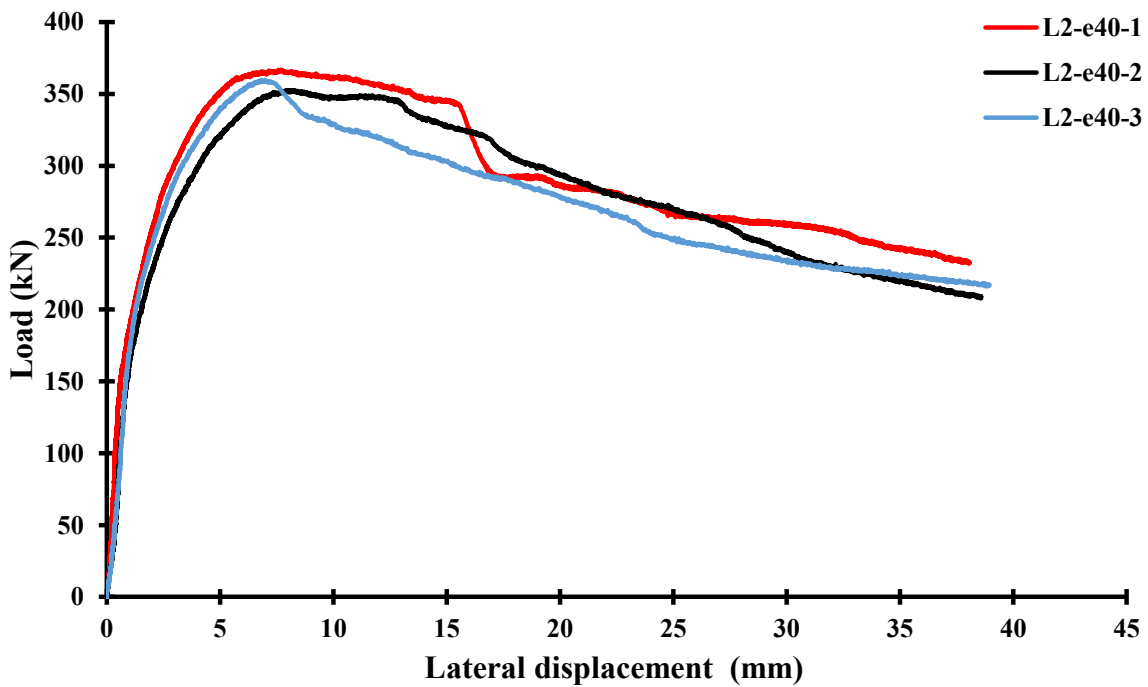Figure C.37 Axial load- lateral displacements curves of L2-e20.

Figure C.38 Axial load- lateral displacements curves of L2-e40.